YUNIBESITI YA BOKONE-BOPHIRIMA
NORTH-WEST UNIVERSITY
NOORDWES-UNIVERSITEIT

TECHNO-ECONOMIC COMPARISON OF POWER CONVERSION UNITS FOR THE NEXT GENERATION NUCLEAR PLANT

R. GREYVENSTEIN B. Eng.

Dissertation submitted for the degree Masters of Engineering at the School of Mechanical and Material Engineering at the North-West University

Study Leader: Prof. P. G. Rousseau

2005

Potchefstroom

EXECUTIVE SUMMARY

The choice of thermodynamic cycle configuration is a vital first step in the development of a new nuclear power plant. Various cycle configurations for High Temperature Gas Reactor power conversion are under investigation. The choice of optimum cycle configuration is a complex problem influenced by a large number of interdependent parameters such as component and material limitations, maintenance, risk and cost. Because identifying the optimum PCU is such a complex and integrated problem it is often difficult to assess the comparative cost and feasibility of each cycle during the concept phase. This forces developers to mainly consider performance and practical considerations when justifying the choice of cycle configuration. Unfortunately, the effect of many of these interdependent parameters on the plant cost can be overlooked when only the cycle performance and practicality are evaluated. An integrated approach is needed in order to highlight the underlying parameters that will impact on the feasibility of a particular cycle. There is therefore a need for an integrated decision-support tool that can systematically compare various cycle configurations and evaluate the efficiency and cost as a function of various design parameters.

The objective of this study was to compare the most promising one-, two- and three-shaft Brayton-, Rankine- and Combined-cycle configurations in order to evaluate the technical performance, practical considerations and economical competitiveness when employed in conjunction with a given Pebble Bed Reactor. The objective was to identify a near-optimum design for each cycle configuration from which the optimum Power Conversion Unit (PCU) configuration for the Next Generation Nuclear Plant could then be identified. The order-of-magnitude plant cost was the main parameter used to compare the various cycle configurations. The following methodology was used in the investigation in order to arrive at the order-of-magnitude plant cost and ultimately at the optimum PCU configuration:

- Ten promising cycle configurations were identified.
- A thermodynamic cycle analysis was done for each configuration.
- Component models were developed for the turbine, compressor, heat exchanger and blower. These component models were used together with the boundary values from the cycle analyses to perform a conceptual design of each component.
- The results from each component model were used to translate the component's geometry into cost, using postulated costing models for each component.
- The power output for each cycle was translated into a capitalised income resulting in a reduction in capital cost.

The temperatures, pressures, efficiency, component capital costs and the order-of-magnitude plant cost of each configuration were then calculated for various pressure ratios, reactor outlet temperatures and power turbine speeds. Based on these results, the different operational parameter envelopes were identified for which each of the different cycle configurations would be most appropriate.

The performance, practical considerations and economical competitiveness of each of the ten selected cycles were evaluated. The single-shaft inter-cooled recuperative direct Brayton cycle (Cycle B) is recommended only when the reactor outlet temperature is lower than 900 °C and the reactor power is lower than 400 MW. Altertatively, at higher reactor outlet temperaures and at higher power levels the single-shaft recuperative direct Combined Cycle without inter-cooling (Cycle J) is recommended. The results from this study suggest that the single-shaft recuperative direct Combined Cycle without inter-cooling (Cycle J) is the most appropriate PCU for the PBMR for the Next Generation Nuclear Plant.

Copyright 2005 by PBMR

UITVOERENDE OPSOMMING

Die keuse van die termodinamiese kringloop uitleg is 'n kritiese eerste stap in die ontwikkeling van 'n nuwe kern aanleg. Verskeie kringloop opsies vir koppeling aan 'n Hoë Temperatuur Gas Reaktor word tans wêreldwyd ondersoek. Die keuse van optimum kringloop uitleg is 'n komplekse probleem wat deur verskeie inter-afhanklike parameters beïnvloed word. Omdat die kringloop keuse deur soveel parameters beïnvloed word, is dit dikwels moeilik om die toepaslikheid van 'n kringloop te kan evalueer tydens die konsep fase van die projek. Daarom gebeur dit dikwels dat navorsers slegs die effektiwiteit en praktiese oorwegings van 'n kringloop in ag neem en nie na die kostes ook kyk nie. Ongelukkig gebeur dit dan dat die effek van baie van die ontwerpsparameters op die koste oorsien word. 'n Geïntegreerde benadering is nodig om die effek van die verskeie ontwerpsparameters op die aanleg koste te kan vasstel. Daar was 'n behoefte by PBMR vir die onwikkeling van 'n geïntegreerde keuse-ondersteunings gereedskapstuk wat sistematies verskeie kringlope kan evalueer en die koste kan bereken as funksie van die ontwerpsparameters.

Die doelwit van hierdie studie was om die mees belowendste enkel-, twee- en drie as Brayton-, Rankine- en Gekombineerde kringlope te evalueer om sodoende elkeen se tegniese vermoë, praktiese beperkinge en kostes te kan vergelyk vir 'n gegewe Korrel Bed Reaktor. Die doelwit is dan om die optimum ontwerp vir elk van die kringloop uitlegte te identifiseer waaruit die optimum kringloop vir die *Next Generation Nuclear Plant* gekies kan word. Die orde-grote aanleg koste is gebruik as hoof parameter om die verskeie kringlope mee te vergelyk. Die volgende metodologie is gevolg om by die optimum kringloop uit te kom:

- Tien belowende kringlope is geïdentifiseer.
- 'n Termodinamies kringloop analise is gedoen vir elke kringloop.
- Komponente modelle is ontwikkel vir die turbine, kompressor, hitteruiler en pomp. Hierdie komponent modelle is gebruik saam met die randwaardes van die kringloop analise om 'n konsep ontwerp vir elke komponent te voltooi.
- Die resultate van die komponent model konsep ontwerp is gebruik om 'n koste te bereken vir elke komponent. Die kostes is bereken met gepostuleerde koste modelle.
- Die krag uitset van elke kringloop is omgeskakel in 'n gekapitaliseerde inkomste wat lei tot 'n reduksie in die kapitale koste.

Die temperature, drukke, termiese kringloop effektiwiteit, komponent kapitale kostes en die orde-grote aanleg koste vir elke kringloop is bereken vir verskeie druk verhoudings, reaktor uitlaat temperature en turbine spoede. Operasionele gebiede is geïdentifiseer waarvoor elk van die onderskeie kringlope mees van pas voor sal wees.

Die tegniese vermoë, praktiese beperkinge en ekonomiese kompeterendheid van elk van die tien kringloop opsies is geëvalueer. Die enkel-as tussen-verkoelde direkte Brayton kringloop met 'n rekuperator word aanbeveel vir kringlope waar die reaktor uitlaat temperatuur onder 900 °C is en die reaktor drywingsvlak minder as 400 MW is. Vir kringlope wat hoër temperature en drywing vereis word die enkel-as direkte gekombineerde kringloop met 'n rekuperator aanbeveel. Die resultate van hierdie studie wys dat die enkel-as direkte gekombineerde kringloop met 'n rekuperator die mees geskikte krinloop is om te koppel aan die Korrel Bed Reaktor vir die *Next Generation Nuclear Plant*.

ACKNOWLEDGEMENTS

This work was performed for and funded by PBMR (Pty) Ltd. I would like to express my appreciation to PBMR (Pty) Ltd. for allowing publication of this document. I am grateful to management for being given the opportunity to conduct this study, specifically to both Dieter Matzner (Power Plant Director) and Abrie Botma (Manager US Projects). Thank you to Michael Correia (THAG Manager) for his support over the last 18 months. I am grateful to Lieb Liebenberg (Heat Exchanger System Engineer) and Peet Venter (Turbo Machinery System Engineer) for their technical support, input and review.

Thank you to M-Tech Industrial (Pty) Ltd. management who initiated this project and for their continued interest and insights. Specifically I would like to thank Jan van Ravenswaay (Manager Consulation Services) and Bennie du Toit (Simulation Design Engineer) for their support, input, review and editorial suggestions.

Especially I also want to thank my study leader, Prof. P. G. Rousseau, who guided and encouraged me througout this study.

Very special thanks to my mom and dad. Thank you for giving me the opportunity to study and for believing in me and encouraging me all the way. I give all the credit to my Heavenly Father.

CONTENTS

EXECUTIVE SUMMARY **2**

UITVOERENDE OPSOMMING **3**

ACKNOWLEDGEMENTS **4**

ABBREVIATIONS **11**

LIST OF VARIABLES **13**

1. INTRODUCTION **17**

1.1 Background 17
1.2 Problem statement 19
1.3 Objective of study 19
1.4 Cycles under investigation 20
1.5 Methodology 25
1.6 Outline of study 26

2. LITERATURE STUDY **28**

2.1 Introduction 28
2.2 Overview of the HTGR 30
2.3 History of the HTGR 32
2.4 Current International HTGR programs 40
2.5 NGNP requirements 50
2.6 Summary 51
2.7 Conclusion 54

3. SYSTEM THERMO-HYDRAULIC DESIGN **56**

3.1 The power conversion unit 56
3.2 System design methodology 57
3.3 Brayton cycle 61
3.4 Combined Cycle 70
3.5 Indirect cycle 84
3.6 Hydrogen Plant 86
3.7 Gas mixture properties 88

4. COSTING MODELS **90**

4.1 Overview 90
4.2 Power Conversion Unit 93
4.3 Building 94
4.4 Reactor 95
4.5 Steam Plant 95
4.6 Marginal Cost 96

5. COMPONENT MODELS **98**

5.1 Turbo-Machine 98

5.2 Compressor 109
5.3 Turbine 112
5.4 Recuperator 115
5.5 Pre- and Inter-cooler 117
5.6 IHX 118
5.7 Blower 118

6. RESULTS 120

6.1 Introduction 120
6.2 Input parameters 122
6.3 Brayton Cycles 123
6.4 Combined Cycles 131
6.5 Design Envelopes 140
6.6 General results 147
6.7 Validation and verification of Results 159
6.8 Combined Cycle Practicalities 164
6.9 Summary of Results 171

7. RECOMMENDATION AND CONCLUSION 176

7.1 Recommendation 176
7.2 Conclusion 180
7.3 Future Work 181

8. REFERENCES 184

9. APPENDICES 189

9.1 Appendix I – Input parameters 189
9.2 Appendix II – Stage prediction 193
9.3 Appendix III – Turbo machine equations in explicit form 197
9.4 Appendix IV – The Howell compressor loss model 199
9.5 Appendix V – The Ainley & Matthieson turbine loss model 202
9.6 Appendix VI – Verification by means of EES-Models 205

FIGURES

Figure 1.1 Fuel for electricity generation (percent) (WNA, 2004a) 17
Figure 1.2 Practicality and efficiency of PCUs vs. cost 19
Figure 1.3 Option tree for choosing the PCU 20
Figure 1.4 T-s diagram indicating lost work for (i) Combined Cycle and (ii) Steam cycle 20
Figure 1.5 Brayton t-s diagram for Combined Cycle for various cycle configurations – not recommended 21
Figure 1.6 Brayton t-s diagram for Combined Cycle for various cycle configurations – recommended 22
Figure 1.7 Brayton cycles under investigation 23
Figure 1.8 Combined Cycles under investigation 24
Figure 1.9 Overview of study 25
Figure 2.10 Arrangement of primary systems for the Prototype and Demonstration Plants 33
Figure 2.11 Schematic diagram of the PBMR PCU (Matzner, 2004) 42
Figure 2.12 Schematic diagram of the GT-MHR (Kostin et al, 2004) 43
Figure 2.13 Schematic diagram of the GT-MHR (Kostin et al, 2004) 44
Figure 2.14 Schematic diagram of the HTR-10 GT PCU (Jie et al, 2004) 45
Figure 2.15 Schematic diagram of the HTR-10 and HTR-10 GT (Jie et al, 2004) 45
Figure 2.16 Cooling system of HTTR (Kunitomi et al, 2004). 46
Figure 2.17 Schematic of MPBR (Wang et al, 2002) 47
Figure 2.18 Schematic of Framatome's Combined Cycle with two levels of pressure and reheat (Copsey et al, 2004) 48
Figure 3.19 PCU for Brayton Cycle B and Combined Cycle I (used as examples) 56
Figure 3.20 Overview of Systems solution – see next page 57
Figure 3.21 Cycle layout and t-s diagram – Cycle D 62
Figure 3.22 T-s diagrams of Cycles A, B, C and E 63
Figure 3.23 T-s diagram: Solution points 1-7 64
Figure 3.24 T-s diagram explaining total turbo isentropic efficiency 69
Figure 3.25 Cycle layout - Cycle H 71
Figure 3.26 T-s diagram i) Cycle H & I Brayton ii) Cycles G,H,I Rankine iii) Cycle G Brayton 72
Figure 3.27 T-s diagram for Brayton & Rankine cycle – Cycles H & I 74
Figure 3.28 T-s diagram and p-h diagrams for Cycle G at 600 MW and pressure ratio 2.1 77
Figure 3.29 Work output and RIT for Combined Cycle H – Brayton and Rankine separately 78
Figure 3.30 Thermal efficiency of Cycles G, H, I and J for various RIT's at a fixed pressure ratio 79
Figure 3.31 Thermal efficiency vs. pressure ratio 79
Figure 3.32 Optimised RIT vs. pressure ratio 79
Figure 3.33 Numbering used for all indirect cycles 84
Figure 3.34 Graphical representation of SIHX in series and parallel 86
Figure 4.35 Cost breakdown for Brayton and Combined Cycle 90
Figure 4.36 Steam plant costs 95
Figure 4.37 Marginal costs 96
Figure 5.38 Axial Compressor stage blade rows and simple velocity diagram [1:p186] 99
Figure 5.39 Axial Turbine stage blade rows and simple velocity diagram [1:p306] 99
Figure 5.40 TS diagram 102
Figure 5.41 Compressor stage and t-s diagram [1:p185] 103
Figure 5.42 Turbine stage and t-s diagram [1:312] 103

Copyright 2005 by PBMR

Figure 5.43 Schematic overview of program methodology 108
Figure 5.44 Creep strength for material: DS1400 (PBMR-MHI-032, 2003:1.6-1.14, [25]) 113
Figure 5.45 Recuperator efficiency vs heat transfer area for recuperator 116
Figure 5.46 Heat exchanger efficiency vs heat transfer area for coolers 117
Figure 6.47 Thermal efficiency vs. pressure ratio for Brayton cycles 123
Figure 6.48 Reactor inlet temperature vs. pressure ratio for Brayton cycles 124
Figure 6.49 Mass flow vs. pressure ratio for Brayton cycles 124
Figure 6.50 Turbo unit capital cost vs. pressure ratio for Brayton cycles – 1 125
Figure 6.51 Turbo unit capital cost vs. pressure ratio for Brayton cycles – 2 separate 126
Figure 6.52 Heat exchangers capital cost vs. pressure ratio for Brayton cycles 127
Figure 6.53 Total order-of-magnitude plant cost vs. pressure ratio for Brayton cycles 127
Figure 6.54 Turbo machine isentropic efficiency vs. pressure ratio for Brayton cycles 128
Figure 6.55 Turbo unit capital cost vs. reactor outlet temperature for Brayton cycles 129
Figure 6.56 Turbo unit capital cost vs. power turbine rotational speed for Brayton cycles 130
Figure 6.57 T-s diagrams 132
Figure 6.58 Heat transfer vs. Temperature 132
Figure 6.59 Thermal efficiency vs. pressure ratio for Brayton & Combined Cycles 133
Figure 6.60 Reactor inlet temperature vs. pressure ratio for Brayton & Combined Cycles 134
Figure 6.61 Mass flow vs. pressure ratio for Brayton & Combined Cycles 134
Figure 6.62 Turbo unit capital cost vs. pressure ratio for Brayton & Combined Cycles 135
Figure 6.63 Heat exchangers capital cost vs. pressure ratio for Brayton & Combined Cycles 135
Figure 6.64 PCU order-of-magnitude capital cost vs. pressure ratio for Brayton & Combined Cycles 136
Figure 6.65 Power output vs. pressure ratio for Brayton & Combined Cycles 136
Figure 6.66 Total order of magnitude plant cost vs. pressure ratio for Brayton & Combined Cycles NCC=2000$/kW 137
Figure 6.67 Total order of magnitude plant cost vs. pressure ratio for Brayton & Combined Cycles NCC=1000$/kW 137
Figure 6.68 Steam plant capital cost vs. pressure ratio for Brayton & Combined Cycles 138
Figure 6.69 Thermal efficiency vs. pressure ratio at ROT 850 °C 141
Figure 6.70 Reactor inlet temperature vs. pressure ratio at ROT 850 °C 141
Figure 6.71 Mass flow vs. pressure ratio at ROT 850 °C 142
Figure 6.72 Total plant order of magnitude capital cost vs. pressure ratio at ROT 850 °C cycles 142
Figure 6.73 Thermal efficiency vs. pressure ratio at ROT 900 °C 143
Figure 6.74 Reactor inlet temperature vs. pressure ratio at ROT 900 °C 143
Figure 6.75 Mass flow vs. pressure ratio at ROT 900 °C 144
Figure 6.76 Total plant order of magnitude capital cost vs. pressure ratio at ROT 900 °C cycles 144
Figure 6.77 Thermal efficiency vs. pressure ratio at ROT 1100 °C 145
Figure 6.78 Reactor inlet temperature vs. pressure ratio at ROT 1100 °C 145
Figure 6.79 Mass flow vs. pressure ratio at ROT 1100 °C 146
Figure 6.80 Total plant order of magnitude capital cost vs. pressure ratio at ROT 1100 °C cycles 146
Figure 6.81 Thermal efficiency vs. pressure ratio for Cycles G, H and J without the intermediate loop 147
Figure 6.82 Blower Sizes 148
Figure 6.83 Steam generator inlet temperatures 148
Figure 6.84 Turbine blade stresses 149
Figure 6.85 Thermal efficiencies of PBMR (k=40, helium, 90bar) vs. Framatome (k=4, mixture, 50bar)

..... 150
Figure 6.86 Graphical representation of SIHX in series and parallel 151
Figure 6.87 Thermal efficiencies for Hydrogen plant: series vs. parallel 152
Figure 6.88 Turbo unit capital cost vs. pressure ratio for Cycle H with Helium, Mixture and Nitrogen 153
Figure 6.89 Heat exchangers capital cost vs. pressure ratio for Cycle H with Helium, Mixture and Nitrogen 154
Figure 6.90 PCU order-of-magnitude capital cost vs. pressure ratio for Cycle H with Helium, Mixture and Nitrogen 154
Figure 6.91 Thermal efficiency vs. pressure ratio for Cycle H with Helium, Mixture and Nitrogen 155
Figure 6.92 Direct vs. Indirect thermal efficiency 156
Figure 6.93 Thermal efficiency sensitivity to reactor outlet temperature 157
Figure 6.94 Thermal efficiency sensitivity to cooling water temperature 157
Figure 6.95 Thermal efficiency sensitivity to maximum Brayton cycle pressure 158
Figure 6.96 Thermal efficiency sensitivity to turbine isentropic efficiency 158
Figure 6.97 Validation of the thermal efficiency of Cycle A and Cycle B 162
Figure 6.98 Validation of the thermal efficiency of Cycle F 162
Figure 6.99 Validation of the thermal efficiency of Cycle H and Cycle I 162
Figure 6.100 Schematic drawing for Cycle H and Cycle I – Brayton (CC) 164
Figure 6.101 Schematic drawing for Cycle H and Cycle I – Steam plant (CC) 165
Figure 6.102 T-s diagram for off-the-shelf Combined Cycle operated at off-design conditions 167
Figure 6.103 Schematic drawing for Cycle H and Cycle I – Standard off-the shelf CC 168
Figure 6.104 Identification Diagram – Cycle H 169
Figure 6.105 Identification Diagram – Cycle I 170
Figure 7.106 Alternative: Combining Cycle B and Cycle C 177
Figure 7.107 Recommendation tree 179
Figure 9.108 Variation of mean blockage factor with number of stages (PBMR-MHI-032, 2003:1-68, [25]) 194
Figure 9.109 Design deflection curves (i) compressor (Saravanamuttoo, 2001:233) (ii) turbine (Saravanamuttoo, 2001:332) 195
Figure 9.110 Drag coefficient for cascade of fixed geometrical form 199
Figure 9.111 Profile loss coefficient for conventional blading with t/c = 0.2 203
Figure 9.112 EES identification diagram - (B) Single-shaft with inter-cooling 206
Figure 9.113 EES identification diagram - (G) Single-shaft recuperative Brayton with inter-cooling .. 207
Figure 9.114 EES identification diagram - (H) Single-shaft Brayton without inter-cooling 208
Figure 9.115 EES identification diagram - (I) Indirect Single-shaft Brayton without inter-cooling – HELIUM 209
Figure 9.116 EES identification diagram - (J) Single-shaft recuperative Brayton without inter-cooling 210

TABLES

Table 2.1 Overview of HTR plants which have been built and operated in the past (Kugeler et al, 2003) 36
Table 2.2 Overview of HTR plants which have been planned in the past (1970s and 1980s) 39
Table 2.3 Overview of HTR plants which have been planned in the past (1970s and 1980s) 41
Table 4.4 Costing Models 92
Table 5.5 Design variables for turbo machines 106
Table 5.6 Summary of compressor model inputs and outputs 109
Table 5.7 Summary of turbine model inputs and outputs 112
Table 6.8 Cost Breakdown for Cycles B, F, G, H, I and J 138
Table 6.9 Cycle input parameters 161
Table 6.10 Cycle input parameters 163
Table 9.11 Guessed input variables 189
Table 9.12 Brayton input variables 189
Table 9.13 Rankine input variables 190
Table 9.14 Fluid input variables 190
Table 9.15 Hydrogen Plant input variables 190
Table 9.16 Turbo machine input variables 191
Table 8.17 Heat exchanger input variables 191
Table 9.18 Costing input variables 192
Table 9.19 Leak flow input variables 192

ABBREVIATIONS

This list contains the abbreviations as used in this study.

Abbreviation	*Definition*
AVR	*Arbeitsgemeinshaft Versuchsreaktor*
BOP	*Balance of plant*
BWXT	*?*
CD	*Condenser*
CEA	*The French Atomic Energy Commission*
D.L	*Derek Lee*
D.M.	*Dieter Matzner*
DOE	*Department of Energy*
EU	*European Union*
FNR	*Fast Neutron Reactors*
GB	*Gear box*
GEN	*Generator*
GFR	*Gas-cooled fast reactor*
GIF	*Generation IV International Forum*
HP	*High-pressure*
HPC	*High-pressure compressor*
HPT	*High-pressure turbine*
HPT	*High-pressure turbine*
HTGR	*High temperature gas reactor*
HTTR	*High Temperature Engineering Test Reactor*
HWR	*Heavy Water Reactors*
IAEA	*International Atomic Energy Agency*
IC	*Inter-cooler*
INEEL	*Idaho National Engineering and Environmental Laboratory*
INET	*Institute of Nuclear and New Energy Technology*
ITRG	*Independent Technical Review Group*
JAERI	*Japan Atomic Energy Research Institute*
KAERI	*Korean Atomic Energy Research Institute*
LP	*Low-pressure*
LPC	*Low-pressure compressor*
LPT	*Low-pressure turbine*
LWR	*Light Water Reactors*
MIT	*Massachusetts Institute of Technology*
NCC	*Nuclear capacity cost*
NCC	*Nuclear capacity cost*
NEA	*Nuclear Energy Agency*
NGNP	*Next Generation Nuclear Plant*
OECD	*Organisation for Economic Co-operation and Development*
OKBM	*Experimental Design Bureau of Mechanical Engineering*
ORNL	*?*

Abbreviation	Definition
PBMR	Pebble Bed Modular Reactor Pty. (Ltd.)
PBR	Pebble Bed Reactor
PC	Pre-cooler
PCU	Power conversion unit
P_{MAX}	Maximum cycle pressure
PT	Power turbine
REC	Recuperator
RIT	Reactor inlet temperature
ROT	Reactor outlet temperature
RX	Recuperator
SBS	Start-up blower system
TBC	To be Completed
TBD	To be Determined
T_{MAX}	Maximum cycle temperature
T_{MIN}	Minimum cycle temperature
TWG-GCR	Technical Work Group on Gas-cooled Reactors
VHTR	Very High Temperature Reactor

LIST OF VARIABLES

This list contains the variables as used in this study.

α	[rad]	rotor blade angle
Λ	[-]	reaction
ρ_{blade}	[kg/m^3]	compressor / turbine blade density
σ	[Pa]	compressor / turbine blade stress
C_{GEN_GB}	[m$]	fixed capital cost for the generator and gearbox combined
C_{SBS_RB}	[m$]	fixed capital cost for the SBS blower and resister bank combined
$C_{Building}$	[m$]	fixed capital cost for the building - Brayton
$C_{Building\_CC}$	[m$]	fixed capital cost for the building – Combined Cycle
$C_{Reactor}$	[m$]	fixed capital cost for the reactor
$\%dP_{HXs}$	[-]	0.7% pressure loss on each side for each heat exchanger in cycle
$\%dP_{PIPING}$	[-]	0.3% pressure loss assumed for each pipe in the cycle
$\%dP_{RH}$	[%]	losses in re-heater
$\%dP_{SG}$	[%]	losses in steam generator
β , α	[rad]	rotor blade angle
ρ / rho	[kg/m^3]	fluid density
A	[m^2]	area
BLOCK	[MWth]	block reactor thermal power
C	[m$]	capital cost
C_a	[m/s]	compressor / turbine axial velocity
CDx	[-]	minimum allowable condenser two-phase quality fraction
$C_{Generator\_Gearbox}$	[m$]	capital cost: Generator and Gearbox
Cp	[J/kg. K]	specific heat at constant pressure
Cr	[-]	heat capacity ratio
$C_{Reactor\_Buiding}$	[m$]	capital cost: reactor and building (incl. balance of plant) - Brayton
$C_{Reactor\_Buiding\_CC}$	[m$]	capital cost: reactor and building (incl. balance of plant) - CC
C_{SBS_RB}	[m$]	capital cost: SBS blower and Resistor bank
C_{w1}	[m/s]	absolute tangential velocity at the inlet
C_{w2}	[m/s]	absolute tangential velocity at the outlet
d_{IHX}	[m]	hydraulic diameter - IHX
dT	[°C] / [K]	total temperature difference over turbo machine
dT_{IHX}	[°C]	temperature difference over the IHX for indirect cycles
$dT_{IHXsteam}$	[°C]	temperature difference over the IHX for direct cycles
F_{u1}	[kg.m/s^2]	tangential force on rotor from entering fluid
Gamma	[-]	ratio of specific heats
h	[m]	blade height
$H2_{eff-parallel}$	[%]	hydrogen process efficiency – parallel configuration
$H2_{eff-serie}$	[%]	hydrogen process efficiency – series configuration

$H2_{MW\text{-}parallel}$	[MW]	power available for Hydrogen plant - parallel configuration
$H2_{MW\text{-}serie}$	[MW]	power available for Hydrogen plant - series configuration
k	[W/m K]	conductivity as function of temperature
$Kbase_{IHX}$	[m$]	cost offset: IHX (development cost)
k_{BLOCK}	[-]	loss coefficient for Block reactor - fixed
K_{C1}	[-]	proportionality constant: compressor (material)
k_{comp}	[-]	loss coefficient for diffuser - compressor
K_{IC}	[-]	proportionality constant: Inter-cooler (material)
K_{IHX}	[-]	proportionality constant: IHX (material)
k_{PBMR}	[m^{-4}]	loss coefficient for PBR - fixed
K_{PC}	[-]	proportionality constant: Pre-cooler (material)
$K_{Recuperator}$	[-]	proportionality constant: recuperator (material)
K_{T1}	[-]	proportionality constant: turbine (material)
k_{turb}	[-]	loss coefficient for diffuser - turbine
Leak flows	[%]	percentage of total mass flow
mflow	[kg/s]	mass flow – Brayton cycle
ms	[kg/s]	mass flow – Rankine cycle
N	[rev/s]	turbo machine rotational speed
NCC	[m$/MW]	nuclear capacity cost
p	[Pa]	total pressure
PBR	[MWth]	Pebble bed reactor thermal power
p_{max}	[bar]	maximum cycle pressure
R	[J/kg. K]	gas constant
Re	[-]	Reynolds number
r_h	[m]	turbine / compressor hub radius
r_h	[m]	turbine / compressor tip radius
s	[m]	turbine / compressor blade pitch
SF	[-]	turbine / compressor blade safety factor
$Steam_{marginal}$	[$/kW]	Y=ax+b… (a) marginal cost
$Steam_{offset}$	[m$]	Y=ax+b… (b) cost offset
t	[K]	temperature
T_1	[$kg.m^2/s^2$]	torque on rotor at the inlet
t_{max}	[°C]	maximum cycle coolant temperature
t_{min}	[°C]	minimum cycle coolant temperature
T_n	[$kg.m^2/s^2$]	net torque on rotor
t_{Pinch}	[°C]	pinch temperature for steam generator
U	[$W/m^2.K$]	heat transfer coefficient
U_{IC}	[-]	heat transfer coefficient for the inter-cooler
U_m	[m/s]	turbine / compressor mean speed
U_{PC}	[-]	heat transfer coefficient for the pre-cooler
$U_{Recuperator}$	[-]	heat transfer coefficient for the recuperator
U_t	[m/s]	turbine / compressor tip speed
w	[MW.s/kg]	work per unit mass flow
W	[MW]	work
z	[-]	compressor / turbine number of stages

η_{blower}	[%]	*blower isentropic efficiency*
η_c	[%]	*compressor isentropic efficiency*
η_{cycle}	[%]	*thermal cycle efficiency*
η_{IC}	[%]	*inter-cooler efficiency*
$\eta_{mechanical}$	[%]	*mechanical shaft efficiency*
η_{PC}	[%]	*pre-cooler efficiency*
η_{pump}	[%]	*pump efficiency for Rankine cycle*
$\eta_{Recuperator}$	[%]	*recuperator effectiveness*
η_s	[%]	*stage efficiency*
η_t	[%]	*turbine isentropic efficiency for Brayton cycle*
$\eta_{turbine}$	[%]	*turbine efficiency for Rankine cycle*
σ_{max}	[MPa]	*blade material maximum allowable yield strength*
Φ	[-]	*flow coefficient*
Ψ	[-]	*work coefficient*

Chapter 1

Introduction

In this chapter, the background to the study is given and the problem statement and objective of the study are stated. The cycles under investigation are discussed and the methodology used for the study is explained where-after an outline of the study is given.

1. INTRODUCTION

1.1 BACKGROUND

There is a continuing increase in the demand for electrical power in most industrialized countries. The *Bush Energy Policy* warns that declining supplies of oil and gas threaten to drag the United States into the worst energy-supply crisis since the 1970's (Anon, 2002). Since 1980 the total world energy use grew by nearly 50 percent, with electricity growth even stronger (WNA, 2002a). The renewable energy sources for electricity constitute of solar, tidal, hydro, geothermal and biomass-based power generation. Except for hydropower in the few places where it is plentiful, none of the renewable energy sources are suitable for large-scale power generation where continuous, reliable supply is needed (WNA, 2002a). The world relies on fossil fuels to produce almost half of all base-load electricity production. Unfortunately carbon dioxide emissions from fossil fuels contribute to significant global warming. The world needs an alternative energy source which will be sustainable, economically viable and which will minimize global pollution.

Technological advances have made nuclear power safer, more efficient and less expensive than it has been in the past. Nuclear power generation is an established part of the world's electricity mix providing over 16% of world electricity today, see *Figure 1.1*. On a global scale nuclear power is reducing carbon dioxide emissions by some 2.4 billion tons per year (WNA, 2002a). The relative costs of generating electricity from coal, gas and nuclear plants vary considerably depending on location. Coal is economically attractive in countries with abundant and accessible domestic coal resources as long as carbon emissions are cost-free. Gas is also competitive for base-load power in many places, particularly using Combined Cycle plants, although rising gas prices have removed much of the advantage (WNA, 2004b). Nuclear energy is, in many places, competitive with fossil fuel for electricity generation, despite relatively high capital costs and the need to internalize all waste disposal and decommissioning costs. A recent OECD comparative study (OECD, 2003) shows that in 7 of 13 countries considering nuclear energy, nuclear would be the preferred choice for new base-load capacity commissioned by 2010. Nuclear holds the promise of sustainable and economically viable energy whilst minimizing global pollution. If the social, health and environmental costs of fossil fuels are also taken into account, nuclear seems to be the only solution to the world's energy needs.

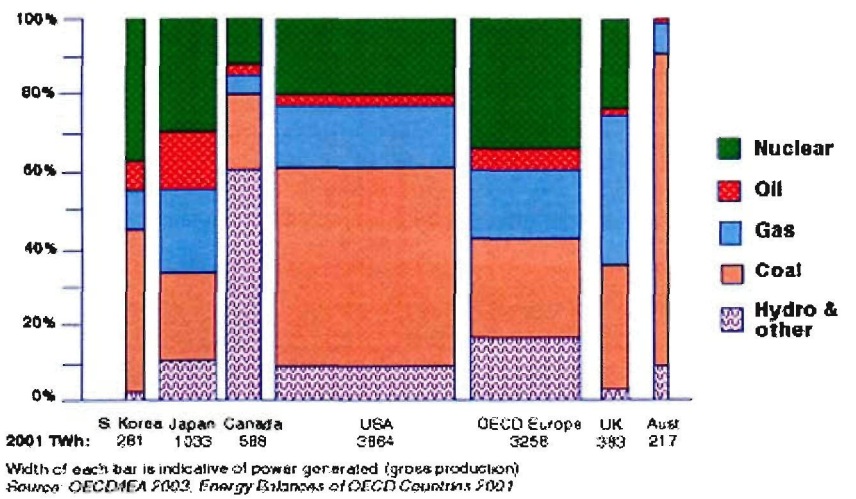


Figure 1.1 *Fuel for electricity generation (percent) (WNA, 2004a)*

Substantial interest has been generated in advanced reactors over the last few years. This interest is motivated by the view that new nuclear power reactors will be needed to provide low carbon generation of electricity and possibly hydrogen to support the future growth in demand for both of these commodities. Some governments feel that substantially different designs will be needed to satisfy the desires for public perception, improved safety, proliferation resistance, reduced waste and competitive economics. This has motivated the creation of the Generation IV Nuclear Energy Systems program in which ten countries have agreed on a framework for international cooperation in research for advanced reactors. Six designs have been selected for continued evaluation with the objective of deployment by 2030. One of these designs is the Very High Temperature Reactor (VHTR). The Department of Energy (DOE) has selected the Very High Temperature Reactor (VHTR) as the concept to demonstrate the use of nuclear power for both electricity and hydrogen production and authorized INEEL to be the vehicle to meet the NGNP functional objectives.

The Pebble Bed Modular Reactor (PBMR), being developed in South Africa through a world wide international collaborative effort led by ESKOM, the national utility, will represent a key milestone on the way to achievement of the VHTR design objectives (Matzner *et al*, 2003). The choice of thermodynamic cycle configuration is a vital first step in the development of a new nuclear power plant. The cycle configuration directly influences the cycle efficiency, power output and cost, as well as maintenance, construction time and risk of the plant. It is therefore essential to investigate various cycle configurations in order to assess each cycle's feasibility with regard to these parameters. In order to partake in this Generation IV initiative, PBMR needs a PCU that can operate at higher temperatures, higher power levels, and which is practical, efficient and cost effective.

Cycle configurations for the PCU under investigation are the Rankine- , Brayton and Combined Cycle. The early nuclear plants operated on a Rankine cycle with steam conditions similar to modern fossil plants. VHTRs offer temperatures in excess of 900 °C. Conventional steam plants do not gain from reactor outlet temperatures in excess of 650 °C, due to the maximum steam temperature being limited to 600 °C. Studies indicated that considerable cost savings could result from the application of a closed loop Brayton cycle using advances in technology for gas turbines, compact heat exchangers, manufacturing and electronics (IAEA, 2001a). Although the Brayton cycle designs are mainly based on existing technology, the specific configurations and operating environment differ considerably from existing applications. These differences introduce uncertainties that need to be understood in order to identify the most competitive cycle design for today's nuclear market. Combined Cycles hold the promise of high cycle efficiencies, while utilising conventional steam plant technology which is coupled to a small Brayton cycle. When investigating the Combined Cycle, the financial gain due to the higher cycle efficiency needs to be compared to the additional capital costs.

Various cycle configurations for high temperature gas reactor (HTGR) power conversion are currently under investigation. The choice of optimum cycle configuration is a complex problem influenced by a large number of interdependent parameters such as component and material limitations, maintenance, risk, and cost. Because identifying the optimum PCU is such a complex and integrated problem it is often difficult to assess the comparative cost and feasibility of each cycle during the concept phase. This forces developers to mainly consider performance and practical considerations when justifying the choice of cycle configuration. Unfortunately, the effect of many of these interdependent parameters on the plant cost can be overlooked when only the cycle performance and practicality are evaluated.

The growing demand for electrical power is urgently pressing the nuclear industry for clean, inherently safe, efficient and cost competitive nuclear power plants. If PBMR wants to participate in the NGNP initiative, it is crucial to propose a PCU that is not only practical and efficient, but also cost competitive.

1.2 PROBLEM STATEMENT

An integrated approach is needed in order to highlight the underlying parameters that will impact on the feasibility of a particular cycle. A need has been identified to develop an integrated decision-making tool that could systematically compare various cycle configurations based on the same input parameters which could evaluate the efficiency and cost as function of various design parameters.

1.3 OBJECTIVE OF STUDY

The objective of this study is to compare the most promising one-, two- and three-shaft Brayton-, Rankine- and Combined-cycle configurations in order to evaluate the technical performance, practical considerations and economical competitiveness when employed in conjunction with a given Pebble Bed Reactor. The objective is to identify a near-optimum design for each cycle configuration from which the optimum PCU configuration can be identified.

This study was conducted for PBMR Pty. Ltd. in support of the NGNP initiative in order to identify the most practical, efficient and cost effective PCU design for today's nuclear market.

- This study aims to assist in long-term strategic planning as to which PCU is best for VHTR application.
- This study aims to integrate knowledge from within PBMR.
- This study aims to provide PBMR with a tool which will give quick, meaningful results of PCU temperatures, pressures, mass flows, cycle efficiencies, comparative costs and PCU component designs.
- This study will also assist in identifying a working point for a particular chosen cycle.

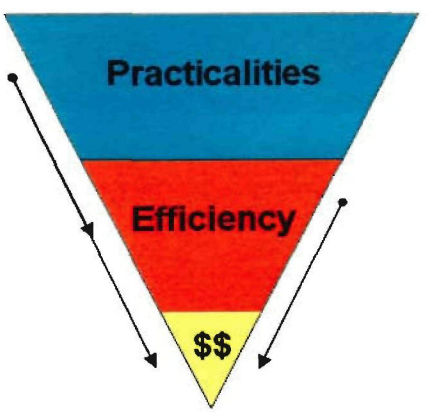


Figure 1.2 *Practicality and efficiency of PCUs vs. cost*

1.4 CYCLES UNDER INVESTIGATION

In this section the Rankine-, Brayton- and Combined Cycle configurations under investigation are mentioned and it is explained why specifically only these were chosen. For a specific PCU, one needs to assess whether a direct or indirect cycle is best. Should one choose an indirect cycle, the choice of which fluid to use arises. These questions will be addressed in the study. It is assumed that a fixed PBR will be used and that Helium will therefore be used as coolant for all the direct cycles.

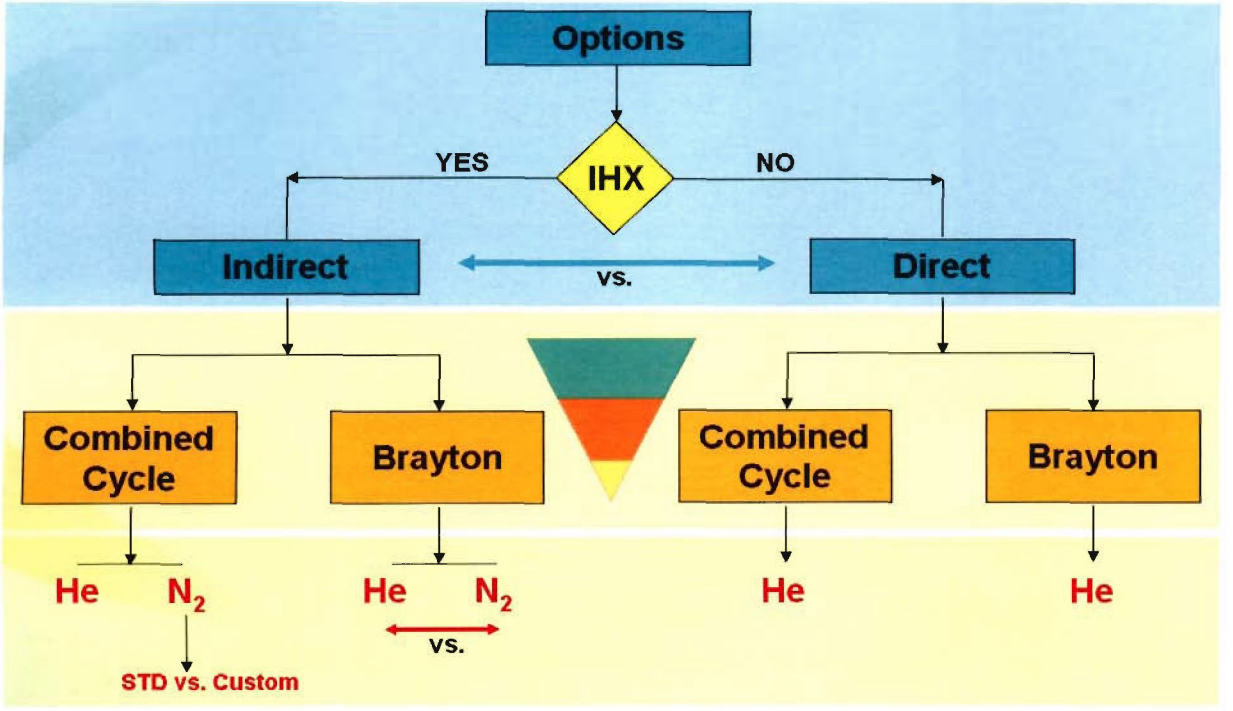


Figure 1.3 *Option tree for choosing the PCU*

1.4.1 Rankine

The maximum steam temperature for conventional steam plants vary between 540 °C and 600 °C. Thus steam plants effectively utilize only heat below 650 °C. The shaded areas in *Figure 1.4* indicate lost work in the system – heat which is available, but not utilized. For temperatures in excess of 650 °C it is recommended that a Combined Cycle be used. A conventional steam plant is therefore not recommended as PCU for VHTR application.

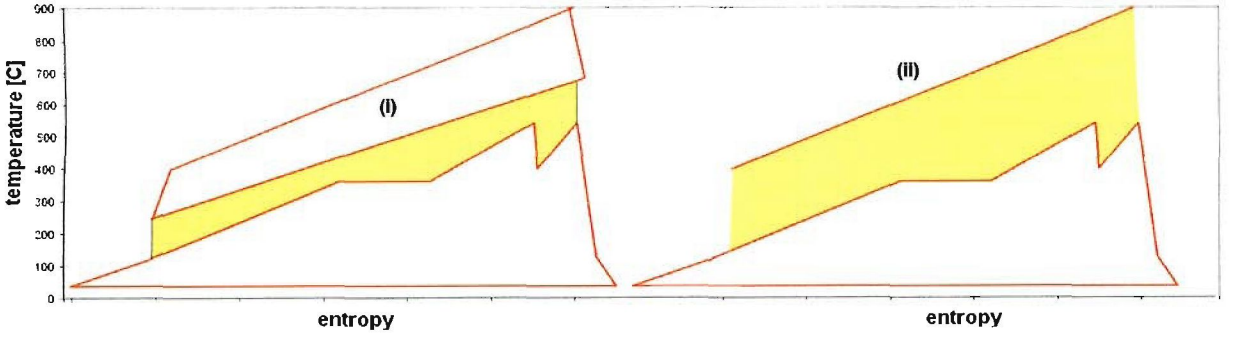


Figure 1.4 *T-s diagram indicating lost work for (i) Combined Cycle and (ii) Steam cycle*

1.4.2 Brayton

Because the Brayton cycle and its operating environment differ from existing applications, it is not clear which Brayton cycle is the best option. Brayton cycle configurations mainly differ from each other with regard to the number of shafts, inter-cooling or not and whether or not a recuperator is employed for waste heat recovery. The number of shafts impacts directly on the plant controllability, the number of compressors and turbines, the turbo machine design, risk and cost. The turbo machine design impacts on the turbo efficiency, which influences the cycle efficiency, which in turn influences the plant economics. Inter-cooling and waste heat recovery directly impact on the plant efficiency, but also the capital cost. The effect of each of these parameters on the plant cost, efficiency and practicalities need to be evaluated for each of the various options. Cycles A – E of *Figure 1.7* were chosen as the representative cycles for possible Brayton configurations:

- Cycle A : Single shaft, recuperative direct Brayton cycle
- Cycle B and F: Single shaft, recuperative Brayton cycle with inter-cooling
- Cycle C: Two shaft, recuperative direct Brayton cycle with inter-cooling
- Cycle D: Three shaft, recuperative direct Brayton cycle with inter-cooling
- Cycle E: Three shaft, recuperative direct Brayton cycle with two-step inter-cooling

1.4.3 Combined

Combined Cycles hold the promise of high cycle efficiencies, while utilising conventional steam plant technology which is coupled to a small custom designed Brayton cycle. A variety of cycle configurations are possible. For the Brayton section of the Combined Cycle, as in section 1.4.2, the question remains as to how many shafts to use and whether inter-cooling and waste heat recovery are necessary. Added complexities are the questions of where the steam generator should be situated in the Brayton cycle layout and how to customise the steam plant to fit the Brayton cycle.

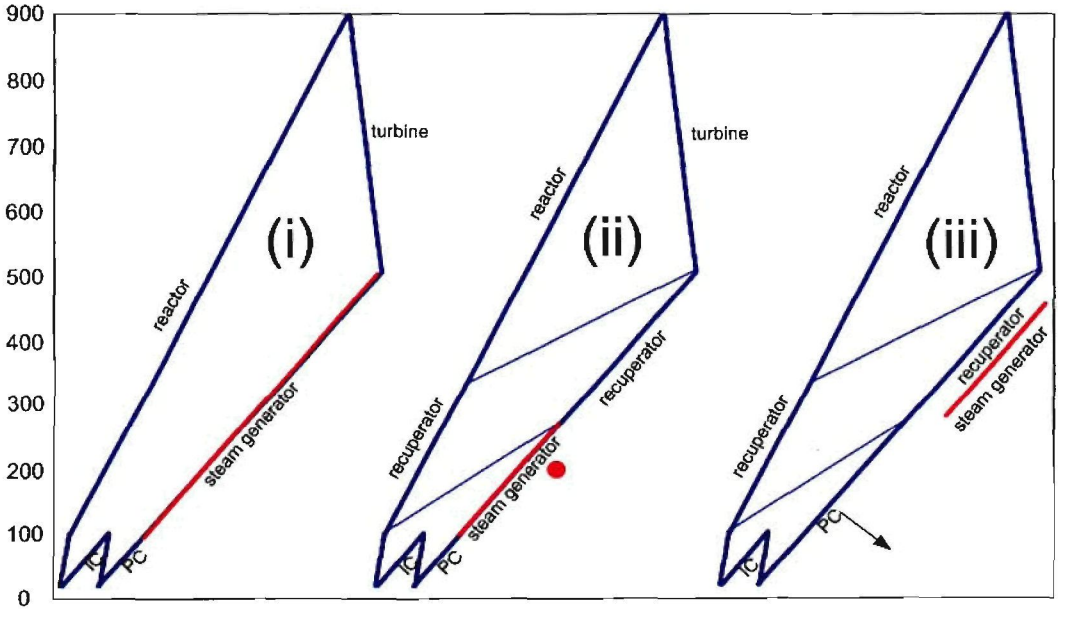


Figure 1.5 *Brayton t-s diagram for Combined Cycle for various cycle configurations – not recommended*

Figure 1.5 (i) represents the t-s diagram of a single-shaft inter-cooled Brayton cycle, where the recuperator has been replaced with a steam generator. The reactor inlet temperature for the PBR is limited to around 300 °C. In the absence of the recuperator, the reactor inlet temperature has dropped to around 100 °C. This is below the minimum inlet temperature and therefore Cycle (i) is not an option. Because of the reactor inlet temperature limit, a recuperator is introduced. *Figure 1.5* (ii) represents the t-s diagram of a single-shaft inter-cooled Brayton cycle, with both a recuperator and steam generator. The problem with placing the steam generator at the lower end is that the recuperator is very ineffective, and that the maximum temperature for the steam plant is limited to around 200 °C. Cycle (ii) will therefore have both an inefficient Brayton due to low recuperator effectiveness and also a low Rankine cycle efficiency due to the low steam temperature. Cycle (ii) is not advised. *Figure 1.5* (iii) represents the t-s diagram of a single-shaft inter-cooled Brayton cycle, where the steam generator is coupled in parallel with the recuperator through a three-pass heat exchanger. Although the steam plant efficiency will be increased because of the higher temperatures, the Brayton is still inefficient due to the ineffective recuperator. Cycle (iii) is also not advisable.

Figure 1.6 (iv-A) represents the t-s diagram of a single-shaft inter-cooled recuperative Brayton cycle, where the steam generator is utilized at the higher end with the recuperator at the lower end. The advantage is that the steam plant has a high steam temperature while the recuperator is still working effectively. Note that the reactor inlet temperature is low and also that the recuperator is relatively small due to lower mass flows. This cycle is proposed to be investigated – see Cycle G of *Figure 1.8*. An alternative to Cycle G is to compress through the low-pressure compressor (LPC) only by discarding both the inter-cooler and high-pressure compressor (HPC) – see Cycle J of *Figure 1.8*. It is noted that the recuperator size is smaller now and also that more heat is available in the pre-cooler to be effectively used to pre-heat the water in the Rankine cycle before entering the steam-generator. An alternative is to leave out the pre-cooler and directly compress from after the steam generator. In this case a recuperator will not be needed since the reactor inlet temperature is already in the region of 400 °C - see Cycle H and Cycle I of *Figure 1.8*.

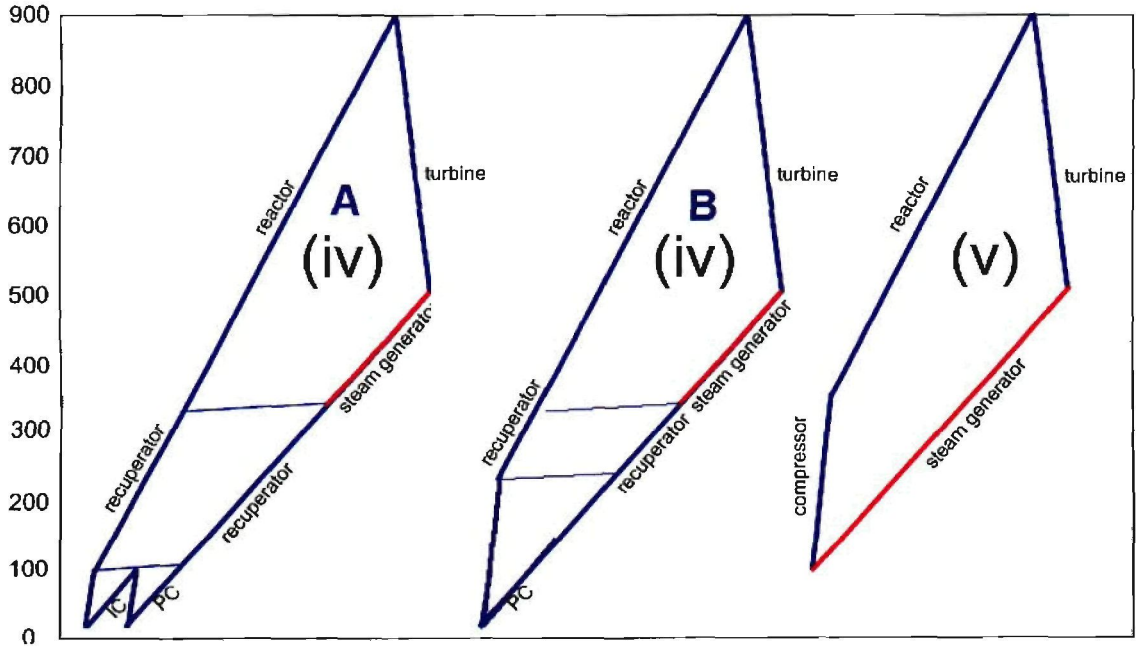


Figure 1.6 *Brayton t-s diagram for Combined Cycle for various cycle configurations – recommended*

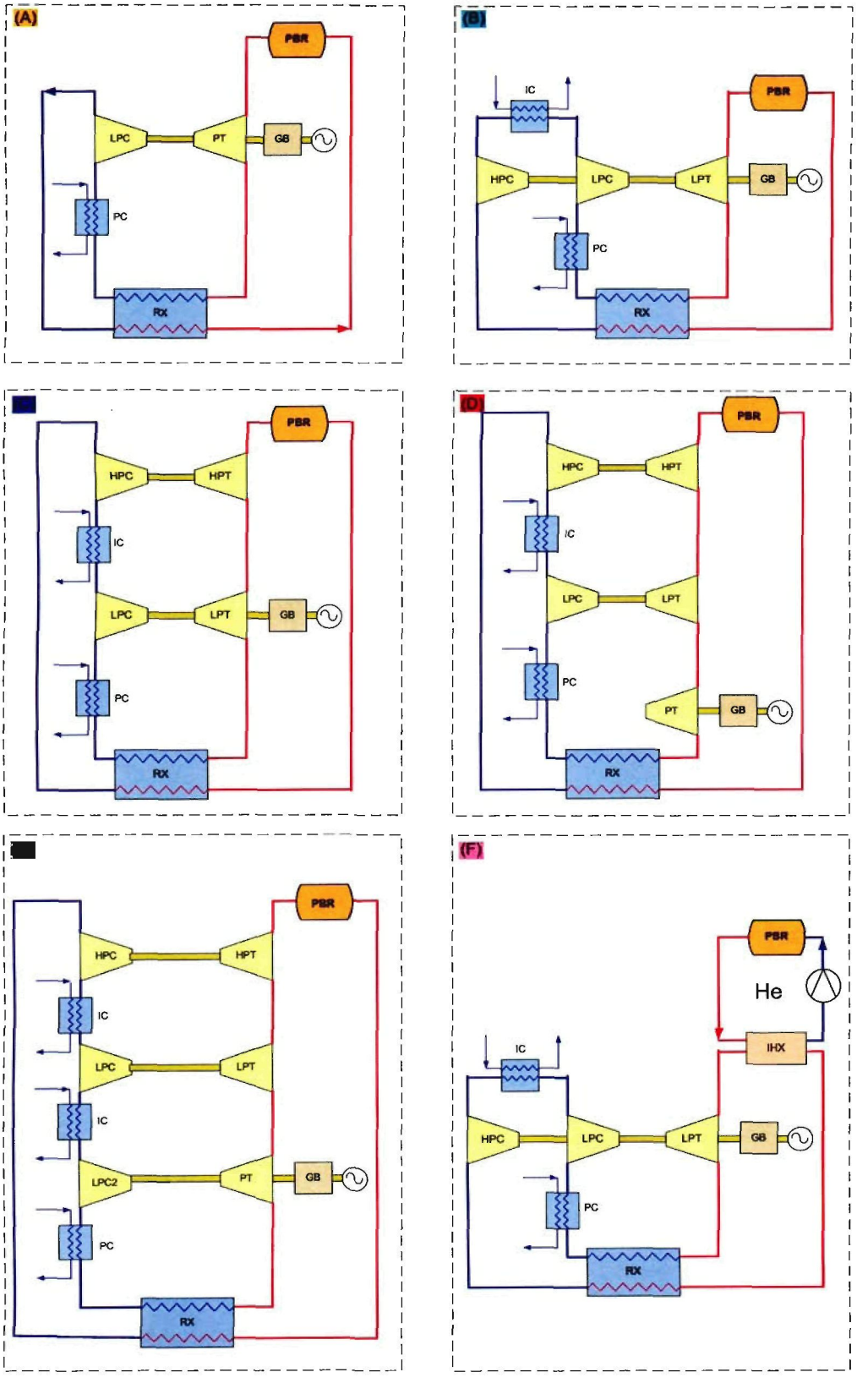


Figure 1.7 *Brayton cycles under investigation*

(A) Single-shaft (B) Single-shaft with inter-cooling (C) Two-shaft with inter-cooling (D) Three-shaft with inter-cooling (E) Three-shaft with two-step inter-cooling (F) Indirect single-shaft with inter-cooling

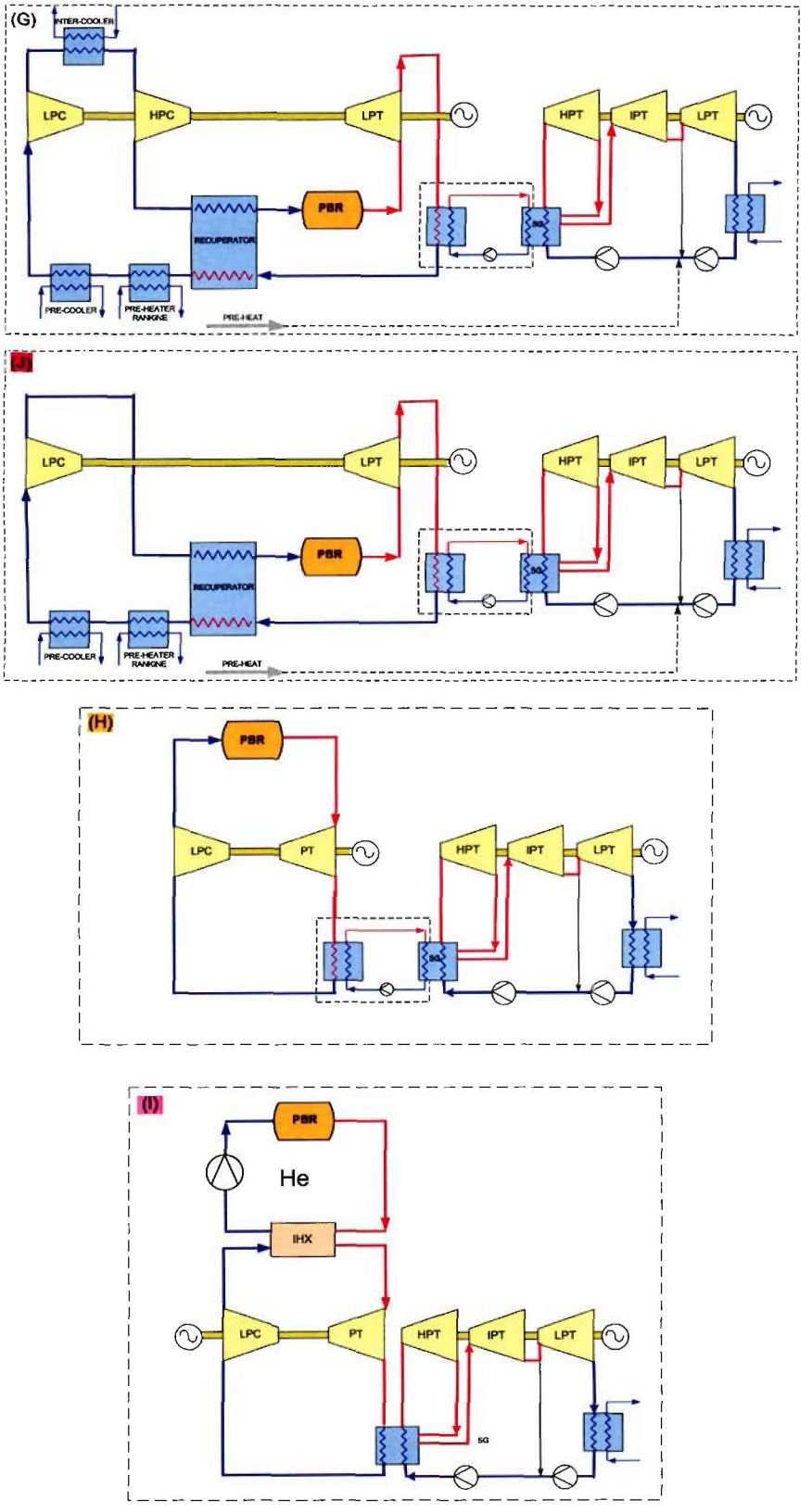


Figure 1.8 *Combined Cycles under investigation*

(G) Single-shaft recuperative Brayton with inter-cooling (J) Single-shaft recuperative Brayton without inter-cooling (H) Single-shaft Brayton without inter-cooling (I) Indirect Single-shaft Brayton without inter-cooling

1.5 METHODOLOGY

The cost is used as main parameter to assess the feasibility of a particular cycle. The order-of-magnitude capital cost is only a comparative value between the cycles and does not portray the absolute total cost of the PCU. The philosophy was to include only those component costs that would result in notable overall cost differences between the cycles. For the PCU, these include only the cost of the turbo machines, heat exchangers and blowers as well as the effect of the capitalised income from the power delivered to the grid. The following methodology was used in the investigation:

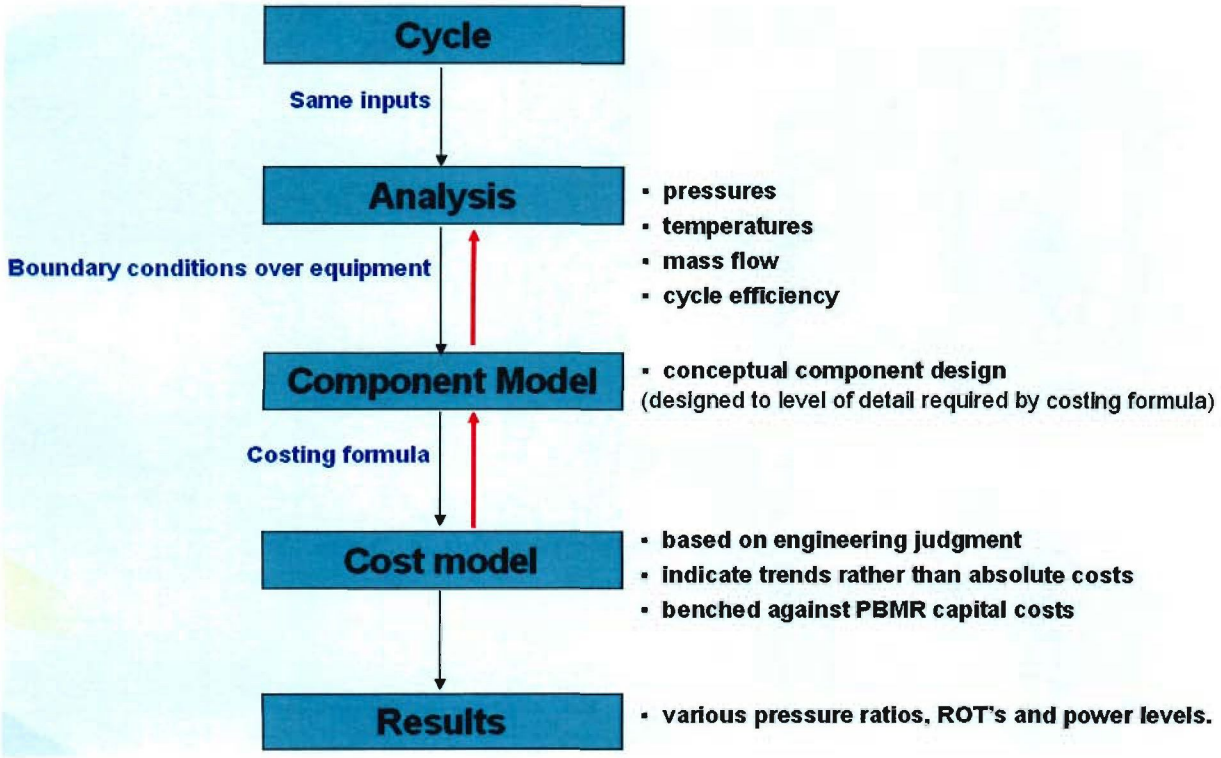


Figure 1.9 *Overview of study*

- Ten cycle configurations were chosen to be investigated (see previous section).
- A thermodynamic cycle analysis was done for each configuration based on a fixed reactor pressure loss coefficient, fixed heat exchanger efficiencies and fixed percentages for the pressure losses through the piping and heat exchangers. The leak flows for each cycle was calculated as fixed percentages of the total cycle flow. The isentropic efficiency of each turbo machine is calculated at each specified cycle pressure ratio as function of the stage efficiency and number of stages (only applied to Brayton cycles).
- Component models for the turbine, compressor, heat exchanger and blower were used together with the boundary values from the cycle analyses to perform a conceptual design of each component. Since the same reactor will be utilized in all the cycles, the reactor cost will not influence the comparative order-of-magnitude cost. The components were only designed to the level of detail that is required by the costing formula. After the components have been designed, certain cycle analysis input was updated with these newly calculated values.
- The results from each component model were used to translate the component's geometry into cost, using postulated costing models for each component. The turbo machine designs

were optimized to ensure minimum capital cost of the machine.

- The power output for each cycle was translated into a capitalised income resulting in a reduction in capital cost. This means that higher thermal cycle efficiencies and higher power levels effectively reduce the order-of-magnitude capital cost.

The temperatures, pressures, efficiency, component capital costs and the order-of-magnitude cost of each configuration was then calculated for various pressure ratios, reactor outlet temperatures and power turbine rotational speeds. Based on these results, the different operational parameter envelopes are identified for which each of the different cycle configurations would be most appropriate.

CYCLE-C is the computer tool that was developed in Visual C++ for this study with the objective to systematically compare various cycle configurations in order to evaluate their technical performance, practical considerations and economical competitiveness when employed in conjunction with a given Pebble Bed Reactor (PBR).

1.6 OUTLINE OF STUDY

The study is presented in the following 6 chapters:

CHAPTER 1: Background and Purpose of study

The background to the study is given and the problem statement and objective of the study is stated. The cycles under investigation are discussed and the methodology used for the study is explained.

CHAPTER 2: Literature survey

An extensive literature survey is documented, placing the problem of identifying a PCU in perspective.

CHAPTER 3: System thermo-hydraulic design

The theory and methodology used to solve the thermodynamic cycle analyses is presented. All relevant input parameters are discussed.

CHAPTER 4: Costing Models

The costing models used are discussed and motivated.

CHAPTER 5: Component Models

The theory and methodology of each component model is discussed:

- compressor, turbine,
- recuperator, pre-cooler, inter-cooler, IHX and
- blower.

CHAPTER 6: Results

Based on the results of the cycle analyses, component designs and cost of each configuration, different operational parameter envelopes are identified for which each of the different cycle configurations would be most appropriate.

CHAPTER 7: Recommendation and Conclusion

Recommendations are made, conclusions are drawn and future work is mentioned.

Copyright 2005 by PBMR

Chapter 2

Literature Study

There are a large number of international programs focussed on developing the first Generation III nuclear plants (which will precede the Next Generation Nuclear Plant). Consequently PBMR is faced with strong competition. A variety of PCU designs are being investigated by the international community and it is not straight-forward to assess which of these PCUs are most suitable for the NGNP. In this chatper, the literature survey is documented placing the problem of identifying a PCU in perspective.

2. LITERATURE STUDY

2.1 INTRODUCTION

There is a continuing increase in the demand for electrical power in most industrialized countries. The renewable energy sources for electricity constitute of solar, tidal, hydro, geothermal and biomass-based power generation. Except for hydropower in the few places where it is plentiful, none of the renewable energy sources are suitable for large-scale power generation where continuous, reliable supply is needed (WNA, 2002b). The world relies on fossil fuels to produce almost half of all base-load electricity production. Unfortunately carbon dioxide emissions from fossil fuels significantly contribute to global warming. The world needs an alternative energy source which will be sustainable, economically viable and which will minimize global pollution. Technological advances have made nuclear power safer, more efficient and less expensive than it has been in the past. On a global scale nuclear power is reducing carbon dioxide emissions by some 2.4 billion tons per year (WNA, 2002b). Nuclear holds the promise of sustainable and economically viable energy whilst minimizing global pollution. If the social, health and environmental costs of fossil fuels are also taken into account, nuclear seems to be the only solution to the world's energy needs. Humankind cannot conceivably achieve a global clean-energy revolution without a huge expansion of nuclear power – to generate electricity, to produce hydrogen for tomorrow's vehicles, and to desalinate seawater in response to the world's rapidly emerging fresh-water crisis.

The nuclear power industry has been developing and improving reactor technology for almost five decades and is preparing for the next generations of reactors. Several generations of reactors are commonly distinguished. Generation I reactors were developed during the 1950-60s and relatively few are still running today. Generation II reactors are typified by the present US fleet and most reactors in operation elsewhere. Generation III reactors are the advanced nuclear reactors, which include the LWR, HWR, HTGR and the FNR. The first are in operation in Japan (HTTR) and in China (HTR-10) and others are under development. Generation IV designs are still on the drawing board. About 85% of the world's nuclear electricity is generated by reactors derived from designs originally developed for naval use. These and other second-generation nuclear power units have been found to be safe and reliable, but they are being superseded by better designs. Reactor suppliers in North America, Russia, South Africa, China, Japan and Europe have a dozen new nuclear reactor designs in advanced stages of planning, while others are at a research and development stage. The greatest departure from current designs is that many new generation nuclear plants incorporate passive or inherent safety features which require no active controls or operational intervention to avoid accidents in the event of malfunction. Traditional reactor safety systems are 'active' in the sense that they involve electrical or mechanical operation on command (WNA, 2003a).

Substantial interest has been generated in advanced nuclear reactors over the last few years. This interest is motivated by the view that new nuclear power reactors will be needed to provide low carbon generation of electricity and possibly hydrogen to support the future growth in demand for both of these commodities. Some governments feel that substantially different reactor designs will be needed to satisfy the desires for public perception, improved safety, proliferation resistance, reduced waste and competitive economics. The high capital cost of large power reactors (generating electricity via the steam cycle) has motivated the movement to develop smaller units. The IAEA defines "small' as

under 300 MWe. These units may be built independently or as modules in a larger complex, with capacity added incrementally as required. These smaller units can also be used on remote sites. Generally, modern small reactors for power generation are expected to have greater simplicity of design, economy of mass production and reduced siting costs.

This interest in advanced nuclear reactors has motivated the creation of the Generation IV Nuclear Energy Systems program in which ten countries have agreed on a framework for international cooperation in research for advanced nuclear reactors. The Generation IV International Forum (GIF) is an international collective representing governments of countries where nuclear energy is significant and also seen as vital for the future. The members of the GIF are Argentina, Brazil, Canada, France, Japan, South Africa, South Korea, Switzerland, the UK and the USA. Six *Generation IV* reactor designs have been selected for continued evaluation with the objective of deployment by 2030. The six reactor designs are the Gas-cooled fast reactor, the Lead-cooled fast reactor, the Molten Salt reactor, the Sodium-cooled fast reactor, the Supercritical water-cooled reactor and the Very High Temperature Reactor (VHTR) (WNA, 2003b).

Along with the Sodium-cooled fast reactor (SFR), the VHTR is the nearest term possibility of the reference *Generation IV* reactor concepts. The VHTR is a graphite-moderated helium-cooled reactor which is based on substantial experience with the High Temperature Gas-cooled Reactor (HTGR). Technology developed in the last decade makes HTGRs more practical than it has been in the past (WNA, 2005a). The VHTR can potentially operate at very high core outlet temperatures (1000 °C +). The core can be built of prismatic blocks such as the *HTTR*-project (Japan) and the *GT-MHR*-project (USA and Russia), or it may be built of pebble fuel such as the *HTR-10*-project (China) and the *PBMR*-project (South Africa).

The Generation IV International Forum is committed to joint development of the Next Generation Nuclear Plant (NGNP) which will utilize a VHTR. If successful, the NGNP will be smaller, safer, more flexible and more cost–effective than any commercial nuclear plant in history. In 2004 the United States Department of Energy (US DOE) sought a partner to develop the NGNP as its leading concept for developing advanced power systems and selected the VHTR as the reactor concept to demonstrate the use of nuclear power for both electricity and hydrogen production. A pilot plant demonstrating technical feasibility is envisaged by 2020 at Idaho National Engineering and Environmental Laboratory (INEEL). The VHTR will enable direct gas turbine electricity generation, thermo-chemical hydrogen production via an intermediate heat exchanger or cogeneration (WNA, 2003b). Reactor modules of 600 MW thermal are envisaged (US DOE, 2004). The NGNP will secure a major role for nuclear energy for the long-term future and also provide a practical path toward replacing imported oil with domestically produced, clean and economic hydrogen (WNA, 2005b).

The NGNP objectives, as presented by the NGNP Program Manager for INEEL on 16 November 2004 (MacDonald, 2004a) are:

- To demonstrate a full-scale prototype NGNP that is commercially licensed by the US Nuclear Regulatory Commission and to
- Demonstrate safe and economical nuclear-assisted production of hydrogen and/or electricity.

The VHTR and NGNP research and development needs are structured in the following five specific R&D projects (US DOE, 2004):

- Design and Safety
- Fuel and Fuel Cycle
- Materials and Components
- Hydrogen Production Technologies
- **Power Conversion Unit (Balance of Plant)

This study was conducted for PBMR Pty. Ltd. in support of the NGNP initiative in order to identify the most practical, efficient and cost effective **PCU design for today's nuclear market. As mentioned, various cycle configurations for HTGR power conversion are currently under investigation. The choice of optimum PCU is a complex problem influenced by a large number of interdependent parameters such as component and material limitations, maintenance, risk, and cost. Because identifying the optimum PCU is such a complex and integrated problem it is difficult to assess the comparative cost and feasibility of each PCU during the concept phase. The NGNP-project is a large commercial project with very strong international competition. Cost data are not readily available and the NGNP-designs are still in concept-phase. It is therefore imperative that PBMR conduct its own comparative study of various PCUs in order to arrive at an optimum design for the NGNP.

Even though such a study does not exist in the open literature, the following information from literature serves as crucial background before this study can be undertaken:

- The NGNP will utilize a VHTR. The VHTR builds on the experience of several innovative HTGRs built in the 1960s and 1970s. It is important to understand the history of the HTGR in order to place the NGNP in context and also to learn from previous HTGR programs. Section 2.2 gives a brief overview of the advantages of the HTGR and section 2.3 gives an overview of the development of the HTGR nuclear plants.
- There are a large number of international programs focussed on developing the first *Generation III* nuclear plants which will precede the NGNP. Consequently PBMR is faced with strong competition. It is important to know what each of these parties are doing in order to better understand the market and competition and also to learn from our competitors. Section 2.4 gives an overview of the current international programs and discusses the basic designs of each of these *Generation III* programs.
- The PCU chosen should comply with the NGNP requirements. It is therefore important to understand the requirements as set out by the ITRG. Although these requirements are not fixed in stone, it is important to keep them in mind when choosing a PCU for the NGNP. Section 2.5 discusses the NGNP requirements as set out by the ITRG.

2.2 OVERVIEW OF THE HTGR

This section will provide a brief overview of the HTGR and will list the six ideas on which the HTGR are

based and mention some common characteristics to all HTGRs.

High Temperature Gas Reactors (HTGRs) are very different from light water (LWR) and heavy water (HWR) reactors. The HTGR is the latest development of the gas cooled reactors which started with the Magnox reactors and later on the Advanced Gas-cooled Reactors (AGR). The use of helium as coolant and the use of graphite as structural material allow much higher helium temperatures compared to the systems mentioned above. The higher helium temperatures result in higher cycle efficiencies. Helium is chemically inert and has a high heat capacity.

The fuel is also very different from today's well known pellets for the LWR. The HTGR uses coated fuel particles. Three layers of pyrolytic carbon, silicon carbon and again pyrolytic carbon protect the fuel itself. Around the fuel kernel there is a porous buffer layer. The coated particle was one of the main inventions in the development of the HTGR. These very small fuel particles are embedded in graphite. The HTGR allows high fuel temperatures under normal conditions (max. 1350 °C) and in accident conditions (max. 1600 °C) without the release of fission products. The coolant gas helium can be heated to very high temperatures (700 °C to 950 °C). The reactor core inlet temperature is somewhere between 250 °C and 550 °C dependent on the power conversion unit. The helium pressure is between 30 Bar and 90 Bar. The core power density is chosen between 3 and 6 MW/m^3 because of safety reasons. The limited power density will realise the principle of self-acting decay heat removal and will avoid overheating of fuel elements in severe accident conditions. All of today's HTGR designs propose a thermal power of modular reactors between 200 and 600 MW_{th}. Higher power can be realised by several parallel working modular reactors on a site.

Originally the HTGR-concept was based on six ideas, which are still important today (Kugeler *et al*, 2003):

- In order to prevent the unproductive capture of neutrons, there should be only fissile and fertile material inside the reactor core together with a very weak absorbing moderator.
- A gaseous coolant (Helium) should be used to avoid chemical reactions with the materials inside the core.
- An all-ceramic core should be used which could be operated at very high temperatures.
- High reactor outlet temperatures suitable for closed cycle gas turbine power conversion should be achieved.
- The fuel should be distributed as uniformly as possible in order to provide a larger heat transfer surface and achieve higher power density in the fuel.
- The good neutron economy should be used to exploit the U-235- , Th-232-, U-233- fuel cycle.

All of the above aspects are realised in modern designs of the modular HTGR. *All HTGR reactor concepts, whether one considers old or new designs, have some common characteristics independent of the form of the fuel elements* (Kugeler *et al*, 2003):

- The HTGR has full ceramic fuel elements which cannot melt, even in extreme accidents such as total loss of active cooling.

- The HTGR uses coated particle-fuel (TRISO) which retains the fission products very effectively inside the fuel and allows very high burn-up of fuel.
- The HTGR uses Helium as an effective and inert coolant medium.
- The HTGR has full ceramic (graphite) core structures which allow for high temperatures.
- The HTGR has a reactor core with a low power density which is very robust and which has a high heat capacity in order to make the reactor thermally inert in all operational and control procedures.
- The HTGR has a core design which can even tolerate loss of coolant and loss of all active decay heat removal. Self-acting decay heat removal is possible and fuel temperatures stay below admissible values. The core can never melt.
- The HTGR has a very strong negative temperature coefficient to contribute to the very good inherent safety characteristic of these reactors, even in hypothetical reactivity accidents.
- The very efficient retention of fission products in the coated particle fuel in normal operation allows relatively clean helium circuits and as a consequence allows the operation of plants with low contamination of cooling gas and low release of radioactivity and small radiation dose values to the operation staff.
- The very efficient retention of fission products in the coated particles in extreme accidents allows the design of a reactor without catastrophic release to the environment in severe accidents.

As a consequence of this safety behaviour of a well designed modular HTGR it will be possible to realise nuclear reactors which never can cause catastrophic damages outside the nuclear power plant.

2.3 HISTORY OF THE HTGR

This section discusses the development of the HTGR Prototype plants (*DRAGON, AVR, Peach Bottom)* and Demonstration plants (*Fort St. Vrain, THTR-300*) which have been built and operated. This section also discusses several HTGR plants which were planned and designed during the 1970s and 1980s. *Table 2.1* gives an overview of HTGR plants that have been built and operated and *Figure 2.10* presents the arrangement of the primary systems of the Prototype and Demonstration plants.

2.3.1 HTGRs built and operated - Prototype Plants

The initial HTGRs included the *DRAGON* reactor experiment, the Arbeitsgemeinshaft Versuchsreaktor (*AVR*) and *Peach Bottom*. Common among these plants were the utilization of steel vessels to contain the primary system and the attainment of high core outlet temperatures culminating in the *AVR* achieving extended operation at 950 °C (IAEA, 2001b). A lot of work has been done on different prototype plants and specifically on the development of fuel, materials and components related to the application for steam-turbine processes, gas-turbine processes and process heat applications (Kugeler *et al*, 2003). The *AVR* and *Peach Bottom* were designed to produce steam for a steam turbine process. The *DRAGON* reactor dumped the process heat into the environment via a heat exchanger.

2.3.1.1 DRAGON

The development of helium cooled HTGRs started in Great Britain with the *DRAGON* project as a common project of several European countries. In this reactor a tabular ceramic fuel element was used and coated particle fuel was inserted for the first time. The reactor has been operated successfully from 1966 to 1975 after which the project was cancelled due to political and financial reasons (Kugeler *et al*, 2003).

The helium (reactor outlet temperature of 750 °C) was circulated through primary heat exchangers and returned at 350 °C. The *DRAGON* did not generate electric power. The reactor demonstrated many components e.g. the helium circuit purification system, the control rod drives, the fuel handling equipment, the gas-bearing circulators and the reactor fuel. As a test bed, it provided much information on fuel and material irradiation tests and component tests under high-purity helium conditions (IAEA, 2001b).

2.3.1.2 Peach Bottom

At the same time the development of the HTGR with tabular type fuel elements had been initiated with the *Peach Bottom* reactors. The *Peach Bottom* was the first prototype HTGR in the US. The 40 MWe plant was built as part of the US Atomic Energy Commission (USAEC) Power Reactor Demonstration program and the High Temperature Reactor Development Associates (HTRDA) Program to demonstrate the feasibility of a high performance, helium cooled, nuclear power plant. The operation behaviour of this reactor from 1965 to 1988 was good. It was stopped as the *Fort St. Vrain* came into operation. Decommissioning was a planned economic decision, based on the additional costs associated with satisfying revised USAEC safety requirements (IAEA, 2001b).

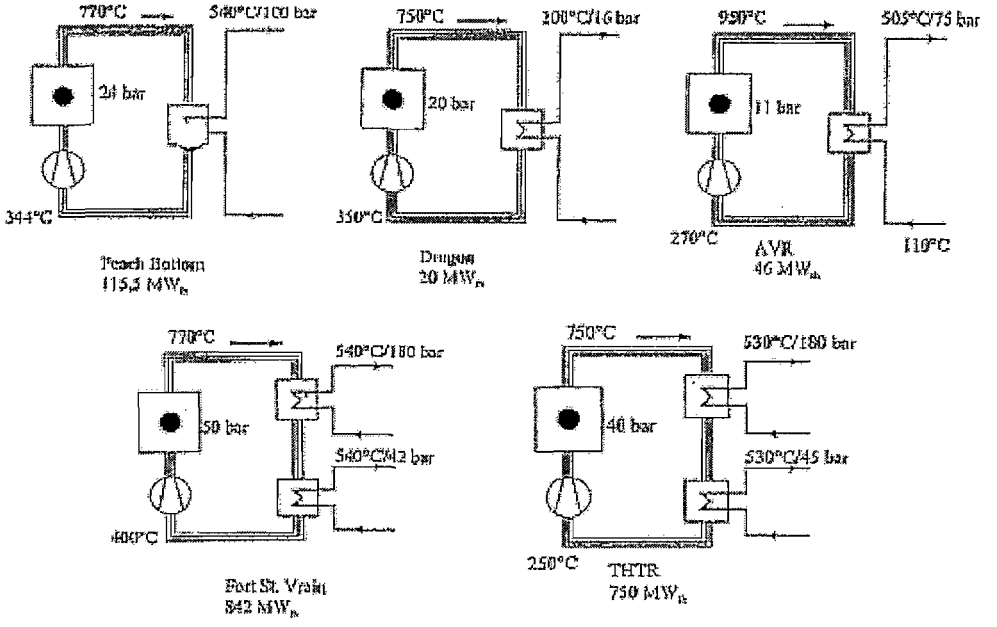


Figure 2.10 *Arrangement of primary systems for the Prototype and Demonstration Plants*

Peach Bottom made a major contribution to fuel technology, to the concept of block-type fuel and the technology of components for the HTGR (Kugeler *et al*, 2003). *Peach Bottom* provided a valuable

demonstration of the HTGR concept by confirming the core physics calculations, verifying the design analysis methods and providing a data base for further design activities. Design activities were conducted in the areas of the reactor core, mechanisms in high-temperature helium, helium purification systems and steam generator tube materials.

Throughout the operation of *Peach Bottom*, excellent agreement was found between the predicted and the actual plant design characteristics, verifying the methods used and providing a reference data base for application to larger HTGR plants. The overall plant control system functioned exceptionally well and the plant was operated in a load-following manner during the majority of its lifetime, demonstrating the ability of the HTGR to function in this manner (IAEA, 2001b).

2.3.1.3 AVR

In Germany the HTGR-technology started with pebble shaped fuel elements and the *AVR*-reactor (1965). The *AVR* was operated successfully for more than 20 years and showed that an HTGR with pebble type fuel is proven technology. This reactor was only three years on the grid. Despite all the difficulties during construction and start-up of this plant, the design data of the power plant were fully achieved and the availability of the plant was good. Operation was finished because the *THTR-300* was taken into operation and also because of financial and political reasons after the accident at Chernobyl (Kugeler *et al*, 2003).

In February 1974, the mean gas outlet temperature, which had initially been set at 850 °C, was increased to 950 °C. Operation of the *AVR* continued until December 1988. In completing 21 years of service, the plant had accumulated more than 122,000 hours of operation with a 66.4 % overall availability and had generated 1.67 billion kWhr of electricity. The core of the reactor consisted of a pebble bed containing 100,000 fuel spheres in a graphite reflector pot. The steam generator was located above the core and shielded against radiation from the core by a 50 cm thick top reflector made of graphite and two additional 50 cm thick layers of carbon bricks. The coolant was helium, pressurized to 10 Bar and circulated by two blowers located in the lower section of the reactor vessels. The helium was heated in the core from 270 °C to 950 °C after which it passed through the steam generator, where it transferred the energy to the water/steam circuit. The generated steam had a pressure of 73 Bar and a temperature of 505 °C. The core, steam generator and blowers were surrounded by two concentrically arranged reactor vessels. The inter-space between the vessels was filled with helium at a pressure slightly above the coolant gas pressure.

In addition to continuous component testing and the collection of operating experience and results, the plant was also used during its operating period for the implementation of several experiments. In particular, these included the testing of various types of fuel elements, investigations of fission product behaviour in the circuit, experiments on the chemistry of coolant gas impurities and the performance of several tests related to HTGR safety.

2.3.2 HTGRs built and operated - Demonstration Plants

The HTGR pants that followed the successful *AVR* and *Peach Bottom* included construction of the Thorium High Temperature Reactor *(THTR-300)* and the *Fort St. Vrain* (FSV). The power levels for

these two plants were significantly higher than the *AVR* and *Peach Bottom*. The *THTR-300* and *FSV* also changed over to pre-stressed concrete reactor vessels and the whole primary system was integrated into this vessel. These vessels are burst-safe, which means they can never fail like a forged steel vessel by bursting. Some further differences include aspects of core, of heat transfer systems and of important systems like the control and shut down system as well as fuel handling systems (Kugeler *et al*, 2003). Performance of the *THTR-300* and the *FSV* in validating reactor safety characteristics and the TRISO coated fuel particle was very good. However, *FSV* was beset with inconsistent operation and a corresponding low capacity factor throughout its life. The *THTR-300* was also plagued with problems primarily associated with changing regulatory requirements that contributed to delays that eventually ended up with a construction period of ~14 years. Financial concerns by the operating utilities led to the premature shutdown of both these plants in the 1988-1989 timeframe. These plants came on line at a time when the commercial industry was in decline, limiting the resources available to resolve issues associated with the commissioning and operation of new power plant designs.

2.3.2.1 THTR-300

The *THTR-300* power plant was sponsored by the Federal Republic of Germany and Nordhein Westfalen (NRW). Construction of this 300 MWe plant began in 1971, but (primarily due to the increasing licensing requirements) was not completed until 1984. This pebble bed reactor plant was connected to the electrical grid of the utility Hochtemperatur-Kernkraftwerk (HKG) in November 1985.

The *THTR-300* nuclear power plant included a steam cycle for the generation of electric power with a net output of 296 MWe. The heat generated in the reactor core was transported via the helium circuit (primary system) to the steam generators where it was transferred to the steam-feedwater circuit (secondary system) and then transported to the turbine generator. The secondary system was cooled by means of a 108 m high natural draught dry cooling tower. Operation of the *THTR-300* was successful in validating the safety characteristics and control response of the pebble bed reactor, primary system thermodynamics and the good fission product retention of the fuel elements. The plant operated over 16,000 hrs and generated 2.891 billion kWhr of electricity (IAEA, 2001b).

2.3.2.2 Fort St. Vrain

The *FSV* HTGR was operated by Public Service Company of Colorado as part of the United States atomic Energy Commission's Advanced Reactor Demonstration program. The *FSV* reactor used hexagonal, graphite block fuel in the form of ceramic coated (TRISO) particles. At its rated capacity, the *FSV* plant generated 852 MWth to achieve a net output of 334 MWe. The steam cycle was essentially conventional, utilizing a standard reheat turbine. The steam conditions were comparable to those of modern fossil plants. Once-through steam generator modules produced 538 °C superheated main and reheat steam.

Although ~5.5 billion kWhr of electricity was generated at *FSV*, the plant operated at low availability primarily because of excessive downtime due to problems with the water-lubricated bearings of the helium circulators. In spite of low availability, the plant was a valuable technology test-bed, successfully demonstrating the performance of several major systems, including the reactor core, reactor internals, steam generators, fuel handing and helium purification (IAEA, 2001b).

PLANT	Thermal Power	Fuel Element	Net Efficiency	Country / Site	Operation	Status	Purpose of Plant
DRAGON	20 MW_{th}	Tabular fuel	-	Winfrith / Great Brittain	1966-1975	Safe enclosure.	• Experimental reactor. • Demonstration of rod-type fuel.
Peach Bottom	115 MW_{th}	Tabular fuel	34 %	Susquehanna / USA	1965-1988	Safe enclosure.	• Experimental reactor. • Demonstration of rod-type fuel.
AVR	46 MW_{th}	Pebble fuel	33 %	Julich / Germany	1965-1988	Decommissioning in preparation.	• Experimental reactor. • Demonstration of pebble core.
THTR-300	750 MW_{th}	Pebble fuel	40 %	Schmehausen / Germany	1985-1988	Safe enclosure.	• Prototype. • Operation experience.
Fort St. Vrain	852 MW_{th}	Block fuel	39.2 %	Platteville / USA	1976-1989	Partly decommissioned.	• Prototype. • Operation experience.
PLANT	**Pressure vessel**	**Coolant pressure**	**Coolant heat up**	**Steam pressure**	**Steam temperature**	**Re-heat conditions**	**Arrangement of primary system**
DRAGON	Steel vessel	20 Bar	350 ---> 750 °C	16 Bar	200 °C	-	Loop design of core, steam generators and helium circulators.
Peach Bottom	Steel vessel	24 Bar	344 ---> 770 °C	100 Bar	540 °C	-	Loop design of core, steam generators and helium circulators.
AVR	Steel vessel (double)	11 Bar	270 ---> 950 °C	73 Bar	505 °C	-	Core, steam generator and helium circulations integrated in one vessel.
THTR-300	Pre-stressed concrete	40 Bar	250 ---> 750 °C	180 Bar	530 °C	42 Bar / 530 °C	Core, steam generator and helium circulations integrated in one vessel.
Fort St. Vrain	Pre-stressed concrete	49.2 Bar	400 ---> 770 °C	173 Bar	538 °C	45 Bar / 538 °C	Core, steam generator and helium circulations integrated in one vessel.

Table 2.1 *Overview of HTR plants which have been built and operated in the past (Kugeler et al, 2003)*

2.3.3 Planned HTGR concepts of the 1970s and 1980s

The primary focus of international HTGR designers in the 1970s and early 1980s was associated with the development of large HTGR units. The interest in development of larger steam cycle HTGR plants included the German *PR-500, HHT, PNP-Prototype, HTR-500, HTR-MODUL* and the *HTR-100*; the Russian *VGM-400* and the American *HTGR-SC, HTGR-GT* and *MHTGR*. *Table 2.2* gives an overview of plants that had been planned in the 1970s and 1980s. These plants had a very high effort of man power and money. The results of this development work are still available and can be used for the new projects on HTGRs.

The *PR-500* realised the principle of self-acting decay heat removal. This reactor concept was worked out for co-generation applications, especially the delivery of process steam for industry. The containment for the reactor was proposed to be filled with N_2 to prevent burn up of Carbon by air. Furthermore there was the proposal to arrange the containment under ground with a hill above it to give safety against airplane crashes and terrorist attacks.

For the *HHT-project* a gas turbine cycle was planned and a broad program on research of relevant components and materials for the HTGR application has been worked out. In this project several reactor designs (block versus pebble) have been investigated.

The *PNP-Project* (Prototype Nuclear Process Heat) developed and tested new heat exchanger components and high temperature materials. The main process applications in this project were steam reforming of methane or light hydrocarbons and coal gasification.

The *HTR-500-project* made considerable use of the technology development for the *THTR-300*, with simplifications and optimizations based on practical experiences with the *THTR-300*. This plant features a simple design with the primary system components located within a single cavity PCRV and included a pebble bed reactor power level of 1200 MWth.

The *HTR-MODUL* and the *HTR-100* have been designed on the basis of *AVR* technology. The *HTR-MODUL* had nearly passed the licensing procedure, but it was stopped due to political reasons in Germany. In this reactor system the 1600 °C concept for the fuel under conditions of severe accidents was introduced.

The 80 MWe *HTR-MODUL* concept was develop by Siemens/Interatom. It was the first small, modular type HTGR concept to be proposed. The safety features of the *HTR-MODUL* were based on the design condition that, even in the case of failure of all active cooling systems and complete loss of coolant, the fuel element temperatures would remain within limits such that there is virtually no realise of radioactive fission products from the fuel elements.

Brown, Boveri and Cie and Hochtemperatur-Reacktorbau initiated the design of the *HTR-100* pebble

bed plant. The design featured a net electric output of 100 MWe. The *HTR-100* was based on the *AVR* concept and utilised the advanced technologies of the *THTR-300* components and systems. The primary system included the reactor, steam generator and helium circulator in a single, vertical steel pressure vessel. The basic design for this plant incorporated two *HTR-100* units with overall capability of producing 170 to 500 t/hr of industrial steam at 270 °C and 16 bar, with 100 – 175 gross output.

The Russian HTGR development program included the VG series of plants primarily developed at OKBM in Nizhny Novgorod. Of these, the *VGM-400* design incorporated a pebble bed reactor with a final power level of 1060 MWth for the co-generation applications of electricity production and had an intended final helium core outlet temperature design of 950 °C (IAEA, 2001c). During the pre-liminary phase of the design development the pebble bed and prismatic fuel block variants of the core were analyzed. As a result of the design and engineering analysis, the pebble bed core was chosen for further development. Also considered was a gas turbine cycle reactor plant.

In the USA the focus in the early 1970s was on *HTGR-SC* (steam cycle) designs of 770 to 1160 MWe. Contracts to General Atomics from US utilities included 10 plants that did not materialize due to the 1973 oil crisis and corresponding economic setback and the collapse of the US nuclear power market of 1975. These plants incorporated cores of hexagonal graphite blocks with TRISO coated fuel particles similar to *FSV* (IAEA, 2001c).

One of the early gas turbine designs was the *HTGR-GT* by General Atomics. This plant was projected to have the potential for high plant efficiencies (40%) under dry cooling conditions and even higher efficiencies (50%) when bottoming cycles were incorporated. An assessment of this plant was conducted ~1980 with a core outlet temperature of 850 °C. The principal findings of the assessment were 1) that the *HTGR-GT* is feasible, but with significantly greater development risk that was associated with the *HTGR-SC*; 2) at the level of performance corresponding to the reference design, no incremental economic incentive can be identified for the *HTGR-GT* to offset the increased development costs and risk relative to those for the *HTGR-SC*; 3) the relative economics of the *HTGR-GT* and *HTGR-SC* are not significantly affected by dry cooling considerations; and 4) although the reduced complexity of the cycle may ultimately result in a reliability advantage for the *HTGR-GT*, the value of that potential advantage could not be quantified. Although these findings did not provide the basis for the *HTGR-GT* as the preferred lead commercial plant (for General Atomics), the *HTGR-GT* continued to engender interest from participating utilities.

Following a detailed evaluation in the spring and summer of 1985, a side-by-side concept similar in configuration to the German *HTR-MODUL* design was chosen as the reference concept for further design and development by the US program. This module was designed to deliver superheated steam at 17.3 MPa and 538 °C. The power was 450 MWth. For a standard steam cycle *MHTGR* plant, the steam output from each of four modules was connected to an individual turbine generator. The four module plant consists of two separate areas, the nuclear island and the power conversion unit.

These programs of the 1970s and 1980s today still provide valuable information for current HTGR programs.

PLANT	Thermal Power	Fuel Element	Core outlet temperature	Country / Site	Planning	Status	Type and purpose of Plant
PR-500	500 MW	Pebble fuel	-	Germany	1968-1973	Conceptual design	Steam generator + steam cycle (process steam extraction)
HHT	1200 MW	Pebble fuel	-	Germany	1970-1980	Basic engineering	Gas turbine cycle
PNP-Prototype	500 MW	Pebble fuel	-	Germany	1975-1985	Basic engineering	Steam reformer + intermediate heat exchanger
HTR-500	1200 MW	Pebble fuel	700 °C	Germany	1980-1988	Basic engineering	Steam generator + steam cycle
HTR-MODUL	200 MW	Pebble fuel	700 °C	Germany	Early 1980s	Nearly licensed	Steam generator (steam cycle + process heat)
HTR-100	250 MW	Pebble fuel	740 °C	Germany	-	Basic engineering	Steam generator (steam cycle + process heat)
VGM-400	1060 MW	Pebble fuel	950 °C	Russia	-	Conceptual design	• Co-generation plant • Gas turbine plant
HTGR-SC	1160 MW	Block fuel	-	USA	Early 1970s	Conceptual design	Steam cycle
HTGR-GT	2000 MW	Block fuel	850 °C	USA	~ 1980	Conceptual design	Gas turbine cycle
MHTGR	450 MW	Block fuel	686 °C	USA	~1985	Conceptual design	Steam plant

Table 2.2 *Overview of HTR plants which have been planned in the past (1970s and 1980s)*

2.4 CURRENT INTERNATIONAL HTGR PROGRAMS

It has long been recognized that substantial gains in the generation of electricity from nuclear fission can be achieved through the direct coupling of a gas turbine to a HTGR. This advanced nuclear power plant is unique in its use of the Brayton cycle to obtain a net electrical efficiency approaching 50%. This plant provides a promising alternative for the utilization of nuclear energy to produce electricity. Although evaluation of this concept was initiated over twenty years ago, it was terminated due to the technical risks primarily in the components areas of magnetic bearings, compact plate-fin heat exchangers and turbo machinery development. Subsequent technological advancements in the design and operation of these components, coupled with the international capability for their fabrication and testing have resulted in renewed interest in the Brayton cycle HTGR concept.

In order to be competitive, the thermal efficiency of nuclear power had to be markedly improved to compete with modern, high efficiency fossil plants. HTGR technology has always held the promise for electricity generation at high thermal efficiency by means of a direct Brayton cycle and fortuitously, technological developments during the past decade provided the key elements to realize this promise. These key elements are as follows (IAEA, 2001b):

- The HTGR reactor size had been reduced in developing the passively safe module design. At the same time, the size of industrial gas turbines had increased. The technology was now available for a single turbo-machine to accommodate the heat energy from a single HTGR module.
- Highly effective compact recuperators had been developed. Recuperator size and capital equipment costs are key economic considerations. Highly effective plate-fin recuperators are much smaller than equivalent tube-and-shell heat exchangers, and also less complex and less expensive. The recuperator is a key requirement for achieving high plant cycle efficiency.
- The technology for large magnetic bearings had been developed. The use of oil lubricated bearings for the turbo-machine with the reactor coolant directly driving the turbine was problematic with regard to the potential coolant contamination by the oil. The availability of magnetic bearings eliminates this potential problem.

The gas turbine modular HTGR has the potential for significant gains in plant efficiency and also for lowering capital and operating costs due to the plant simplification. The possibilities presented by the gas turbine modular HTGR have brought about an increasing interest by international research organisations and plant developers.

It was the development of the HTGR steam plants (previous section) that provided the key emphasis to initiation of the HTGR coupled to a gas turbine power conversion unit. With few exceptions, it is the German *HTR-MODUL* and the *HTR-100* reactor designs that are being utilized by the South African *PBMR*. The United States' *MHTGR* forms the basis for the *GT-MHR* project (IAEA, 2001c). *Table 2.3* gives an overview of the current international programs together with certain of their design parameters.

PLANT	Cycle	REF.	Country / Site	Thermal power	Fuel Element	Thermal Efficiency	Core outlet temperature	Coolant pressure	Status	Type and purpose of Plant
PBMR	B	[21]	South Africa	400 MW	Pebble fuel	45 %	900 °C	90 Bar	Basic design	• Direct gas turbine cycle • Inter-cooled, recuperative Brayton cycle. Horizontal shaft.
GT-MHR	B	[15]	General Atomics Russia	600 MW	Block fuel	48 %	850 °C	71 Bar	Preliminary design	• Direct gas turbine cycle. • Inter-cooled, recuperative Brayton cycle. Vertical shaft.
HTR-10	-	[16]	China	10 MW	Pebble fuel	-	950 °C	30 Bar	In operation since 2002	• Steam generator with helium circulator • Interim heat exchanger
HTR-10 GT	B	[45]	China	10 MW	Pebble fuel	22 %	750 °C	16 Bar	Basic design	• Direct gas turbine cycle. • Inter-cooled, recuperative Brayton cycle. Vertical shaft.
HTTR	-	[7]	Japan	30 MW	Block fuel	-	950 °C	40 Bar	In operation since 1998	• Intermediate heat exchanger • Pressurized water coolers
GTHTR300	A	[44]	Japan	600 MW	Block fuel	46.7 %	850 °C	70 Bar	Basic design	• Gas turbine cycle (non inter-cooled Brayton cycle)
ANTARES	I	[4]	Framatome ANP	600 MW	Block fuel	53 %	1000 °C	50 Bar	Conceptual design	• Indirect Combined Cycle
MPBR	E	[14]	MIT (USA)	250 MW	Pebble fuel	48 %	900 °C	80 Bar	Conceptual design	• Three-shaft twice inter-cooled recuperative indirect Brayton cycle.
ACACIA	-	[34]	The Netherlands	60 MW	Pebble fuel	70% (Co-gen) 38% (Combined Cycle)	900 °C	?	Conceptual design	• Combined Cycle AND/OR • Cogeneration

Table 2.3 *Overview of HTR plants which have been planned in the past (1970s and 1980s)*

2.4.1 South Africa

The Pebble Bed Modular Reactor (PBMR) is being developed in South Africa through a world wide international collaborative effort led by ESKOM, the national utility. The project to construct the *PBMR* Demonstration Plant on the Koeberg site near Cape Town has now been approved with a planned fuel load date of April 2010. The South African Government has announced the intention to include some 4000 MW to 5000MW of *PBMR* plants in the new construction program. The design of the *PBMR* turbine plant has been revised following a review of the availability of dry gas seals (that allow conventional oil bearings) and compact, high performance gearboxes. Both these technologies were not commercially available when the original three-shaft PCU was laid out. With their availability the revised layout now is a horizontal, single shaft design (TWG-GCR, 2005).

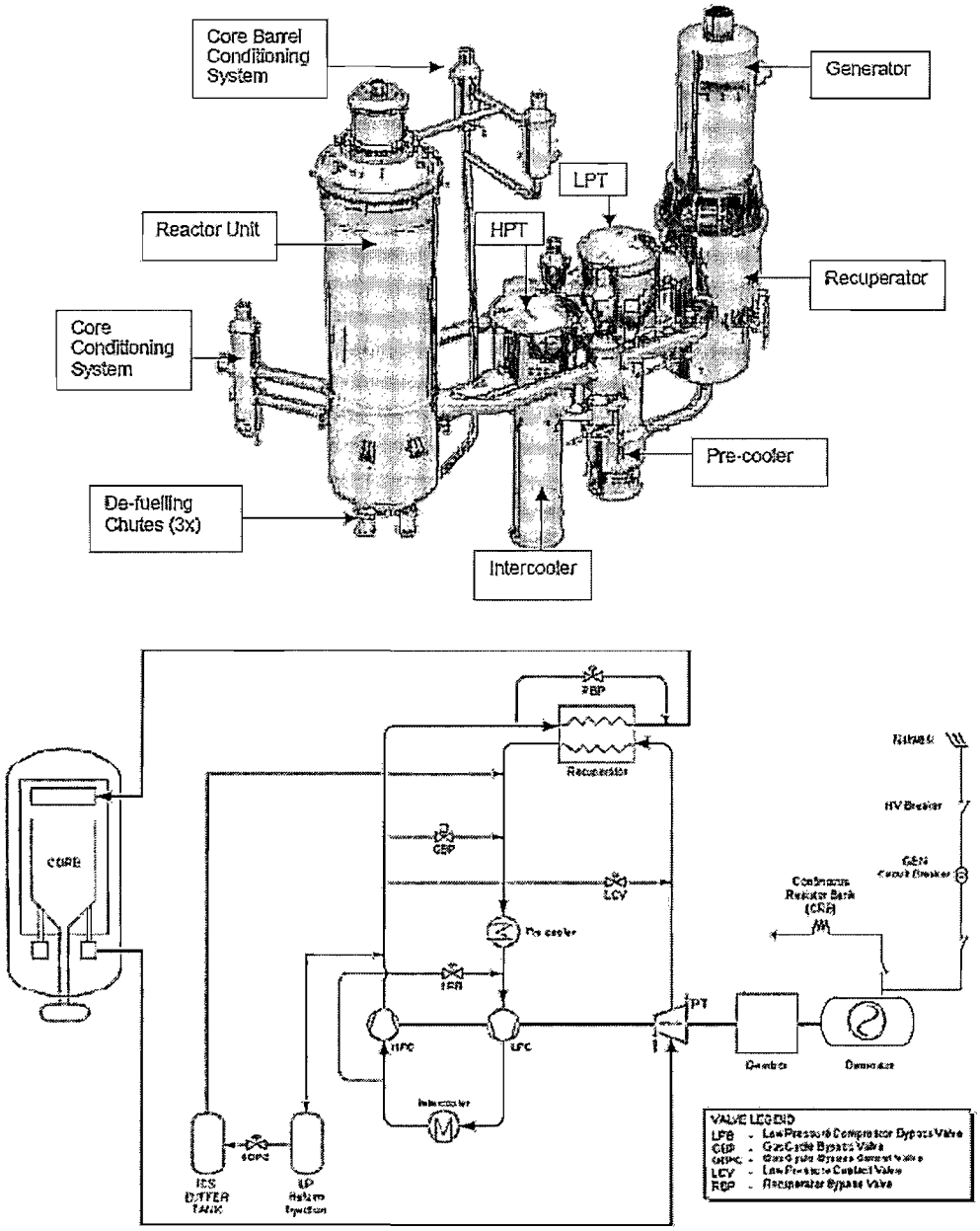


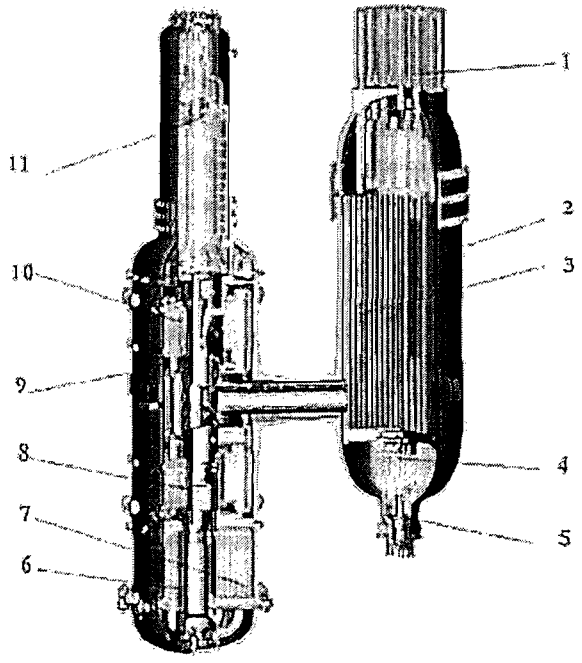
Figure 2.11 *Schematic diagram of the PBMR PCU (Matzner, 2004)*

PBMR has chosen a horizontal single-shaft, inter-cooled recuperative direct Brayton cycle as baseline design (Matzner, 2004). The compressors and turbine run an 6000 rpm with a 2:1 gearbox allowing a generator speed of 3000 rpm (TWG-GCR, 2005). See *Figure 2.11* for the schematic diagram of PBMR.

2.4.2 USA

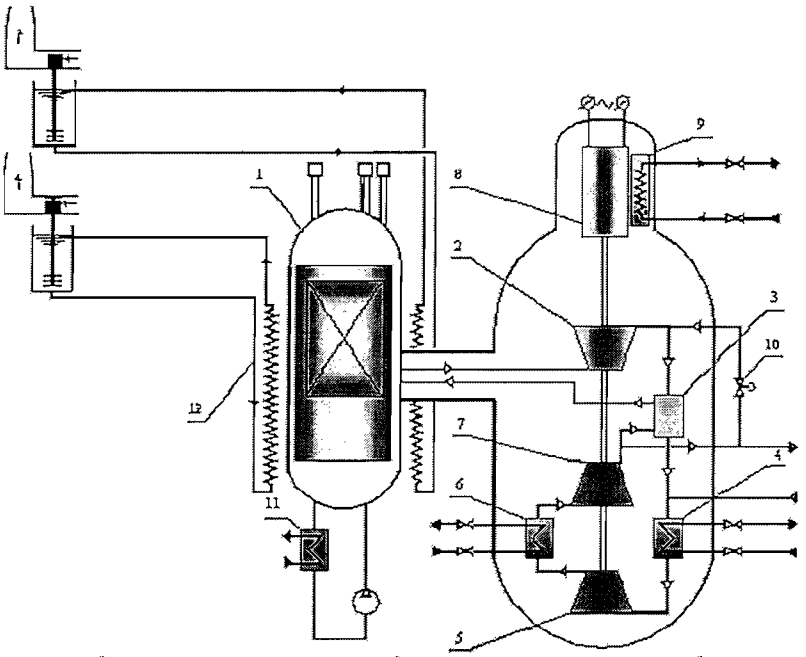
The US HTGR program is currently focused on fuel design, fabrication and qualification. Termed the Advanced Gas Reactor (AGR) program, it consists of eight stages including a shakedown of the reference German design, test fuel fabrication, characterization, irradiation and testing, as well as fuel performance and fission product transport modelling. Participants include INEEL, ORNL and BWXT. INEEL is in charge of the design and irradiation setup at the ATR reactor. BWXT is in charge of kernel manufacturing and ORNL of coating and characterization (TWG-GCR, 2005).

The *GT-MHR* is a vertical single-shaft, inter-cooled recuperative direct Brayton cycle under development by a joint effort by the USA and Russia. This Russian-America project aims to build a demonstration plant with a reactor power of 600 MW and reactor outlet temperature of 850 °C. Currently the GTMHR design is developed for surplus weapons plutonium disposition. For commercial use the 600 MWth power will use low enriched uranium fuel (14%) (Kostin et al, 2004). The generator speed is 3000 rpm. See *Figure 2.12* and *Figure 2.13* for the schematic diagram of the GT-MHR.



1 – control rod drive mechanisms / refueling channels; 2 – reactor vessel; 3 – annular zone of reactor; 4,5 – heat exchanger and gas blower of reactor shutdown cooling system; 6,7 – end and intermediate heat exchanger; 8 – compressor; 9 – turbine; 10 – recuperator; 11 – generator.

Figure 2.12 *Schematic diagram of the GT-MHR (Kostin et al, 2004)*



1–reactor; 2–turbine; 3–recuperator 4 - precooler; 5 - compressor; 6 - intercooler; 7 – compressor; 8 – generator; 9 – generator cooler; 10 – valve of turbine control and protection system; 11 –SCS auxiliary heat exchanger; 12 – SCS heat exchanger.

Figure 2.13 *Schematic diagram of the GT-MHR (Kostin et al, 2004)*

2.4.3 China

HTR-10

China started the construction of a 10 MW-HTR in 1995 and the reactor has begun operation in the year 2002. The technology of this reactor is based on the *AVR* experience. The *HTR-10* reached full power in 2003. In all, six safety demonstration tests were carried out. The results showed that the *HTR-10* has inherent safety features and computer codes for the design of the *HTR-10* were validated. (TWG-GCR, 2005).

The *HTR-10* is the first reactor worldwide which has inherent safety features. The power conversion system of the *HTR-10* is a steam turbine generator system. The reactor is in one pressure vessel and is connected by a horizontal hot gas duct to the steam generator. The steam generator and helium circulator are in another pressure vessel. Based on the success of the *HTR-10* project a new project called *HTR-10 GT* (the gas turbine power conversion system) has been launched recently (Jie et al, 2004).

HTR-10 GT

For the *HTR-10 GT* the gas turbine direct cycle is utilized instead of the steam generator. The Institute of Nuclear and New Energy Technology (INET) of China and the Experimental Design Bureau of Mechanical Engineering (OKBM) of Russia jointly completed the conceptual design of the power conversion unit in 2002. The basic design was completed in 2003. The main components are under manufacture and are scheduled for operation in 2006 (TWG-GCR, 2005).

The power conversion unit (PCU) will be inserted into the original *HTR-10* steam generator pressure vessel. The PCU configuration includes a pressure vessel, turbine, high-pressure compressor, low-pressure compressor, recuperator, pre-cooler, inter-cooler and generator. The gas turbine direct cycle is expected to have higher efficiency and better performance theoretically. The single-shaft arrangement is selected and the helium turbine and the electric generator have identical speeds which are designed for 15000 r/min. The rotors are supported by active magnetic bearings to avoid the contamination from any lubricant. The recuperator is vertical with a plate-fin heat exchange surface. The reactor core outlet temperature is 750 °C and the reactor inlet temperature is 330 °C (Jie et al, 2004) and (Zhiyong et al, 2004). See *Figure 2.14* and *Figure 2.15* for the schematic diagram of the *HTR-10* and *HTR-10 GT*.

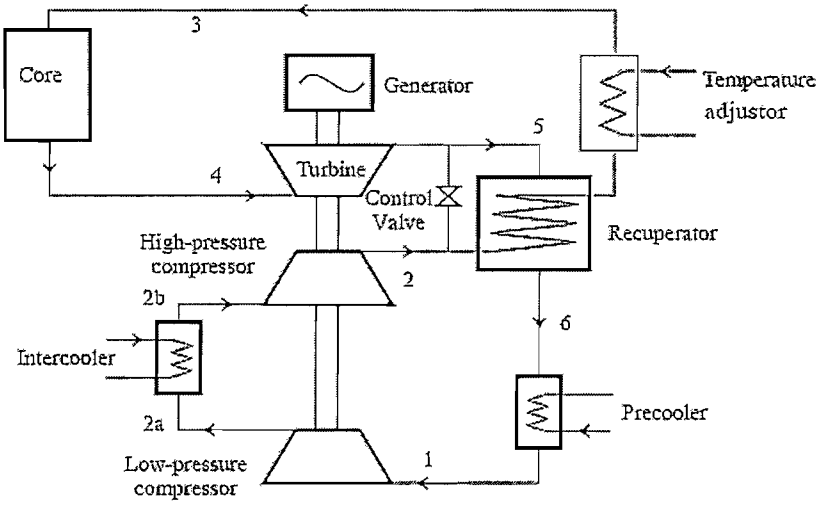


Figure 2.14 *Schematic diagram of the HTR-10 GT PCU (Jie et al, 2004)*

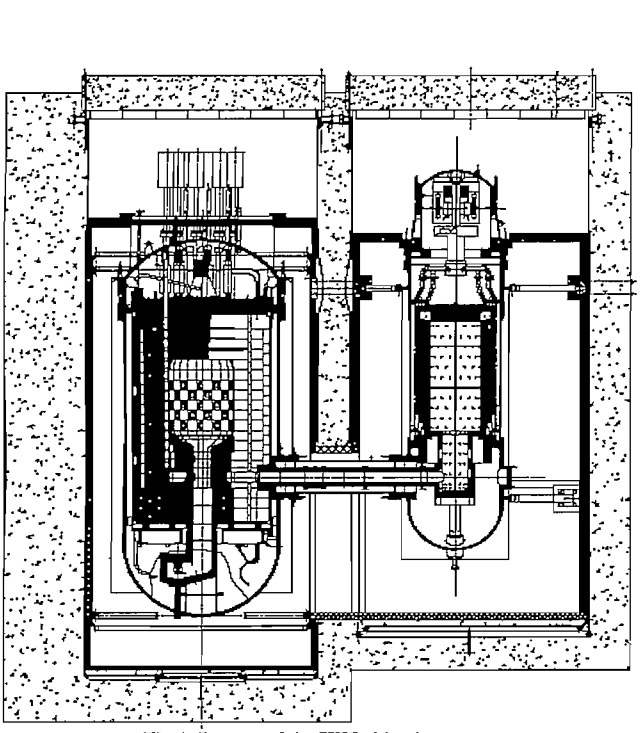


Fig.1. Layout of the HTR-10 primary system

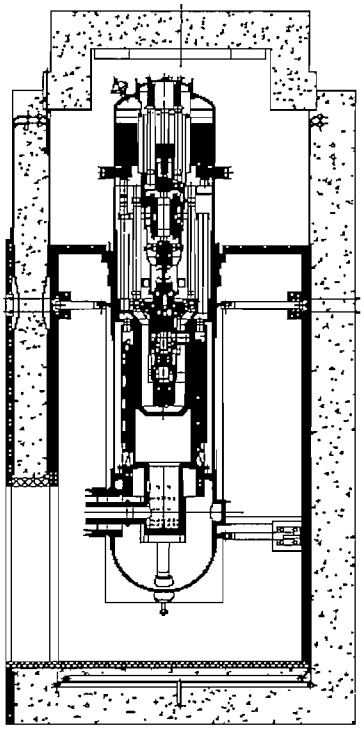


Fig.2. Layout of the power conversion system of the HTR-10GT

Figure 2.15 *Schematic diagram of the HTR-10 and HTR-10 GT (Jie et al, 2004)*

HTR-PM

A demonstration plant of the pebble bed modular reactor (*PBMR*) is being proposed by three parties, namely China Huanneng Group, China Nuclear Engineering and Construction Corporation and Tsinghua University. The parties signed the investment agreement to build the *HTR-PM* on 16th of December 2004. The project proposal will soon be submitted to authorities for approval. The location of the *HTR-PM* will be decided following the completion of the pre-feasibility study. Start of construction is foreseen for 2007 and first criticality may be reached by 2010 (TWG-GCR, 2005).

2.4.4 Japan

In Japan, the Japan Atomic Energy Research Institute (JAERI) has carried out the research and development of HTGRs since 1960. JAERI has three major HTGR development programs namely 1) Hydrogen production, 2) reactor technology development and advanced design and 3) gas turbine technology development.

HTTR

The High Temperature Engineering Test Reactor (*HTTR*) is the first HTGR in Japan with 30 MWth and a reactor outlet temperature of 950 °C. This is the highest outlet coolant temperature in the world (Fujimoto, 2004). The construction of the *HTTR* started in 1991. The *HTTR* reached full power in December 2000 (Sawa & Ueta, 2004). The reactor core consists of an array of hexagonal graphite fuel assemblies. The core is supported by a graphite support structure. The reactor cooling system is composed of a single main cooling system, an auxiliary cooling system and a vessel cooling system. The main cooling system is operated in normal operation to remove heat from the core and is sent to the environment via an intermediate heat exchanger (IHX) of 10 MW and a primary pressurized water cooler of 20 MW in parallel (called parallel loaded operation) or via only the pressurized water cooler of 30 MW (called single loaded operation).

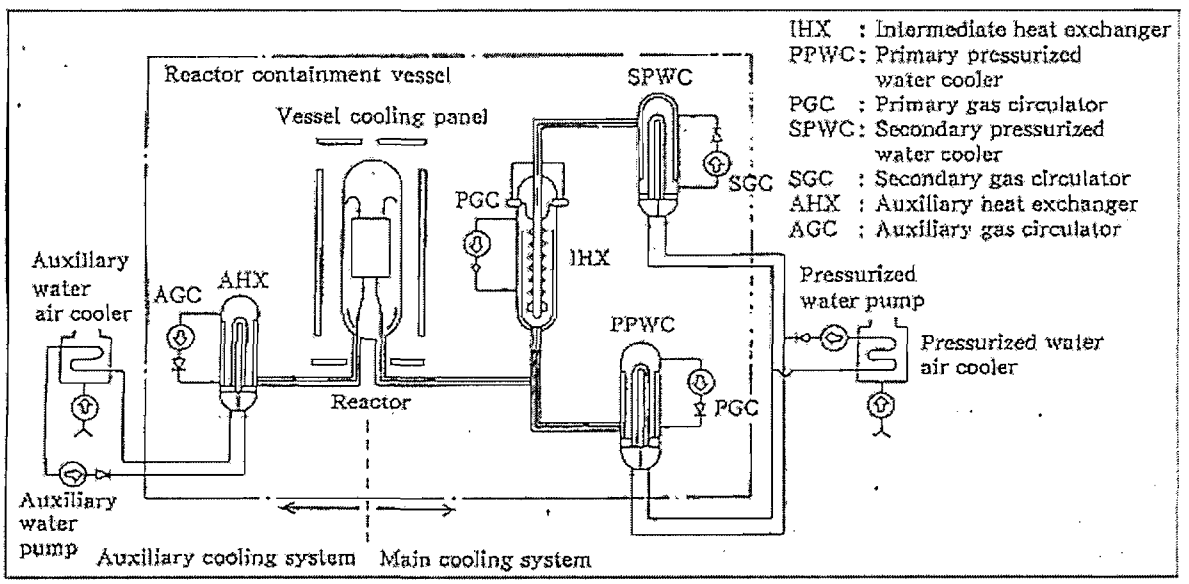


Figure 2.16 *Cooling system of HTTR (Kunitomi et al, 2004).*

GTHTR300

JAERI has undertaken the feasibility study on various types of HTGR power conversion units. Since 2001, the basic design of Japan's original gas turbine high temperature reactor (*GTHTR300*) has been conducted. The *GTHTR300* is expected to be deployed in the 2010 as a safe and economically competitive electric generation system in Japan (Kunitomi et al, 2004).

The *GTHTR300* is a horizontal single-shaft, non inter-cooled recuperative direct Brayton cycle. According to (Yan et al, 2003) the inter-cooled cycle is ruled out because it results in substantial complexities in turbo machine and system design, but provides no compelling advantage in plant economy. The helium gas turbine in the non inter-cooled cycle exhibits superior aerodynamic efficiency by a fewer number of stages and its rotor is lighter, shorter and more rigid, resulting in more robust rotor dynamics.

2.4.5 MIT

The modular pebble bed reactor (MPBR) project at Massachusetts Institute of Technology (MIT) was initiated in 1998 as part of an effort to re-invigorate thinking about how to improve the overall safety of nuclear plants, making the plants less complex and more competitive with fossil fuel plants. Numerous studies, designs, experiments and analyses have been conducted leading to a conceptual design that addressed some of the fundamental issues regarding new nuclear plants (Kadak & Ballinger, 2004). The MPBR consists of an indirect, three-shaft twice inter-cooled recuperative Brayton cycle.

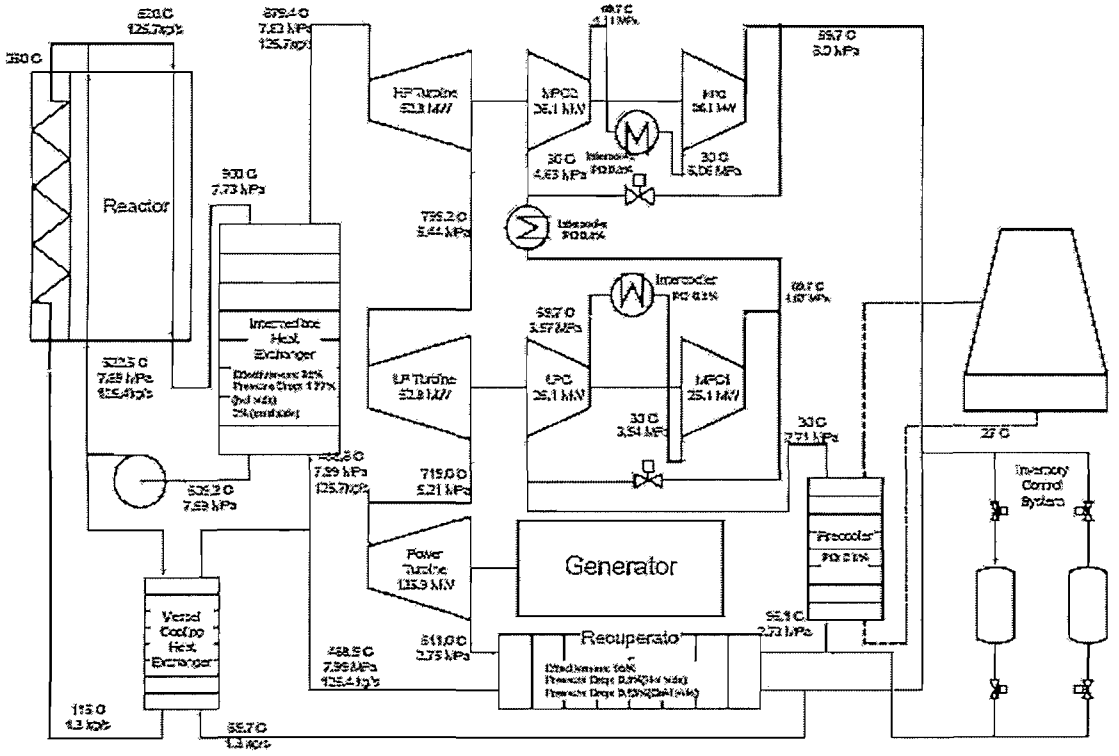


Figure 2.17 *Schematic of MPBR (Wang et al, 2002)*

2.4.6 European Union (EU)

Under the 5th framework program (FP5, 1998-2002), 10 HTR projects have been co-funded by the European Commission (EC). These projects have dealt with fuel technology, components, core physics, fuel cycle, materials, licensing and educational training. Under the 6th framework program (FP6, 2002-2006) an ambitious integrated VHTR project with a consortium of 35 partners worldwide is due to start in 2005 for a period of 48 months. With a total budget of 20 Million Euros the project will cover reactor physics, safety fuel, technology, fuel cycles, materials components and the VHTR plants design (TWG-GCR, 2005). About twenty organisations from industry, research and higher education in Europe (e.g. BNFL, CEA, Cogema, EDF, Framatome ANP, Forschungszentrum Julich (FZJ), NRG etc.) and the Joint Research Centre (JRC) of the European Commission joined forces and created the (European) HTR Technology Network (HTR-TN) in 2000. The objectives are to create the technological basis for an industrial deployment of modern modular HTRs in Europe by the next decade and to prepare longer term evolution of HTRs. The European programme will be covering most of the areas that have to be addressed by R&D for the development of modern modular HTGRs. It is organising the European effort in a consistent way, avoiding overlapping and redundancies (Hittner, 2004).

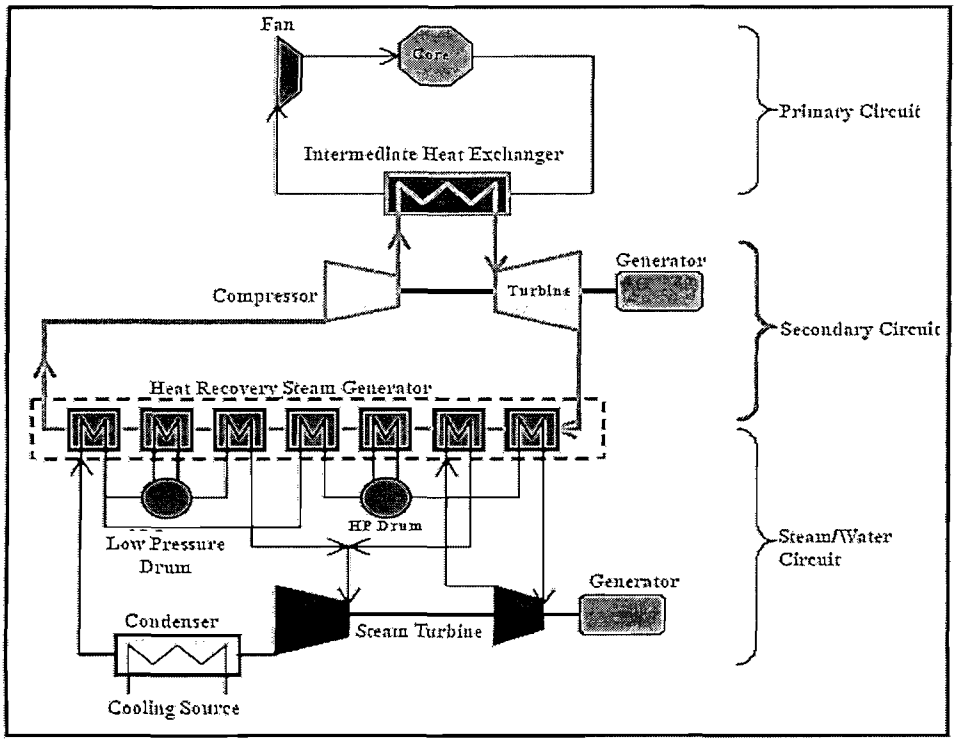


Figure 2.18 Schematic of Framatome's Combined Cycle with two levels of pressure and reheat (Copsey et al, 2004)

Framatome ANP is developing a VHTR design, relying on its previous experience with high temperature reactor designs, from its participation in the *GT-MHR* design. The Framatome ANP VHTR design is based on an indirect cycle coupled to an "off-the-shelf" Combined Cycle gas turbine. Although direct cycle HTGRs are being promoted for their high efficiency, preliminary evaluations showed that the Framatome ANP design efficiency is on par with a direct cycle while avoiding PCU developments and keeping the PCU contamination free. This concept was independently evaluated with sensitivity analysis by EDF. Moreover, the nuclear heat source of the indirect cycle could also be

used to qualify the direct cycle components without risk of contamination behind the IHX, thus assisting in the preparation for the later introduction of that technology. The PCU will rely to the maximum extent on available technology (Copsey et al, 2004)

2.4.7 The Netherlands

Most of the HTGRs activities are framed in the European Union (EU) RTD policies and international collaborations with EU co-funding. The Netherlands R&D activities concentrate on VHTR core physics, safety technology, components technology, materials and fuels as well as GFR core physics. New activities are on nuclear hydrogen technologies and system studies for HTGR applications in the energy market (TWG-GCR, 2005).

Sunergy, the largest private investor in photovoltaic energy in The Netherlands, has started an initiative with the aim of series production of a modular pebble bed reactor on a relatively short term. The markets aimed for will be both industrial and industrialising, and the unit power level will be around 80 MWe. Sunergy's approach to the market is a mix of solar and nuclear energy: nuclear electricity will be used in the production process of photovoltaic cells, in this way decreasing the solar energy cost. As the production of solar cells will not match electricity demand in the future, this gap between supply and demand of clean electricity will also be a market for the selected pebble bed reactor (Van Heek et al, 2004).

A 60 MWth pebble bed reactor with an indirect Brayton cycle is proposed for the applications of heat and power cogeneration or distributed electricity generation. The reactor will be cooled by helium, whereas for the secondary cycle nitrogen is proposed as a heat carrier. Economic performance is being optimized by simplification of the nuclear part and by the exclusive use of commercially proven systems in the energy conversion part (Cruz et al, 2002).

2.4.8 Russia

The main field of HTGRs activity in Russia is the joint US/Russia *GT-MHR* design.

2.4.9 Germany

The German government has decided to phase out of nuclear energy. This implies to keep competence especially on safety and waste issues for the safe operation of existing plants and management of wastes. Gas-cooled reactor activities mainly comprise of the decommissioning of the *AVR*, code validation for safety analysis and management of spent HTR fuel. Most R&D on HTGRs is embedded into the EURATOM-Framework program (TWG-GCR, 2005).

2.4.10 Indonesia

Nuclear Energy in Indonesia is considered as a part of the Energy Mix policy in order to realize security of the energy supply and long-term sustainable development. Based on results of the energy planning study done together with ISAS, a medium-large Nuclear Power Plant (NPP) could be accommodated in the Java-Bali electricity grid around 2016. Smaller units could be installed on the other islands, after 2020. The small NPPs could be operated as cogenerations systems in order to provide process heat for other purposes, such as desalination and oil recovery. In this regard, a HTGR could be selected as a potential NPP (TWG-GCR, 2005).

2.4.11 Korea

The KAERI VHTR program, i.e., Nuclear Hydrogen Development and Demonstration (NHDD) project was introduced focusing on the R&D on fuel, materials and nuclear graphite after a brief review (TWG-GCR, 2005).

2.4.12 France

The French program on Gas Cooled Reactors (GCRs) is focussed on the VHTR and the Gas-cooled fast reactor (GFR). The VHTR program focuses on developing technology in order to be able to propose a commercial plant up to 2017. The major technology developments include TRISO fuel particle fabrication, tests on specific materials are planned, graphite characterization, helium test benches, a 1MW helium technological loop, a waste management strategy and development of the Sulfur Iodine process to produce Hydrogen using a nuclear reactor (TWG-GCR, 2005).

2.4.13 Nuclear Energy Agency (NEA)

The NEA is an international organization, part of the OECD in Paris. Seven technical committees cover nuclear energy aspects, under the aegis of the Steering Committee for Nuclear Energy (28 member countries). Two working parties of the Nuclear Science committee are involved in reactor studies and fuel cycle studies, including activities for advanced HTGRs. In parallel to these projects, NEA holds the technical secretariat for the Generation IV International Forum (GIF).

2.4.14 International Atomic Energy Agency (IAEA)

The IAEA HTGR activities continue to focus on coordinated research projects (CRPs), information exchange and educational training. Current CRPs include benchmarking codes used in HTGR core physics and thermal-hydraulics. With the participation of 10 international institutes, the CRP has made use of data from *HTR-10*, *HTTR*, ASTRA and the *PBMR* micro model, in addition to *PBMR* and *GT-MHR* calculations.

2.5 NGNP REQUIREMENTS

The basic technology for the NGNP has been established in the former HTGR test and demonstration plants (*DRAGON*, *Peach Bottom*, *AVR*, *Fort St. Vrain*, and THTR). In addition, the technologies for the NGNP are being advanced in the *GT-MHR* Project and *PBMR* project. Furthermore, the Japanese *HTTR* and Chinese *HTR-10* test reactors are demonstrating the feasibility of some of the planned NGNP components and materials. The NGNP project is focused on building a demonstration reactor, rather than simply confirming the basic feasibility of the concept (MacDonald, 2004b).

The United States Department of Energy (DOE) authorized the Idaho National Engineering and Environmental Laboratory (INEEL) to have the Independent Technology Review Group (ITRG) conduct a review of technology alternatives for meeting the functional objectives for the Next Generation Nuclear Plant (NGNP). The following highlights some of the important recommendations as found in (INEEL ITRG, 2004):

- The reactor outlet temperature should be limited to below 1000 °C due to technology limitations.

- The reactor thermal power (about 600 MWth) and core configuration will be designed to ensure passive decay heat removal without fuel damage during accidents (US DOE, 2004).
- It is recommended that resources be dedicated to developing the complex intermediate heat exchanger (IHX) to operate at high reactor outlet temperatures. This implies that materials need to be officially qualified.
- The H_2 process should be capable of utilizing 50 MWth power from the PBR.
- The co-generation plant should reach a 60 year operating life.
- Thermal efficiencies of between 45% and 47% are anticipated.
- The capacity factor should exceed 95%.
- Reactor dimensions should be such as to allow transportation to minimize on-site manufacturing.
- The maximum metal temperature is 900 °C.
- The pressure boundary materials should be operated outside the time dependant deformation (creep) range.
- Use materials for which a database exists today.
- Indirect cycles are favourable because they reduce the risk of contaminated PCU components.
- Indirect cycles provide the infrastructure to test bench the direct cycle.
- Maintenance should allow easy access.
- It is advised to possibly combine more than one reactor with larger PCU.
- It is advised to investigate Molten Salt as working fluid for Secondary Loop.
- The capital cost for the n^{th} plant is strongly recommended to be < $1000/kWe.
- The electricity cost is strongly recommended to be < 1.0 c/kW-hr (MacDonald, 2004a).
- The decommissioning costs should be < $100m/unit.

The focus of this study is to select a PCU for the NGNP plant. And in selecting a PCU, one needs to remember the above mentioned criteria.

2.6 SUMMARY

The following is a brief summary of what has been covered in this Chapter:

- In section 2.2 an overview of the HTGR was given. The six ideas on which the HTGR are based were mentioned as well as the common characteristics to all HTGRs. It was emphasized and explained that the HTGR is inherently safe.
- In section 2.3 the history and development of the HTGR was discussed.
    - Prototype Plants - The initial HTGRs included the *DRAGON,* the *AVR* and *Peach Bottom*. Common among these plants were the utilization of steel vessels. These three plants were successfully built and operated (1965-1988) and valuable lessons were learned from their operation. The *AVR* and *Peach Bottom* produced steam for a steam turbine process. The *DRAGON* reactor dumped the process heat to the

environment via a heat exchanger.

- Demonstration Plants - The *THTR-300* and *FSV* followed the successful *AVR* and *Peach Bottom*. The power levels for these two plants were significantly higher than the *AVR* and *Peach Bottom*. The *THTR-300* and *FSV* also changed over to pre-stressed concrete reactor vessels and the whole primary system was integrated into this vessel. These two plants operated from 1976 to 1989.
- Planned HTGR concepts of the 1970s and 1980s – The primary focus of international HTGR designers in the 1970s and early 1980s was associated with the development of large HTGR units. The interest in development of larger steam cycle HTGR plants included the German PR-500, HHT, PNP-Prototype, HTR-500, HTR-MODUL and the HTR-100; the Russian VGM-400 and the American HTGR-SC, HTGR-GT and MHTGR. Many man hours and a lot of money were invested in these projects. The results of this development work are still available and can be used for the new projects on HTGRs. None of these plants were commissioned.

- In section 2.4, the current international HTGR programs were discussed. It was the development of the HTGR steam plants that provided the key emphasis to initiation of the HTGR coupled to a gas turbine power conversion unit. With few exceptions, it is the German *HTR-MODUL* and the *HTR-100* reactor designs that are being utilized by the South African *PBMR*. The United States' *MHTGR* forms the basis for the *GT-MHR* project (IAEA, 2001c). The most notable of the current international programs are the following:
  - PBMR - The *PBMR* (400 MWt_h) is being developed in South Africa and the planned fuel load date is April 2010. *PBMR* consists of a horizontal single-shaft, inter-cooled recuperative direct Brayton cycle.
  - GT-MHR - The *GT-MHR* (600 MW_{th}) is a vertical single-shaft, inter-cooled recuperative direct Brayton cycle under development by a joint effort by the USA and Russia. Currently the GTMHR design is developed for surplus weapons plutonium disposition.
  - HTR-10 - China started the construction of a 10 MW-HTR in 1995 and the reactor has begun operation in the year 2002. The *HTR-10* reached full power in 2003. The *HTR-10* is the first reactor worldwide which has inherent safety features. The power conversion system of the *HTR-10* is a steam turbine generator system.
  - HTR-10 GT - INET of China and OKBM of Russia jointly completed the conceptual design of the *HTR-10 GT* power conversion unit in 2002. The basic design was completed in 2003. The main components are under manufacture and are scheduled for operation in 2006. The PCU will be inserted into the original *HTR-10* steam generator pressure vessel. The PCU configuration includes a pressure vessel, gas turbine, high-pressure compressor, low-pressure compressor, recuperator, pre-cooler, inter-cooler and generator.
  - HTR-PM - A demonstration plant of the pebble bed modular reactor is being proposed by China Huanneng Group, China Nuclear Engineering and Construction Corporation and Tsinghua University. The project proposal will soon be submitted to authorities for approval. The location of the *HTR-PM* will be decided following the completion of the pre-feasibility study. Start of construction is foreseen for 2007 and first criticality may be reached by 2010.
  - HTTR - The *HTTR* is the first HTGR in Japan with 30 MWth and a reactor outlet

temperature of 950 °C. This is the highest outlet coolant temperature in the world. The *HTTR* reached full power in December 2000.

- GTHTR300 - JAERI has undertaken the feasibility study on the *GTHTR300*. The design is expected to be deployed in 2010 as a safe and economically competitive electricity generation system in Japan. The *GTHTR300* is a horizontal single-shaft, non inter-cooled recuperative direct Brayton cycle.
- Framatome Combined Cycle - The Framatome ANP VHTR design is based on an indirect cycle coupled to an "off-the-shelf" Combined Cycle gas turbine. The nuclear heat source of the indirect cycle could be used to qualify the direct cycle components without risk of contamination behind the IHX, thus assisting in the preparation for the later introduction of that technology.
- MPBR - The *MPBR* project at MIT was initiated in 1998 as part of an effort to re-invigorate thinking about how to improve the overall safety of nuclear plants, making the plants less complex and more competitive with fossil fuel plants. The MPBR consists of an indirect, three-shaft twice inter-cooled recuperative Brayton cycle.
- ACACIA - The Netherlands' R&D activities concentrate on VHTR core physics, safety technology, components technology, materials and fuels as well as GFR core physics. New activities are on nuclear hydrogen technologies and system studies for HTGR applications in the energy market. The ACACIA project is a 60 MWth pebble bed reactor with an indirect Brayton cycle and is proposed for the applications of heat and power cogeneration or distributed electricity generation.
- Under the 5^{th} framework program 10 HTR projects have been co-funded by the European Commission (EC). These projects have dealt with fuel technology, components, core physics, fuel cycle, materials, licensing and educational training. Under the 6^{th} framework program an ambitious integrated VHTR project with a consortium of 35 partners worldwide is due to start in 2005 for a period of 48 months. The European programme will be covering most of the areas that have to be addressed by R&D for the development of modern modular HTGRs. It is organising the European effort in a consistent way, avoiding overlapping and redundancies.
- The German government has decided to phase out nuclear energy. Gas-cooled reactor activities mainly comprise of the decommissioning of the *AVR*, code validation for safety analysis and management of spent HTR fuel.
- The KAERI VHTR program was introduced focusing on the R&D on fuel, materials and nuclear graphite after a brief review.
- Two working parties of the Nuclear Science committee are involved in reactor studies and fuel cycle studies, including activities for advanced HTGRs. The NEA holds the technical secretariat for the Generation IV International Forum (GIF).
- The IAEA HTGR activities continue to focus on coordinated research projects (CRPs), information exchange and educational training.

2.7 CONCLUSION

There are a large number of international programs focussed on developing the first *Generation III* nuclear plants which will precede the NGNP. Consequently PBMR is faced with strong competition. A variety of PCU designs are being investigated by the international community and it is not straight-forward to assess which of these PCUs are most suitable for the NGNP. Cost comparisons for these various PCUs are not available in open literature because of its confidentiality and commercial value. Efficiencies quoted for each of the PCU designs are often contradictory.

If PBMR wants to participate in the NGNP project, it is important to conduct a separate independent study as to which PCU would be best for the NGNP. The objective of this study is to compare the most promising one-, two- and three-shaft Brayton-, Rankine- and Combined-cycle configurations in order to evaluate the technical performance, practical considerations and economical competitiveness when employed in conjunction with a given Pebble Bed Reactor. The objective is to identify a near-optimum design for each cycle configuration from which the optimum PCU configuration for the NGNP can be identified.

Chapter 3

System thermo-hydraulic design

In this chapter, the theory and methodology used to solve the thermodynamic cycle analyses are presented and all relevant input parameters are discussed. The definitions used to calculate the efficiency of a co-generation plant (producing electricity and hydrogen) are given and the theory regarding gas mixtures is mentioned.

3. SYSTEM THERMO-HYDRAULIC DESIGN

Chapter 3 discusses the methodology, optimization and theory used to solve the system thermodynamic cycle analyses for the Brayton and Combined Cycle configurations under investigation. An overview of the PCU is given in section 3.1. Section 3.2 gives an overview of how these cycles are solved and integrated together with the costing formulas. The theory and methodology used to solve the Brayton cycles are presented in section 3.3. The theory used to solve the Combined Cycles and the methodology used to optimize the plant for maximum combined efficiency are explained in section 3.4.2. The optimization of the steam plant is also discussed in section 3.4.2.2. The methodology used and assumptions made to solve the indirect loop for the indirect cycles are discussed in section 3.5. The applicable theory for the hydrogen plant is discussed in section 3.6 and the theory for deriving the gas mixture properties is discussed in section 3.7. All the relevant input parameters are listed in Appendix 9.1.

The ten cycle configurations under investigation were discussed in Chapter 1. As mentioned, the objective is to compare these ten cycles in order to identify a near-optimum design for each cycle from which the most practical, efficient and economical PCU for the NGNP can be chosen.

3.1 THE POWER CONVERSION UNIT

For the purpose of this study, only the PCU is simulated and analysed. The PCU includes all the system components necessary to convert the heat energy of the heated helium through the reactor into electricity. The Brayton PCU consists of a combination of a high pressure gas turbine (HPT), low pressure gas turbine (LPT), power turbine (PT), recuperator (RX), pre-cooler (PC), low pressure compressor (LPC), inter-cooler (IC), high pressure compressor (HPC), valves, generator (GEN), gearbox (GB) and possibly a start-up blower (SBS). The Rankine PCU consists of a combination of a steam generator (SG), high pressure steam turbine (HPT), intermediate pressure steam turbine (IPT), low pressure steam turbine (LPT), condenser (CD) and feed-water pumps. The Combined Cycle comprises of both the Brayton- and Rankine cycle which is connected through the steam generator. Additional components for the indirect cycles would be the primary side blower and the intermediate heat exchanger (IHX). The indirect cycle comprises of a primary and secondary loop which is connected through the intermediate heat exchanger (IHX). Only Cycle B and Cycle I are discussed as examples - see *Figure 3.19* for the schematic layout. The schematic layout of Cycle G is discussed in section 3.4.2.3

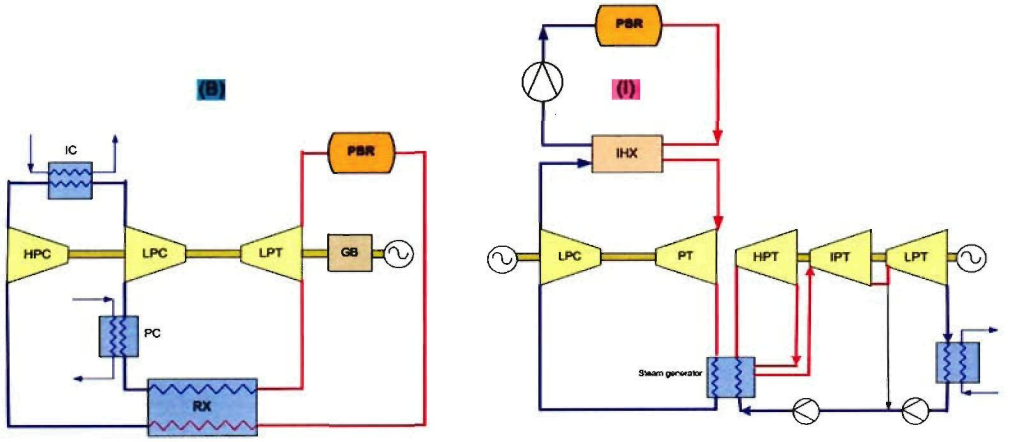


Figure 3.19 *PCU for Brayton Cycle B and Combined Cycle I (used as examples)*

Brayton B

The hot helium leaving the core flows through the turbine that drives the compressors. The flow is then cooled in the recuperator, which also heats the helium before it enters the core, and is further cooled down to the minimum cycle temperature in the pre-cooler. The flow enters the compressors between which it is inter-cooled and finally passes through the recuperator before entering the core. The turbine is the main power generating component, where the net work available equals the turbine work minus the work required by the compressor. The thermal cycle efficiency is defined as:

$$W_{Brayton} = \eta_{Mechanical} W_{Gas-turbine} - W_{Compressors} \tag{3.1}$$

$$\eta_{cycle} = \frac{W_{Brayton}}{PBR_{th}} \tag{3.2}$$

Combined Cycle I

The recuperator, pre-cooler and inter-cooler of the Brayton cycle are replaced with a steam generator. The hot steam leaving the steam generator passes through the high pressure steam turbine, where after the steam is re-heated in the steam generator. The flow then passes through both the intermediate- and low- pressure steam turbines. From the LPT, the flow enters the condenser, passes through the low-pressure pump and is then pre-heated before entering the high pressure pump and returning to the steam generator. The bleed-flow is extracted between the IPT and LPT. The combined thermal cycle efficiency is defined as:

$$W_{Rankine} = W_{Steam-turbines} - W_{Pumps} \tag{3.3}$$

$$\eta_{cycle} = \frac{(W_{Brayton} - W_{Blower}) + W_{Rankine}}{PBR_{th}} \tag{3.4}$$

3.2 SYSTEM DESIGN METHODOLOGY

This section gives an overview of how the cycle analyses are integrated with both the component- and costing models in order to arrive at the integrated model used to analyse the PCU. The cycle analyses, component designs and costs are solved simultaneously in CYCLE-C. All relevant theory regarding the cycle analyses is documented in sections 3.3 and 3.4, while all relevant theory regarding the component designs and costing formulas are documented in Chapters 5 and 4 respectively. The optimization of the turbo machines is documented in Chapter 5. See *Figure 3.20* for the overview of the discussion to follow.

3.2.1 Input variables

All the input parameters to the analyses are listed in *Figure 3.20*. The meaning of each variable and its value is documented in Appendix 9.1. Except for the leak flows, these input values are kept the same for all the cycles. Since the turbo machines have not yet been designed at the onset of the cycle analyses, the turbo machine efficiencies and outlet axial velocities are guessed and updated once the machines have been designed. The turbo machine isentropic efficiencies are not calculated as function of the appropriate loss models, but merely as function of the stage efficiency and number of stages (see Chapter 5).

Figure 3.20 *Overview of Systems solution – see next page*

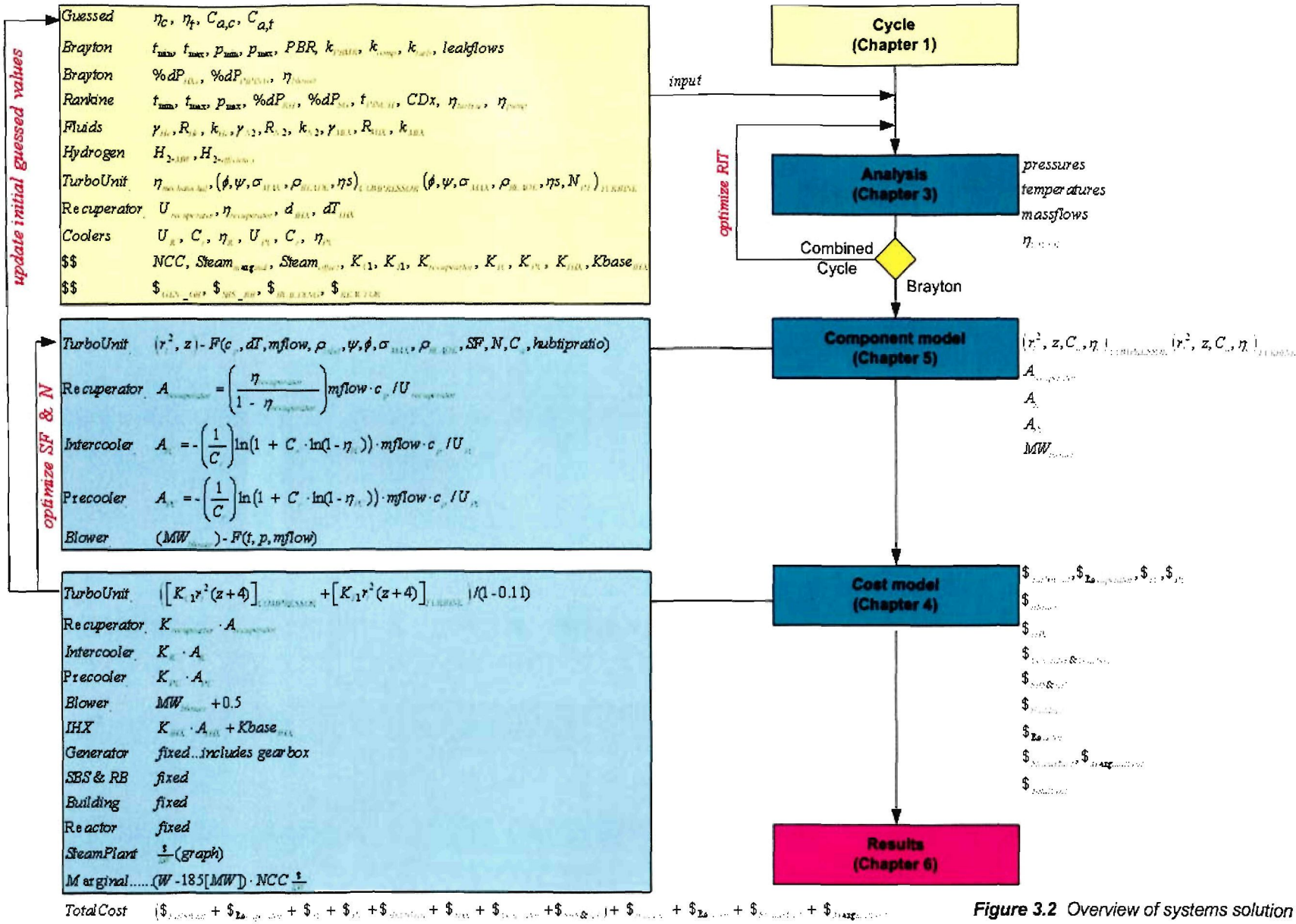


Figure 3.2 *Overview of systems solution*

3.2.2 Cycle Analyses

These input values are used together with basic thermodynamic relations (see section 3.3.3) to solve for all the pressures and temperatures in the cycle, for each component's inlet and outlet.

A thermodynamic cycle analysis was done for each configuration based on a fixed reactor pressure loss coefficient (k_{PBMR}), fixed heat exchanger efficiencies ($\eta_{Recuperator}$, η_{IC}, η_{PC}) and fixed percentages for the pressure losses through the piping ($\%dP_{PIPING}$) and heat exchangers ($\%dP_{HXs}$). This implies that a fixed reactor design is used for all the cycles and also that the heat exchangers and piping geometry are scaled with each pressure ratio to ensure the specified pressure loss. The leak flows for each cycle was calculated as fixed percentages of the total cycle flow. The isentropic efficiency of each turbo machine is calculated at each specified cycle pressure ratio as function of the stage efficiency and number of stages. See section 3.3 for the detailed discussion on the Brayton cycle.

Brayton input variables

$$assumed: \ \eta_c,\ \eta_t,\ C_{a,c},\ C_{a,t}$$

$$fixed: \quad t_{\min}, t_{\max}, p_{\min}, p_{\max}, PBR, k_{PBMR}, k_{comp}, k_{turb}, dT_{IHX}, \%dP_{HXs},\ \%dP_{PIPING}, \eta_{Blower}, \eta_{Mechanichal}, \eta_{Recuperator}, \eta_{IC}, \eta_{PC}$$

For the Rankine cycle, the maximum pressure is fixed and an upper limit is set for the maximum steam temperature. Both the turbine and pump efficiencies are fixed and the condenser fraction is limited to 88%. The pressure loss through the steam generator is calculated as fixed percentages of its inlet pressure. The reactor inlet temperature determines the fraction of work that is performed by the Brayton and Rankine respectively. The reactor inlet temperature is optimized to ensure the maximum combined efficiency. See section 3.4 for the detailed discussion on the Combined Cycle.

Rankine input variables

$$fixed: \quad t_{\min}, t_{\max} >, p_{\max}, \%dP_{RH}, \%dP_{SG}, t_{PINCH}, CDx, \eta_{turbine}, \eta_{pump}$$

3.2.3 Component Models

Component models for the turbine, compressor, recuperator, inter-cooler, pre-cooler, intermediate heat exchanger and blower are used together with the boundary values from the cycle analyses to perform a conceptual design of each component. The components are only designed to the level of detail that is required by the costing formula – see next section.

The turbo machine model needs to solve only for the tip radius (r_t), number of stages (z), isentropic efficiency (η) and axial velocity (C_a). See Chapter 5 for the detailed theory used to solve these variables.

The model is a function of: $\left(r_t^2,\ z\right) - F(c_p, dT, mflow, \rho_{inlet}, \psi, \phi, \sigma_{MAX}, \rho_{Blade}, SF, N, C_a, hubtipratio)$

The recuperator model needs to solve only for the heat transfer area ($A_{Recuperator}$) – see Chapter 5.

$$A_{Recuperator} = \left(\frac{\eta_{Recuperator}}{1 - \eta_{Recuperator}} \right) mflow \cdot C_p / U_{Recuperator}$$

The inter-cooler model needs to solve only for the heat transfer area (A_{IC}) – see Chapter 5.

$$A_{IC} = -\left(\frac{1}{C_r} \right) \ln\left(1 + C_r \cdot \ln(1 - \eta_{IC})\right) \cdot mflow \cdot C_p / U_{IC}$$

The pre-cooler model needs to solve only for the heat transfer area (A_{PC}) – see Chapter 5.

$$A_{PC} = -\left(\frac{1}{C_r} \right) \ln\left(1 + C_r \cdot \ln(1 - \eta_{PC})\right) \cdot mflow \cdot C_p / U_{PC}$$

The blower model needs to solve only for the blower size, which is determined by the inlet and outlet temperatures and pressures as well as the mass flow through the blower - see Chapter 5.

$$(MW_{Blower}) - F(t, p, mflow)$$

3.2.4 Costing Models

The order-of-magnitude plant cost is only a comparative value between the cycles and does not portray the absolute total cost of the plant. The philosophy was to include only those component costs that will result in notable overall cost differences between the cycles. The costing formulas are postulated based on engineering judgement. The cost of each component will rather indicate a trend, than an absolute cost. The designs were benchmarked against the PBMR capital costs. The order-of-magnitude plant cost is defined as the sum of all the major PCU component capital costs, the capital cost of the building, the capital cost of the reactor and the capital cost of the steam plant, minus the capitalized income due to the power output.

$$\left[C_{Turbo\ Unit} + C_{Recuperator} + C_{IC} + C_{PC} + C_{Blower} + C_{IHX} + C_{Generator} + C_{SBS\&RB} \right]_{PCU} + C_{Building} + C_{Reactor} + C_{Steam\ Plant} - C_{Marginal\ Cost}$$

The capital cost of the generator, gearbox, SBS blower, resistor bank, building and reactor was fixed. The steam plant is calculated from a certain $/kW. The power output for each cycle was translated into a capitalised income resulting in a reduction in capital cost. This means that a higher thermal cycle efficiency effectively reduces the order-of-magnitude plant cost ($C_{MarginalCost}$). The cost models used for the PCU are as follows (see Chapter 4 for more details):

$C_{TurboUnit}$: $\left(\left[K_{C1} r_t^2 (z+4) \right]_{Compressor} + \left[K_{T1} r_t^2 (z+4) \right]_{Turbine} \right) / (1 - 0.11)$

$C_{Recuperator}$: $K_{Recupeartor} \cdot A_{Recuperator}$

C_{IC}: $K_{IC} \cdot A_{IC}$

C_{PC}: $K_{PC} \cdot A_{PC}$

C_{Blower}: $MW_{Blower} + 0.5$

C_{IHX}: $K_{IHX} \cdot A_{IHX} + Kbase_{IHX}$

Once the parameters mentioned in the previous section have been solved, the capital costs of the turbo unit, recuperator, inter-cooler, pre-cooler, intermediate heat exchanger and blower are calculated, using the cost models together with the proportionality constants (K) derived from PBMR design data.

3.2.5 Optimization

The reactor inlet temperature is optimized to ensure the maximum Combined Cycle efficiency – see section 3.4.2.3. Each turbo machine is optimized to ensure the minimum capital cost. The cost of *each turbo machine is minimised by varying the blade stress safety factor and the rotational speed.* For a specific combination of safety factor and rotational speed, the tip radius and number stages are determined using a design routine and these values are then used to determine the cost of the machine. By repeating this calculation for a large number of combinations of safety factor and speed, the minimum cost can be determined. All this is done while staying within all design limitations – see Chapter 5 for more details. The number of stages calculated from this optimized design is used to calculate the compressor and turbine isentropic efficiency. Both the initial guessed values for the turbo machine axial velocities and isentropic efficiencies are updated and the cycle analysis is repeated until *the solution converges.*

3.2.6 Results

The temperatures, pressures, thermal cycle efficiency, component capital costs and the order-of-magnitude plant cost of each configuration were then calculated for various pressure ratios, reactor outlet temperatures, reactor power levels and power turbine rotational speeds. Based on these results, the different operational parameter envelopes are identified for which each of the different cycle *configurations would be most appropriate – see Chapter 6.*

3.3 BRAYTON CYCLE

Six Brayton cycle configurations are investigated. In this section, the system thermo-hydraulic design *of the three-shaft recuperative* direct Brayton with inter-cooling is discussed (D). Only Cycle D is discussed as representative example, since the same equations and methodology are applicable for the other five cycles – see Chapter 1 for the schematic layout of all the cycles.

- Cycle A: Single shaft, recuperative direct Brayton cycle
- Cycle B: Single shaft, recuperative direct Brayton cycle with inter-cooling
- Cycle C: Two shaft, recuperative direct Brayton cycle with inter-cooling
- Cycle D: Three shaft, recuperative direct Brayton cycle with inter-cooling
- Cycle E: Three shaft, recuperative direct Brayton cycle with two-step inter-cooling
- Cycle F: Two shaft, *recuperative indirect Brayton cycle with inter-cooling*

3.3.1 Input

The input to the Brayton cycle is listed in Appendix 9.1 *Table 6.9.* These input values are kept the same for each of the Brayton cycles. The primary working fluid for the direct Brayton cycles is Helium. Nitrogen is also investigated for the indirect cycles. It is assumed that ideal gas law properties apply. The minimum cycle coolant temperature is limited by the available cooling water temperature of 18 °C using an approach temperature of 6 °C. The maximum coolant temperature is limited by the turbine blade materials and the allowable reactor inlet temperature, which is 500 °C. The maximum pressure in the cycle is limited by pressure boundary limitations. The loss coefficient for the reactor is based on the PBMR reactor, where

$$K_{PBMR} = \frac{\rho_{avg}\Delta P}{mflow^2} = \frac{4.5 \cdot 307}{185^2} \approx 40 \frac{kg/m^3 \cdot kPa}{(kg/s)^2} \quad (3.5)$$

See reference [24] for the Flownex network details on which the pressure difference (ΔP), mass flow ($mflow$) and average density (ρ_{avg}) were based. The percentages for the pressure losses through all heat exchangers and piping were based on typical values. The power turbine speed was fixed at 6000 rpm, assuming a 180 MW gearbox. The rest of the input values are assumed to be typical values. The initial guessed values for the turbo machines are updated once the turbo machines have been designed.

The turbine leak flow values are different for each cycle configuration and each pressure ratio since the leak flow is a function of the number of turbines, the size of the turbines and the mass flow in the cycle. The turbine leak flow is calculated as fixed percentages of the total cycle mass flow. The leak flows for the three-shaft designs were assumed to be 7.3%, based on the three-shaft PBMR design [24], while the leak flows for the single-shaft designs were assumed to be 5.6%, based on the single-shaft PBMR design [23]. For the two-shaft design, the averaged value of 6.1 % was used. For the single-shaft indirect Nitrogen cycle, the turbo machines are presumed to be smaller and therefore a smaller leak flow of 5.2% was assumed. See *Table 9.19* for the leak flow input data. The leak flows referred to in this document only apply to the turbo machine cooling flows.

3.3.2 Design methodology

The t-s diagrams and more importantly the numbering for all the cycles are presented in *Figure 3.21* and *Figure 3.22*. All the analyses are done in a program written in *Visual C++*; therefore the equations need to be written in the explicit form. The equations, as listed, are in the exact sequence as they appear in CYCLE-C and the same variable names are used.

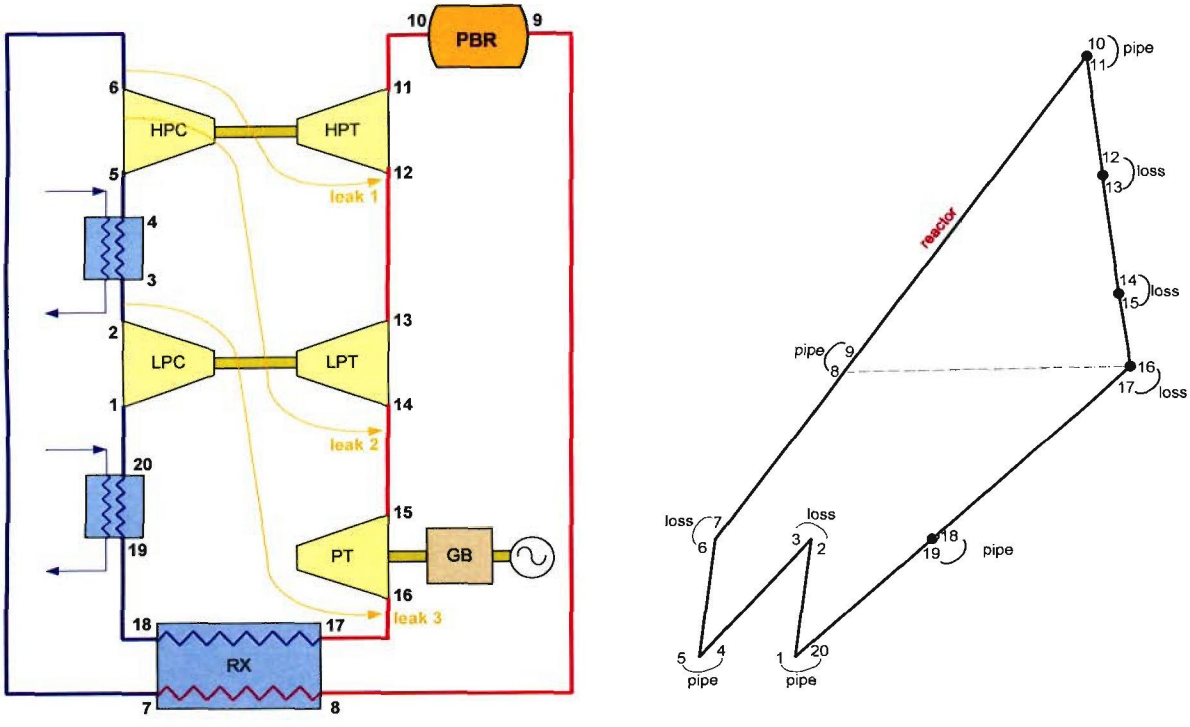


Figure 3.21 *Cycle layout and t-s diagram – Cycle D*

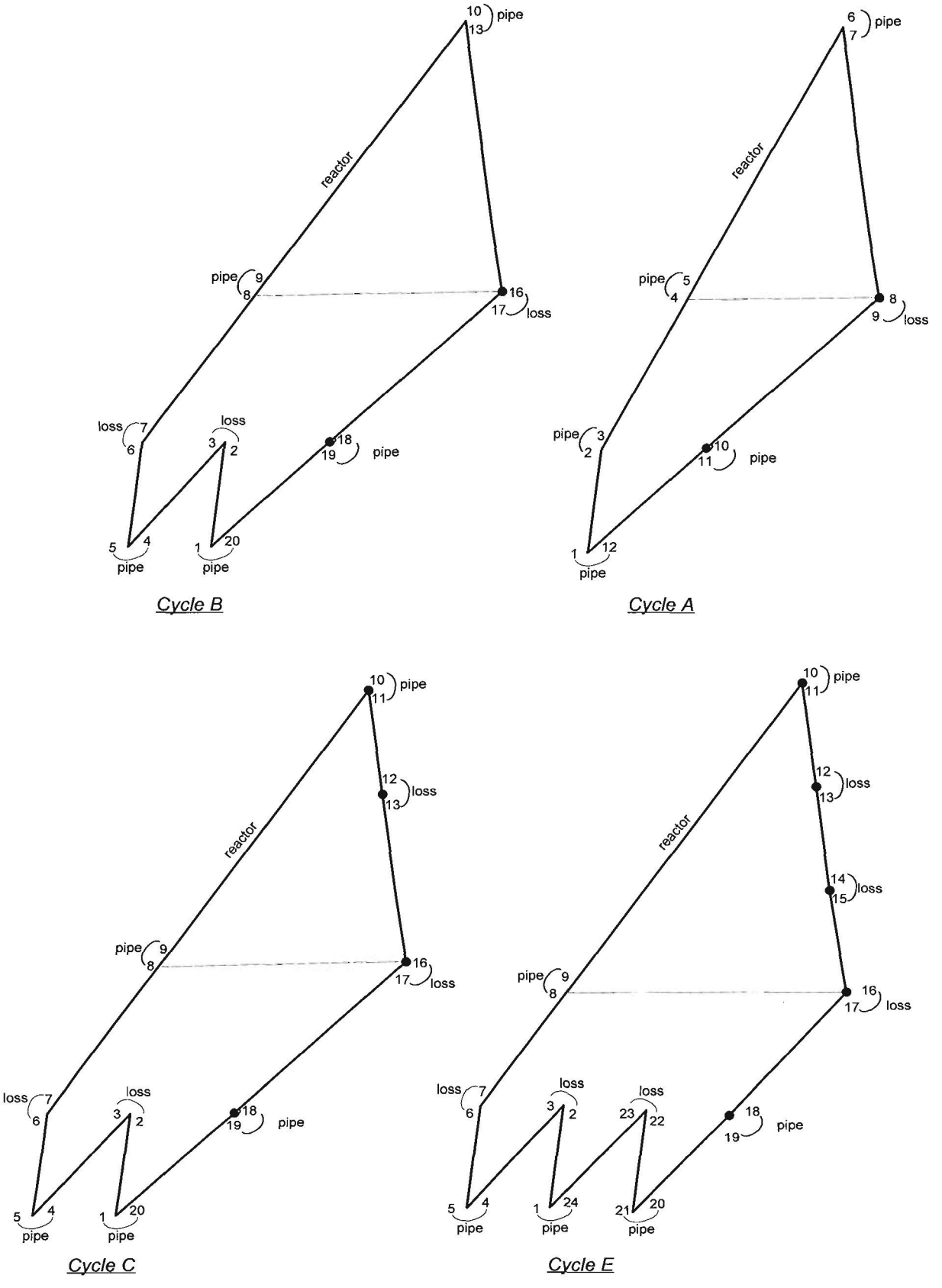


Figure 3.22 *T-s diagrams of Cycles A, B, C and E*

Discussion and numbering – see Cycle D Figure 3.21:

The numbers in brackets refer to the equation numbers of section 3.3.3. NOTE: The turbo machine intake losses were not taken into account.

Low-pressure Compressor (LPC)

The minimum cycle temperature (3.6) , maximum cycle pressure (p_{max}) and the total pressure ratio over all the compressors (PR) are specified. The minimum cycle pressure (3.7) and the inlet density (3.8) are calculated. It was decided to equally split the work between all the compressors. Next, the LPC outlet pressure (3.9), temperature (3.10) and density (3.11) are calculated. The diffuser outlet pressure (3.13) based on the axial velocity is calculated.

Inter-cooler

The inter-cooler outlet temperature is set to the minimum cycle temperature (3.14). The outlet pressure is calculated as a fixed percentage of the inlet pressure (3.15).

High-pressure Compressor (HPC)

The pressure loss over the piping from the inter-cooler outlet to the HPC inlet (3.17) is calculated. The HPC outlet pressure (3.18), outlet temperature (3.19) and outlet density (3.20) are calculated. The diffuser outlet pressure (3.22) based on the axial velocity is calculated.

Recuperator

The high-pressure recuperator pressure loss (3.23) and the pressure loss over the recuperator outlet pipe (3.24) are calculated as fixed percentages of the recuperator inlet pressure. The recuperator outlet temperature (3.51) is calculated later on.

Reactor

The maximum cycle temperature (3.25)(3.26) is specified as fixed input.

All the pressures and temperatures at points 1 through 7 have been calculated. At the reactor inlet (point 8 and 9) only the pressures are known and at the reactor outlet (point 10 and 11) only the temperatures are known.

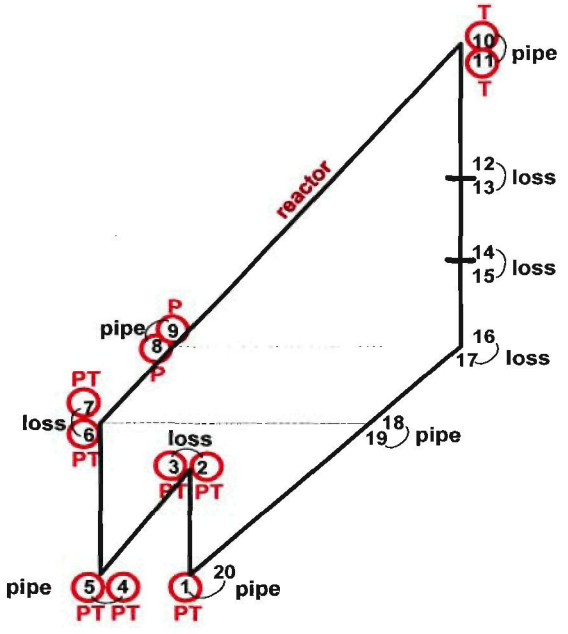


Figure 3.23 *T-s diagram: Solution points 1-7*

The next step is to solve the pressure drop through the reactor. The pressure drop is defined by:

$$\Delta P_{reactor} = \frac{k_{PBMR} \cdot mflow^2 (1 - leak1 - leak2)^2}{(rho_{10} + rho_9)/2}.$$

At this stage, neither rho_9, rho_{10} nor the mass flow rate is known. The mass flow (mflow) referred to onwards is the mass flow through the LPC. The mass flow, p_{10} and t_9 are solved by iterating for the mass flow. The following initial guessed values were assumed, based on the PBMR plant:

mflow	= 190 kg/s	(calculated with Eq. (3.56))
p_{10}	= p9 – 100 kPa	(calculated with Eq. (3.29))
t_9	= t10 – 400 °C	(calculated with Eq. (3.53))

Reactor

The assumed values for p_{10} and t_9 are used to calculate the reactor's inlet (3.27) and outlet density (3.28). The pressure drop over the reactor (3.29) is calculated using the assumed mass flow. The pressure loss over the reactor outlet pipe (3.30) is calculated.

Pressure losses

The assumed percentages for the pressure losses over the heat exchangers and piping are used to calculate the pressures at points 20 (3.31), 19 (3.32), 18 (3.33) and 17 (3.34).

HPT

The work produced by the HPT is fully absorbed by the HP compressor. Assuming $Q_{HPC} = Q_{HPT}$, the outlet temperature (3.35), pressure (3.36) and density (3.37) are solved. The pressure (3.38) after the diffuser is calculated next. Leak flow 1 is extracted from point 6 and mixes with t_{12} to produce t_{13}. The mixing formula of Eq. (3.39) is used to calculate t_{13}.

LPT

The work produced by the LPT is fully absorbed by the LP compressor. Assuming that $Q_{LPC} = Q_{LPT}$, it follows that Eq. (3.40) can be used to solve for t_{14}. Eq. (3.41) is used to solve for the LPT outlet pressure. The density is calculated with Eq. (3.42). The diffuser outlet pressure is calculated with Eq. (3.43). Leak flow 2 is extracted from point 6 and mixes with t_{14} to produce t_{15}. The mixing formula of Eq. (3.44) is used to calculate t_{15}.

Power Turbine

The pressure loss over the power turbine diffuser is defined by: $p_{16} = p_{17} + k_{turb}\left(\frac{1}{2} rho_{16} V_{PT}^{\ 2}\right)$.

The initial guessed value for p_{16} is assumed to be: $p_{16} = p_{17} / lossfact1$.

Since both p_{16} and t_{16} are still unknown, rho_{16} is not known and therefore the power turbine outlet pressure (p_{16}) will need to be solved for iteratively. An initial value for p_{16} is assumed. With p_{16} fixed, t_{16} (3.46) is calculated. Next rho_{16} (3.47) can be calculated. A new updated value for p_{16} (3.48) can now be calculated. With this newly calculated value for p_{16}, the process is repeated until convergence. Leak flow 3 is extracted from point 2 and mixes with t_{16} to produce t_{17} (3.49).

Work output

The work output per unit mass flow of the power turbine is calculated with Eq. (3.50).

Recuperator

The recuperator efficiency is used to calculate the recuperator HP temperature (3.51) and LP

temperature (3.52). Next, the reactor inlet temperature (3.53) is solved.

Mass flow

The heat input per unit mass flow (3.54) is calculated where after the mass flow (3.56) can be calculated, using the fixed power level input. Remembering that the mass flow was initially assumed to calculate the pressure loss through the reactor, this mass flow needs to be updated and all calculations from the reactor pressure loss calculation onwards need to be repeated. This will be done until the solution converges. The assumed values for p_{10} and t_9 was re-calculated with equations (3.29) and (3.53). All pressures and temperatures from points 1 through 20 have now been solved.

3.3.3 Design equations

All pressures referred to are total pressures

$input: \ \eta_C, \ \eta_t, \ C_{a,c}, \ C_{a,t}$

$input: \ t_{\min}, t_{\max}, p_{\min}, p_{\max}, PBR, k_{PBMR}, k_{comp}, k_{turb}, dT_{IHX}, \%dP_{HXs}, \ \%dP_{PIPING}, \eta_{blower}, \eta_{mechanichal}, \eta_{recuperator}, \eta_{IC}, \eta_{PC}$

LPC	$t_1 = t_{cold}$	(3.6)
	$p_1 = \frac{p_{\max}}{pr}$	(3.7)
	$rho_1 = \frac{p_1}{t_1 R}$	(3.8)
	$p_2 = p_1 \sqrt{pr}$	(3.9)
	$t_2 = t_1 + \frac{t_1}{etac_{LP}}\left[\left(\frac{p_2}{p_1}\right)^{(\gamma-1)/\gamma} - 1\right]$	(3.10)
	$rho_2 = \frac{p_2}{t_2 R}$	(3.11)
	$t_3 = t_2$	(3.12)
	$p_3 = p_2 - k_{comp}(\frac{1}{2} rho_2 V_{LPC}{}^2)$	(3.13)
Inter-cooler	$t_4 = t_{cold}$	(3.14)
	$p_4 = lossfact2 * p_3$	(3.15)
HPC	$t_5 = t_{cold}$	(3.16)
	$p_5 = lossfact1 * p_4$	(3.17)
	$p_6 = p_5 \sqrt{pr}$	(3.18)
	$t_6 = t_5 + \frac{t_5}{etac_{HP}}\left[\left(\frac{p_6}{p_5}\right)^{(\gamma-1)/\gamma} - 1\right]$	(3.19)
	$rho_6 = \frac{p_6}{t_6 R}$	(3.20)
	$t_7 = t_6$	(3.21)
	$p_7 = p_6 - k_{comp}(\frac{1}{2} rho_6 V_{HPC}{}^2)$	(3.22)

Recuperator HP	$p_8 = lossfact2 * p_7$	(3.23)
	$p_9 = lossfact1 * p_8$	(3.24)
Reactor	$t_{10} = t_{hot}$	(3.25)
	$t_{11} = t_{hot}$	(3.26)
ITERATIVE LOOP (blue indent)	The pressure drop through the reactor is defined by: $p_{10} = p_9 - \frac{k_{PBMR} mflow^2}{(rho_{10} + rho_9)/2}$	
	assume: mflow = 190 kg/s; $p_{10} = p_9$ - 100e3; $t_9 = t_{10} - 400$	
Reactor	$rho_9 = \frac{p_9}{t_9 R}$	(3.27)
	$rho_{10} = \frac{p_{10}}{t_{10} R}$	(3.28)
	$p_{10} = p_9 - \frac{k_{PBMR} mflow^2 (1 - leak1 - leak2)^2}{(rho_{10} + rho_9)/2}$	(3.29)
	$p_{11} = lossfact1 * p_{10}$	(3.30)
Pressure losses	$p_{20} = p_1 / lossfact1$	(3.31)
	$p_{19} = p_{20} / lossfact2$	(3.32)
	$p_{18} = p_{19} / lossfact1$	(3.33)
	$p_{17} = p_{18} / lossfact2$	(3.34)
HPT	$t_{12} = t_{11} - \frac{(t_6 - t_5) * (1 - leak3)}{(1 - leak1 - leak2 - leak3) eta_{mech}}$	(3.35)
	$p_{12} = p_{11} \left(1 - \frac{t_{11} - t_{12}}{t_{11} etat_{HP}}\right)^{\gamma/(\gamma-1)}$	(3.36)
	$rho_{12} = \frac{p_{12}}{t_{12} R}$	(3.37)
Mixing flow	$p_{13} = p_{12} - k_{turb} \left(\frac{1}{2} rho_{12} * V_{HPT}^{\ 2}\right)$	(3.38)
	$t_{13} = \frac{t_{12}(1 - leak1 - leak2 - leak3) + t_6 leak1}{1 - leak2 - leak3}$	(3.39)
LPT	$t_{14} = t_{13} - \frac{t_2 - t_1}{(1 - leak2 - leak3) eta_{mech}}$	(3.40)
	$p_{14} = p_{13} \left(1 - \frac{t_{13} - t_{14}}{t_{13} etat_{LP}}\right)^{\gamma/(\gamma-1)}$	(3.41)
	$rho_{14} = \frac{p_{14}}{t_{14} R}$	(3.42)
Mixing flow	$p_{15} = p_{14} - k_{turb} \left(\frac{1}{2} rho_{14} V_{LPT}^{\ 2}\right)$	(3.43)
	$t_{15} = \frac{t_{14}(1 - leak2 - leak3) + t_6 leak2}{1 - leak3}$	(3.44)

ITERATIVE LOOP
(red indent)

The pressure loss over the diffuser:

$$p_{16} = p_{17} + k_{turb}\left(\frac{1}{2} rho_{16} V_{PT}^{\ 2}\right)$$

Power Turbine

$GUESS:$ (3.45)

$$p_{16} = p_{17} / lossfact1$$

{

$$t_{16} = t_{15} - t_{15} etat_{PT}\left[1 - \left(\frac{p_{16}}{p_{15}}\right)^{(\gamma-1)/\gamma}\right] \quad (3.46)$$

$$rho_{16} = \frac{p_{16}}{t_{16} R}$$

$$p16 = p_{16} \quad (3.47)$$

$$p_{16} = p_{17} + k_{turb}\left(\frac{1}{2} rho_{16} * V_{PT}^{\ 2}\right) \quad (3.48)$$

Convergence testing

$$\} \; while \left(fabs \frac{p16 - p_{16}}{p_{16}}\right) > 1.0e-8$$

Power Turbine

$$t_{17} = t_{16}(1 - leak3) + t_2 \; leak3 \quad (3.49)$$

Work output

$$work = cp * (t_{15} - t_{16}) * (1 - leak3) * eta_{mech} \quad (3.50)$$

Recuperator

$$t_8 = t_7 + eta_{recup} \; (t_{17} - t_7) \quad (3.51)$$

$$t_{18} = t_{17} - (t_8 - t_7) * (1 - leak1 - leak2 - leak3) \quad (3.52)$$

$$t_9 = t_8 \quad (3.53)$$

Mass flow

$$heat = (1 - leak1 - leak2 - leak3) * cp * (t_{10} - t_9) \quad (3.54)$$

$$massflow = mflow \quad (3.55)$$

$$mflow = \frac{PBMR}{heat} \quad (3.56)$$

Convergence testing

$$\} \; while \left(fabs \frac{massflow - mflow}{mflow}\right) > 1.0e-8$$

Recuperator Power

$$W_{recuperator} = C_p \; (t_{17} - t_{18}) \quad (3.57)$$

Work

$$work = C_p \; (t_{15} - t_{16}) \; (1 - leak3) \; eta_{mech} \quad (3.58)$$

Thermal efficiency

$$\eta_{TOTAL} = \frac{work}{heat} = \frac{C_p (t_{15} - t_{16})(1 - leak3) eta_{mech}}{(1 - leak1 - leak2 - leak3) C_p (t_{10} - t_9)} \quad (3.59)$$

3.3.4 Total isentropic efficiency (compressor & turbine)

Not all the cycle configurations have the same amount of turbines and compressors, therefore making it difficult to compare the turbo machine isentropic efficiencies. In order to compare these efficiencies the total isentropic efficiency for all the compressors combined and for all the turbines combined was calculated. These results are presented in Chapter 6. This section presents the definition used for the combined compressor and the combined turbine isentropic efficiency.

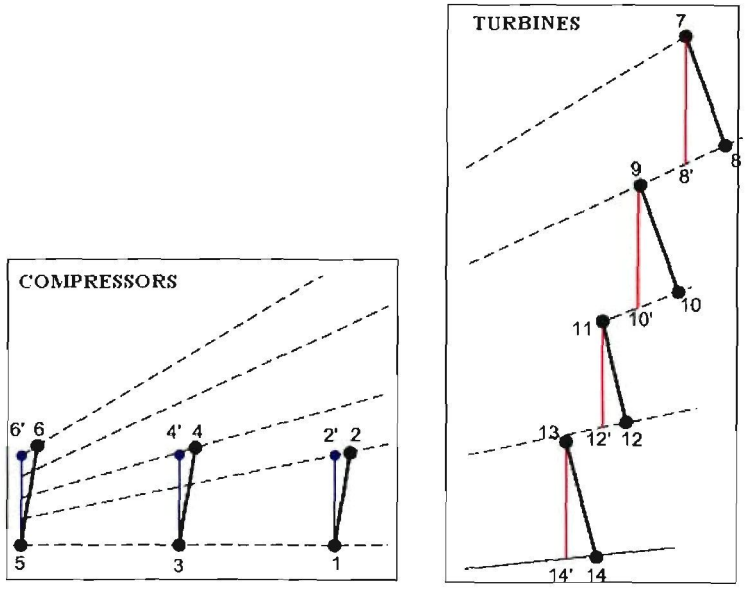


Figure 3.24 *T-s diagram explaining total turbo isentropic efficiency*

The compressor and turbine isentropic efficiencies are dependent on the stage efficiency and the number of stages. The number of stages is proportional to the pressure ratio over the turbo machine. For a fixed stage efficiency, the compressor isentropic efficiency will always decrease with increasing pressure ratio and the turbine efficiency will increase with increasing pressure ratio. This theoretical phenomenon corresponds with what would be expected in practice, where the boundary layer losses cause a compressor's efficiency to decrease with increasing number of stages. From a turbo machine efficiency point of view, one would like to have as few compressor stages as possible and as many turbine stages as possible.

At each pressure ratio, the turbo machine was optimized with regard to cost and the number of stages was calculated. The temperatures at points 2, 4, 6, 8, 10, 12 and 14 were calculated using the compressor and turbine isentropic efficiencies as calculated by the component model. The combined isentropic efficiency over all the turbines and compressors are defined respectively by equations (3.60) and (3.61).

$$\eta_{turbines} = \frac{\sum\left(m \cdot c_p \Delta T_{actual}\right)}{\sum\left(m \cdot c_p \Delta T_{isentropic}\right)} = \frac{m_{7/8}(T_7 - T_8) + m_{9/10}(T_9 - T_{10}) + m_{11/12}(T_{11} - T_{12}) + m_{13/14}(T_{13} - T_{14})}{m_{7/8}(T_7 - T_{8'}) + m_{9/10}(T_9 - T_{10'}) + m_{11/12}(T_{11} - T_{12'}) + m_{13/14}(T_{13} - T_{14'})} \quad (3.60)$$

$$\eta_{compressor} = \frac{\sum\left(m \cdot c_p \Delta T_{isentropic}\right)}{\sum\left(m \cdot c_p \Delta T_{actual}\right)} = \frac{m_{1/2}(T_2 - T_1) + m_{3/4}(T_4 - T_3) + m_{5/6}(T_6 - T_5)}{m_{1/2}(T_{2'} - T_1) + m_{3/4}(T_{4'} - T_3) + m_{5/6}(T_{6'} - T_5)} \quad (3.61)$$

3.4 COMBINED CYCLE

Only four Combined Cycles are investigated. In this section, the system thermo-hydraulic design of the single-shaft direct Combined Cycle, without inter-cooling is discussed (H). Only Cycle H is discussed as a representative example. The methodology of Cycle G is a combination of the theory discussed in this section and section 3.3.2 – see 3.4.2.3 for more details on Cycle G and Cycle J.

- Cycle G: Single-shaft recuperative Brayton with inter-cooling
- Cycle H: Single-shaft Brayton without inter-cooling
- Cycle I: Indirect Single-shaft Brayton without inter-cooling
- Cycle J: Single-shaft recuperative Brayton without inter-cooling

3.4.1 Input

The input to the Brayton cycle is the same as mentioned in section 3.3.1. The input to the Rankine cycle is listed in Appendix 9.1 *Table 9.13*. The thermodynamic properties of water substance have been implemented using the thermodynamic property correlation of *Harr, Gallagher, and Kell, NBS/NRC Steam Tables, Hemisphere Publishing Co., 1984.*

In the former German nuclear process heat project the design provided an IHX between the reactor and the coal gasifier. The design had inlet/outlet temperatures of 950/293 °C on the primary side and 220/900 °C on the secondary side respectively. This temperature difference in the IHX of 50 °C (see *Table 8.17*) has been experimentally confirmed and was taken as reference value (Frohling et al, 2002). Over and above the IHX temperature difference, an additional pinch temperature of 10 °C was assumed. Typical approach temperatures for condensers vary between 15 °C and 20 °C. The minimum Rankine cycle temperature is limited by the available cooling temperature of 18 °C. The minimum condenser temperature is 35 °C, choosing an approach temperature of 17 °C. In advanced coal-fired steam plants, supercritical steam parameters (up to 300 bar and 600 °C) are applied. We have chosen a maximum live steam temperature of 540 °C as a reference, and a live steam pressure of 180 bar. The maximum steam pressure for all the steam cycles are fixed at 180 bar, while the maximum steam temperature may be below 540 °C, depending on the Brayton cycle. Normally the quality of the exhaust steam should not be lower than 85% (Frohling et al, 2002), conservatively we set the maximum condenser quality to 88%. The isentropic efficiency of an optimized steam turbine is 90% for an advanced power plant (Frohling et al, 2002). We set the steam turbine isentropic efficiency to 89%. According to manufacturers information the overall efficiency of the feed-water pump can be 75-85% according to the size. Optimistically we chose a pump efficiency of 85%. The pressure losses in the water piping were ignored. The pressure loss in both the steam-generator and re-heater are assumed to be 3% of the inlet pressure.

3.4.2 Design methodology

The t-s diagrams and more importantly the numbering for all the Combined Cycles are presented in *Figure 3.25* and *Figure 3.26*. See Chapter 1 for the schematic layout of all four Combined Cycles.

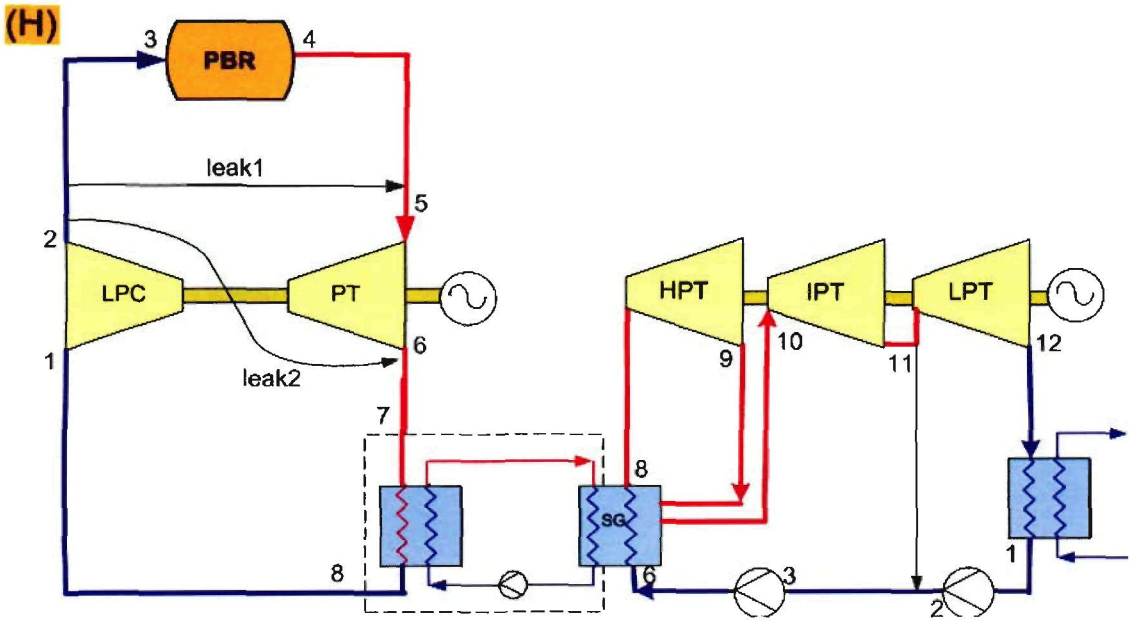


Figure 3.25 *Cycle layout - Cycle H*

3.4.2.1 Brayton

Discussion and numbering – see Cycle H *Figure 3.25:*

Low-pressure Compressor (LPC)

The maximum cycle pressure and the total pressure ratio over all the compressors (PR) are specified; therefore the minimum cycle pressure (3.63) is calculated. The LPC inlet temperature is not known. It can not be fixed as with the standard Brayton cycles, but needs to be solved. The reactor inlet temperature (RIT) is optimized to ensure both a possible fit with the steam cycle and to identify the maximum Combined Cycle efficiency (see section 3.4.2.3). For a fixed RIT (3.65), the LPC inlet temperature (3.66), inlet density (3.67) and outlet density (3.68) are calculated. The diffuser outlet pressure (3.69) based on the axial velocity is calculated.

The maximum cycle temperature (3.71) is specified as fixed input.

All the pressures and temperatures at points 1, 2 and 3 have been calculated. At point 4 only the temperature is known.

The next step is to solve the pressure drop through the reactor. The pressure drop is defined by:

$$p_4 = p_3 - \frac{k_{PBMR}\, mflow^2}{(rho_4 + rho_3)/2}.$$

At this stage, neither rho_4 nor the mass flow is known. Since the mass flow is unknown at this stage, a value will be assumed, then calculated and later updated with the newly calculated value.

assume: $p_4 = p_3$ (initial guessed value)

assume: mflow = 330 (initial guessed value)

Reactor

The reactor inlet density (3.72) is calculated. The assumed value for p_4 is used to calculate the reactor's outlet density (3.73). The pressure drop over the reactor (3.74) is calculated by using the

assumed mass flow. Lastly, the pressure loss over the reactor outlet pipe (3.75) is calculated.

Pressure losses

The assumed percentages for the pressure losses over the heat exchangers and piping are used to calculate the pressures at points 8 (3.76) and 7 (3.77).

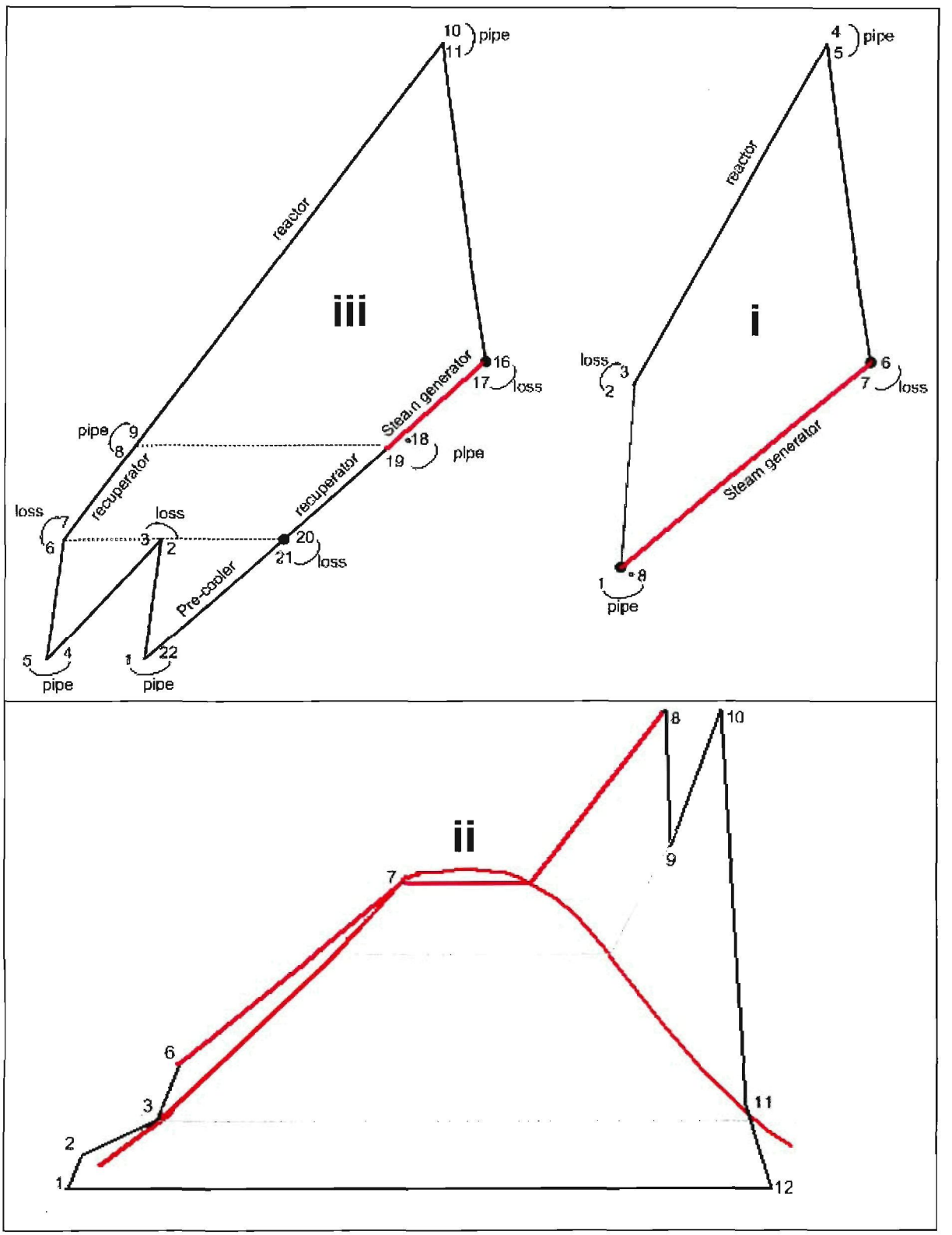


Figure 3.26 *T-s diagram i) Cycle H & I Brayton ii) Cycles G,H,I Rankine iii) Cycle G Brayton*

Leak flow 1 is extracted from point 2 and mixes with t_4 to produce t_5 (3.79).

Power Turbine

The pressure loss over the power turbine diffuser is defined by: $p_6 = p_7 + k_{turb}\left(\frac{1}{2} rho_6 \cdot V_{PT}^2\right)$

The initial guessed value for p_{16} is assumed to be: $p_6 = p_7 / lossfact1$

Since both p_6 and t_6 are still unknown, rho_{16} is not known and therefore the power turbine outlet pressure (p_6) will need to be solved for iteratively. An initial value for p_6 is assumed. With p_6 fixed, t_6 (3.80) and rho_{16} (3.81) are calculated. A new updated value for p_{16} (3.82) can now be calculated. With this newly calculated value for p_{16}, the process is repeated until convergence.

Leak flow 2 is extracted from point 2 and mixes with t_6 to produce t_7 (3.85).

Work output

The work output per unit mass flow of the power turbine is calculated with Eq. (3.87)

Mass flow

The heat input per unit mass flow (3.86) is calculated after which the mass flow (3.90) can be calculated, using the fixed power level input. Remembering that the mass flow was initially assumed to calculate the pressure loss through the reactor, this mass flow needs to be updated and all calculations from the reactor pressure loss calculation onwards need to be repeated. This will be done until the solution converges. The assumed value for p_4 was re-calculated with Eq. (3.83). All pressures and temperatures from points 1 through 8 have now been solved.

The mass flow of the Brayton cycle, t_7 and t_8 determines the heat available for the steam cycle. The steam cycle needs to be custom designed to fit between t_7 and t_8. The steam fitting is explained in the next section.

3.4.2.2 Rankine

The steam cycle needs to be custom designed to fit in between $t_{7\text{-Brayton}}$ and $t_{8\text{-Brayton}}$. Both $t_{7\text{-Brayton}}$ and $t_{8\text{-Brayton}}$ fall 50 °C to temperatures t10g and t6g respectively – see *Figure 3.27*. From temperatures t7g and t8g, both temperatures fall 10 °C (pinch temperature) to t_7 and t_8 respectively.

***Discussion and numbering – see Cycle H** Figure 3.27:*

The minimum cycle temperature (3.91) is set to the condenser temperature. The maximum cycle temperature (3.92) is equal to the Brayton temperature ($t_{7\text{-Brayton}}$) minus the IHX temperature difference minus the pinch temperature. The maximum steam temperature is calculated, but is limited to 540 °C (3.93).

Condenser Inlet

The condenser inlet quality (3.94) is specified. The condenser inlet enthalpy (3.95) and pressure (3.96) are interpolated from the steam data by specifying the inlet temperature and quality.

IPT inlet: iterate: p_{10}

Next, the IPT inlet pressure needs to be solved. To solve p_{10}, points 10 and 12 are connected to operate as one turbine (although there are in fact two turbines). The pressure (3.97) is solved iteratively. Since p_{12}, p_{10} and t_{10} are known, the turbine efficiency from points 10 to 12 can be calculated (3.101). The pressure (p_{10}) is varied until the calculated efficiency equals the actual specified turbine efficiency.

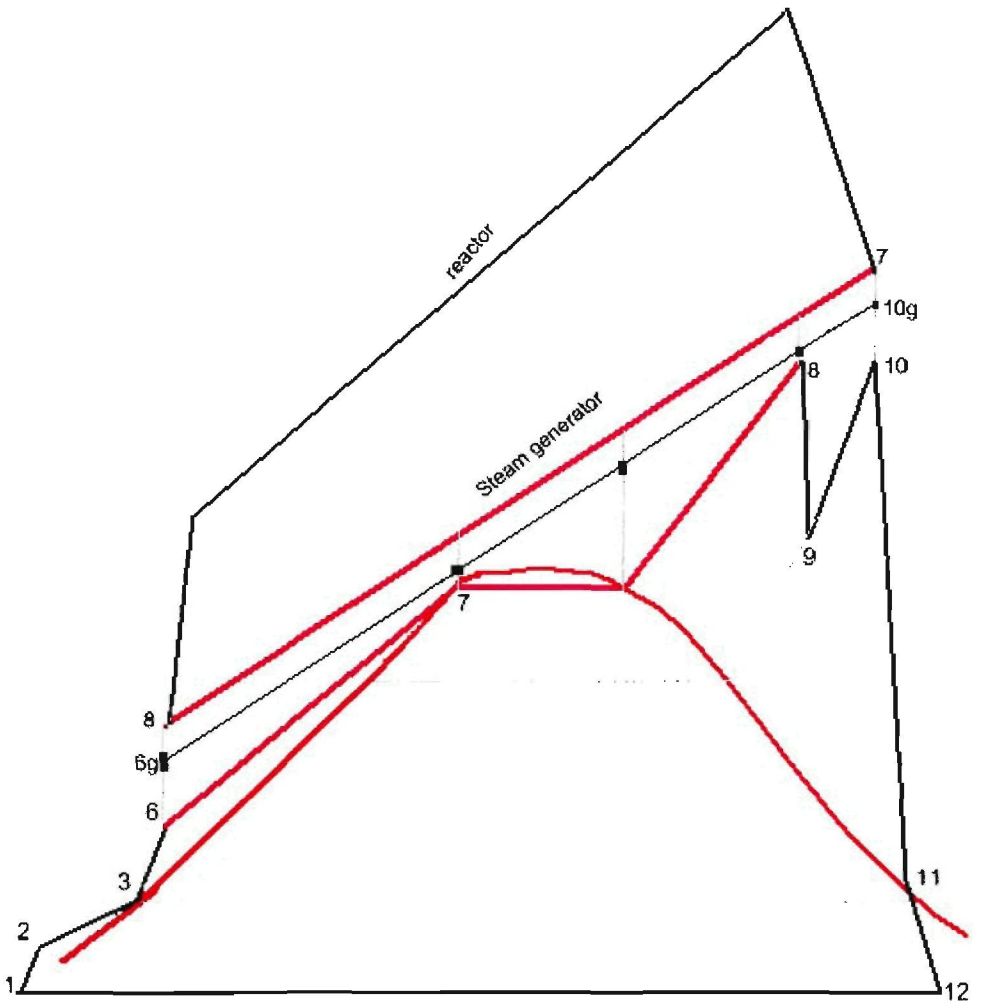


Figure 3.27 *T-s diagram for Brayton & Rankine cycle – Cycles H & I*

Pressures

The HPT outlet pressure (3.102) is calculated by assuming a 3% pressure loss through the re-heater. P_8 (3.103) is set equal to the maximum steam pressure. The steam generator inlet pressure (3.104) is calculated by assuming a 3% pressure loss through the steam-generator.

Steam-generator saturation

The steam generator saturated enthalpy (3.106), entropy (3.107) and temperature (3.108) at a quality of 0 is calculated.

HPT inlet temperature: iterate t_8

At this stage t10g, t_{10}, tg7 and t_7 are known. It is clear that

$$\left[(h_{10}-h_9)+(h_8-h_7)\right]\cdot ms = mflow_{Brayton}Cp_{Brayton}\left[(t_{7-Brayton}-dT_{IHX})-(t_7+t_{PINCH})\right].$$

This relationship is used to first solve for the steam mass flow (3.119), and secondly for t_8 (3.122). For all the relations, see equations (3.110) through (3.122)

Steam generator

The steam generator inlet enthalpy (3.123) is calculated from Eq. (3.62). The steam generator inlet temperature (3.124) is interpolated from the steam data from the specified pressure and enthalpy. Lastly, tg6 (3.125) is calculated.

$$ms \cdot (h_7 - h_6) = (tg_7 - (t_{8,Brayton} - dT_{IHX}))mflow_{Brayton} Cp \quad (3.62)$$

LPT outlet

Equations (3.126), (3.127) and (3.128) are used to calculate the condenser outlet conditions.

HP pump inlet pressure: iterate p_3

The steam generator inlet temperature t_6 was calculated in order to fit the steam cycle between Brayton temperatures $t_{7\text{-}Brayton}$ and $t_{8\text{-}Brayton}$. The pressure at point 3 needs to be calculated to ensure that point 6 equals t_6. P_3 is varied until point 6 equals t_6. See equations (3.129) to (3.132). Next, the LP pump outlet enthalpy (3.133) can be calculated.

IPT

The IPT outlet pressure (3.134) and enthalpy (3.136) are calculated next.

Cycle G: Pre-heating

Additional Pre-heating is used in Cycle G, where heat from the Brayton pre-cooler is used to pre-heat the water before entering the steam-generator – see equations (3.138) to (3.142).

Bleed-off flow

The bleed-flow (3.143) required to produce t_3 (and by implication t_6) is calculated.

Lastly t_{12} (3.144), t_1 (3.145), t_{11} (3.146) and t_9 (3.147) are calculated.

3.4.2.3 Optimization

Steam fit

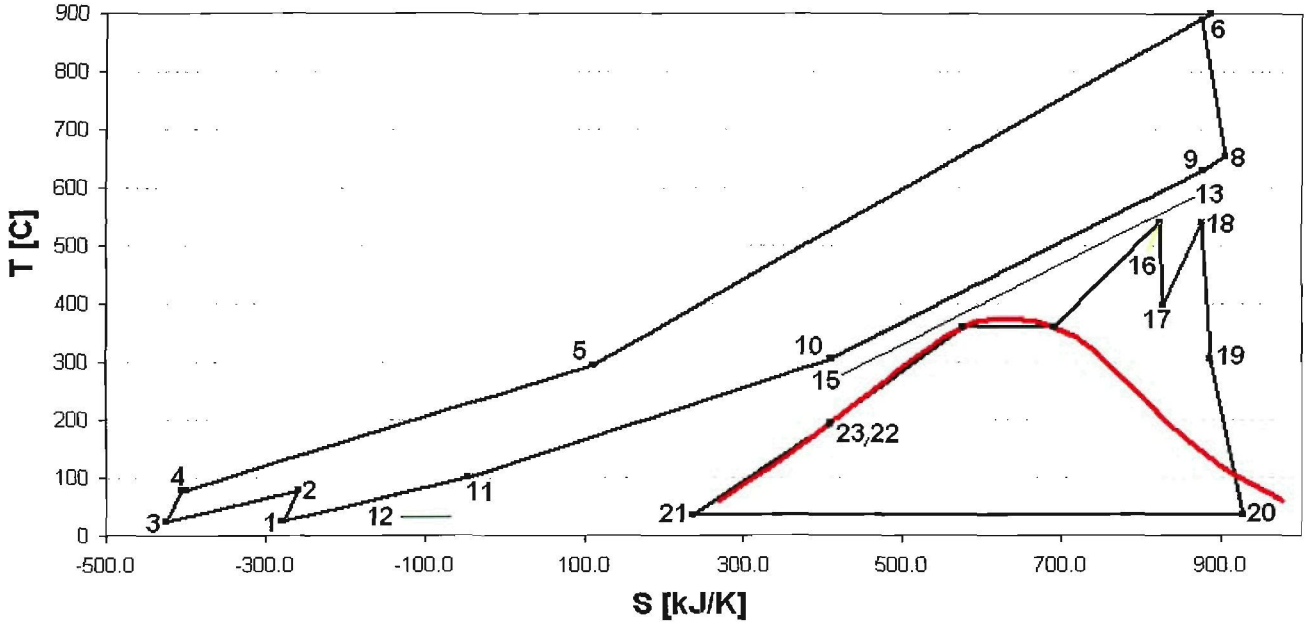
For all the Combined Cycles (G, H, I, J) the exact correct bleed-off pressure (3.129) need to be identified which will enable the exact correct bleed-off flow (3.143) to pre-heat the LP pump's outlet temperature (3.139) in order to arrive at the required steam generator inlet temperature (3.124).

Both Cycle G and Cycle J first use heat from the Brayton cycle to pre-heat the Rankine cycle. The flow from after the LP pump's outlet (T_a) is heated by the Brayton cycle to temperature T_b before the bleed-off flow is extracted from the turbines. The bleed-off flow heats the water from T_b to T_{22} in order to arrive at the required temperature, T_{23}. See *Figure 3.28* for the discussion to follow (only applicable to Cycle G and Cycle J). The hot helium leaving the PBR (6) expands through the LPT (6-8) that drives both the LPC (1-2) and HPC (3-4). The helium flow is then cooled in the IHX (9-10) to temperature T_{10}. Temperature T_{10} is determined by the reactor inlet temperature. The IHX rejects all its heat to the steam plant through the steam generator (23-16-17-18). After the IHX (9-10), the helium is further cooled down in the recuperator (10-11) to temperature T_{11}. The Rankine cycle is preheated from T_a to T_b. Temperature T_b equals temperature T_{11}-10 °C. The energy required to heat the Rankine cycle from T_a to T_b is calculated. This calculated energy is subtracted from T_{11} to arrive at temperature T_{12}. The heat is rejected from T_{12} to the minimum cycle temperature in the pre-cooler (12-1). The flow enters the LPC (1-2), between which it is inter-cooled and finally passes through the recuperator (4-5) before entering the PBR (5).

The hot steam leaving the steam generator (16) passes through the high pressure steam turbine (16-

17), after which the steam is re-heated (17-18) in the steam generator. The flow then passes through both the intermediate-pressure (18-19) and low-pressure (19-20) steam turbines. Next, the flow enters the condenser (20-21), passes through the low-pressure pump (21-a) and is then pre-heated from points a to b by utilising the heat from the Brayton cycle (T_{11}). After the water has been pre-heated from points a to b, bleed-flow is extracted from point 19 in order to further pre-heat the water from points b to 22 before entering the high pressure pump (22-23) and returning to the steam generator (23).

For a given reactor inlet temperature, the challenge is to custom fit the Rankine cycle between points 9 and 10 – see *Figure 3.28* . Temperatures 23, 16 and 18 were calculated to minimize the lost work between the Brayton and the Rankine cycle and also to ensure that the steam generator does not pinch. For a given reactor inlet temperature, temperatures 23, 16 and 18 are calculated. Next, the Rankine cycle was optimised to exactly fit between temperatures 23, 16 and 18 by calculating the correct Rankine pressure levels, Rankine bleed-off flows and Brayton pre-heating. The reactor inlet temperature determines the fraction of work that is done by the Brayton and Rankine cycle respectively. The reactor inlet temperature was optimised in order to identify the maximum combined efficiency at each pressure ratio.



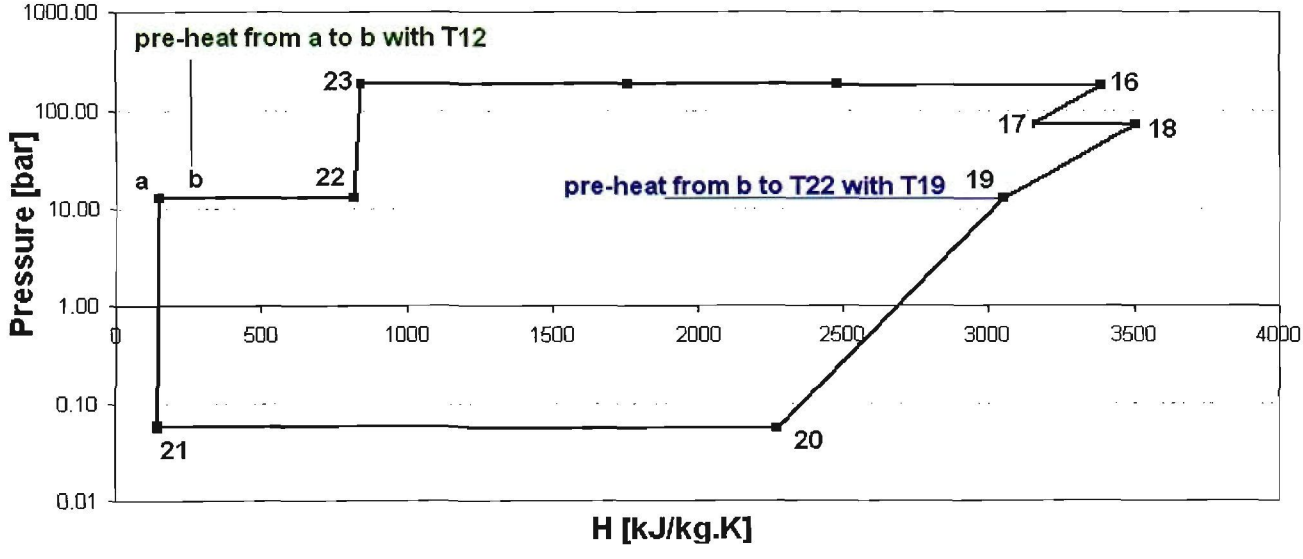


Figure 3.28 *T-s diagram and p-h diagrams for Cycle G at 600 MW and pressure ratio 2.1.*

Reactor inlet temperature (RIT)

It was mentioned in the previous section how the RIT is optimized for Cycle G and Cycle J. *Figure 3.30* shows the work output separately for the Brayton (Combined) and Rankine (Combined) cycle. It is seen that the Rankine work output slightly decreases with increasing pressure ratio. The Brayton work output first increases and then decreases with increasing pressure ratio. The maximum Rankine work is at a lower pressure ratio than the maximum Brayton work. The question arises as to what pressure ratio results in the highest combined efficiency. The RIT is the parameter that determines the ratio of work that is done by the Brayton versus the Rankine. The combined efficiency was calculated over a large range of RIT's and the RIT corresponding with the highest combined efficiency was identified as that pressure ratios optimized RIT. *Figure 3.30* shows the results of the optimized RIT. At low pressure ratios the Rankine cycle is more efficient and therefore a larger fraction of work needs to be done by the Rankine and therefore the low RIT. At higher pressure ratios, a larger fraction of work needs to be done by the Brayton and therefore the larger RIT.

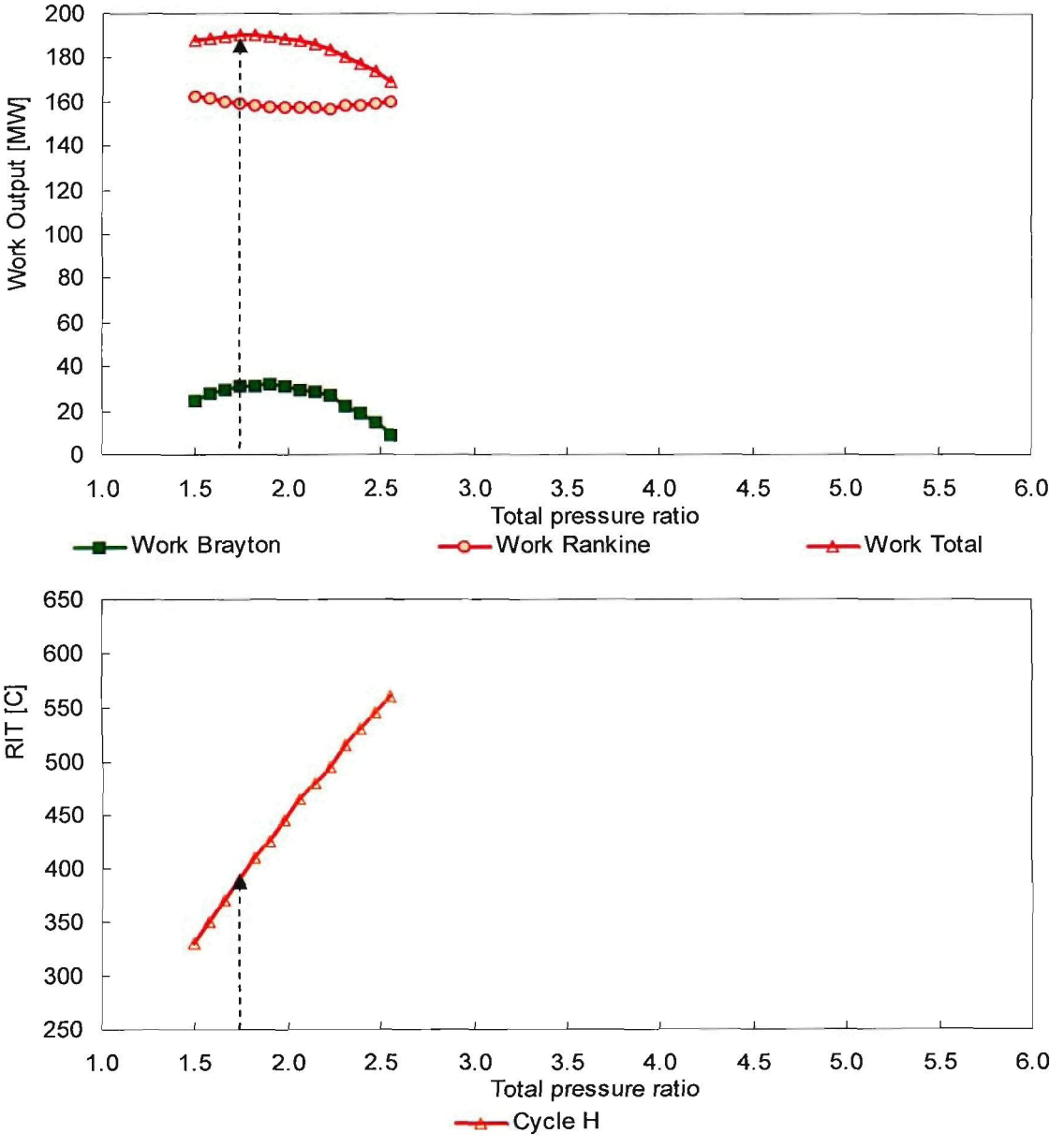


Figure 3.29 *Work output and RIT for Combined Cycle H – Brayton and Rankine separately*

Figure 3.30 shows how the thermal cycle efficiency is influenced by the RIT at a fixed pressure ratio. The pressure ratio of Cycle G was fixed at 2.4, Cycle H at 1.8, Cycle I at 1.8 and Cycle J at 2.1. It is clear from *Figure 3.30* that certain RIT's will not yield any solution and therefore one needs to operate within a fixed envelope of RIT's in order to get optimum results.

For Cycle H, the optimum RIT is 400 °C. See *Figure 3.31* for both the thermal efficiency and optimized RIT versus pressure ratio for all the Combined Cycles. See Chapter 6 for more results.

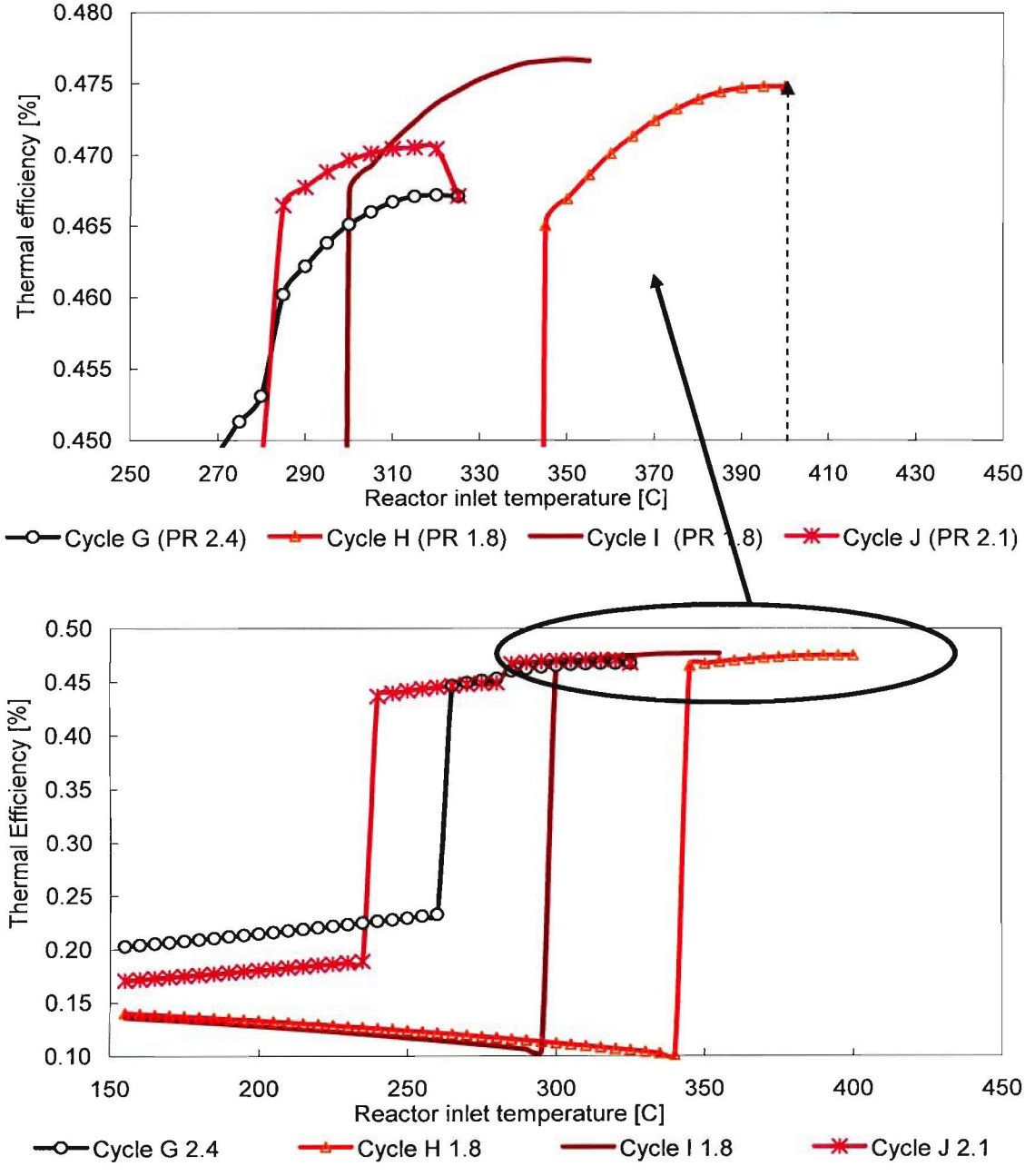


Figure 3.30 *Thermal efficiency of Cycles G, H, I and J for various RIT's at a fixed pressure ratio*

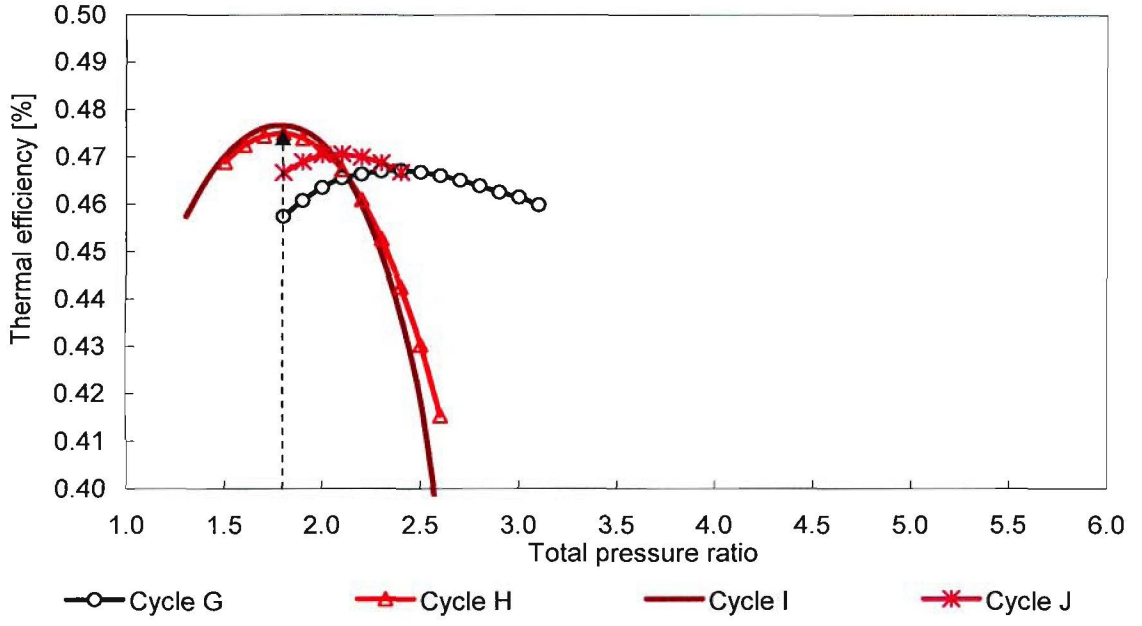


Figure 3.31 *Thermal efficiency vs. pressure ratio*

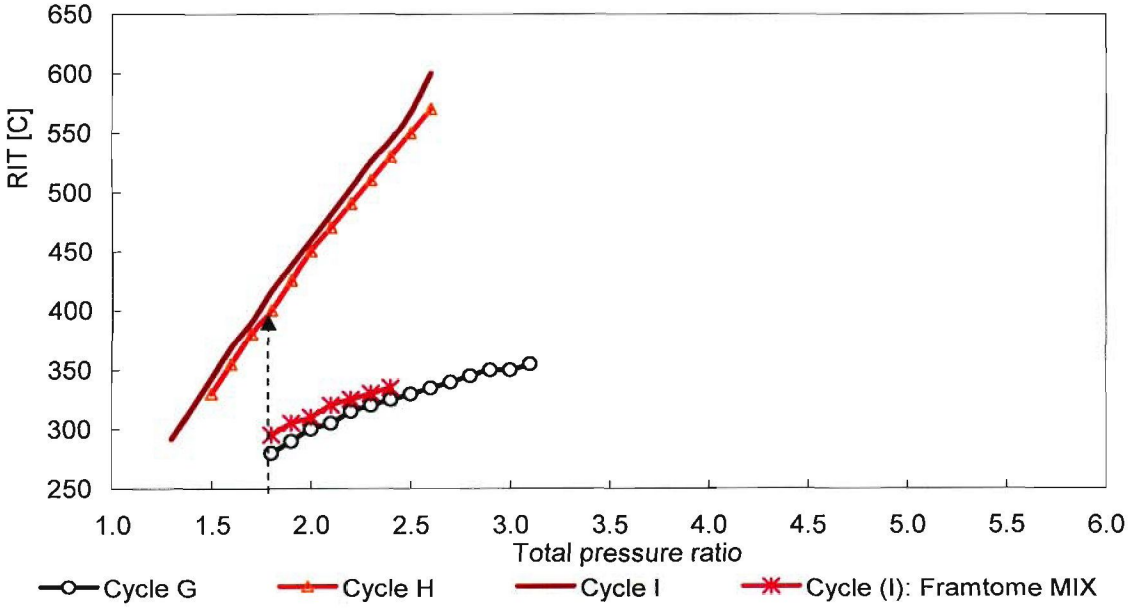


Figure 3.32 *Optimised RIT vs. pressure ratio*

3.4.3 Design equations

3.4.3.1 Brayton (only Cycle H and I)

All pressures referred to are total pressures

$input:\ \eta_c,\ \eta_t,\ C_{a,c},\ C_{a,t}$

$input:\ t_{\max}, p_{\min}, p_{\max}, PBR, k_{PBMR}, k_{comp}, k_{turb}, dT_{IHX}, \%dP_{HXs},\ \%dP_{PIPING}, \eta_{blower}, \eta_{mechanichal}$

$optimize: RIT$

LPC	$p_1 = \frac{p_{\max}}{pr}$	(3.63)
	$p_2 = p_1 \cdot pr$	(3.64)
	$t_2 = RIT$	(3.65)
	$t_1 = t_2 / \left(1 + \frac{1}{etac_{LP}}\left[\left(\frac{p_2}{p_1}\right)^{(\gamma-1)/\gamma} - 1\right]\right)$	(3.66)
	$rho_1 = \frac{p_1}{t_1 R}$	(3.67)
	$rho_2 = \frac{p_2}{t_2 R}$	(3.68)
	$p_3 = p_2 - k_{comp}(\frac{1}{2} rho_2 {V_{LPC}}^2)$	(3.69)
	$t_3 = t_2$	(3.70)
Reactor	$t_4 = t_{hot}$	(3.71)
ITERATIVE LOOP (blue indent)	The pressure drop through the reactor is defined by: $p_4 = p_3 - \frac{k_{PBMR} mflow^2}{(rho_4 + rho_3)/2}$ assume: $p_4 = p_3$ (initial guessed value) assume: mflow = 330 (initial guessed value)	
Reactor	$rho_3 = \frac{p_3}{t_3 R}$	(3.72)
	$rho_4 = \frac{p_4}{t_4 R}$	(3.73)
	$p_4 = p_3 - \frac{k_{PBMR} mflow^2 (1 - leak1 - leak2)^2}{(rho_4 + rho_3)/2}$	(3.74)
	$p_5 = lossfact1 * p_4$	(3.75)
Pressures	$p_8 = p_1 / lossfact1$	(3.76)
	$p_7 = p_8 / lossfact2$	(3.77)
	$p_6 = p_7 / lossfact1$ (initial guessed value)	(3.78)
Mixing flow	$t_5 = \frac{t_4 (1 - leak1 - leak2) + t_2\ leak1}{1 - leak2}$	(3.79)

ITERATIVE LOOP (red indent) *Power Turbine*	{	
	$t_6 = t_5 - t_5 etat_{PT}\left[1 - \left(\frac{p_6}{p_5}\right)^{(\gamma-1)/\gamma}\right]$	(3.80)
	$rho_6 = \frac{p_6}{t_6 R}$	(3.81)
	$p6 = p_6$	(3.82)
	$p_6 = p_7 + k_{turb}\left(\frac{1}{2} rho_6 \cdot V_{PT}^{\ 2}\right)$	(3.83)
	$\}\ while\left(fabs\frac{p6 - p_6}{p_6}\right) > 1.0e-8$	(3.84)
Mixing Flow	$t_7 = t_6(1-leak2) + t_2\ leak2$	(3.85)
Heat	$heat = (1-leak1-leak2)\cdot Cp\cdot(t_4 - t_3)$	(3.86)
Work output	$work = Cp\cdot(t_5 - t_6)\cdot(1-leak2)\cdot eta_{mech} - Cp\cdot(t_2 - t_1)$	(3.87)
	$t_8 = t_1$	(3.88)
Mass flow	$massflow = mflow$	(3.89)
	$mflow = \frac{PBMR}{heat}$	(3.90)
	$\}\ while\left(fabs\frac{massflow - mflow}{mflow}\right) > 1.0e-8$	
Intermediate Loop	See coding	
Rankine	SolveRankine(.....), See section 3.4.3.2	

3.4.3.2 Rankine

All pressures referred to are total pressures

input : $t_{\min}$, $t_{\max}$ >, $p_{\max}$, $\%dP_{RH}$, $\%dP_{SG}$, t_{PINCH}, CDx, $\eta_{turbine}$, η_{pump}

	$t_1 = t_{\min}$	(3.91)
	$t_{10} = t_{7-Brayton} - dT_{IHX} - t_{PINCH}$	(3.92)
	$t_{10} < 540^o C \quad \& \quad t_8 < 540^o C$	(3.93)
Condenser	$x_{12} = 0.88$	(3.94)
	$h_{12} = function(temperature, quality) \rightarrow t_1, x_{12}$	(3.95)
	$p_{12} = function(temperature, quality) \rightarrow t_1, x_{12}$	(3.96)
ITERATIVE LOOP: p_{10} (blue indent) *IPT*	**With Newton-Raphson:** Vary p_{10} until $\eta_{turbine}$ =89% for the given x_{12}.	
	$p_{10} = guessed\ value$	(3.97)
	$h_{10} = function(pressure, temperature) \rightarrow p_{10}, t_{10}$	(3.98)
	$s_{10} = function(pressure, temperature) \rightarrow p_{10}, t_{10}$	(3.99)
	$hs_{12} = function(pressure, entropy) \rightarrow p_{12}, s_{10}$	(3.100)
	$\eta_{turbine-NewtonRaphson} = \frac{h_{10} - h_{12}}{h_{10} - hs_{12}}$	(3.101)
	[see coding for complete Newton Raphson]	

Pressures	$p_9 = \frac{p_{10}}{\%dP_{RH}}$	(3.102)
	$p_8 = p_{\max}$	(3.103)
	$p_6 = \frac{p_8}{\%dP_{SG}}$	(3.104)
	$p_7 = p_6$	(3.105)
SGsaturation	$hsat_7 = function(pressure, quality) \rightarrow p_7, 0$	(3.106)
	$ssat_7 = function(pressure, quality) \rightarrow p_7, 0$	(3.107)
	$tsat_7 = function(pressure, quality) \rightarrow p_7, 0$	(3.108)
	$psat_7 = p_7$	(3.109)
ITERATIVE LOOP: t_8 (blue indent)	**Solve for t_8 by using $Q_{Brayton}$7-7g = $W_{Rankine}$10-9-8-7**	
HPT	$t_8 = guessed\ value$	(3.110)
	$h_8 = function(pressure, temperature) \rightarrow p_8, t_8$	(3.111)
	$s_8 = function(pressure, temperature) \rightarrow p_8, t_8$	(3.112)
	$hs_9 = function(pressure, entropy) \rightarrow p_9, s_8$	(3.113)
	$h_9 = h_8 - eta_{turbine}(h_8 - hs_9)$	(3.114)
	$x_9 = function(pressure, enthalpy) \rightarrow p_9, h_9$	(3.115)
SG saturation	$h_7 = function(pressure, quality) \rightarrow p_7, 0$	(3.116)
	$t_7 = function(pressure, quality) \rightarrow p_7, 0$	(3.117)
Heat balance	$q = (h_{10} - h_9) + (h_8 - h_7)$	(3.118)
	$ms = \frac{mflow_{Brayton} Cp_{Brayton} \left[(t_{7-Brayton} - dT_{IHX}) - (t_7 + t_{PINCH} \right]}{q}$	(3.119)
	$tg_8 = \left[\left(t_{7,Brayton} - dT_{IHX} \right) - \frac{ms \cdot (h_{10} - h_9)}{mflow_{Brayton} Cp_{Brayton}} \right]$	(3.120)
	$tg_7 = tg_8 - \frac{ms \cdot (h_8 - h_7)}{mflow_{Brayton} Cp}$	(3.121)
	Update	
	$t_8 = tg_8 - t_{PINCH}$	(3.122)
SG	$h_6 = h_7 - \frac{(tg_7 - (t_{8,Brayton} - dT_{IHX}))mflow_{Brayton} Cp}{ms}$	(3.123)
	$t_6 = function(pressure, enthalpy) \rightarrow p_6, h_6$	(3.124)
	$tg_6 = tg7 - \frac{ms(h_7 - h_6)}{mflow_{Brayton} Cp}$	(3.125)
LPT	$p_1 = p_{12}$	(3.126)
	$h_1 = function(pressure, quality) \rightarrow p_1, 0$	(3.127)
	$v_1 = function(pressure, quality) \rightarrow p_1, 0$	(3.128)
	Test whether steam plant fit Brayton...see coding	
ITERATIVE LOOP: p_3	**With Newton-Raphson:** Vary p_3 to find $frac_2$ so that h6=h_6	

(blue indent) *HP Pump*	$p_3 = guessed\ value$	(3.129)
	$h_3 = function(pressure, quality) \rightarrow p_3, 0$	(3.130)
	$v_3 = function(pressure, quality) \rightarrow p_3, 0$	(3.131)
	$h_6 = h_3 + \frac{v_3(p_6 - p_3)}{\eta_{pump}}$	(3.132)
	$h_2 = h_1 + \frac{v_1(p_3 - p_1)}{\eta_{pump}}$	(3.133)
IPT	$p_{11} = p_3$	(3.134)
	$hs_{11} = function(pressure, entropy) \rightarrow p_{11}, s_{10}$	(3.135)
	$h_{11} = h_{10} - \eta_{turbine}(h_{10} - hs_{11})$	(3.136)
*Only applicable to **Cycle G*** **ITERATIVE LOOP: pre-heating** **(red indent)**	$p_2 = p_3$	(3.137)
	$t_2 = function(pressure, enthalpy) \rightarrow p_2, h_2$	(3.138)
	$t_3 = function(pressure, quality) \rightarrow p_3, 0$	(3.139)
	$t2a = t_{20-Brayton} - t_{PINCH}$	(3.140)
	$cpw = function(pressure, temperature) \rightarrow p_2, t_2$	(3.141)
	Check whether $t_3 > t2a$.. If yes,	
	$h2a = h_2 + cpw(t2a - t_2)$	(3.142)
Bleed-off flow	$frac2 = \frac{h_3 - h2a}{h_{11} - h2a}$	(3.143)
	$t_{12} = function(pressure, quality) \rightarrow p_{12}, x_{12}$	(3.144)
	$t_1 = function(pressure, quality) \rightarrow p_1, 0$	(3.145)
	$t_{11} = function(pressure, enthalpy) \rightarrow p_{11}, h_{11}$	(3.146)
	$t_9 = function(pressure, enthalpy) \rightarrow p_9, h_9$	(3.147)

For Cycle H, the work output per unit mass flow for the Brayton cycle is defined as:

$$w_{Brayton} = Cp \cdot (t_5 - t_6) \cdot (1 - leak2) \cdot eta_{mech} - Cp \cdot (t_2 - t_1) \quad (3.148)$$

For Cycle H, the work output per unit mass flow for the Rankine cycle is defined as:

$$w_{Rankine} = [ms \cdot (h_8 - h_9 + (h_{10} - h_{11}) + (1 - frac_2)(h_{11} - h_{12}))] - [ms \cdot ((1 - frac_2)(h_2 - h_1) + (h_6 - h_3))] \quad (3.149)$$

For Cycle H, the Brayton thermal efficiency of the plant is defined as:

$$\eta_{Brayton} = \frac{w_{Brayton}}{heat_{Brayton}} = \frac{Cp \cdot (t_5 - t_6) \cdot (1 - leak2) \cdot eta_{mech} - Cp \cdot (t_2 - t_1)}{(1 - leak1 - leak2) \cdot Cp \cdot (t_4 - t_3)} \quad (3.150)$$

For Cycle H, the Rankine thermal efficiency of the plant is defined as:

$$\eta_{Rankine} = \frac{w_{Rankine}}{heat_{Rankine}} = \frac{[ms \cdot (h_8 - h_9 + (h_{10} - h_{11}) + (1 - frac2)(h_{11} - h_{12}))] - [ms \cdot ((1 - frac2)(h_2 - h_1) + (h_6 - h_3))]}{Cp(t_7 - t_8)} \quad (3.151)$$

For Cycle H, the Combined total thermal efficiency of the plant is defined as:

$$\eta_{Total} = \frac{W_{Total}}{PBR} = \frac{(mflow \cdot w_{Brayton} - w_{blower}) + ms \cdot w_{Rankine}}{PBR} \quad (3.152)$$

3.5 INDIRECT CYCLE

The secondary side (Brayton) of the indirect cycles is solved in the same manner as explained in the previous sections. This section will focus on the indirect cycle primary side solution. In the primary loop, one aims to solve for the mass flow and blower size. The primary side mass flow will directly determine the secondary side mass flow and the blower size will impact the thermal efficiency of the cycle. The following variables are given as input to the calculation (see *Table 6.9* and *Table 9.14*):

$t_{max}, PBR, k_{PBMR}, dT_{IHX}, \%dP_{HXs}, \%dP_{PIPING}, \eta_{blower}, \gamma_{He}, R_{He}, k_{He}, \gamma_{N2}, R_{N2}, k_{N2}, \gamma_{MIX}, R_{MIX}, k_{MIX}$.

The following values are known from the secondary side cycle analysis:

p_9 = IHX inlet pressure

t_9 = IHX inlet temperature

p_{10} = IHX outlet pressure

t_{10} = IHX outlet temperature

The following values are fixed for the primary side analysis.

p_1 = p9

t_3 = t_{10} + dT_{IHX}

t_4 = t_9 + dT_{IHX}

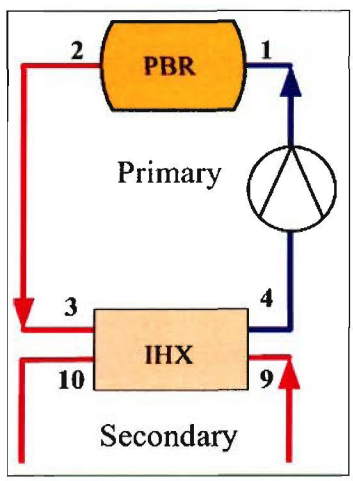


Figure 3.33 *Numbering used for all indirect cycles*

The mass flow (secondary and primary) and blower power need to be solved for iteratively. For initial guessed values, the following values are assumed for Q_{IHX}, p_2, t_1 and the mass flows:

Q_{IHX}	= PBR power	(initial guessed value)
p_2	= p_1	(initial guessed value)
t_1	= t_4	initial guessed value)

Mass flow (secondary) = $\frac{PBR}{Cp(t_{10} - t_9)}$ (initial guessed value)

Mass flow (primary) = $\frac{m_{secondary}(1 - leak1 - leak2) \cdot Cp_{secondary}}{Cp_{primary}}$ (initial guessed value)

note: *it is assumed that* $(m \cdot Cp)_{primary} = (m \cdot Cp)_{secondary}$

To start with, p_1 is known and an initial guessed value for t_1 is known. The value for t_2 is known and an initial guessed value for p_2. From these four values, the reactor inlet and outlet density is calculated. Using the assumed mass flow (primary), a new value can be calculated for p_2:

$$p_2 = p_1 - \frac{K_{PBMR} mflow^2}{(rho_1 + rho_2)/2}.$$

t_2 is equal to t_3 and p_3 is calculated with $p_3 = p_2 \cdot lossfact1$. p_4 is calculated with $p_4 = p_3 \cdot lossfact2$. A new value for t_1 can now be calculated using the blower equation:

$$t_1 = t_4 + \frac{t_4}{\eta_{blower}}\left[\left(\frac{p_1}{p_4}\right)^{(\gamma-1)/\gamma} - 1\right]$$

With a new value for t_1, the primary side mass flow can be updated:

$$m_{primary} = \frac{Q_{PBR}}{Cp_{primary}(t_2 - t_1)}$$

A new value for the IHX power can now be calculated:

$$Q_{IHX} = m_{primary} \cdot Cp(t_3 - t_4).$$

All this is repeated until the calculated value for the primary side mass flow converges. Next, with the converged solution, the secondary side mass flow is updated; after which the primary side mass flow can again be calculated.

$$m_{secondary} = \frac{Q_{IHX}}{Cp_{secondary}(t_{10} - t_9)}$$

$$m_{primary} = \frac{m_{secondary}(1 - leak1 - leak2) \cdot Cp_{secondary}}{Cp_{primary}}$$

With p_2, t_1, Q_{IHX} and the mass flows updated, the entire process is repeated again until convergence.

The blower power is given by:

$$Q_{Blower} = m_{primary} Cp_{primary}(t_1 - t_4) \quad (3.153)$$

The work output per unit mass flow for the Brayton cycle is defined as:

$$work = Cp_{secondary}(t_{13} - t_{16}) \cdot (1 - leak2) \cdot eta_{mech} - cp_{secondary}(t_2 - t_1) \quad (3.154)$$

The thermal efficiency of the plant is defined as:

$$\eta_{TOTAL} = \frac{work \cdot m_{secondary} - Q_{Blower}}{PBR} \quad (3.155)$$

3.6 HYDROGEN PLANT

This section only documents the input and theory used to calculate the co-generation plant efficiency. The results and conclusions are presented in Chapter 6. The hydrogen plant requires 50 MWth heat, provided by the SIHX. Four questions arise:

- Should the Secondary IHX be in series or parallel with the Primary IHX?
- What are the practicalities and efficiency associated with both?
- What is the co-generation efficiency?
- Does this efficiency merit a co-generation plant?

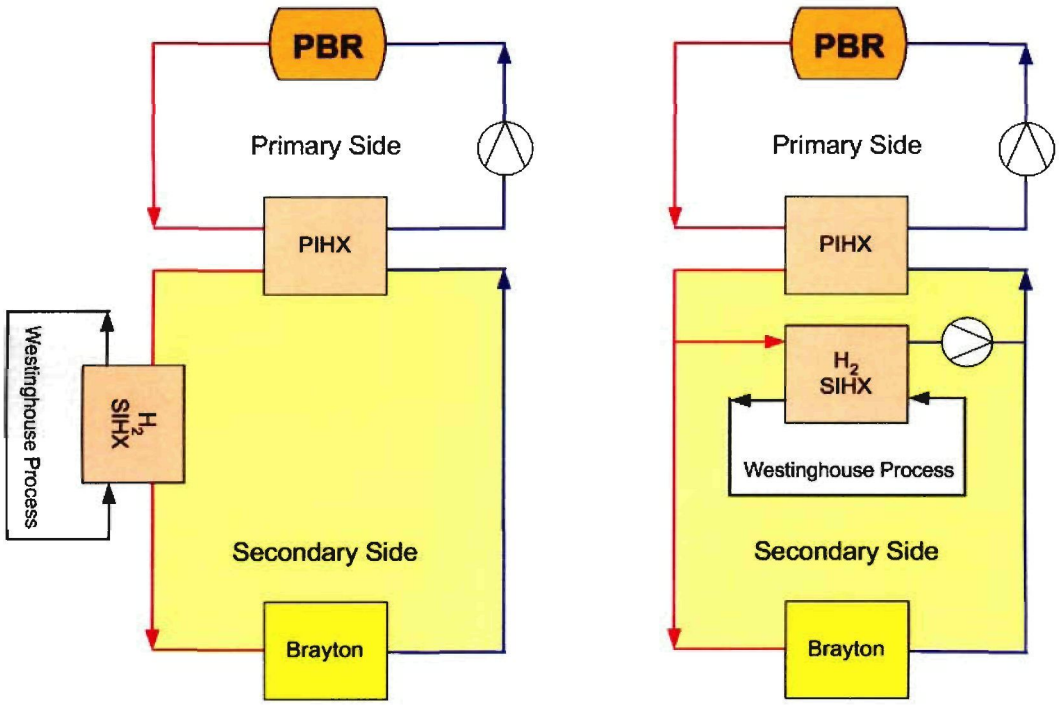


Figure 3.34 *Graphical representation of SIHX in series and parallel*

PBMR Pty. Ltd has joined a US-based Consortium led by Westinghouse Electric Company to bid for the INEEL project. The important parameters from **Error! Reference source not found.** for the calculations to follow are:

- Hydrogen plant process heat 900 °C.
- Hydrogen plant return-temperature 547 °C.
- Electric power needed for process
  - Electrolyser: 10.21 MWe
  - Pumps: 0.502 MWe

The Westinghouse Process efficiency is defined as:

$$\eta_{hydrogen} = \frac{LHV_{Hydrogen}}{50 + \frac{EE}{\eta_{cycle}}} \qquad (3.156)$$

where LHV = Lower heating value of hydrogen [MW_{th}]

EE = Electrical equipment [MWe]

η_{cycle} = Brayton thermal cycle efficiency [%]

Westinghouse quotes their process to be 45 % efficient. It was assumed that the PBR Brayton cycle is typically 42.5% efficient. From Eq. (3.156) it follows that $LHV_{hydrogen}$ equals 33.84 [MW_{th}]. The co-generation efficiency is defined as:

$$\eta_{total} = \frac{\left[W_{Brayton} - W_{Blower}\right] + \left[LHV_{Hydrogen} - EE\right]}{PBR} \tag{3.157}$$

The net output of the hydrogen plant is 23.1MW_{th}, resulting in a net hydrogen efficiency of $\frac{23.1}{50} = 46.2\%$.

3.7 GAS MIXTURE PROPERTIES

The choice of working fluid has a direct impact on the capital cost of the PCU components. The fluids under investigation are helium, nitrogen and a mixture of helium and nitrogen. Nitrogen is favourable from a turbo machine viewpoint, resulting in small machines because of a higher compressibility than helium (smaller gas constant). Helium is favourable from a heat exchanger viewpoint, resulting in small designs due to better heat transfer characteristics (large Cp value). The conductivity of the fluid has a direct impact on the heat exchanger heat transfer coefficient, which determines the size of the heat exchanger. The capital cost of each component for helium, nitrogen and the gas mixture is presented in Chapter 6. See *Table 9.14* for the fluid properties.

In this section the theory used to derive the gas properties for the gas mixture is presented. It was decided to use a gas mixture of 20% Helium and 80% Nitrogen. An 80% Nitrogen concentration will still allow conventional off-the-shelf air gas turbines to be used. The gas mixture can be described by a mass fraction and mole fraction of each component:

$$c_{He} = 20\% \tag{3.158}$$

$$c_{N2} = 80\% \tag{3.159}$$

$$y_{He} = \frac{\frac{0.2}{M_{He}}}{\frac{0.2}{M_{He}} + \frac{0.8}{M_{N2}}} = 0.636 \tag{3.160}$$

$$y_{N2} = \frac{\frac{0.8}{M_{N2}}}{\frac{0.8}{M_{N2}} + \frac{0.2}{M_{He}}} = 0.364 \tag{3.161}$$

where c = mass fraction

y = mole fraction

M_{He} = molecular weight of Helium - 4

M_{N2} = molecular weight of Nitrogen - 28

The molecular weight of the mixture becomes:

$$M_{MIX} = \gamma_{He} M_{He} + \gamma_{N2} M_{N2} = 12.736 \tag{3.162}$$

The gas constant for the mixture becomes:

$$R_{MIX} = \frac{\bar{R}}{M_{MIX}} = 652.8 \frac{J}{kgK} \text{ where } \bar{R} \text{ = ideal gas constant, } 8314.5 \frac{N \cdot m}{kmol \cdot K} \tag{3.163}$$

$$Cp_{MIX} = 0.2 \cdot Cp_{He} + 0.8 \cdot Cp_{N2} = 1873.6 \frac{J}{kg \cdot K} \tag{3.164}$$

where Cp_{He} = specific heat at constant pressure of Helium, $5200 \frac{J}{kg \cdot K}$

Cp_{N2} = specific heat at constant pressure of Nitrogen, $1042 \frac{J}{kg \cdot K}$

$$Cv_{MIX} = Cp_{MIX} - R_{MIX} = 1220.8 \frac{J}{kg \cdot K} \tag{3.165}$$

$$\gamma_{MIX} = \frac{Cp_{MIX}}{Cv_{MIX}} = 1.5347 \tag{3.166}$$

Thus, the fluid properties of the gas mixture are: $R_{MIX} = 652.8 \frac{J}{kgK}$; $Cp_{MIX} = 1873.6 \frac{J}{kg \cdot K}$; $\gamma_{MIX} = 1.5347$.

Chapter 4

Costing Models

In this chapter, the costing models used in this study are discussed and motivated.

4. COSTING MODELS

4.1 OVERVIEW

The order-of-magnitude plant cost is the main parameter used to compare the various cycle configurations. The order-of-magnitude plant cost is only a comparative value between the cycles and does not portray the absolute cost of the plant. The philosophy was to include only those component costs that will result in notable overall cost differences between the cycles. The order-of-magnitude plant cost is defined as the sum of all the major PCU component capital costs, the capital cost of the building, the capital cost of the reactor and the capital cost of the steam plant, minus the capitalized income due to the power output.

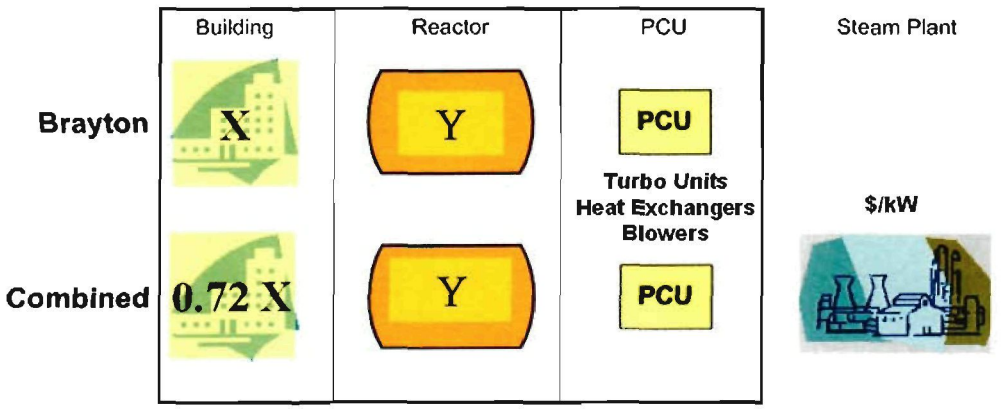


Figure 4.35 *Cost breakdown for Brayton and Combined Cycle*

The order-of-magnitude cost is defined as:

$$\left[C_{Turbo\ Units}+C_{Recuperator}+C_{IC}+C_{PC}+C_{Blower}+C_{IHX}+C_{Generator}+C_{SBS\&RB}\right]_{PCU}+C_{Building}+C_{Reactor}+C_{Steam\ Plant}-C_{Marginal\ Cost}$$

The capital cost of the generator, gearbox, start-up blower (SBS), resistor bank (RB), building and reactor was fixed. The steam plant is calculated from a given $/kW. The power output for each cycle was translated into a capitalised income resulting in a reduction in capital cost. This means that a higher cycle thermal efficiency or power level effectively reduces the order-of-magnitude plant cost ($C_{MarginalCost}$). The cost models used for the PCU are as follows (see next sections for more details):

$C_{TurboUnit}$: $\left(\left[K_{C1}r_t^2(z+4)\right]_{Compressor}+\left[K_{T1}r_t^2(z+4)\right]_{Turbine}\right)/(1-0.11)$

$C_{Recuperator}$: $K_{Recupeartor}\cdot A_{Recuperator}$

C_{IC}: $K_{IC}\cdot A_{IC}$

C_{PC}: $K_{PC}\cdot A_{PC}$

C_{Blower}: $MW_{Blower}+\frac{1}{2}$

C_{IHX}: $K_{IHX}\cdot A_{IHX}+Kbase_{IHX}$

The capital costs of the turbo machines, recuperator, inter-cooler (IC), pre-cooler (PC), intermediate heat exchanger (IHX) and blower are calculated using the cost models together with the proportionality constants (K) derived from PBMR design data. The costing formulas are postulated based on engineering judgement. The cost of each component will rather indicate a trend, than an absolute cost. See *Table 4.4* for an overview of the cost models and costs.

COMPONENT	COST FUNCTION	VARIABLE PBMR		REF.	COST m$	REF.	K*	Output
Turbo machines	$\frac{\left(\left[K_{C1}r_t^2(z+4)\right]_{Compressor}+\left[K_{T1}r_t^2(z+4)\right]_{Turbine}\right)}{1-0.11}$				m$ 8.00	S.E		
24%	$\left[K_{C1}r_t^2(z+4)\right]_{Compressor}$	r_t =	0.4719 m	[28] : p1-60	m$ 1.92		0.4311	$K_{C1}=0.4311$
		z =	16	[28] : p1-60	-		-	-
65%	$\left[K_{T1}r_t^2(z+4)\right]_{Turbine}$	r_t =	0.5640 m	[27]: p1-4	m$ 5.20		2.0400	$K_{T1}=2.0400$
		z =	4	[27]: p1-4	m$ 0.88		-	-
11%	Shaft & Bearings	-		-	-		-	-
Recuperator	$K_{Recupeartor}\cdot A_{Recuperator}$	$A_{Recuperator}$ =	31000 m^2	[24]	m$ 8.00	D.M	0.0002581	$K_{Recupeartor}=0.0002581$
Inter-cooler	$K_{IC}\cdot A_{IC}$	A_{IC} =	10193 m^2	[24]	m$ 0.75	D.M	0.0000736	$K_{IC}=0.0000736$
Pre-cooler	$K_{PC}\cdot A_{PC}$	A_{PC} =	10193 m^2	[24]	m$ 0.75	D.M	0.0000736	$K_{PC}=0.0000736$
Blower	$MW_{Blower}+\frac{1}{2}$	MW =	solve	-	-	D.M	-	Calculate $
IHX	$K_{IHX}\cdot A_{IHX}+Kbase_{IHX}$	A_{IHX} =	solve	Benched:	m$ 25.0	D.M	-	
	40 % material	K_{IHX} =	0.001255	7968 m^2			0.001255	$K_{IHX}=0.001255$
	60 % development	$Kbase_{IHX}$ =	15 m$	D.M	$15.0	D.M	15 m$	$Kbase_{IHX}=15$ m$
Generator	*fixed*				m$ 5.00	D.M		$C_{Generator\&Gearbox}$
Gearbox	*fixed*				m$ 1.00	D.M		
SBS	*fixed*				m$ 3.00	D.M		$C_{SBS\&RB}$
Resister Bank	*fixed*				m$ 3.80	D.M		
Building – Brayton	*fixed*				m$ 113	D.M		$C_{Building}$
Building – Combined	*fixed*				m$ 82	D.L		$C_{Building}$
Reactor	*fixed*				m$ 77	D.M		$C_{Reactor}$

COMPONENT	COST FUNCTION	VARIABLE PBMR	REF.	COST m$	REF.	K*	Output
Steam Plant	$a \cdot x + b$, *where* x = *net power* $[MW]$	a = 0.26 b = 24					*see graph*
Marginal Cost	$(W - 185) \cdot NCC \frac{\$}{kW}$	NCC = 2.0	Section 4.6				NCC

Table 4.4 *Costing Models*

4.2 POWER CONVERSION UNIT

4.2.1 Cost Models

4.2.1.1 Turbo machines

Data for the cost breakdown of turbo machines is not readily available due to the fact that manufacturers regard this information as important intellectual property. Therefore, the costing model used for the turbo machines could not be based on exact information. The compressor was assumed to contribute 24 % to the total turbo machine cost and the turbine 65 %. The remaining 11 % of the cost is attributable to the shaft and bearings. The reasoning behind this was that since the turbine blades need to withstand higher inlet temperatures, it would require more exotic materials and would therefore be more expensive. Furthermore, it was simply assumed that the cost of the compressor and turbine is directly proportional to the number of stages (z) and proportional to the square of the tip radius (r_t). The cost of the casing and other peripherals was accounted for by adding the cost of 4 *additional stages. The capital cost estimates and geometries of the PBMR preliminary low-pressure* turbo machine designs were used in order to arrive at realistic values for the proportionality constants K_{C1} and K_{T1}. The component models are used to determine the compressor and turbine tip radius and number of stages for each cycle configuration and at each specific operating point.

$$C_1 = C_{Compressor} + C_{Turbine} + C_{Shaft\&Bearings}$$

$$C_{Turbo\ Unit} = 0.24\ C_1 + 0.65\ C_1 + 0.11\ C_1$$

$$C_{Turbo\ Unit} = \left(\left[K_{C1} r_t^2 (z+4)\right]_{Compressor} + \left[K_{T1} r_t^2 (z+4)\right]_{Turbine}\right)/(1-0.11)$$

$C_{Compressor}$	= capital cost of compressor [m$]
$C_{Turbine}$	= capital cost of turbine [m$]
$C_{Shaft+Bearings}$	= capital cost of shaft and bearings [m$]
K_{C1}	= fixed constant (calculated from PBMR data) for compressor [-]
K_{T1}	= fixed constant (calculated from PBMR data) for turbine [-]
r_t	= tip radius [m]
z	= number of stages [-]

From the 3-shaft PBMR preliminary turbo machine designs found in documents (PBMR-MHI-035, 2003) and (PBMR-MHI-036, 2003), the values for the tip radius (r_t) and number of stages (z) for a particular machine is known. According to the system engineer, the LP turbo machine costs 8 m$.

K_{c1} = 0.4907 (see *Table 4.4*)

K_{T1} = 2.0400 (see *Table 4.4*)

The compressor and turbine component models will need to solve for:

r_t	= compressor tip radius [m]
z	= compressor number of stages [-]

r_t = turbine tip radius [m]

z = turbine number of stages [-]

For the turbine and compressor, the aim is to identify the design that will ensure the minimum turbo machine cost, using the costing formula as evaluation criteria. Optimizing the machine for minimum cost effectively means that one is trying to arrive at the smallest possible machine, while staying within all the design limitations.

4.2.1.2 Heat exchangers

The cost of the heat exchangers is assumed to be directly proportional to the heat transfer area. The constants, K, are calculated from the data obtained from the three-shaft PBMR design [24]. The component models are applied within the algorithm to determine the appropriate heat transfer area.

$$C_{Recuperator} = K_{Recupeartor} \cdot A_{Recuperator}$$

$$C_{IC} = K_{IC} \cdot A_{IC}$$

$$C_{PC} = K_{PC} \cdot A_{PC}$$

For the IHX, the development cost is also included, assuming that 40% of the total capital cost is attributed to material and 60 % to development costs. Only 40 % of the cost is scaled with the area.

$$C_{IHX} = K_{IHX} \cdot A_{IHX} + Kbase_{IHX}$$

It is clear that the heat exchanger models need to solve for:

$A_{Recuperator}$ = recuperator heat transfer area

$A_{Inter\text{-}cooler}$ = inter-cooler heat transfer area

$A_{Pre\text{-}cooler}$ = pre-cooler heat transfer area

A_{IHX} = IHX heat transfer area

4.2.1.3 Blower

The cost of the centrifugal blowers is assumed to be directly proportional to the blower size, offset by 0.5 MW.

$$C_{Blower} = MW_{Blower} + \frac{1}{2}$$

4.2.2 Fixed Costs

The capital costs for the generator, gearbox, SBS blower and the resister bank are fixed, based on estimates obtained from D.M.

4.3 BUILDING

The capital cost of the building (and balance of plant) for the Brayton cycles is fixed at 113 m$, based on best estimates obtained from D.M. The capital cost of the building (and BOP) for the Combined Cycle are presumed to be smaller. The capital cost of the steam plant will include the building cost for the steam plant. The capital cost of the Combined Cycle building is fixed at 82 m$, based on best estimates obtained from D.L and the DP2 project.

4.4 REACTOR

It is assumed that the same reactor is used for all the cycle configurations. The cost of the reactor is fixed at 77 m$, based on best estimates obtained from D.M.

4.5 STEAM PLANT

The following estimated costs for a steam plant with reheat were obtained from the Sargent&Lundy study for a turbine island in South Africa (SL-008277, 2004).

190 MWe	668 $/KW
400 MWe	387 $/KW
600 MWe	300 $/KW

Dated June 11, 2004 Rand : $ = 8,07:1.

The cost of 668 $/kW at 190 MWe is considered to be too expensive for a steam plant. The values below were considered to be more realistic [D.M].

Rather, the following values were assumed based on advice from Dieter Matzner:

190 MWe	387 $/KW
600 MWe	300 $/KW

Using these two points, the graph of *Figure 4.36* was constructed with the following equation:

$$C_{Steam} = 0.26 \cdot MW + 24$$

This equation was used to calculate the capital cost of the Rankine cycle portion of the Combined Cycles.

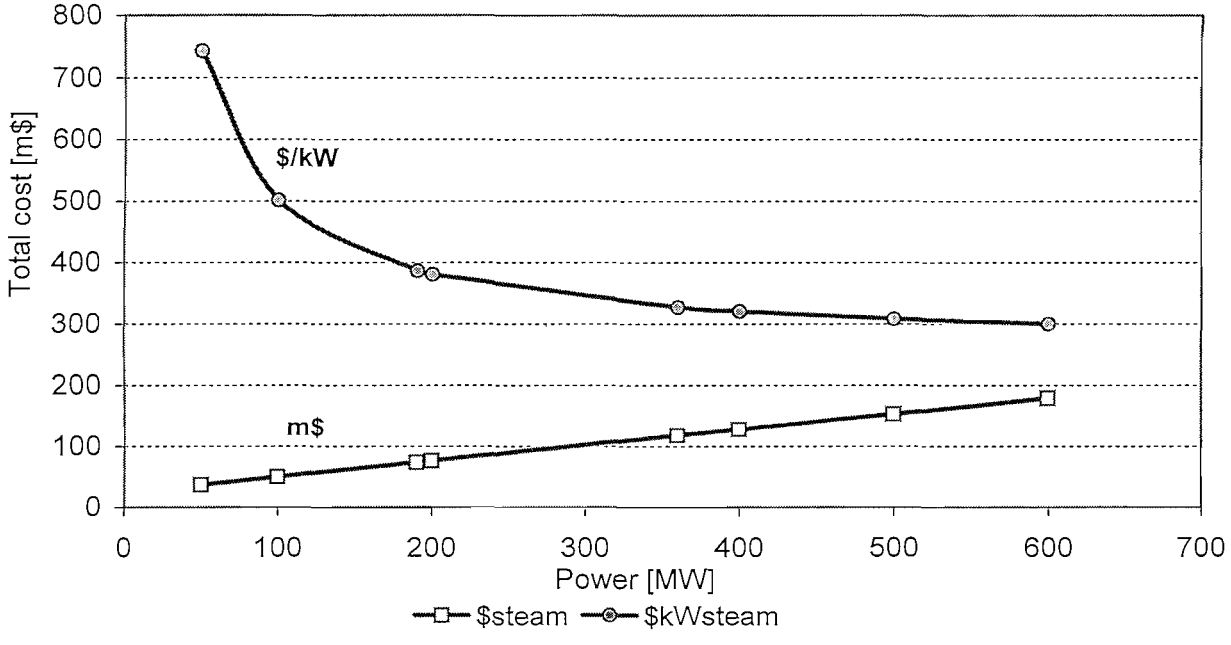


Figure 4.36 Steam plant costs

4.6 MARGINAL COST

It is assumed that the customer of a nuclear plant is willing to pay an additional m$ 2 for every additional MW on the grid. Therefore a more efficient plant or a higher power level plant will be sold for more. This additional income is subtracted from the capital costs. Therefore a more efficient cycle is portrayed as being less expensive. *Figure 4.37* shows how the plant's cost increases with increasing reactor power (remember that the $/kW cost decreases). The dots represent the selling price of the nuclear plant as would be found in literature. The gradient in the graph of *Figure 4.37* below illustrates the marginal cost.

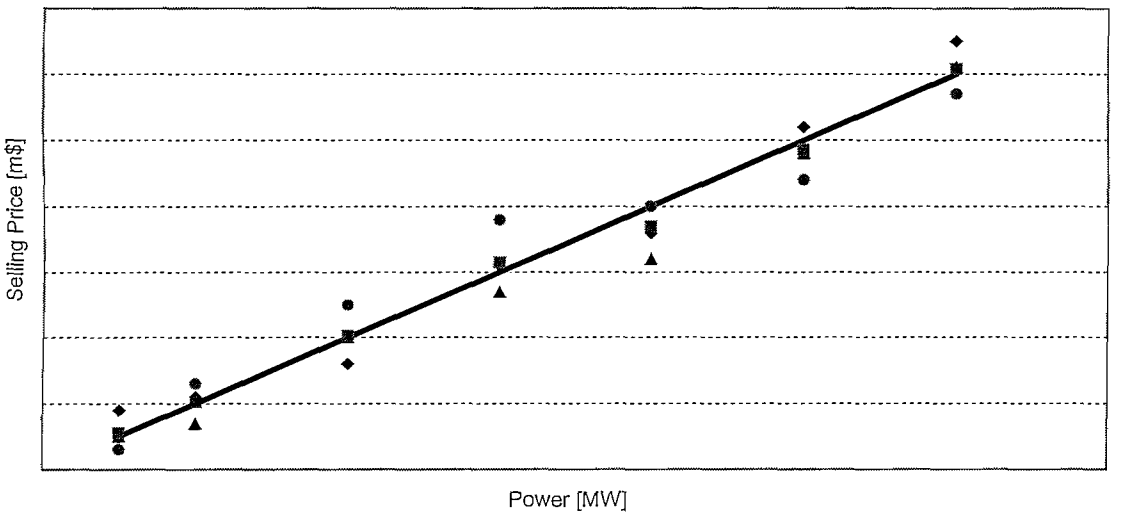


Figure 4.37 *Marginal costs*

$$C_{order\text{-}of\text{-}magnitude} = C_{PCU} + C_{Building} + C_{Reactor} + C_{Steam\ Plant} - C_{Marginal\ Cost}$$

$$C_{order\text{-}of\text{-}magnitude} = C_{PCU} + C_{Building} + C_{Reactor} + C_{Steam\ Plant} - (W - 185) \times NCC \frac{\$}{kW}$$

The value *185* is taken as a reference value (PBMR DP1) and *W* represents the total power output in MW. For every MW above the reference value of 185 MW, 2 m$ is subtracted from the capital costs.

Chapter 5

Component Models

In this chapter, the theory and methodology of the component models of the compressor, turbine, recuperator, pre-cooler, inter-cooler, IHX and blower are discussed and motivated.

5. COMPONENT MODELS

5.1 TURBO-MACHINE

5.1.1 Basic theory

This section gives a brief overview of the basic theory of compressors and turbines as applied in the component models. Knowledge of the theory and definitions discussed here will be necessary for understanding the compressor and turbine models in the following sections.

The Euler equation is used to calculate the stage work for the compressor and turbine by applying the principle of angular momentum and energy conservation. The derivation of and assumptions made for the Euler equation is discussed in section 5.1.1.1. The definition for the *work coefficient (ψ)* and *flow coefficient (Φ)* follows from the Euler and energy equation, which is covered in section 5.1.1.2. Section 5.1.1.3 shows how the stage velocity triangles are obtained. This information will be used to calculate the stage efficiencies. In section 5.1.1.4 the definition of stage reaction is given. Lastly the theory regarding isentropic- and stage efficiencies and stage prediction are presented in sections 5.1.1.5 and 5.1.1.6 respectively.

5.1.1.1 Euler's equation

Consider the flow of V_1 that enters the rotor of a turbo machine at one radius with one relative velocity and leaves at another radius with another relative velocity. The change in momentum between the flow entering and leaving the rotor can be used to calculate the force on the rotor and equal and opposite forces on the fluid. The three principal components of this force are: axial, radial and tangential. At the mean radius, the axial and radial components do not contribute to the work transfer between the working fluid and the rotor. Only the tangential component of the force can produce a change in enthalpy through a work transfer. The flow enters the rotor at a radius r_1, with a tangential component of the absolute velocity U_1, defined positive in the direction of the rotor rotation ω. Applying Newton's law and then calculating the torque, it follows that:

$$F_{u1} = \dot{m} C_{w1} \tag{5.1}$$

$$T_1 = F_{u1} r_1 = \dot{m} C_{w1} r_1 \tag{5.2}$$

$$T_n = \dot{m}(C_{w1} r_1 - C_{w2} r_2) \tag{5.3}$$

The energy transfer can now be calculated:

$$T_n \omega = \dot{m}\omega(C_{w1} r_1 - C_{w2} r_2) \tag{5.4}$$

$$W_{outlet} - W_{inlet} = \dot{m} U_m (C_{w1} - C_{w2}) \tag{5.5}$$

where F_{u1} = tangential force on rotor from entering fluid

m = mass flow

C_{w1} = absolute tangential velocity at the inlet

C_{w2} = absolute tangential velocity at the outlet

T_1 = torque on rotor at the inlet

T_n = net torque on rotor

Eq. (5.4) is known as Euler's equation. Positive work out W_{outlet} means that work is delivered from the turbo machine shaft and therefore represents the turbine. A compressor will have positive W_{inlet}. In the preliminary design of axial-flow machines, the change of radius of the mean flow can often be ignored; therefore Euler's equation can reduce to (5.5). It is more useful, however, to express the power in terms of the relative rotor blade air angles; β_1 and β_2 (see section 5.1.1.3).

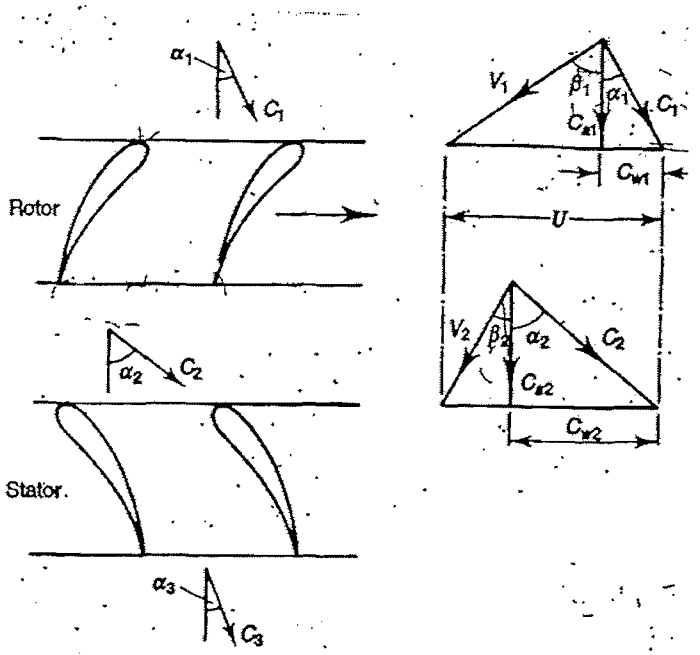


Figure 5.38 Axial Compressor stage blade rows and simple velocity diagram [1:p186]

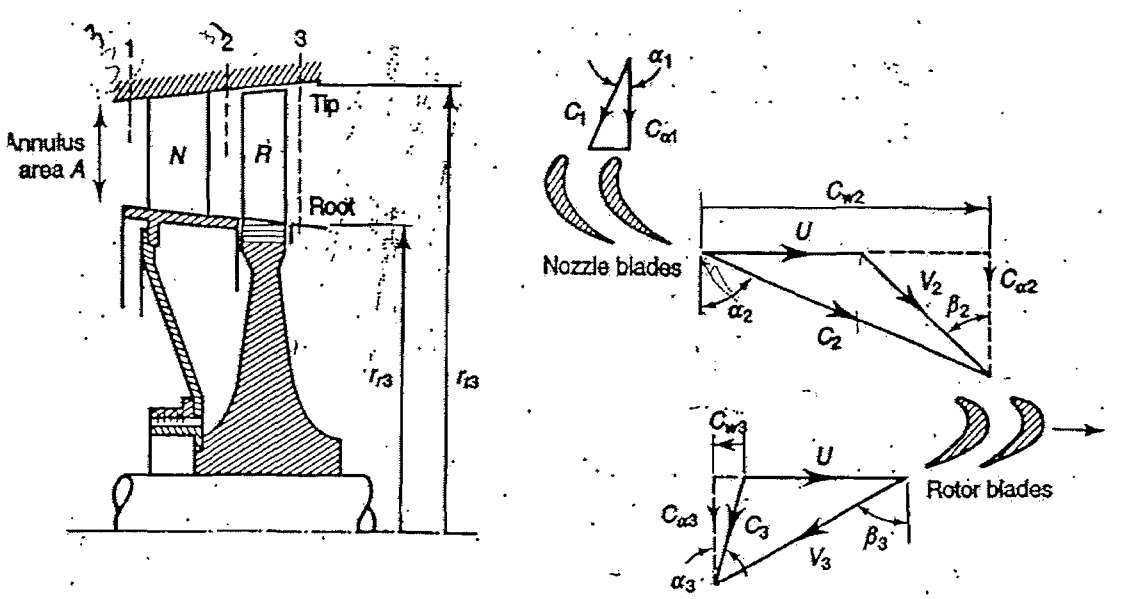


Figure 5.39 Axial Turbine stage blade rows and simple velocity diagram [1:p306]

Compressor *(see Figure 5.38)*

When working at the mean radius, U_1 equals U_2. Using $U_1 = \omega.r_1$ and $U_{2,} = \omega.r_2$, it follows that,

$$W_c = \dot{m}U_m\left(C_{w2} - C_{w1}\right) \tag{5.6}$$

$$\dot{m}C_p\Delta T_{0s} = \dot{m}U_m C_a(\tan\beta_1 - \tan\beta_2) \qquad \text{(see section 5.1.1.3)} \tag{5.7}$$

$$\Delta T_{0s} = \frac{U_m C_a}{C_p}(\tan\beta_1 - \tan\beta_2) \tag{5.8}$$

Turbine *(see Figure 5.39)*

When working at the mean radius, U_2 equals U_3 using again that $U_2 = \omega.r_2$ and $U_{3,} = \omega.r_3$. For the turbine it follows from (5.5) that,

$$W_t = \dot{m}U_m\left(C_{w2} + C_{w3}\right) \tag{5.9}$$

$$\dot{m}C_p\Delta T_{0s} = \dot{m}U_m C_a(\tan\beta_2 + \tan\beta_3) \qquad \text{(see section 5.1.1.3)} \tag{5.10}$$

$$\Delta T_{0s} = \frac{U_m \cdot C_a}{C_p}(\tan\beta_2 + \tan\beta_3) \tag{5.11}$$

Equations (5.8) and (5.11) are the fundamental equations for the compressor and turbine from which the stage work output and blade angles are calculated.

5.1.1.2 The work (ψ) and flow coefficient (Φ)

The *flow coefficient*, Φ and the *work coefficient*, ψ is defined by:

$$\phi = \frac{C_a}{U_m} \tag{5.12}$$

$$\psi = \frac{C_p(dT/z)}{U_{m.}^{\,2}} \tag{5.13}$$

where C_a = axial velocity

dT = total temperature difference over machine

z = number of stages

The combination of these two coefficients determines the blade angles and thus also the efficiency of the machine. It will be explained in following sections how the values for Φ and ψ were determined. The relation of Φ and ψ to the blade angles for the compressor and turbine is given below:

Compressor *(see Figure 5.38)*

From Eq. (5.8) it is known that

$$\Delta T_{0s} = \frac{U_m C_a}{C_p}(\tan\beta_1 - \tan\beta_2) \tag{5.14}$$

$$\psi = \phi(\tan\beta_1 - \tan\beta_2) \tag{5.15}$$

Turbine *(see Figure 5.39)*

From Eq. (5.11) it is known that

$$\Delta T_{0s} = \frac{U_m \cdot C_a}{C_p}(\tan\beta_2 + \tan\beta_3) \tag{5.16}$$

$$\psi = \phi(\tan\beta_2 + \tan\beta_3) \tag{5.17}$$

5.1.1.3 Velocity diagrams

For the purpose of this study, the turbo machine mean radius approach will be followed; thus assuming that flow occurs in a tangential plane at the mean radius.

Compressor *(see Figure 5.38)*

The gas approaches the rotor with an absolute velocity C_1 at an angle α_1 from the axial direction; combining C_1 vectorially with the blade speed U, gives the velocity relative to the blade V_1, at an angle β_1 from the axial direction. After passing through the rotor (which increases the absolute velocity of the gas), the fluid leaves the rotor with a relative velocity V_2 at an angle β_2 determined by the rotor blade outlet angle. It is assumed that the axial velocity, C_a will remain constant throughout all the stages. Assuming that $C_a = C_{a1} = C_{a2}$, two basic equations follow immediately from the geometry of the velocity triangles. These are

$$\frac{U_m}{C_a} = \tan\alpha_1 + \tan\beta_1 \tag{5.18}$$

$$\frac{U_m}{C_a} = \tan\alpha_2 + \tan\beta_2 \tag{5.19}$$

Turbine *(see Figure 5.39)*

The gas enters the row of nozzle blades with a static pressure and temperature p_1, T_1 and absolute velocity C_1, and is expanded to p_2, T_2 and leaves with an increased velocity C_2 at angle α_2. The rotor blade inlet angle will be chosen to suit the direction β_2 of the gas velocity V_2 relative to the blade at inlet. β_2 and V_2 are found by vectorial subtraction of the blade speed U_m from the absolute velocity C_2. After being deflected and usually further expanded, in the rotor blade passage, the gas leaves at p_3, T_3 with relative velocity V_3 at angle β_3. Vectorial addition of U_m yields the magnitude and direction of the gas velocity at exit from the stage, C_3 at α_3. α_3 is known as the *swirl angle*. The geometry of the diagram gives the relations

$$\frac{U_m}{C_a} = \tan\alpha_2 - \tan\beta_2 \tag{5.20}$$

$$\frac{U_m}{C_a} = \tan\beta_3 - \tan\alpha_3 \tag{5.21}$$

The blades are designed from the velocity diagrams. To specify a stage velocity diagram, we need three parameters: the *work coefficient* ψ, the *flow coefficient* Φ and the stage reaction Λ.

5.1.1.4 The stage reaction

The *degree of reaction* Λ expresses the fraction of the stage expansion which occurs in the rotor and it is usual to define it in terms of static temperature differences.

Compressor *(see Figure 5.38)*

The stage reaction for the compressor is defined as:

$$\Lambda_{Compressor} = \frac{T_2 - T_1}{T_3 - T_1} \tag{5.22}$$

For stages with constant C_a, this expression can be written as (Saravanamuttoo, 2001:196)

$$\Lambda_{Compressor} = \frac{C_a}{2U_m}\left(\tan\beta_1 + \tan\beta_2\right) \tag{5.23}$$

Turbine *(see Figure 5.39)*

The stage reaction for the turbine is defined as:

$$\Lambda_{Turbine} = \frac{T_2 - T_3}{T_1 - T_3} \tag{5.24}$$

For stages with constant C_a, this expression can be written as (Saravanamuttoo, 2001:309)

$$\Lambda_{Turbine} = \frac{C_a}{2U_m}\left(\tan\beta_3 - \tan\beta_2\right) \tag{5.25}$$

5.1.1.5 Isentropic vs. Stage efficiency

The stage efficiency (η_s) and isentropic efficiency (η_c) are respectively defined by:

$$\eta_s = \frac{\sum \Delta T_s'}{\Delta T} \tag{5.26}$$

$$\eta_c = \frac{\Delta T'}{\Delta T} \tag{5.27}$$

It follows that

$$\frac{\eta_s}{\eta_c} = \frac{\sum \Delta T_s'}{\Delta T'} \tag{5.28}$$

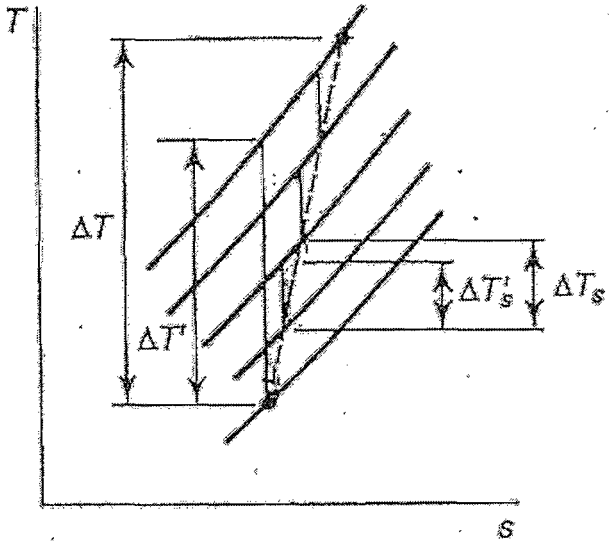


Figure 5.40 *TS diagram*

The vertical distance between a pair of constant pressure lines in the t-s diagram increases as the entropy increases, see *Figure 5.40*. For a compressor, it follows that $\sum \Delta T_s' > \Delta T'$ and therefore that $\eta_c < \eta_s$. This difference will increase with the number of stages, i.e. with increase in pressure. For the turbine, it follows that $\sum \Delta T_s' < \Delta T'$ and therefore that $\eta_c > \eta_s$. Thus, at each pressure ratio, the isentropic efficiency of the compressor and turbine will be different, although the stage efficiency for all the machines at all pressure ratios was kept the same. A sketch of a typical stage for the compressor and turbine is shown in *Figure 5.41* and *Figure 5.42*, respectively.

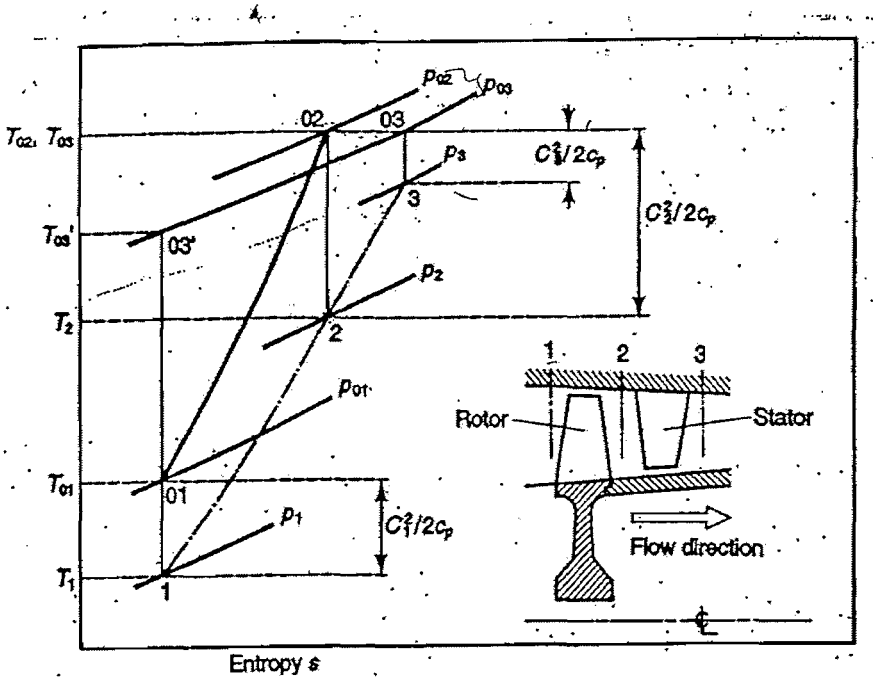


Figure 5.41 *Compressor stage and t-s diagram [1:p185]*

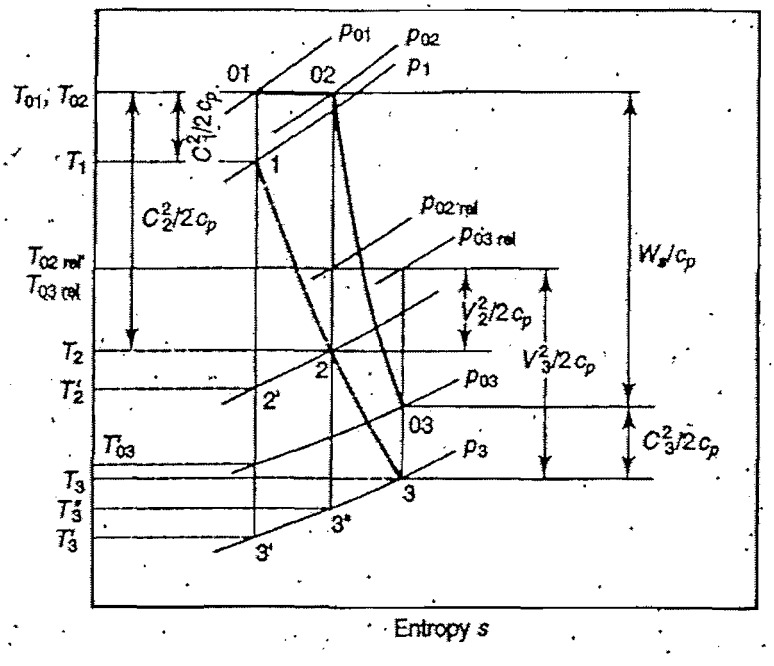


Figure 5.42 *Turbine stage and t-s diagram [1:312]*

5.1.1.6 Stage Prediction

It is emphasized that (at this point in the study) the stage efficiencies were simply fixed and no loss models were used to calculate the stage efficiencies. In a following revision, the loss models will most probably be implemented and are therefore documented in the meantime – see Appendix 9

5.1.2 Optimization

This section explains how the turbo machines are optimized to ensure the minimum capital cost. More attention was given to the turbo machines than to the heat exchangers, and for the following reasons:

- Apart from the reactor, the turbo machines are the most expensive component in the PCU. The turbo machines are almost ten times more expensive than the pre- and inter-cooler and twice as expensive as the recuperator.
- The turbo machines have the largest impact on the cycle efficiency and controllability of the plant.

The axial velocity and efficiencies calculated for the turbo machines will need to be updated in the cycle analyses. The methodology explained here is applicable to both the compressor and turbine, though the differences between these two models will be highlighted. See Figure 5.43 for the discussion to follow. For the compressor and turbine, the following input parameters are obtained from the cycle analyses:

- T_{In} - Inlet temperature
- T_{out} - Outlet temperature (based on *guessed value* for isentropic efficiency)
- P_{in} - Inlet pressure
- P_{out} - Outlet pressure
- m - Mass flow [kg/s]
- Fluid properties
  - C_p – specific heat at constant pressure
  - γ – ratio of specific heats
  - R – gas constant

A large variety of compressor and turbine designs are possible from these input parameters. The goal is to find the optimum design within the design boundaries and limitations. The "optimum" design is defined as the design which ensures the minimum turbo machine capital cost. The turbo unit capital cost is given by (see Chapter 4):

$$C_{TurboUnit} = \frac{\left(\left[K_{C1} r_t^2 (z+4)\right]_{Compressor} + \left[K_{T1} r_t^2 (z+4)\right]_{Turbine}\right)}{1-0.11} \tag{5.29}$$

In order to calculate the turbo machine capital cost, the tip radius (r_t) as well as the number of stages for the compressor and turbine needs to be solved.

The compressor and turbine design are governed by equations (5.30), (5.31), (5.80) and (5.33). The *work coefficient* expresses the work capacity per stage, while the *flow coefficient* relates the axial velocity to the mean rotor speed. The derivation of both these coefficients was documented in section 5.1.1.2. The maximum centrifugal tensile stress at the blade root, is given by Eq. (5.80). For

preliminary design calculations, it is sufficiently accurate (and conservative) to assume that the tapered blade reduces the stress to 2/3 of the value for the untapered blade. The effect of gas bending on the blade stresses was not evaluated. Eq. (5.33) is the fundamental continuity equation.

The *work coefficient* is defined as:
$$\psi = \frac{C_p(dT/z)}{U_m^{\,2}} \tag{5.30}$$

The *flow coefficient* is defined as:
$$\phi = \frac{C_a}{U_m} \tag{5.31}$$

The *centrifugal tensile* stress is defined by:
$$\sigma_{real} = \frac{\sigma_{max}}{SF} = \frac{2}{3}\left[\frac{\rho_b}{2}U_t^2\left(1-\left(\frac{r_r}{r_t}\right)^2\right)\right] \tag{5.32}$$

The *continuity equation* states that:
$$m = \rho C_a \pi r_t^2\left(1-\left(\frac{r_r}{r_t}\right)^2\right) \tag{5.33}$$

Where dT = temperature rise (drop) over compressor (turbine)

SF = blade material safety factor [-]

ρ_b = blade density [kg/m^3]

U_t = tip speed [m/s]

r_r = hub radius [m]

r_t = tip radius [m]

ρ = fluid density [kg/m^3]

σ_{real} = centrifugal tensile stress at blade root

σ_{max} = maximum allowable stress : compressor - based on yield strength

turbine - based on creep strength

The following input to each turbo machine is known from the cycle analysis:

C_p, dT, m, ρ

The following input values need to be fixed for the compressor and turbine:

σ_{max}, ρ_b, SF, N, Ψ, Φ,

For a given blade material (σ_{max}, ρ_b), safety factor (SF), rotational speed (N), work coefficient and flow coefficient, equations (5.30) to (5.33) are used together with the input from the cycle analysis to solve for these four variables:

- z: number of stages [-]
- C_a: axial velocity [m/s]
- r_t: tip radius [m]
- $\frac{r_r}{r_t}$: hub-tip-ratio [-]

Different blade materials are used for the compressor and turbine, but the same materials were used for all the cycles. For the turbine, the maximum allowable creep strength is calculated at each pressure ratio as a function of the blade inlet temperature. The component model needs to identify the optimum combination of SF and N at each different pressure ratio that will ensure minimum plant capital cost. The cost model is the criteria by which the SF and N are identified.

The following variables are optimized for in the component model of the compressor and turbine:

SF - blade material safety factor

N - rotational speed [rev/s]

At lower rotational speeds, the blade stresses will also be lower and therefore higher safety factors will result. Therefore the safety factor is optimized and not fixed. When optimising the turbo machine, the design must be within the design limitations. These design limitations were gathered from experts within PBMR:

Description	Variable	Unit	Lower limit	Upper limit
Compressor				
Hub-tip-ratio	htr	[-]	0.36	0.87
Mach number	mach	[-]	-	0.65
Safety factor	SF	[-]	3	20
Fluid deflection compressor	deHaller	[-]	$\frac{V_2}{V_1} \leq 0.72$	-
Turbine				
Hub-tip-ratio	htr	[-]	0.40	0.90
Mach number	mach	[-]	-	0.65
Safety factor	SF	[-]	1	20

Table 5.5 *Design variables for turbo machines*

Turbo machine optimization methodology

For the discussion on the methodology used to optimize the turbo machines, see Figure 5.43. The goal of the turbo machine optimization is to identify the combination of SF and N that will ensure the minimum plant capital cost while staying within all design limitations. The capital costs can be evaluated once the compressor and turbine tip radii and number of stages are known. The tip radii and number of stages can be calculated using equations (5.30) to (5.33) once Ψ, Φ, N and SF is known. The plant capital cost will be evaluated over a range of N and SF in order to identify the optimum design.

The range over which the rotational speed will be evaluated is:

Minimum: 50 rev/s

Maximum: 200 rev/s

The range over which the safety factor will be evaluated is:

Compressor:	Minimum:	3
	Maximum:	20
Turbine:	Minimum:	1
	Maximum:	20

The choice of Φ and ψ is very significant since these two parameters basically define the geometry of the machine, its performance and also its off-design behaviour. The combination of Ψ and Φ for both the compressor and turbine were fixed – see sections 5.2 and 5.3. To start with the rotational speed is fixed at 50 rev/s.

With Ψ, Φ and N fixed, the capital cost of the compressor is calculated over a range of safety factors. The safety factor yielding the minimum compressor capital cost is identified as the optimum SF for the compressor at the specified rotational speed. For the same rotational speed as for the compressor, the capital cost for the turbine is calculated over its range of safety factors. The turbine safety factor yielding the minimum turbine capital cost is identified as its optimum safety factor. Thus, for a specified rotational speed, the minimum compressor and turbine capital costs were calculated. Using Eq. (5.29), the turbo machine capital cost can now be evaluated for the specified rotational speed, N. The minimum turbo machine cost has thus been identified for a specified N. Next, this process is repeated over the range of rotational speeds, up to 200 rev/s. The minimum turbo machine capital cost is thus calculated at various rotational speeds, but still for the same fixed combination of Ψ and Φ for the turbine. All of this was done for a fixed reaction for the compressor and turbine. For a given Ψ and Φ for the turbine, the optimum rotational speed, and corresponding design is thus identified.

For both the compressor and turbine the tip radius, number of stages and axial velocity have been calculated. The compressor and turbine isentropic efficiencies are calculated from the stage efficiencies, as obtained for a fixed combination of Ψ and Φ. Once calculated, the initial guessed values are updated.

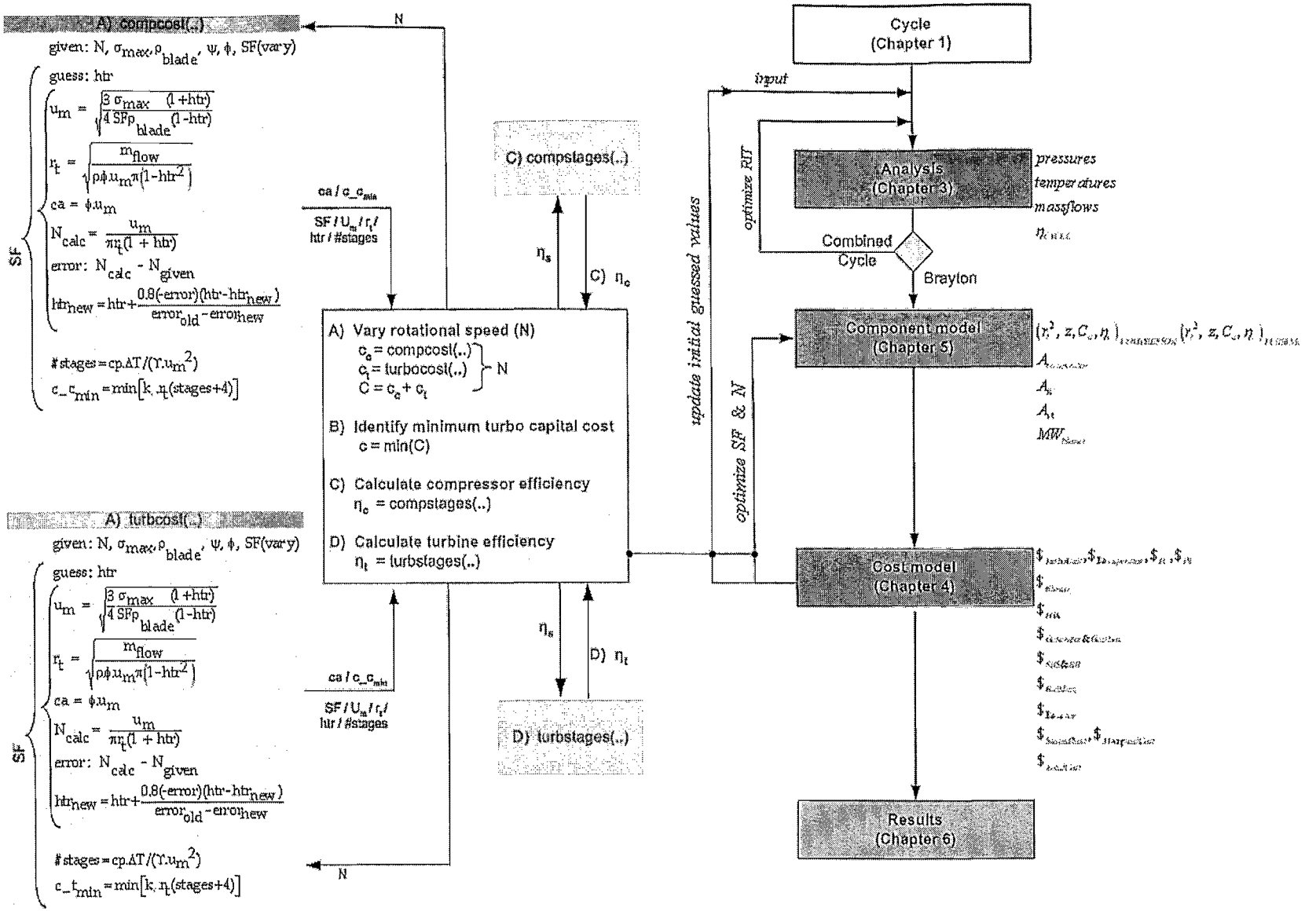


Figure 5.43 *Schematic overview of program methodology*

5.2 COMPRESSOR

The compressor model must calculate the compressor's capital cost, axial outlet velocity and isentropic efficiency. *Table 5.6* summarizes the required input and output.

Fixed input values	Estimated guessed values	Costing Model	To be solved	Output
K_{C1} η_s Φ Ψ Blade material	η_c $C_{a,c}$	$C_{Compressor} = K_{C1} r_t^2 (z+4)$	r_t z η_c $C_{a,c}$	η_c $C_{a,c}$ $C_{Compressor}$

Table 5.6 *Summary of compressor model inputs and outputs*

The following variables are fixed input to the compressor model:

- K_{c1} = 0.4907 - fixed constant for compressor (see Chapter 4)
- η_s = 0.88 - stage efficiency: internal stage (see section 5.2.1)
- Φ = 0.40 - flow coefficient (see section 5.2.1)
- Ψ = 0.36 - work coefficient (see section 5.2.1)
- Blade material: - 10705BX (008472-052 Rev 1, p42)

  σ_{max} =744 MPa - maximum allowable yield strength

  ρ_b =7770 kg/m^3 - blade density [kg/m^3]

The values for the following variables are assumed, and later on updated:

- η_c - isentropic efficiency
- $C_{a,c}$ - axial velocity

The following variables are obtained from the cycle analysis:

- C_p - specific heat at constant pressure
- dT - temperature rise (drop) over compressor (turbine)
- m - mass flow [kg/s]
- rho - fluid density [kg/m^3]

The cost model is used to find the optimum speed and safety factor for the compressor.

- **N - rotational speed [rev/s]**
- **SF - safety factor [-]**

These input values are used together with equations (5.30) to (5.33) to solve for the four variables listed below. In C++ these equations had to be solved explicitly. See Appendix 9.3 for the explicit form of these four equations.

- **z:** **number of stages** [-]
- **C_a:** **axial velocity** [m/s]
- **r_t:** **tip radius** [m]
- $\frac{r_r}{r_t}$: **hub-tip-ratio** [-]

At this stage, both the compressor capital cost (r_t and stages) and the axial velocity of the compressor have been solved. The compressor isentropic efficiency remains to be solved.

The stage efficiencies for the first stage, internal and last stage were specified as fixed input. Ideally, the stage efficiencies should be calculated from the design parameters, using loss models. Typically, the stage efficiency could be calculated if the aspect ratio, tip clearance, Reynolds number and temperatures are known. In section 5.1.1.6 it was explained how to solve for the required input parameters, while the methodology of the loss model of *Howell* is documented in Appendix 9.4. It is emphasized that the stage efficiencies were not calculated with the loss models, but were simply specified. Although not implemented yet, the loss models will be incorporated in future.

The temperature difference over each stage can be calculated next since the total temperature difference over the compressor is known from the cycle analysis and the number of stages has been calculated. The temperature rise over each stage is kept constant. Knowing the inlet temperature and pressure from the cycle analyses and from knowing the temperature rise per stage, the outlet pressure can be calculated using the fixed stage efficiency, using Eq. (5.34).

$$P_{outlet} = P_{inlet}\left[1+\frac{\eta_{stage}\Delta T_{stage}}{T_{inlet}}\right]^{\gamma/(\gamma-1)} \tag{5.34}$$

where P_{inlet} - stage inlet pressure

T_{inlet} - stage inlet temperature

P_{outlet} - stage outlet pressure

T_{outlet} - stage outlet temperature

This process is repeated until the second last stage. For the last stage, the outlet pressure is known (from the cycle analysis) and the outlet temperature is re-calculated using,

$$\Delta T_{last\ stage} = \frac{T_{inlet}}{\eta_{stage}}\left[\left(\frac{P_{outlet}}{P_{inlet}}\right)^{(\gamma-1)/\gamma} - 1\right] \tag{5.35}$$

With the newly calculated outlet temperature for the compressor, the isentropic efficiency for the machine is calculated using,

$$\eta_c = \frac{T_1}{\Delta T}\left[(PR)^{(\gamma-1)/\gamma} - 1\right] \tag{5.36}$$

where T_1 - compressor inlet temperature

ΔT - compressor outlet temperature, as re-calculated with Eq. (5.35).

PR - total pressure ratio over compressor

The initial assumed value for the compressor isentropic efficiency for the specific compressor at the specified pressure ratio will be updated with the newly calculated value. The assumed value for the axial outlet velocity will also be updated. All this will be done until convergence. The next section explains the choice of *work-, flow coefficient* and stage efficiency.

5.2.1 Choice of Φ and ψ (compressor)

The choice of Φ and ψ is very significant since these two parameters basically define the geometry of the machine, its performance and also its off-design behaviour. One would like to have Φ as small as possible to minimize the frontal area and ψ as large as possible to minimize the number of stages. The choice of reaction, Φ and ψ is also influenced by the permissible amount of diffusion in the blades. The de Haller criterion sets the upper limit on the fluid deflection, stating that $\frac{V_2}{V_1} \leq 0.72$. Usually, the goal is to use the maximum deflection in order to minimize the number of stages and therefore the cost. Typical values for reaction, Φ and ψ were chosen based on a combination of (i) information contained in literature on the subject, (ii) experience gained thus far in the development of the PBMR cycle and (iii) discussions with experts in the field. The following values were chosen:

Λ = 50%

Φ = 0.40

Ψ = 0.36

The stage efficiency is largely dependent on the blade inlet and outlet angles. Since the blade inlet and outlet angles are fixed for a certain choice of reaction, Φ and ψ, the stage efficiency can be related to reaction, Φ and ψ. The relative outlet and inlet speed V_2 and V_1 is obtained from β_2 and β_1 (see *Figure 5.38* and *Figure 5.39*) where β_1 and β_2 is only a function of the reaction, Φ and ψ. For a fixed reaction, Φ and ψ, equations (5.37) and (5.38) will solve for β_1 and β_2.

From Eq. (5.15) resulting from the Euler equation we have that

$$\psi = \phi(\tan\beta_1 - \tan\beta_2) \tag{5.37}$$

From Eq. (5.23) we have that

$$\Lambda = \frac{\phi}{2}(\tan\beta_1 + \tan\beta_2) \tag{5.38}$$

For the assumed values of reaction, Φ and ψ, the best estimate (based on engineering judgement) for the compressor stage efficiency is assumed to be

$$\eta_s = 88\%$$

After the loss models have been implemented, one will be able to calculate the stage efficiency for a specified combination of Φ and ψ. This implies that one can optimize for the cost versus thermal efficiency of the plant and in doing so optimize the choice of Φ and ψ.

5.3 TURBINE

The turbine model must also calculate the turbine's capital cost, axial outlet velocity and isentropic efficiency. 5.3.1 summarizes the required input and output.

Fixed input values	Estimated guessed values	Costing Model	To be solved	Output
K_{T1} η_s Φ ψ Blade material	η_T $C_{a,T}$	$C_{Turbine} = K_{T1} r_t^2 (z+4)$	r_t z η_T $C_{a,T}$	η_T $C_{a,T}$ $C_{Turbine}$

Table 5.7 *Summary of turbine model inputs and outputs*

The following variables are fixed input to the turbine model:

- K_{T1} = 2.0434 - fixed constant for turbine (see Chapter 4)
- η_s = 0.90 - stage efficiency: internal stage (see section 5.3.1)
- Φ = 0.50 - flow coefficient (see section 5.3.1)
- ψ = 1.10 - work coefficient (see section 5.3.1)
- Blade material: MGA1400DS (008472-052 Rev 1, p35)

  ρ_b - Blade density = 7830 kg/m^3 at 800 °C

  σ_{max} - Creep strength is calculated from Figure 5.44 as a function of the inlet temperature (minimum safety factor of 1)

The values for the following variables are assumed, and later on updated:

- η_T - isentropic efficiency
- $C_{a,T}$ - axial velocity

The following variables are obtained from the cycle analysis:

- C_p - specific heat at constant pressure
- dT - temperature rise (drop) over turbine (turbine)
- m - mass flow [kg/s]
- rho - fluid density [kg/m^3]

The cost model is used to find the optimum speed and safety factor for the turbine.

- **N - rotational speed [rev/s]**
- **SF - safety factor [-]**

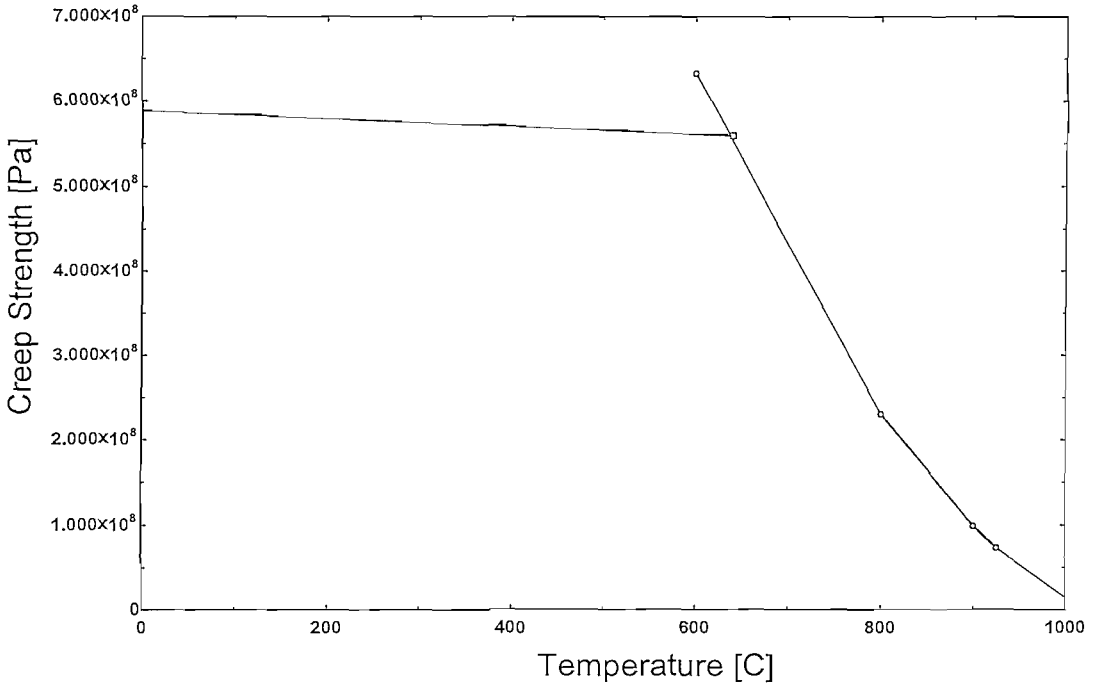


Figure 5.44 *Creep strength for material: DS1400 (PBMR-MHI-032, 2003:1.6-1.14, [25])*

These input values are used together with equations (5.30) to (5.33) to solve for the four variables listed below. In C++ these equations had to be solved explicitly. See Appendix 9.4 for the explicit form of these four equations.

- **z: number of stages [-]**
- **C_a: axial velocity [m/s]**
- **r_t: tip radius [m]**
- **$\frac{r_r}{r_t}$: hub-tip-ratio [-]**

Both the turbine capital cost (r_t and stages) and the axial velocity of the turbine have been solved and only the turbine isentropic efficiency remains to be solved.

The stage efficiencies for the first stage, internal and last stage were specified as fixed input. Ideally, the stage efficiencies should be calculated from the design parameters, using loss models. Again, it is emphasized that the stage efficiencies were not calculated with the loss models, but were simply specified and will be implemented in future. In section 5.1.1.6 it was explained how to solve for the required input parameters, while the methodology of the loss model of *Ainley and Matthiesen* is documented in Appendix 9.5.

The temperature difference over each stage can be calculated next since the total temperature difference over the turbine is known from the cycle analysis and the number of stages has been calculated. The temperature rise over each stage is kept constant. Knowing the inlet temperature and pressure from the cycle analyses and from knowing the temperature difference per stage, the outlet pressure is calculated using the fixed stage efficiency – see Eq. (5.39).

$$P_{outlet} = P_{inlet}\left[1-\frac{\Delta T_{stage}}{\eta_{stage} T_{inlet}}\right]^{\gamma/(\gamma-1)} \tag{5.39}$$

where P_{inlet} - stage inlet pressure

T_{inlet} - stage inlet temperature

P_{outlet} - stage outlet pressure

T_{outlet} - stage outlet temperature

This process is repeated until the second last stage. For the last stage, the outlet pressure is known (from the cycle analysis) and the outlet temperature is re-calculated using,

$$\Delta T_{last\ stage} = \eta_{stage} T_{inlet}\left[1-\left(\frac{P_{outlet}}{P_{inlet}}\right)^{(\gamma-1)/\gamma}\right] \tag{5.40}$$

With the newly calculated outlet temperature for the turbine, the isentropic efficiency is calculated with:

$$\eta_c = \frac{t_{inlet}}{\Delta T}\left(1 - \left(\frac{p_{outlet}}{p_{inlet}}\right)^{(\gamma-1)/\gamma}\right) \tag{5.41}$$

$$\eta_c = \frac{T_1}{\Delta T}\left[1-(PR)^{(\gamma-1)/\gamma}\right]$$

where T_1 - turbine inlet temperature

ΔT - turbine outlet temperature, as re-calculated with Eq. (5.35).

PR - total pressure ratio over turbine

The initial assumed value for the turbine isentropic efficiency for the specific turbine at the specified pressure ratio will be updated with the newly calculated value. The assumed value for the axial outlet velocity will also be updated. All this will be done until convergence. The next section explains the choice of *work-, flow coefficient* and choice of stage efficiency.

5.3.1 Choice of Φ and ψ (turbine)

The choice of Φ and ψ is very significant since these two parameters basically define the geometry of the machine, its performance and also its off-design behaviour. Typical values for reaction, Φ and ψ were chosen based on a combination of (i) information contained in literature on the subject, (ii) experience gained thus far in the development of the PBMR cycle and (iii) discussions with experts in the field. The following values were chosen:

Λ = 50%

Φ = 0.50

ψ = 1.10

The stage efficiency is largely dependent on the blade inlet and outlet angles. Since the blade inlet and outlet angles are fixed for a certain choice of reaction, Φ and ψ, the stage efficiency can be related to reaction, Φ and ψ. From Eq. (5.17) resulting from the Euler equation we have that

$$\psi = \phi(\tan\beta_2 + \tan\beta_3) \tag{5.42}$$

From Eq. (5.25) we have that

$$\Lambda = \frac{\phi}{2}\left(\tan\beta_3 - \tan\beta_2\right) \tag{5.43}$$

For the assumed values of reaction, Φ and ψ, the best estimate (based on engineering judgement) for the turbine stage efficiency is assumed to be

$\eta_s = 90\%$

After the loss models have been implemented, one will be able to calculate the stage efficiency for a specified combination of Φ and ψ. This implies that one can optimize for the cost versus thermal efficiency of the plant and in so doing optimize the choice of Φ and ψ.

5.4 RECUPERATOR

The recuperator component model needs to solve only for the heat transfer area. The heat transfer area can be calculated with the NTU-method. The NTU value for a concentric tube, counter flow heat exchanger is given by:

$$NTU = \frac{\eta_{Recuperator}}{1 - \eta_{Recuperator}} \tag{5.44}$$

$$NTU = \frac{UA}{C_{\min}} = \frac{UA}{\left(\dot{m}C_p\right)_{\min}} \tag{5.45}$$

Substituting Eq. (5.44) into (5.45):

$$UA = \left(\frac{\eta_{Recuperator}}{1 - \eta_{Recuperator}}\right)\dot{m}C_p \tag{5.46}$$

For un-finned, tabular heat exchangers, the AU value is also defined as:

$$\frac{1}{AU} = \frac{1}{A_iU_i} = \frac{1}{A_oU_o} = \frac{1}{h_iA_i} + \ldots + \frac{1}{h_oA_o} \tag{5.47}$$

where i = primary side / low-pressure

o = secondary side / high-pressure

The current PBMR recuperator design is such that $A_i = 2.334A_o$ [24]. Using this relation, it follows that:

$$\frac{1}{A_oU_o} = \frac{1}{h_i(2.334 \cdot A_o)} + \frac{1}{h_oA_o} \tag{5.48}$$

$$\frac{1}{A_iU_i} = \frac{1}{h_iA_i} + \frac{2.334}{h_oA_i} \tag{5.49}$$

where h_i = primary side heat transfer coefficient

h_o = secondary side heat transfer coefficient

Simplifying equations (5.48) and (5.49) lead to *U*,

$$U_o = \left(\frac{1}{h_i \cdot 2.334} + \frac{1}{h_o} \right)^{-1} \quad \text{and} \quad U_i = \left(\frac{1}{h_i} + \frac{2.334}{h_o} \right)^{-1}$$

The heat transfer area of the recuperator's primary and secondary side is defined respectively by equations (5.50) and (5.51):

$$A_o = \frac{\left(\frac{\eta_{Recuperator}}{1 - \eta_{Recuperator}} \right) \dot{m} C_p}{\left(\frac{1}{h_i \cdot 2.334} + \frac{1}{h_o} \right)^{-1}} \tag{5.50}$$

$$A_i = \frac{\left(\frac{\eta_{Recuperator}}{1 - \eta_{Recuperator}} \right) \dot{m} C_p}{\left(\frac{1}{h_i} + \frac{2.334}{h_o} \right)^{-1}} \tag{5.51}$$

From the V704D Flownex results file [24] U was calculated to be 1094 [W/m^2.K]. In calculating the value for U from the Flownex network, the effect of heat conductivity was not taken into account. The model will need to be extended eventually to calculate the heat transfer coefficients for the recuperator. It was decided to use U as a constant value for all the cycles at all the pressure ratios. Thus the heat transfer area used in all the analyses for the recuperator is:

$$A_o = \frac{\left(\frac{\eta_{Recuperator}}{1 - \eta_{Recuperator}} \right) \dot{m} C_p}{1094} \tag{5.52}$$

The optimum efficiency for the recuperator can now be evaluated by using Eq. (5.52) to plot the heat transfer area as function of the recuperator efficiency. The mass flow was taken as 192 kg/s [24], C_p as 5195 [J/kg.K] and U as 1033 [W/m^2.K]. It was decided to use a recuperator efficiency of 96%.

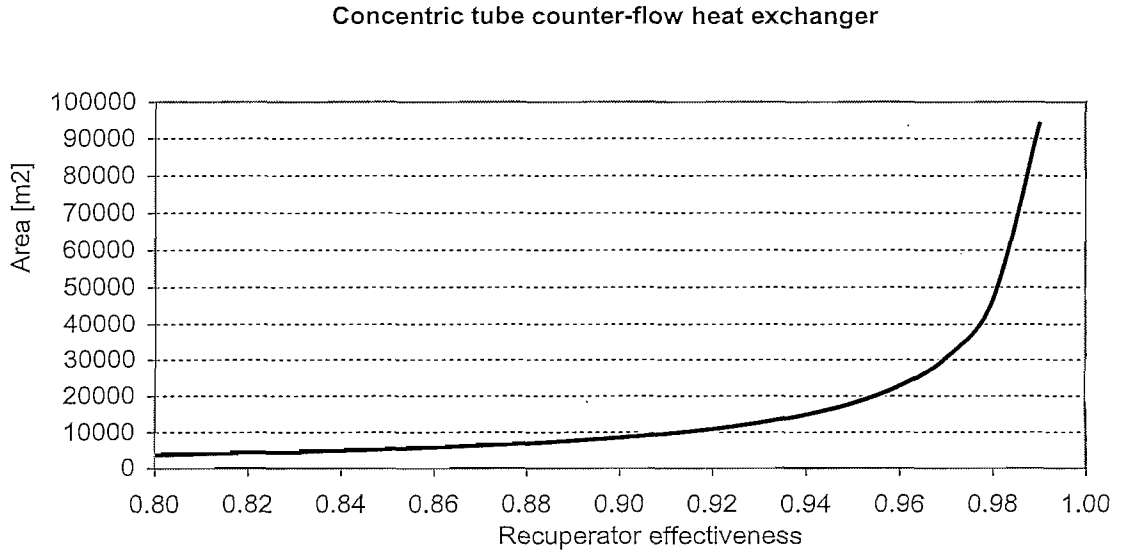


Figure 5.45 *Recuperator efficiency vs heat transfer area for recuperator*

5.5 PRE- AND INTER-COOLER

The heat transfer area for the coolers is also calculated with the NTU-method. The NTU value for a cross-flow (single pass) heat exchanger is given by:

$$NTU = -\left(\frac{1}{C_r}\right)\ln\left(1 + C_r \cdot \ln(1-\eta_{PC})\right) \tag{5.53}$$

$$NTU = \frac{UA}{C_{\min}} = \frac{UA}{\dot{m}C_p} \tag{5.54}$$

where $C_r = \frac{C_{\min}}{C_{\max}}$. Cr was calculated to be 0.4 (Helium-Water).

From equations (5.53) and (5.54) it can be seen that the heat transfer area equals:

$$Ai_{PC} = -\left(\frac{1}{C_r}\right)\ln\left(1 + C_r \ln(1-\eta_{PC})\right)\dot{m}C_p / U \tag{5.55}$$

$$Ai_{IC} = -\left(\frac{1}{C_r}\right)\ln\left(1 + C_r \ln(1-\eta_{IC})\right)\dot{m}C_p / U \tag{5.56}$$

The heat exchanger models will need to be extended to *calculate* the heat transfer coefficient. The total heat transfer area for the current PBMR is 10193 m^2 [24]. When applying Eq.s (5.55) and (5.56) to the PBMR design, the heat transfer coefficient U seems to be in the order of 127. For now, the heat transfer coefficient U is simply assumed to be 320 [$W/m^2.K$], which is a typical value.

The optimum efficiency for the heat exchanger can now be evaluated by using Eq. (5.56) to plot the heat transfer area as function of the heat exchanger efficiency. The mass flow was taken as 200 kg/s [24], Cp as 5195 [J/kg.K] and U as 320 [$W/m^2.K$]. The values of the mass flow, Cp and U are not as important, since they will only shift the graph up or down. It was decided to use a cooler efficiency of 83% - see *Figure 5.46*.

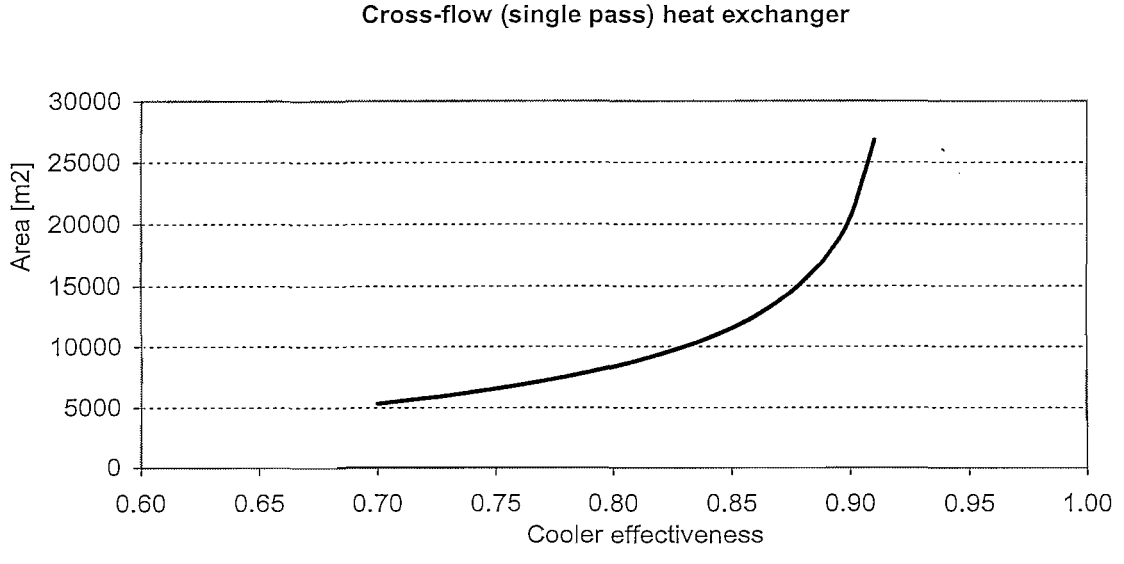


Figure 5.46 *Heat exchanger efficiency vs heat transfer area for coolers*

5.6 IHX

The heat transfer area of the IHX is calculated with the same relationship as explained in section 5.4:

$$A_{IHX} = \frac{\left(\frac{\eta_{IHX}}{1 - \eta_{IHX}}\right)\dot{m}C_p}{U_{IHX}} \tag{5.57}$$

But for the IHX, both the effectiveness (η_{IHX}) and heat transfer coefficient (U_{IHX}) are calculated. The effectiveness is calculated from the specified IHX temperature difference (dT_{IHX}),

$$\eta_{IHX} = \frac{\left(T_{h,i} - T_{h,o}\right)}{C_{\min}\left(T_{h,i} - T_{c,i}\right)} \quad where\ h = hot,\ \ c = cold \tag{5.58}$$

The effect of working fluid on the IHX cost for the indirect cycles is being investigated. The heat transfer coefficient will be different for various working fluids and is calculated as function of the conductivity (k), which is a function of temperature,

$k_1 = function(t)$ - see Chapter 3 (5.59)

$k_2 = function(t)$ - see Chapter 3 (5.60)

$$h_1 = \frac{Nu\ k_1}{d_{IHX}},\ \ where\ Nu\ =\ 3.66 \text{ - see Chapter 3, } d_{IHX} \tag{5.61}$$

$$h_2 = \frac{Nu\ k_2}{d_{IHX}},\ \ where\ Nu\ =\ 3.66 \text{ - see Chapter 3, } d_{IHX} \tag{5.62}$$

$$U_{IHX} = \left(\frac{1}{h_1} + \frac{1}{h_2}\right)^{-1} \tag{5.63}$$

5.7 BLOWER

The blower power is calculated with the following relation:

$$t_{outlet} = t_{inlet} + \frac{t_{inlet}}{\eta_{blower}}\left[\left(\frac{p_{inlet}}{p_{outlet}}\right)^{(\gamma-1)/\gamma} - 1\right]$$

$$Q_{IHX}\ =\ \dot{m}C_p(t_{outlet} - t_{inlet})\,.$$

Chapter 6

Results

Based on the results of the cycle analyses, component designs and cost of each configuration, different operational parameter envelopes are identified for which each of the cycle configurations would be most appropriate. This chapter presents all the results of the study.

6. RESULTS

The ten cycle configurations under investigation were presented in *Figure 1.7* and *Figure 1.8*. The objective was to compare these ten cycles in order to identify a near-optimum design for each cycle from which the most practical, efficient and economical PCU can be chosen. The thermodynamic cycle analyses were used together with the costing- and component models in order to calculate each cycle's temperatures, pressures, efficiency, component capital costs and the order-of-magnitude plant cost for various pressure ratios, reactor outlet temperatures and power turbine rotational speeds. The different operational parameter envelopes were identified for which each of the different cycle configurations are most appropriate.

Figure 1.3 presented a schematic layout of the possible choices when choosing a PCU configuration. Should one decide to use an indirect cycle, it is inevitable to develop the complex advanced IHX. This chapter will recommend a Brayton and a Combined Cycle for both an indirect and a direct configuration. Helium is chosen as working fluid for all the direct cycles. For the indirect cycle, one is free to choose the fluid in the secondary loop. For the indirect Combined Cycle, the question arises whether to custom design the plant or to buy an off-the-shelf Combined Cycle. Each of these issues will be addressed in this document.

The results of the Brayton cycles are discussed in section 6.3. The results of the Combined Cycles and the two chosen Brayton cycles are discussed in section 6.4. A design envelope is drawn for each of the chosen cycles and the boundary conditions are discussed in section 6.5. The PBMR and Framatome designs are compared in section 6.6.5. In section 6.6.6 the effect of the hydrogen plant on the thermal efficiency is presented and the series and parallel configurations are discussed. The effect of Helium, Nitrogen and a mixture of the two on the cost is discussed in section 6.6.7. In section 6.6.8 the effect of the direct and indirect configuration on the thermal efficiency is discussed. The practicalities associated with the Combined Cycles are discussed in section 6.7. Lastly a summary of the study is given (6.9).

6.1 INTRODUCTION

6.1.1 Definitions

The following definitions are used throughout the document:

Thermal efficiency

The thermal cycle efficiency is defined as the ratio of the net work output to the power input. Neither the effect of the generator and switching efficiencies nor the *house load* is taken into account. See Chapter 3 for more details.

Brayton Cycles

$$\eta_{cycle} = \frac{W_{Brayton}}{PBR_{th}}, \text{ where } W_{Brayton} = \eta_{Mechanical} W_{Gas-turbine} - W_{Compressors} \quad (5.64)$$

Combined Cycles

$$\eta_{cycle} = \frac{(W_{Brayton} - W_{Blower}) + W_{Rankine}}{PBR_{th}}, \text{ where } W_{Rankine} = W_{Steam-turbines} - W_{Pumps} \quad (5.65)$$

Total order of magnitude plant cost

The order-of-magnitude plant cost is defined as the sum of all the major PCU component capital costs, the capital cost of the building, the capital cost of the reactor and the capital cost of the steam plant, minus the capitalized income due to the power output.

$$C_{Total\ O\text{-}O\text{-}M} = C_{PCU} + C_{Building} + C_{Reactor} + C_{Steam\ Plant} - C_{Marginal\ Cost} \tag{5.66}$$

where $C_{PCU} = C_{Turbo\ Unit} + C_{Heat\ Exchangers} + C_{Blower} + C_{SBS\&RB}$

PCU order-of-magnitude capital cost

The PCU order-of-magnitude capital cost consists of the capital cost of the turbo units, heat exchangers, blowers, SBS and resister bank.

$$C_{PCU} = C_{Turbo\ Unit} + C_{Heat\ Exchangers} + C_{Blower} + C_{SBS\&RB} \tag{5.67}$$

$$C_{PCU} = C_{TurboUnit} + C_{Generator} + C_{Gearbox} + C_{Recuperator} + C_{IC} + C_{PC} + C_{IHX} + C_{Blower} + C_{SBS\&RB}$$

Turbo unit capital costs

The turbo unit capital cost consists of the capital costs of the turbo units, generator and gearbox.

$$C_{Turbo\ Unit} = C_{TurboUnit} + C_{Generator} + C_{Gearbox} \tag{5.68}$$

Heat exchanger capital costs

The heat exchangers capital cost consists of the capital costs of the recuperator, inter-cooler, pre-cooler and IHX.

$$C_{Heat\ Exchangers} = C_{Recuperator} + C_{IC} + C_{PC} + C_{IHX} \tag{5.69}$$

Steam plant capital cost

The steam plant capital cost includes all capital costs associated with the steam plant, including the steam plant building.

Marginal cost

The nuclear capacity cost (NCC) is taken as $2000 \frac{\$}{kW}$. It is assumed that the customer of a nuclear plant is willing to pay an additional 2 m$ for every additional MW available on the grid. Therefore a more efficient plant or a higher power level plant will be sold for more. This additional income is subtracted from the capital costs. Therefore a more efficient cycle is portrayed as being less expensive. For every MW above the referenced value of 185 MW, 2 m$ is therefore subtracted from the capital costs.

$$C_{Marginal\ Cost} = (W - 185) \cdot NCC \frac{\$}{kW} \tag{5.70}$$

Hydrogen plant efficiency

The co-generation thermal cycle efficiency is defined as: (see Chapter 3)

$$\eta_{total} = \frac{\left[W_{Brayton} - W_{Blower}\right] + \left[LHV_{Hydrogen} - EE\right]}{PBR} \tag{5.71}$$

Turbo machine isentropic efficiency

In order to compare the compressor and turbine isentropic efficiencies for the single, two- and three-shaft Brayton cycles, the total isentropic efficiency for all the compressors combined and

for all the turbines combined was calculated. See Chapter 3 for more details.

$$\eta_{turbines} = \frac{\sum\left(m \cdot c_p \Delta T_{actual}\right)}{\sum\left(m \cdot c_p \Delta T_{isentropic}\right)} \tag{5.72}$$

$$\eta_{compressor} = \frac{\sum\left(m \cdot c_p \Delta T_{isentropic}\right)}{\sum\left(m \cdot c_p \Delta T_{actual}\right)} \tag{5.73}$$

6.2 INPUT PARAMETERS

All the input parameters to the analyses are listed in Chapter 3. Except for the leak flows, these input values are kept the same for all the cycles. The following lists all the input variables to the analyses:

Guessed: $\eta_c,\ \eta_t,\ C_{a,c},\ C_{a,t}$

Brayton: $t_{min},\ t_{max},\ p_{min},\ p_{max},\ PBR,\ k_{PBMR},\ k_{comp},\ k_{turb},\ leakflows\ ,\%dP_{HXs},\ \%dP_{PIPING},\ \eta_{blower}$

Rankine: $t_{\min},\ t_{\max},\ p_{\max},\ \%dP_{RH},\ \%dP_{SG},\ t_{PINCH},\ CDx,\ \eta_{turbine},\ \eta_{pump}$

Fluids: $\gamma_{He}, R_{He},\ k_{He}, \gamma_{N2}, R_{N2},\ k_{N2}, \gamma_{MIX}, R_{MIX},\ k_{MIX}$

Hydrogen: $H_{2\text{-}MW}, H_{2\text{-}efficiency}$

Turbo Unit: $\eta_{Mechanichal}, (\phi, \psi, \sigma_{Max}, \rho_{Blade}, \eta s)_{Compressor}\ (\phi, \psi, \sigma_{Max}, \rho_{Blade}, \eta s, N_{PT})_{Turbine}$

Recuperator: $U_{Recuperator}, \eta_{Recuperator},\ d_{IHX},\ dT_{IHX}$

Coolers: $U_{IC},\ C_r,\ \eta_{IC},\ U_{PC},\ C_r,\ \eta_{PC}$

Costs: $NCC,\ Steam_{marginal},\ Steam_{offset},\ K_{C1},\ K_{T1},\ K_{Recupeartor},\ K_{IC},\ K_{PC},\ K_{IHX}, Kbase_{IHX}$

$C_{GEN\_GB},\ C_{SBS\_RB},\ C_{Building}, C_{Building\_CC},\ C_{Reactor}$

6.3 BRAYTON CYCLES

The isentropic efficiencies of the turbo machines were calculated as function of stage efficiency and tip radius – see also section 6.4.

This section presents the results for the six Brayton cycles. The thermal efficiency (*Figure 6.47*), reactor inlet temperature (*Figure 6.48*), mass flow (*Figure 6.49*), turbo unit capital cost (*Figure 6.50*), heat exchanger capital cost (*Figure 6.52*) and total order-of-magnitude capital cost (*Figure 6.53*) are given as function of total pressure ratio. The turbo unit costs are also presented as function of both the reactor outlet temperature (*Figure 6.55*) and the power turbine rotational speed (*Figure 6.56*).

The following graphs are relevant to the discussions in this section:

- *Figure 6.47 Thermal efficiency vs. pressure ratio for Brayton cycles*
- *Figure 6.48 Reactor inlet temperature vs. pressure ratio for Brayton cycles*
- *Figure 6.49 Mass flow vs. pressure ratio for Brayton cycles*
- *Figure 6.50 Turbo unit capital cost vs. pressure ratio for Brayton cycles – 1*
- *Figure 6.51 Turbo unit capital cost vs. pressure ratio for Brayton cycles – 2 separate*
- *Figure 6.52 Heat exchangers capital cost vs. pressure ratio for Brayton cycles*
- *Figure 6.53 Total order-of-magnitude plant cost vs. pressure ratio for Brayton cycles*
- *Figure 6.54 Turbo machine isentropic efficiency vs. pressure ratio for Brayton cycles*
- *Figure 6.55 Turbo unit capital cost vs. reactor outlet temperature for Brayton cycles*
- *Figure 6.56 Turbo unit capital cost vs. power turbine rotational speed for Brayton cycles*

Figure 6.47 presents the calculated thermal efficiency as function of total pressure ratio for each of the cycles. *Figure 6.47* shows that in general the thermal efficiency of a Brayton cycle is increased when the number of compression stages with inter-cooling is increased. However, the contribution of each additional stage to the thermal efficiency becomes less (from Cycle A to Cycle D to Cycle E).

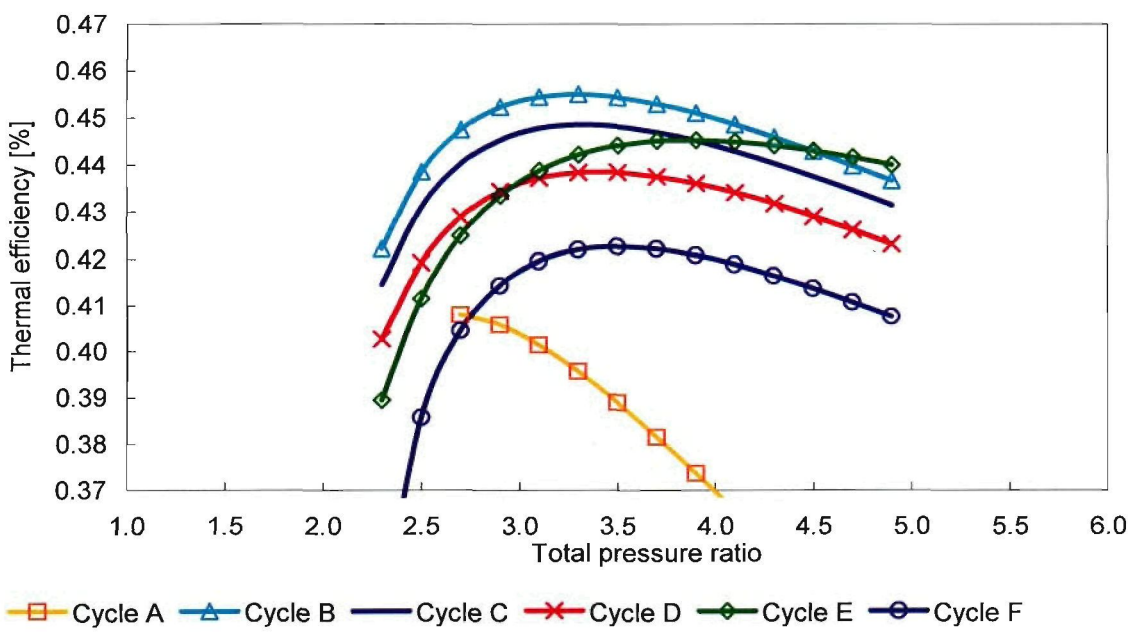


Figure 6.47 *Thermal efficiency vs. pressure ratio for Brayton cycles*

Cycles B, C and D represent single-, two- and three-shaft Brayton cycles with a single inter-cooler. The thermal efficiency of the single-shaft design is higher than the two-shaft and three-shaft designs. The reason for these differences can be ascribed to the different leak flows, turbo machine efficiencies and the turbo machine diffuser losses. The indirect cycle coupled to the single-shaft design (Cycle F) has the lowest efficiency of the single inter-cooled cycles. This is largely attributed to the temperature difference over the IHX.

Figure 6.48 and *Figure 6.49* present the reactor inlet temperature and mass flow as function of total pressure ratio for each of the cycles. The reactor inlet temperature of the PBR is limited to below 500 °C and the mass flow through the reactor to 200 kg/s.

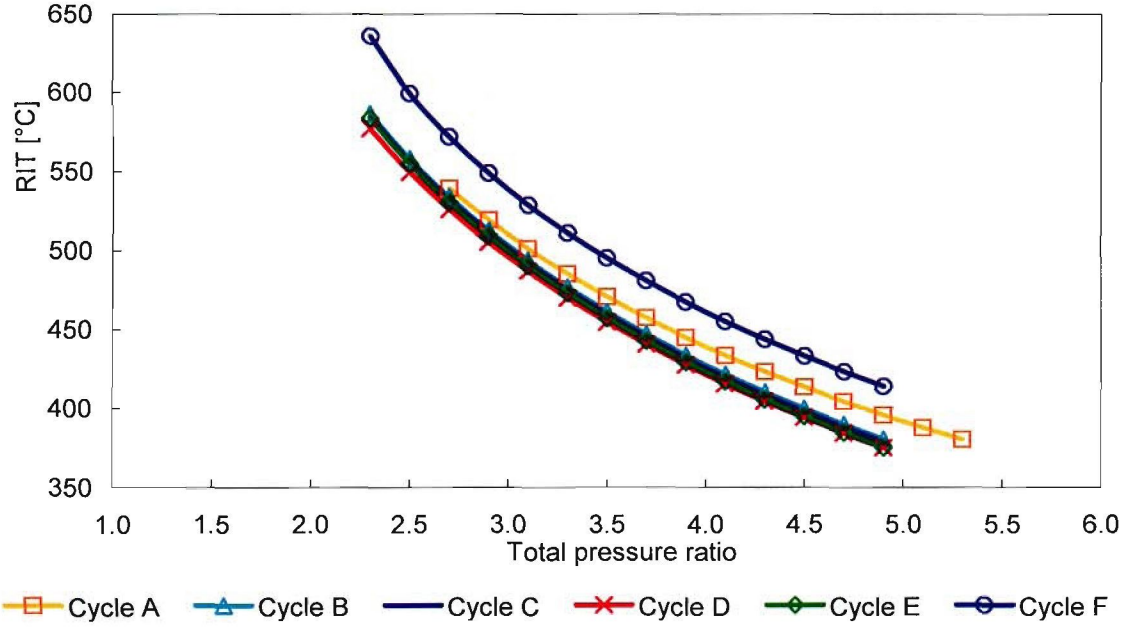


Figure 6.48 *Reactor inlet temperature vs. pressure ratio for Brayton cycles*

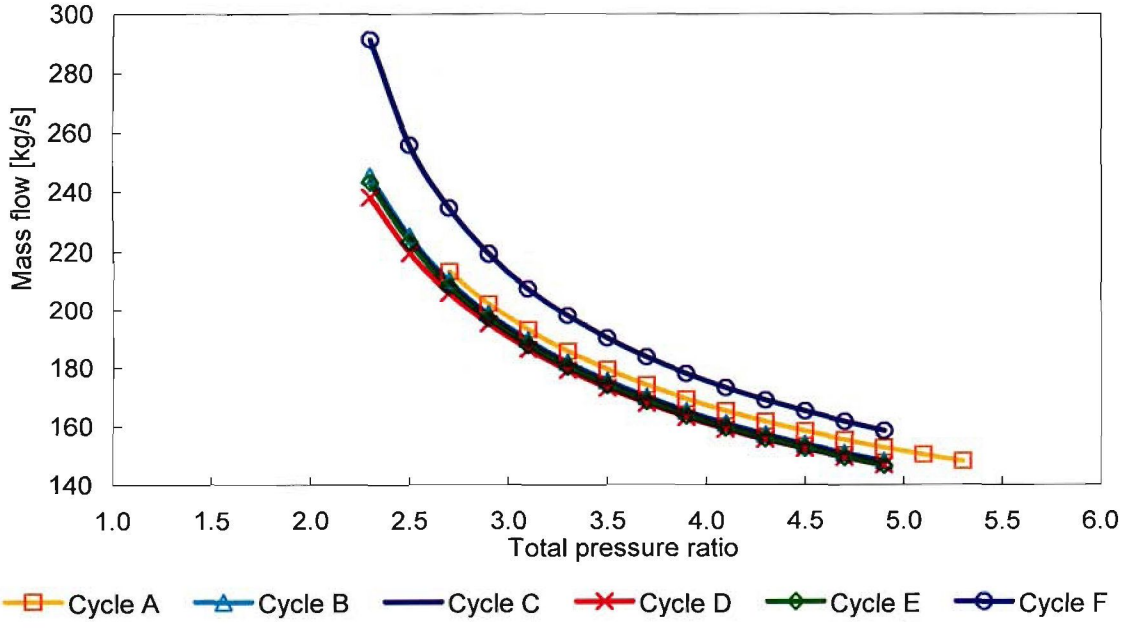


Figure 6.49 *Mass flow vs. pressure ratio for Brayton cycles*

The pressure ratio of the single-shaft design (Cycle A) needs to be higher than 3.1 in order to limit the reactor inlet temperature. The corresponding thermal efficiency is below 40 % and therefore the single-shaft without inter-cooling (Cycle A) does not seem like a viable cycle option from the viewpoint of reactor inlet temperature. The pressure ratio for the two-step inter-cooled Cycle E needs to be above 2.9, which will enable the cycle to still operate at its maximum cycle efficiency. All of the single inter-cooled cycles need to operate above a pressure ratio of 3, which allows these three cycles (B, C, D) to operate at their maximum efficiencies. The total pressure ratio of indirect Cycle F needs to be above 3.5 in order to operate at below the 500 °C RIT limitation.

Figure 6.50 presents the capital costs of all the turbo machines combined as function of the total pressure ratio. The separate capital cost of each cycle's compressors and turbines is presented in *Figure 6.51*. It is interesting to note the gradients in *Figure 6.50* . The three-shaft design (Cycle D) has the lowest gradient and the single-shaft designs (Cycle A, B, F) the highest gradients. *Figure 6.51* explains this phenomenon. The turbo machine cost increases at the same gradient for both of the three-shaft designs. As expected, the cost increases with pressure ratio.

See *Figure 6.50* and *Figure 6.51* for the discussion to follow. The turbo machine rotational speed is fixed for both Cycle A and Cycle B. Because the rotational speed is fixed, the size of all the machines increases with increasing pressure ratio. Therefore the HPC, LPC and LPT costs increase with pressure ratio. Interesting to note is that Cycle B is less expensive than Cycle A. Because the compressor after the inter-cooler (Cycle B) enters at a low temperature, the volumetric flow is smaller and therefore the machine as well. The combined cost of the two compressors of Cycle B is smaller than the cost of the single compressor of Cycle A and this saving is not totally negated by the additional inter-cooler costs. For the two-shaft design (Cycle C) the HPC and HPT speed is not fixed and was optimized with regard to cost. The cost of the HPC and HPT stays basically constant as the pressure ratio increases because the speed is adjusted at each pressure ratio to minimize the cost of the machine, while staying within all design limitations. The resulting gradient of the line for the total turbo machine cost for the two-shaft design is therefore less than for the single-shaft design.

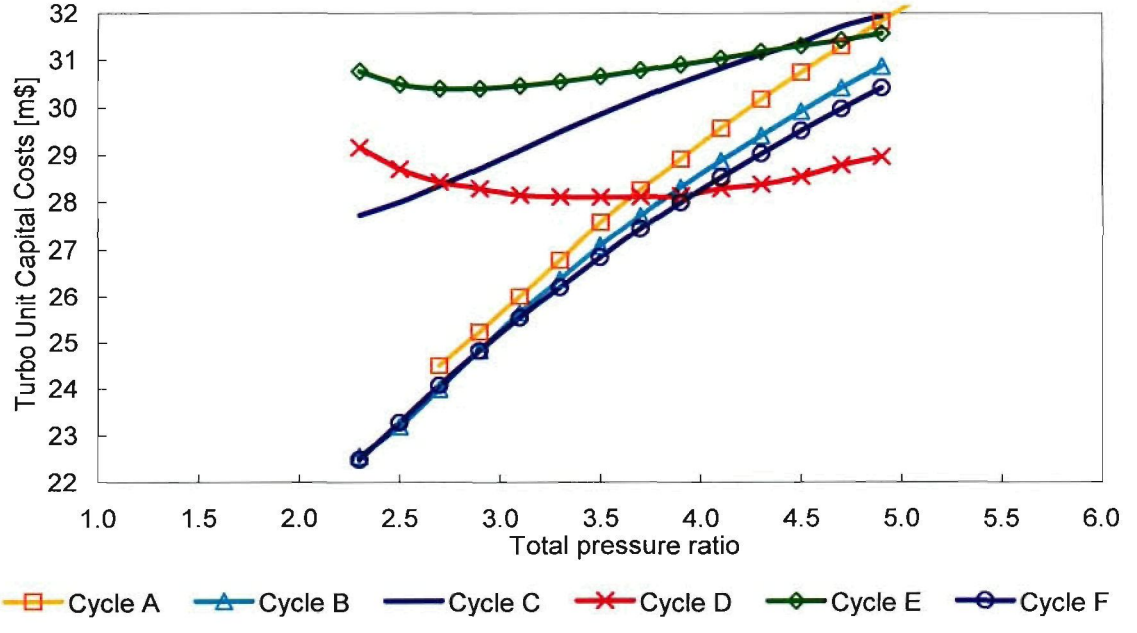


Figure 6.50 *Turbo unit capital cost vs. pressure ratio for Brayton cycles – 1*

For the three-shaft designs, both the HPC, HPT, LPC and LPT speeds are optimized with regard to cost and therefore all their costs stay basically constant with increasing pressure ratio. For Cycle D, only the cost of the power turbine increases with increasing pressure ratio. For Cycle E, both the cost of the power turbine and the cost of the LPC connected to the power turbine increase with pressure ratio. The gradient for the total turbo machine cost for the three-shaft designs is less than that for the two-shaft design.

The difference between the three-shaft designs is due to the additional capital cost of the compressor connected to the power turbine for the two-step inter-cooled Cycle E. At pressure ratios smaller than 4.0, the single-shaft designs (Cycle B) seem to be the cheapest with regard to turbo machine cost, followed by the three-shaft design with a single inter-cooler (Cycle D). Remember that these results are for a certain fixed power turbine speed (100 rev/s) – see *Figure 6.56* for the effect of rotational speed.

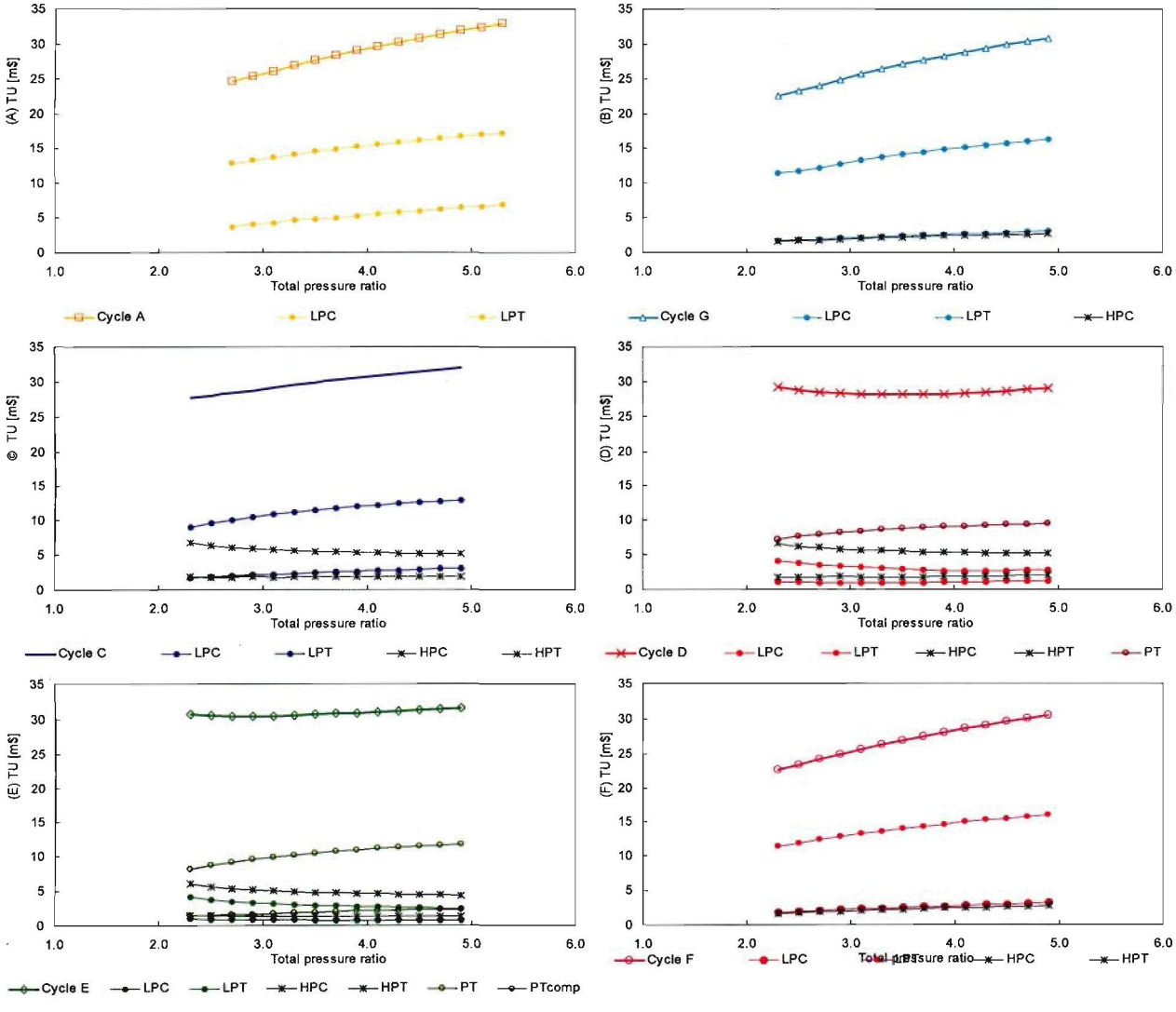


Figure 6.51 *Turbo unit capital cost vs. pressure ratio for Brayton cycles – 2 separate*

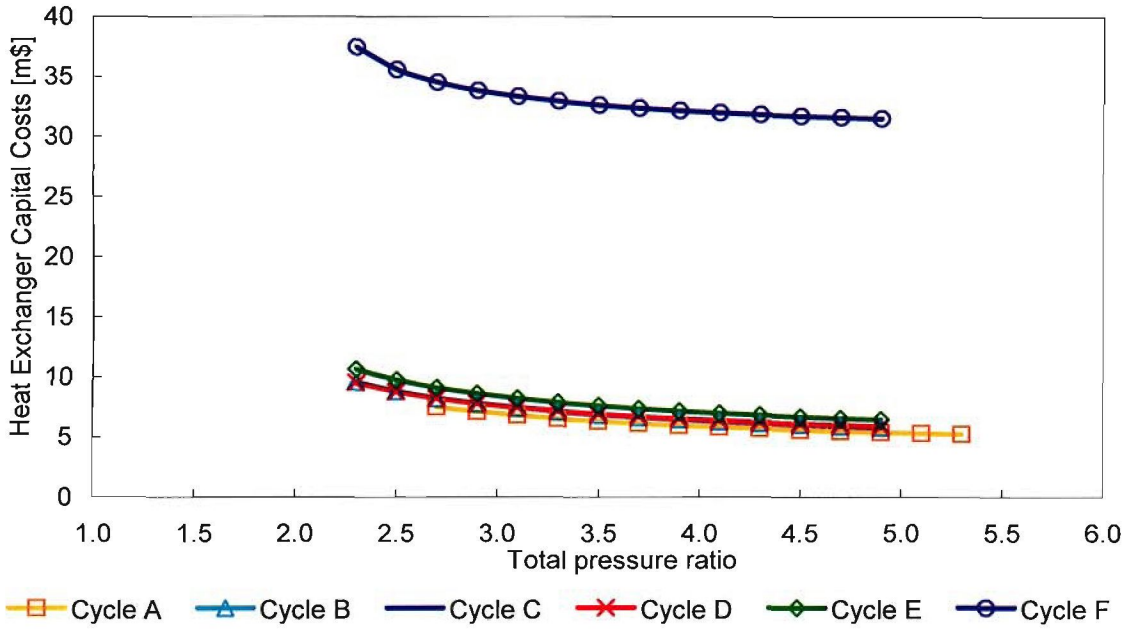


Figure 6.52 *Heat exchangers capital cost vs. pressure ratio for Brayton cycles*

Figure 6.52 shows the total heat exchanger cost as a function of pressure ratio. Since both the heat exchanger effectiveness and the heat transfer coefficient (U) are fixed, the heat transfer area of each heat exchanger is only a function of its mass flow. The mass flow decreases as the pressure ratio increases and therefore the total cost of the heat exchangers steadily decreases as well. The total capital cost of the heat exchangers is the same for the single-, two- and three-shaft inter-cooled Brayton cycles (B, C, D) because their mass flows are the same at each pressure ratio. The heat exchanger cost of Cycle E is the highest of the direct cycles due to the two-step inter-cooling and Cycle A is the least expensive of the direct cycles because there is no inter-cooler. Indirect Cycle F has the highest heat exchanger costs due the additional cost of the IHX (25m$).

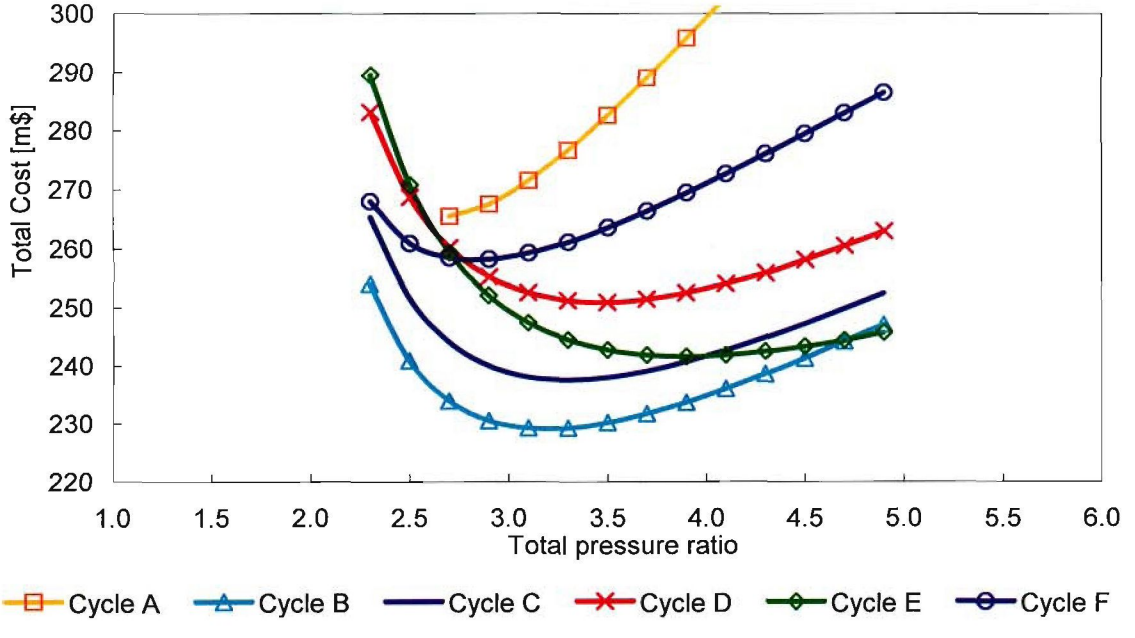


Figure 6.53 *Total order-of-magnitude plant cost vs. pressure ratio for Brayton cycles*

Figure 6.53 represents the total order-of-magnitude plant cost. Because a high cycle efficiency reduces the order-of-magnitude cost, the minimum cost will generally be realised at the maximum thermal cycle efficiency. The results show that the single-shaft inter-cooled design (Cycle B) is the least expensive in relative terms.

Total order-of-magnitude cost:

$$C_{Total\ O\text{-}O\text{-}M} = C_{PCU} + C_{Building} + C_{Reactor} + C_{Steam\ Plant} - C_{Marginal\ Cost}$$

Total turbo machine isentropic efficiency

The turbo machine isentropic efficiency is largely dependent on the number of stages, which is related to the pressure ratio over the turbo machine. For a fixed stage efficiency, the compressor isentropic efficiency will always decrease with increasing pressure ratio and the turbine efficiency will increase with increasing pressure ratio. This theoretical phenomenon corresponds with what would be expected in practice, where the boundary layer losses cause a compressor's efficiency to decrease with increasing number of stages. Generally, one would like to have as few compressor stages as possible and as many turbine stages as possible. At each pressure ratio, the turbo machine was optimized with regard to cost and the number of stages was calculated. The temperatures at points 2, 4, 6, 8, 10, 12 and 14 (see Chapter 5) were calculated using the compressor and turbine efficiencies as calculated by the component model. The combined isentropic efficiency over all the turbines and compressors is defined respectively by equations (5.74) and (5.75).

$$\eta_{turbines} = \frac{\sum\left(m \cdot c_p \Delta T_{actual}\right)}{\sum\left(m \cdot c_p \Delta T_{isentropic}\right)} = \frac{m_{7/8}(T_7 - T_8) + m_{9/10}(T_9 - T_{10}) + m_{11/12}(T_{11} - T_{12}) + m_{13/14}(T_{13} - T_{14})}{m_{7/8}(T_7 - T_{8'}) + m_{9/10}(T_9 - T_{10'}) + m_{11/12}(T_{11} - T_{12'}) + m_{13/14}(T_{13} - T_{14'})} \quad (5.74)$$

$$\eta_{compressor} = \frac{\sum\left(m \cdot c_p \Delta T_{isentropic}\right)}{\sum\left(m \cdot c_p \Delta T_{actual}\right)} = \frac{m_{1/2}(T_2 - T_1) + m_{3/4}(T_4 - T_3) + m_{5/6}(T_6 - T_5)}{m_{1/2}(T_{2'} - T_1) + m_{3/4}(T_{4'} - T_3) + m_{5/6}(T_{6'} - T_5)} \quad (5.75)$$

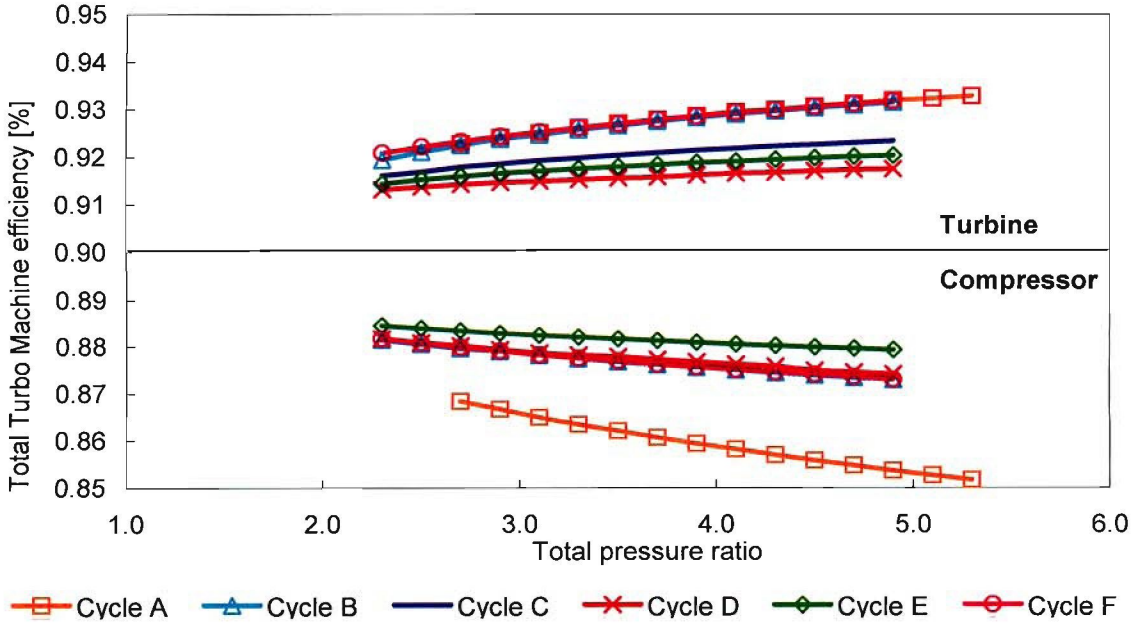


Figure 6.54 *Turbo machine isentropic efficiency vs. pressure ratio for Brayton cycles*

Figure 6.54 shows the effect of the pressure ratio on the total isentropic efficiency for all the compressors and turbines combined for each of the cycles. *Figure 6.54* shows that the single-shaft design (Cycle A) has the lowest compressor efficiency. Because only one compressor is used, the compressor has a large pressure ratio resulting in many stages. Cycles B, C and D all have two compressors and it was found that their efficiencies are very much the same because of the similar pressure ratio over each compressor. Cycle E has the highest compressor efficiency because the three compressors result in fewer number of stages per compressor. The turbine isentropic efficiency for the two single-shaft designs (Cycle A, B and F) is very similar since both cycles have only one turbine. The turbine efficiency decreases as the number of turbines increase.

Figure 6.55 shows how the turbo machine costs increase with increasing reactor outlet temperature for each cycle. The maximum allowable blade stress for the turbines is a function of the turbine inlet temperature. The maximum allowable blade stress decreases with increasing reactor outlet temperature. At higher temperatures, the turbine rotational speed will therefore need to decrease because of the lower permissible blade stresses. At each pressure ratio, the maximum allowable stress for the turbine was calculated as function of the turbine inlet temperature. The pressure ratio for all the cycles was fixed at 3.1. The power turbine speed is 100 rev/s. For the two- and three-shaft designs, the cost increases more rapidly. The advantage of multi-shaft systems is that the high-pressure turbo machine speed is not fixed. But, at higher temperatures the multi-shaft designs looses this advantage because the higher temperatures require that the turbo machine operates at lower speeds in order to reduce the permissible blade stresses. Consequently, at temperatures above 870 °C, the turbo machines for two- and three-shaft concepts are no longer less expensive than those for the single-shaft concept (see *Figure 6.55*).

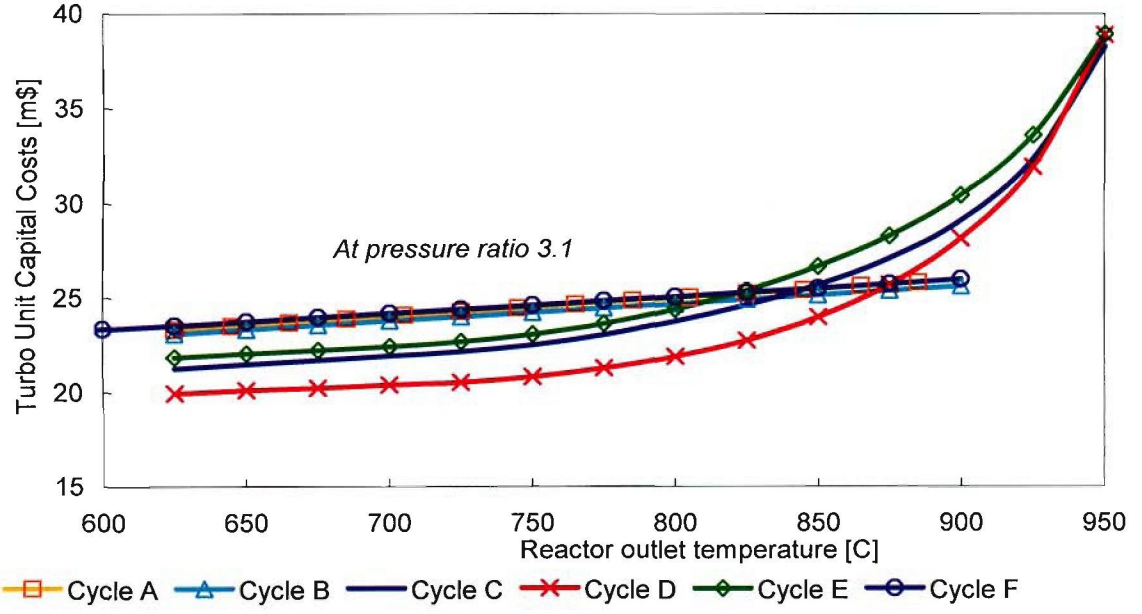


Figure 6.55 *Turbo unit capital cost vs. reactor outlet temperature for Brayton cycles*

Figure 6.56 shows how the turbo machine costs decrease as the power turbine rotational speed increases. The reactor outlet temperature is fixed at 900 °C. *Figure 6.56* shows that the single-shaft design only becomes viable at power turbine speeds above 85 rev/s. Should the single-shaft design be chosen, it would therefore be advisable to have a gearbox connecting it to the low-speed generator.

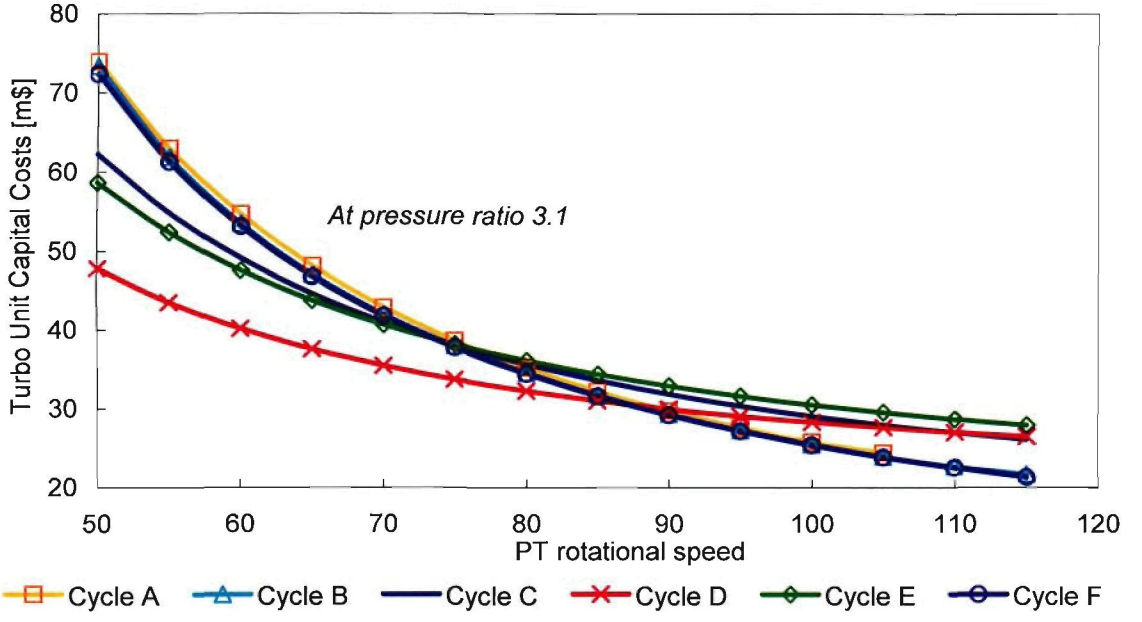


Figure 6.56 *Turbo unit capital cost vs. power turbine rotational speed for Brayton cycles*

6.4 COMBINED CYCLES

The isentropic efficiencies of the turbo machines were **NOT** calculated as function of stage efficiency and tip radius. The isentropic efficiency for the compressor and turbine was fixed for all these results.

In this section, the results are presented for the Combined Cycles G, H, I and J together again with Brayton Cycle B and Cycle F. In section 7.1 it is motivated why Cycle B and Cycle F were chosen as the only Brayton cycles to be further investigated. The final recommendations will be made between these six cycles.

The following graphs are relevant to the discussions in this section:

- *Figure 6.57 T-s diagrams*
- *Figure 6.58 Heat transfer vs. Temperature*
- *Figure 6.59 Thermal efficiency vs. pressure ratio for Brayton & Combined Cycles*
- *Figure 6.60 Reactor inlet temperature vs. pressure ratio for Brayton & Combined Cycles*
- *Figure 6.61 Mass flow vs. pressure ratio for Brayton & Combined Cycles*
- *Figure 6.62 Turbo unit capital cost vs. pressure ratio for Brayton & Combined Cycles*
- *Figure 6.63 Heat exchangers capital cost vs. pressure ratio for Brayton & Combined Cycles*
- *Figure 6.64 PCU order-of-magnitude capital cost vs. pressure ratio for Brayton & Combined Cycles*
- *Figure 6.65 Power output vs. pressure ratio for Brayton & Combined Cycles*
- *Figure 6.68 Steam plant capital cost vs. pressure ratio for Brayton & Combined Cycles*
- *Figure 6.66 Total order of magnitude plant cost vs. pressure ratio for Brayton & Combined Cycles NCC=2000$/kW*
- *Figure 6.67 Total order of magnitude plant cost vs. pressure ratio for Brayton & Combined Cycles NCC=1000$/kW*
- *Table **6.8** Cost Breakdown for Cycles B, F, G, H, I and J*

The temperature-entropy (t-s) diagrams for Cycles B, G, H, I and J at their respective design points are presented in *Figure 6.57*. The line between the Brayton and Rankine sections for Cycles G, H and J represents the temperature loss due to the IHX.

Figure 6.58 presents the temperature in the steam generator as function of heat transfer. Each cycle has two lines. The two lines for each cycle represent the steam generator where the top line represents the Brayton side and the bottom line the Rankine side. This graph indicates how the Rankine was custom-designed to exactly fit the Brayton cycle, with the minimum allowable pinch temperature.

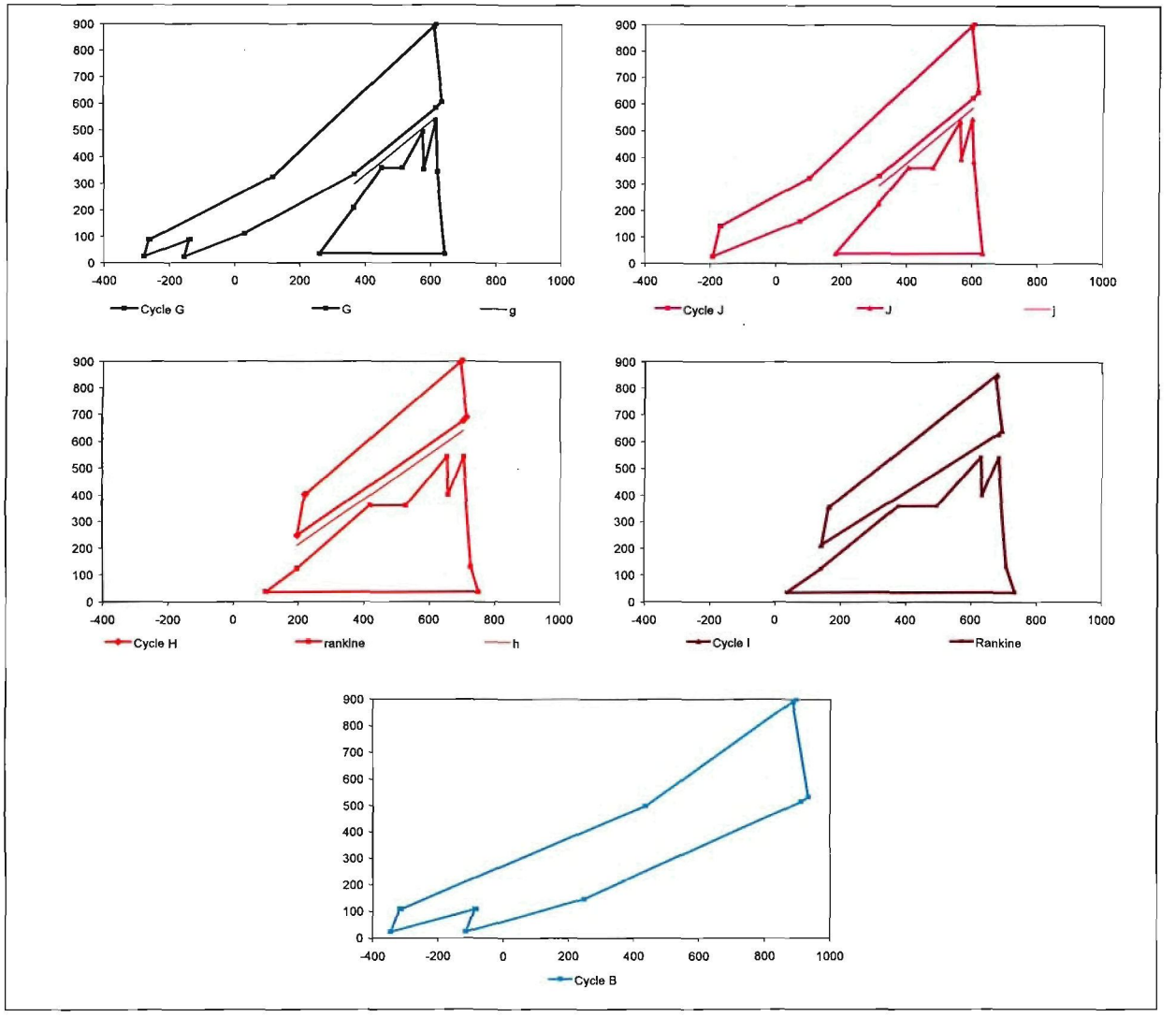


Figure 6.57 *T-s diagrams*

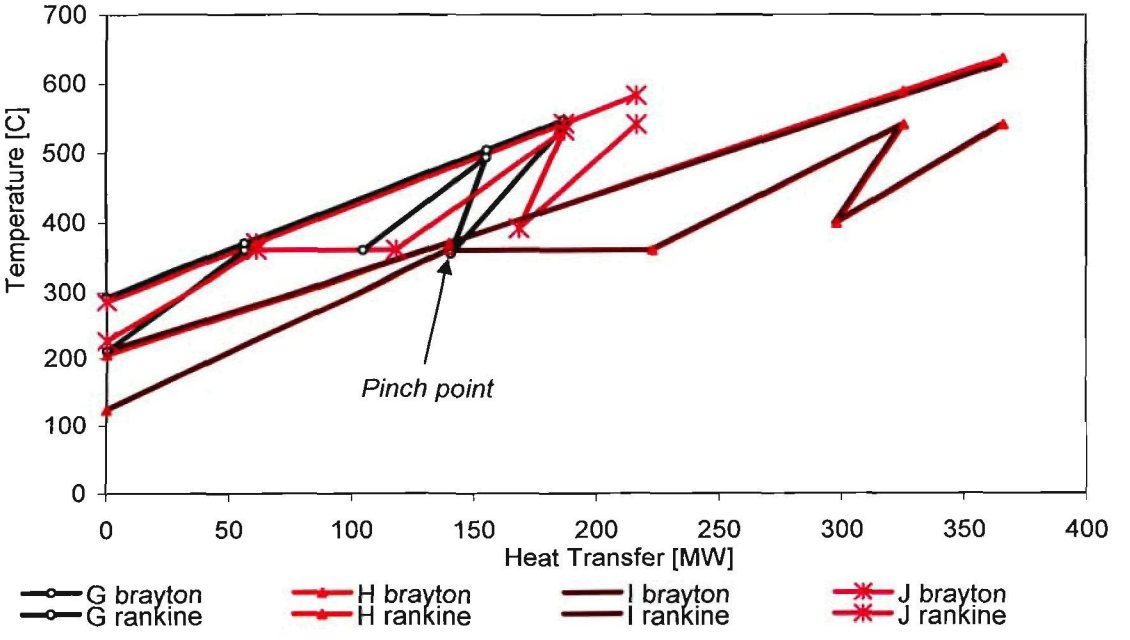


Figure 6.58 *Heat transfer vs. Temperature*

Figure 6.59 presents the thermal cycle efficiency as function of total pressure ratio. The high efficiencies of the Combined Cycles are attributed to the fact that the Combined Cycles reject heat at a lower cycle temperature in the condenser where as the Brayton cycles reject heat at higher temperatures in the inter-cooler and pre-cooler.

It was found that Cycle H and Cycle I have the highest efficiency. Although Cycle H is direct and Cycle I indirect, they have the same efficiency. Both Cycle H and Cycle I have an IHX - Cycle H at the bottom and Cycle I at the top. For the same temperature difference, the IHX for Cycle I is physically larger than for Cycle H. The temperature difference over Cycle I was specified and the size was calculated. The same size was assumed for the IHX of Cycle H, and the temperature difference was calculated. The sizes were thus kept the same and not the temperature difference.

Cycle G rejects all its inter-cooler heat and uses the pre-cooler heat above 35 °C to preheat the Rankine cycle. Cycle J is more efficient that Cycle G because Cycle J does not have an inter-cooler. The pre-cooler of Cycle J uses all the heat (above 35 °C) that would have been rejected in the inter-cooler to preheat the Rankine cycle.

The Brayton cycle rejects all its inter-cooler and pre-cooler heat, resulting in lower cycle efficiencies. The indirect Cycle F is 3 % less efficient than the Brayton cycle due to the temperature loss over the IHX, pressure losses in the piping and IHX and the lower blower efficiency.

The working point for the Brayton cycles is at a pressure ratio of **3.1**, for Combined Cycle H and Cycle I at **1.8**, for Combined Cycle G at **2.4** and for Combined Cycle J at **2.1**.

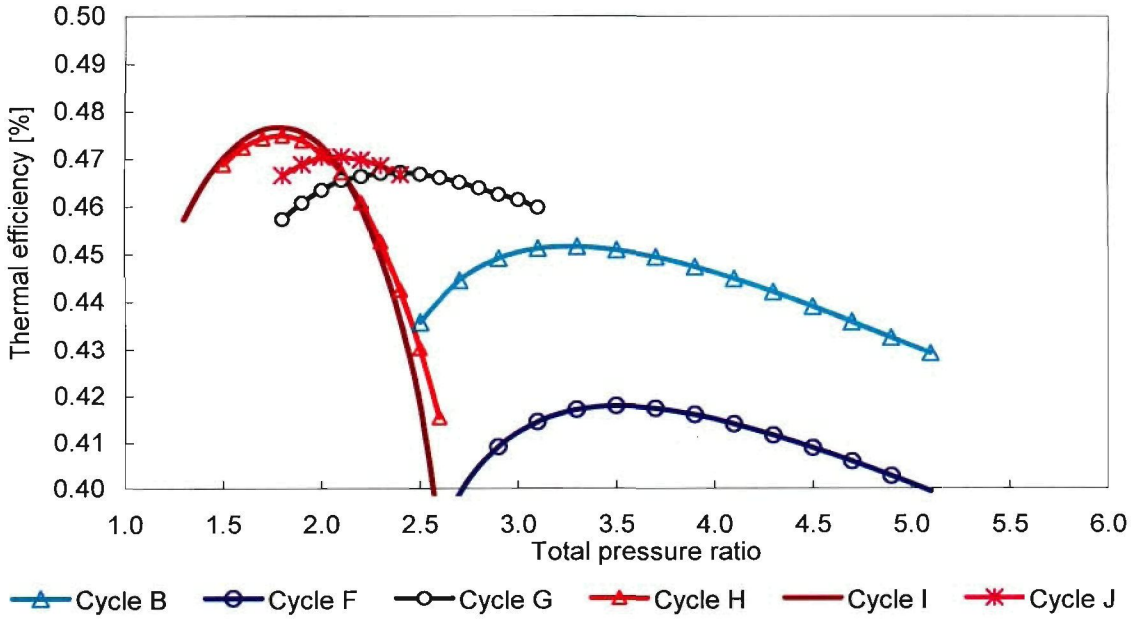


Figure 6.59 *Thermal efficiency vs. pressure ratio for Brayton & Combined Cycles*

Figure 6.60 and *Figure 6.61* presents the reactor inlet temperature and mass flow as function of total pressure ratio. The mass flows of Cycle H and Cycle I are almost 22 % smaller than the Brayton mass flows at the respective design points. Indirect Cycle I has a slightly higher reactor inlet temperature than Cycle H due to the additional temperature rise over the blower. Due to the larger mass flows of the Brayton cycles, the primary loop blower is also larger than for the Combined Cycles. The large blower of Cycle F results in a large temperature difference over the blower which explains the higher reactor inlet temperature of Cycle F. The mass flow of Cycle G and Cycle J are almost 32% smaller than the Brayton mass flow, resulting in favourably low reactor inlet temperatures.

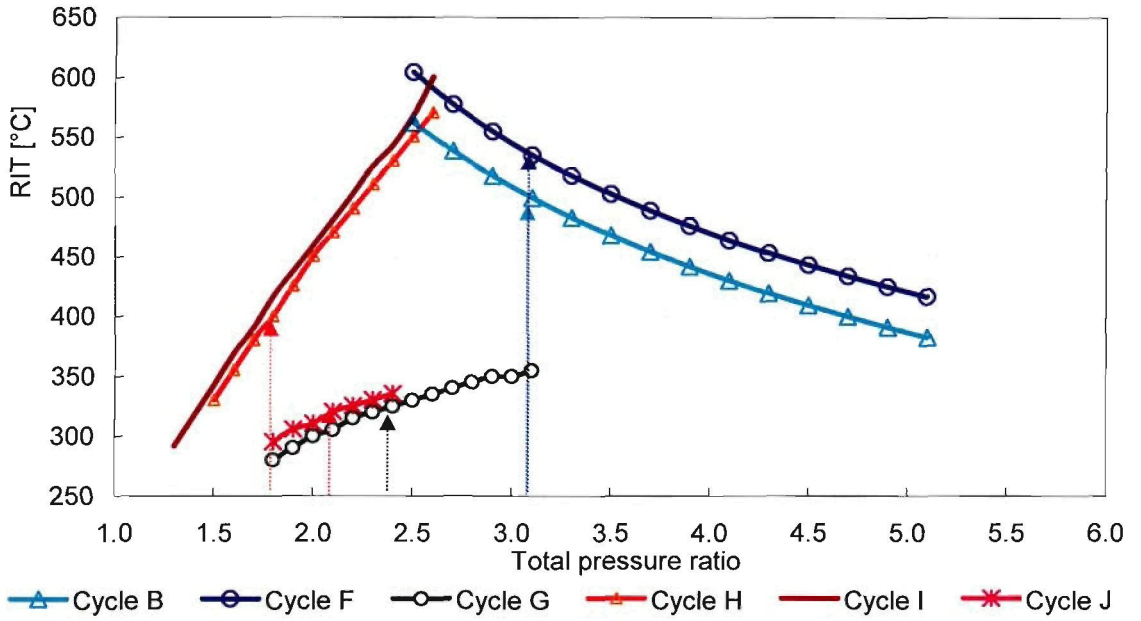


Figure 6.60 *Reactor inlet temperature vs. pressure ratio for Brayton & Combined Cycles*

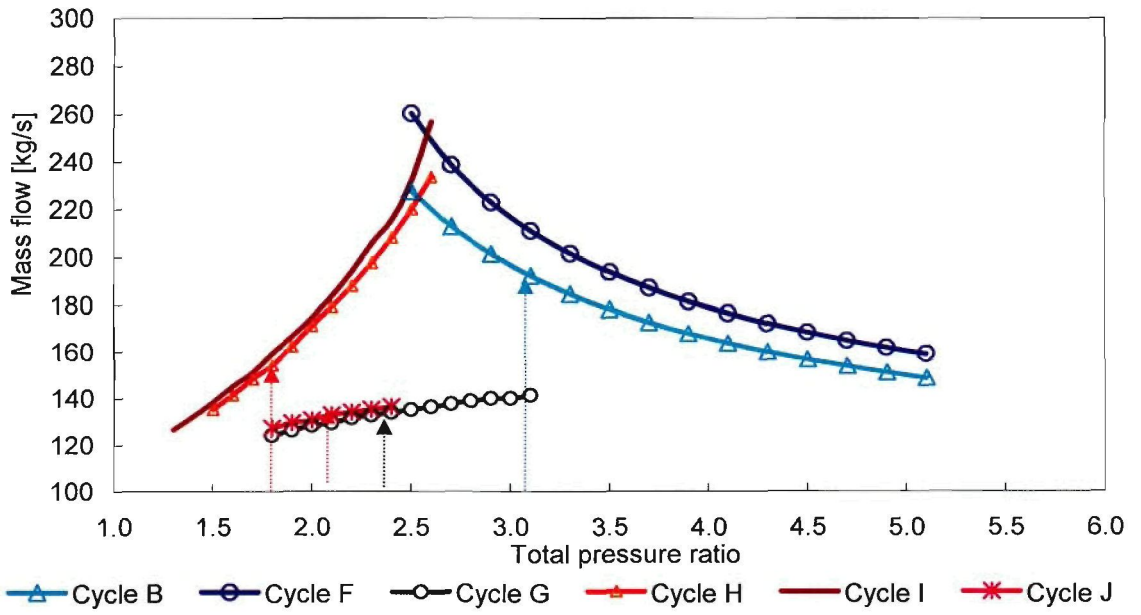


Figure 6.61 *Mass flow vs. pressure ratio for Brayton & Combined Cycles*

Figure 6.62 presents the total turbo unit capital cost as function of total pressure ratio. It was found that the Brayton cycles are almost 28% more expensive than the Combined Cycles. The turbo machines of the Combined Cycles are significantly smaller than the Brayton machines due to the lower mass flows. Cycles H, I and J also have one less compressor than does Cycles B, F and G.

Figure 6.63 presents the total heat exchanger capital cost as function of total pressure ratio. The IHX for the indirect cycles are assumed to cost in the region of 25 m$ (including development costs), making the indirect cycle heat exchanger cost the most expensive. Cycle H is the least expensive, consisting only of one heat exchanger at low inlet (< 700 °C) temperatures. Cycles B, G and J average the same heat exchanger costs. Although Cycle G has the most heat exchangers, they are all relatively small because of the low mass flows.

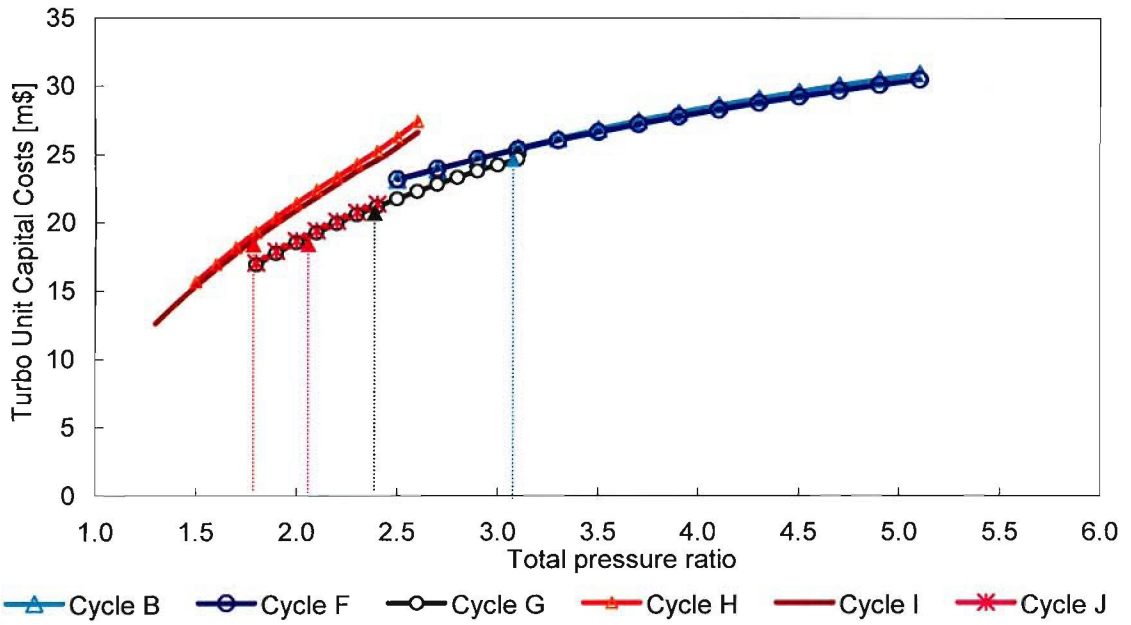


Figure 6.62 *Turbo unit capital cost vs. pressure ratio for Brayton & Combined Cycles*

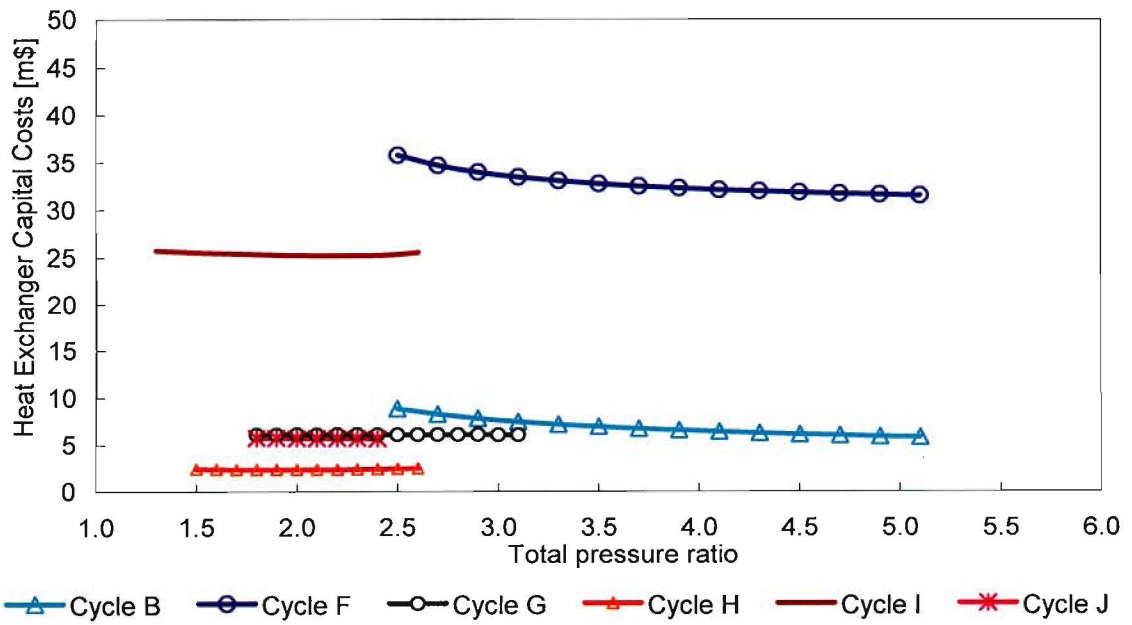


Figure 6.63 *Heat exchangers capital cost vs. pressure ratio for Brayton & Combined Cycles*

Figure 6.64 presents the total PCU order-of-magnitude capital cost as function of total pressure ratio. The PCU order-of-magnitude cost consists of the capital cost of the turbo units, generator, gearbox, heat exchangers and blower. It was found that the direct Combined Cycles have the lowest PCU order-of-magnitude capital cost. *The PCU referred to here is that of the Brayton sections only.*

Figure 6.65 presents the net work output as function of total pressure ratio. The solid lines refer to the total work output and the dotted lines refer to the steam plant work output. For Cycle G and Cycle J, it was found that only about 45 % and 52 % of the total work output at the design point is produced by the steam plant. For Cycle H and Cycle I, it was found that almost 80 % of the total work output is produced by the steam plant. Cycle H and Cycle I consist of large steam plants and small Brayton cycles.

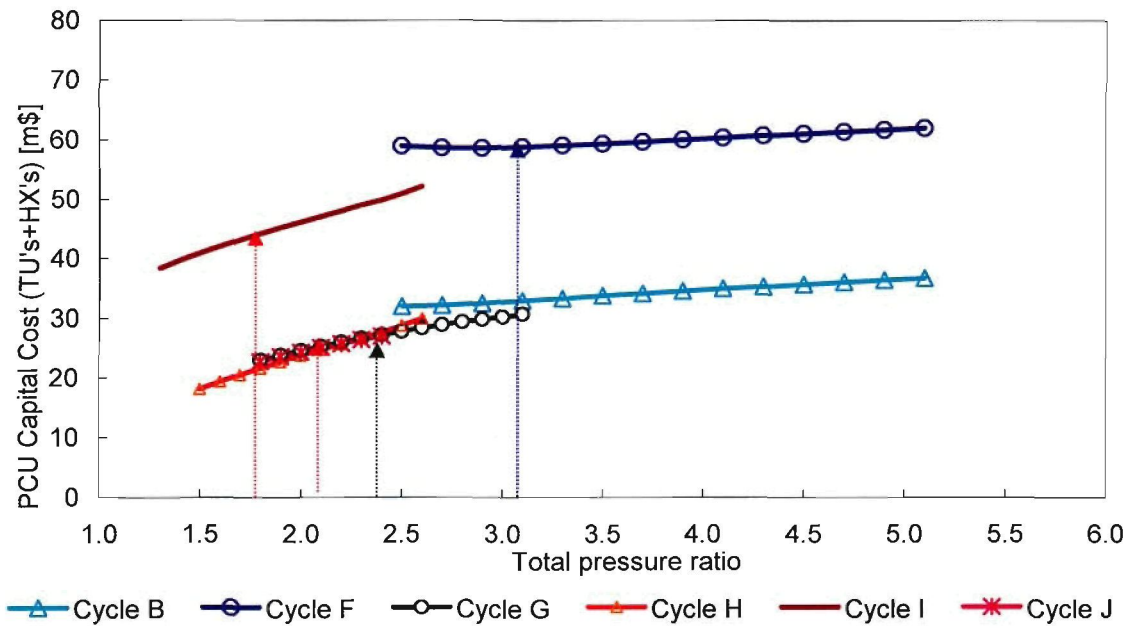


Figure 6.64 *PCU order-of-magnitude capital cost vs. pressure ratio for Brayton & Combined Cycles*

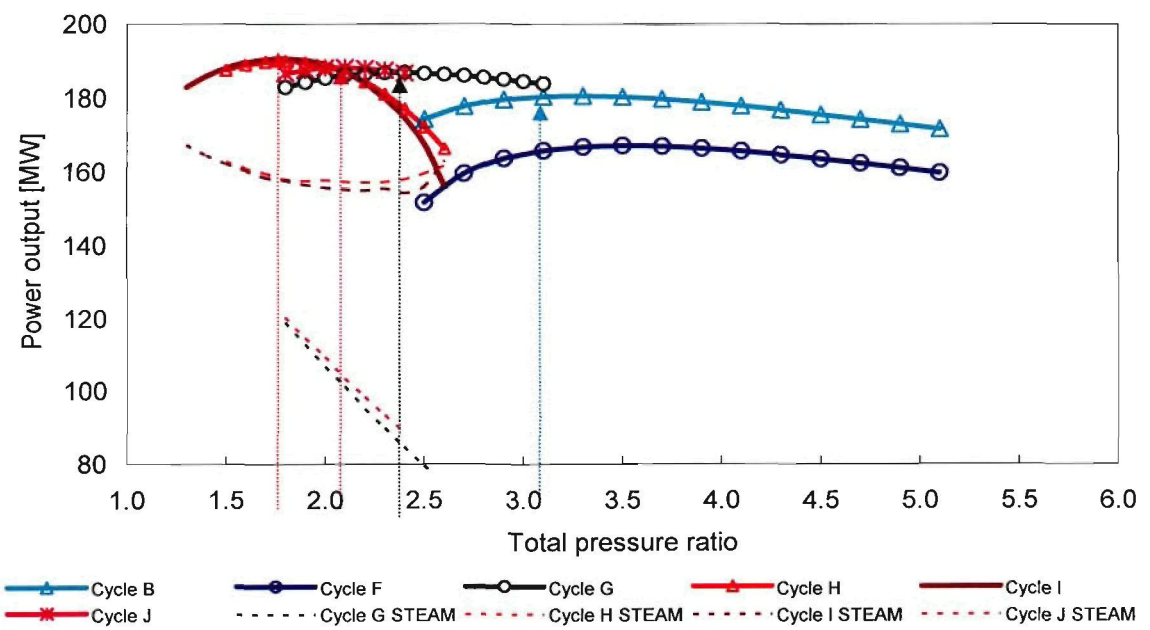


Figure 6.65 *Power output vs. pressure ratio for Brayton & Combined Cycles*

Figure 6.66 and *Figure 6.67* present the total order-of-magnitude cost as function of total pressure ratio for a NCC of 2000 $\frac{\$}{kW}$ and 1000 $\frac{\$}{kW}$ respectively. The total order-of-magnitude plant cost is defined as the sum of all the major PCU component capital costs, the capital cost of the building, the capital cost of the reactor and the capital cost of the steam plant, minus the capitalized income due to the power output.

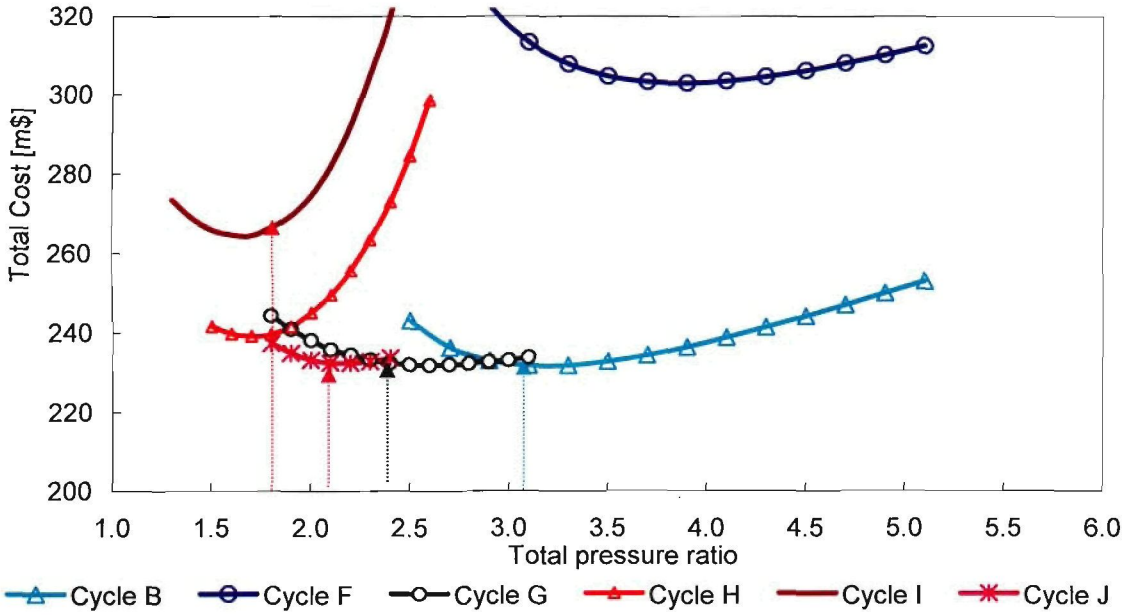


Figure 6.66 *Total order of magnitude plant cost vs. pressure ratio for Brayton & Combined Cycles NCC=2000$/kW*

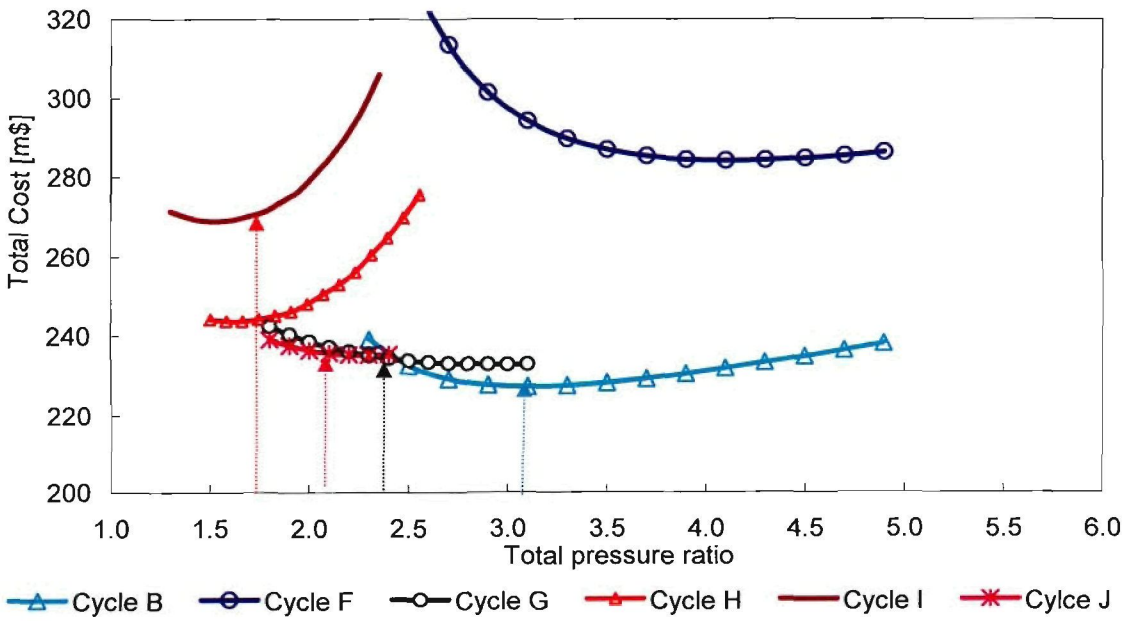


Figure 6.67 *Total order of magnitude plant cost vs. pressure ratio for Brayton & Combined Cycles NCC=1000$/kW*

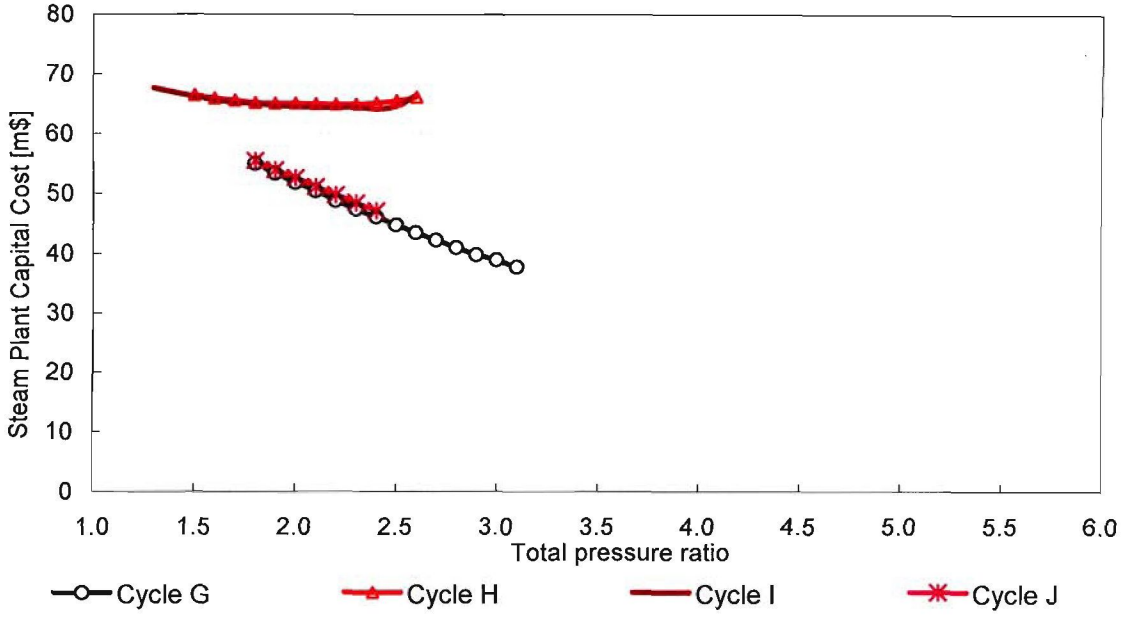


Figure 6.68 *Steam plant capital cost vs. pressure ratio for Brayton & Combined Cycles*

Figure 6.68 presents the steam plant capital cost as function of total pressure ratio. Cycle H and Cycle I are larger and therefore more expensive than Cycle G and Cycle J.

	Cycle	Units	(B)	(F)	(G)	(H)	(I)	(J)	
	Total pressure ratio		**3.1**	**3.1**	**2.4**	**1.8**	**1.8**	**2.1**	**Reference**
a	Turbo Units + GB + Generator	[m$]	25.3	25.3	21.1	19.5	18.6	19.3	Figure 6.62
b	Heat Exchangers	[m$]	7.5	33.4	6.1	2.3	25.3	5.7	Figure 6.63
c	Blower	[m$]	0.0	26.2	4.0	4.0	9.4	4.0	
d	Building	[m$]	113.0	113.0	82.0	82.0	82.0	82.0	Fixed
e	Reactor	[m$]	77.0	77.0	77.0	77.0	77.0	77.0	Fixed
f	Steam Plant	[m$]	0.0	0.0	46.0	64.9	64.9	50.9	Figure 6.68
g	Marginal Cost NCC 2000 $\frac{\$}{kW}$	[m$]	-9.0	-38.4	3.6	9.6	11.4	6.4	-
h	Marginal Cost NCC 1000 $\frac{\$}{kW}$	[m$]	-4.5	-19.2	1.8	4.8	5.7	3.2	-
i	Total o-o-m plant cost 2000 $\frac{\$}{kW}$	[m$]	231.8	313.3	232.6	240.1	265.8	232.5	Figure 6.66
j	Total o-o-m plant cost 1000 $\frac{\$}{kW}$	[m$]	227.3	294.1	234.4	244.9	271.5	235.7	Figure 6.67
k	Work Output	[MWth]	180.5	165.8	186.8	189.8	190.7	188.2	Figure 6.65

Table 6.8 *Cost Breakdown for Cycles B, F, G, H, I and J*

Table 6.8 gives the cost breakdown for each cycle - see equations (5.76) to (5.79).

$$g = (k - 185) \cdot 2 \frac{m\$}{MW} \tag{5.76}$$

$$h = (k - 185) \cdot 1 \frac{m\$}{MW} \tag{5.77}$$

$$i = a + b + c + d + e + f - g \tag{5.78}$$

$$j = a + b + c + d + e + f - h \tag{5.79}$$

Cycle B has the lowest relative cost for a NCC of 1000 $\frac{\$}{kW}$, although Cycles G, H and J compare favourably with Cycle B. The costs of Cycles B, G, H and J are basically the same for a NCC of 2000 $\frac{\$}{kW}$. At the lower NCC of 1000, Cycle B performs better because Cycle G, H and J lose some of the advantage of having a higher cycle efficiency. Cycle I is about 25 m$ more expensive than Cycle H due to the expensive IHX. Interesting to note is that although the cost of Cycle G, H and J include that of an entire steam plant, their total costs still compare favourably with Cycle B. Cycle F is the most expensive due to the low cycle efficiency (low power output) and the expensive IHX.

The costs of Cycle B, G, H and J are relatively close. Although Cycle I is approximately 25 m$ more expensive than Cycle H, the additional advantages of Cycle I need to be evaluated. The question arises as to how these six cycles will compare at different reactor outlet temperatures and power levels – see next section. Comments as to the best cycle are reserved for section 7.1.

6.5 DESIGN ENVELOPES

It is important from a NGNP technology growth potential viewpoint to know how each of these cycles will perform at other power levels and reactor outlet temperatures. The power conversion unit has certain restrictions with regard to mass flow, pressure ratio and reactor inlet temperature and needs to operate within this design envelope.

- The reactor riser channels have a maximum velocity restriction. The velocity restriction translates to a mass flow of around 200 kg/s at 90 Bar.
- The total pressure ratio across the compressors directly influences the turbo machine size. The total pressure ratio across the compressors is limited to 3.5 to ensure a practical turbo machine design.
- The maximum allowable temperature for the core barrel is 500 °C, which limits the reactor inlet temperature to around 500 °C.

In this section the total cost of each cycle is calculated for a reactor outlet temperature of 850 °C, 900 °C and 1100 °C for both 400 MW and 600 MW reactor thermal power options. A design envelope is drawn for each scenario, showing which cycles yield a practical solution. The same PBR reactor design is used for all the cycles at all temperatures and all power levels. At higher power levels, the higher mass flow through the reactor results in larger pressure losses through the reactor and therefore decreases the thermal cycle efficiency. *Figure 6.69*, *Figure 6.73* and *Figure 6.77* indicate that the 600 MW cycles have lower thermal cycle efficiencies than the 400 MW cycles.

The following graphs are relevant to the discussions in this section:

- *Figure 6.69 Thermal efficiency vs. pressure ratio at ROT 850 °C*
- *Figure 6.70 Reactor inlet temperature vs. pressure ratio at ROT 850 °C*
- *Figure 6.71 Mass flow vs. pressure ratio at ROT 850 °C*
- *Figure 6.72 Total plant order of magnitude capital cost vs. pressure ratio at ROT 850 °C cycles*
- *Figure 6.73 Thermal efficiency vs. pressure ratio at ROT 900 °C*
- *Figure 6.74 Reactor inlet temperature vs. pressure ratio at ROT 900 °C*
- *Figure 6.75 Mass flow vs. pressure ratio at ROT 900 °C*
- *Figure 6.76 Total plant order of magnitude capital cost vs. pressure ratio at ROT 900 °C cycles*
- *Figure 6.77 Thermal efficiency vs. pressure ratio at ROT 1100 °C*
- *Figure 6.78 Reactor inlet temperature vs. pressure ratio at ROT 1100 °C*
- *Figure 6.79 Mass flow vs. pressure ratio at ROT 1100 °C*
- *Figure 6.80 Total plant order of magnitude capital cost vs. pressure ratio at ROT 1100 °C cycles*

6.5.1 Reactor outlet temperature: 850 °C

Figure 6.69, Figure 6.70, Figure 6.71 and *Figure 6.72* present the thermal cycle efficiency, reactor inlet temperature, mass flow and total order-of-magnitude plant cost as function of total pressure ratio. The green shaded areas indicate the region where no solutions were found.

Figure 6.71 indicates that for a reactor outlet temperature of 850 °C there are no solutions for the 600 MW cases. There are no solutions for Cycle F at 400 MW. Cycle B at 400 MW has a very small design envelope. *Figure 6.72* shows the practical solutions for a reactor outlet temperature of 850 °C.

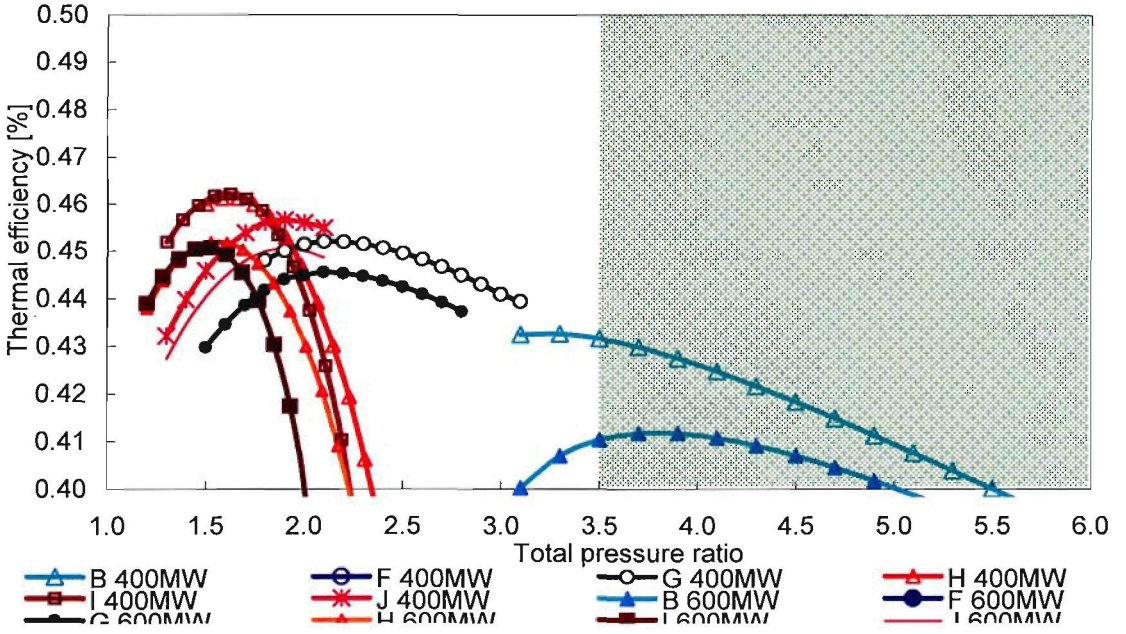


Figure 6.69 *Thermal efficiency vs. pressure ratio at ROT 850 °C*

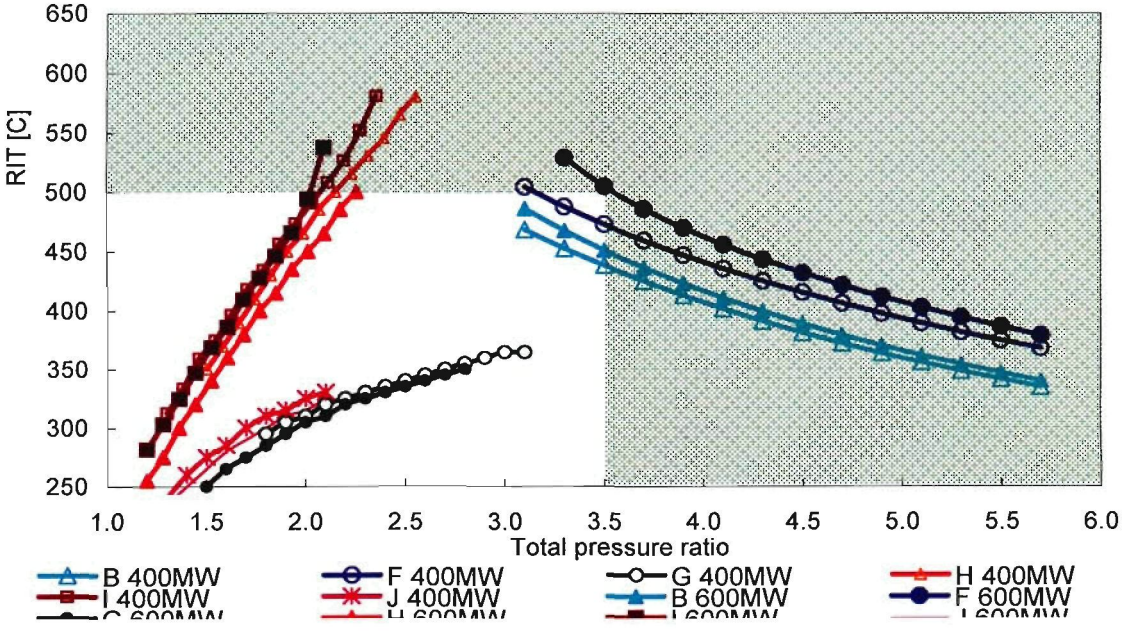


Figure 6.70 *Reactor inlet temperature vs. pressure ratio at ROT 850 °C*

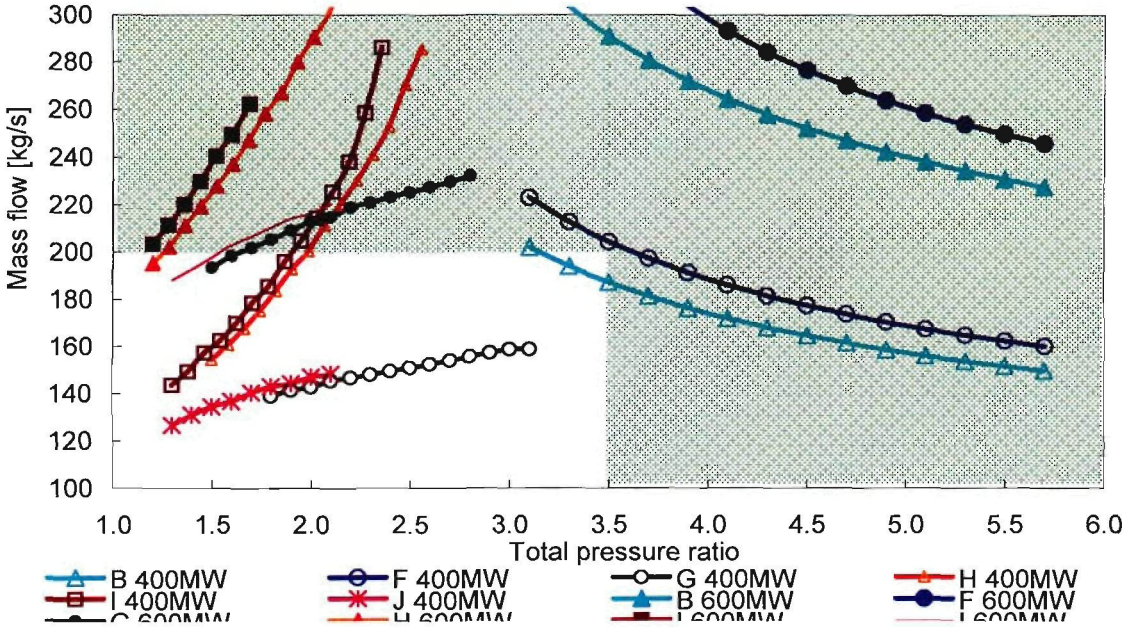


Figure 6.71 *Mass flow vs. pressure ratio at ROT 850 °C*

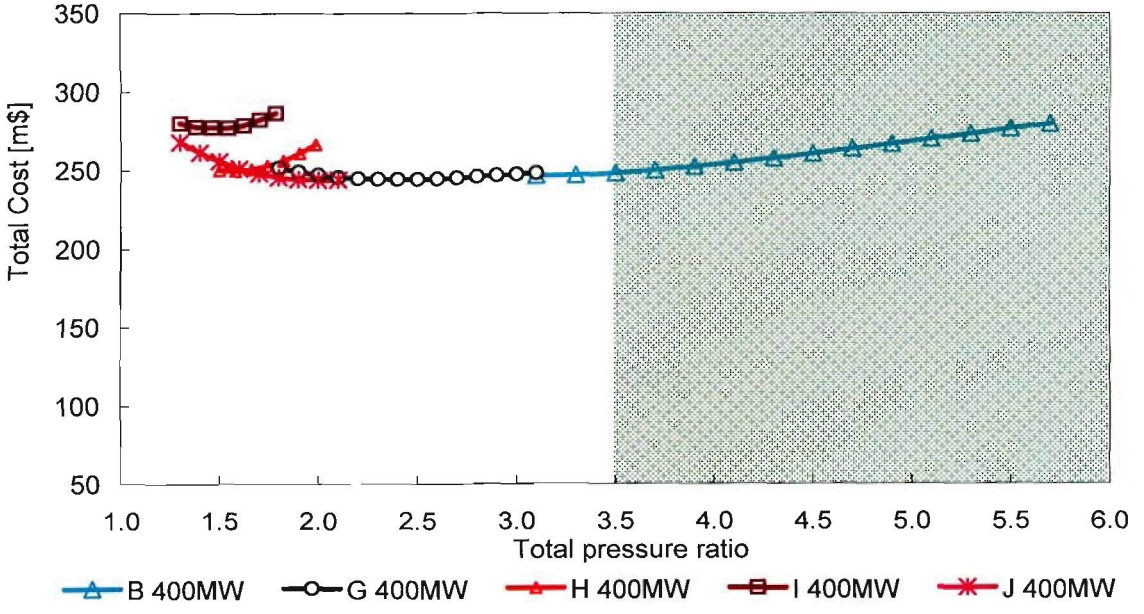


Figure 6.72 *Total plant order of magnitude capital cost vs. pressure ratio at ROT 850 °C cycles*

6.5.2 Reactor outlet temperature: 900 °C

Figure 6.73, *Figure 6.74*, *Figure 6.75* and *Figure 6.76* present the thermal cycle efficiency, reactor inlet temperature, mass flow and total order-of-magnitude plant cost as function of total pressure ratio. The green shaded areas indicate the region where no solutions were found.

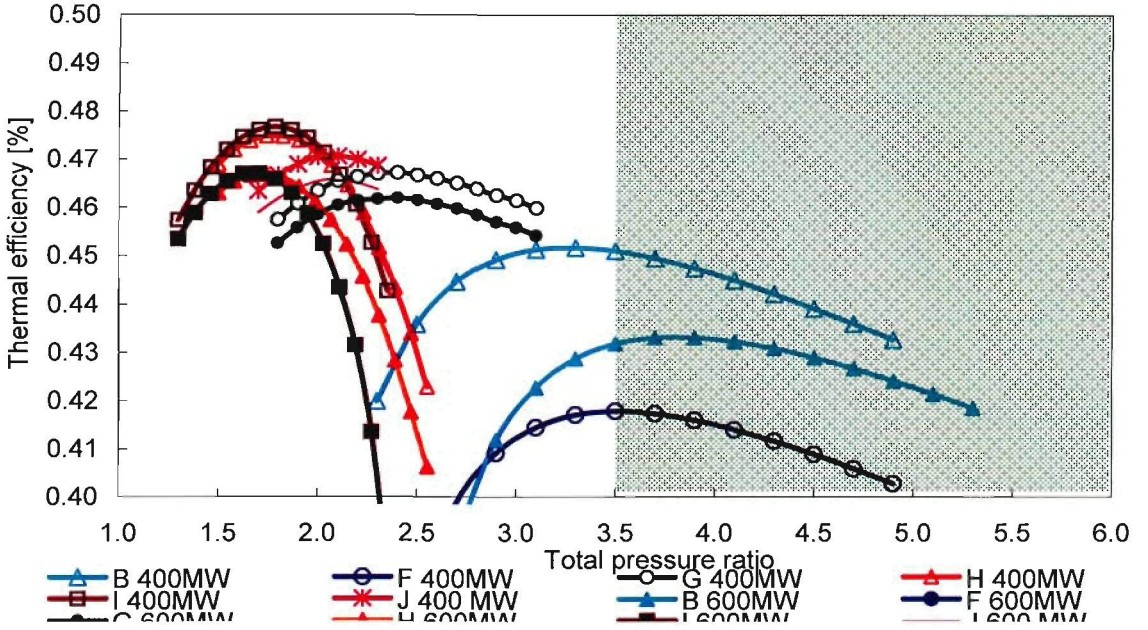


Figure 6.73 *Thermal efficiency vs. pressure ratio at ROT 900 °C*

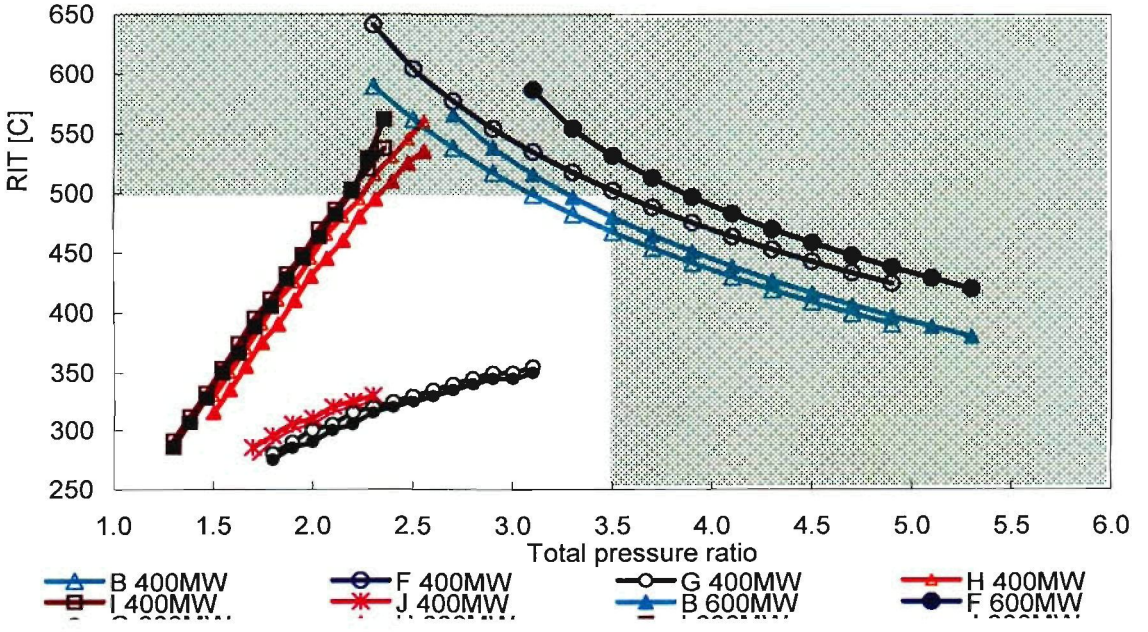


Figure 6.74 *Reactor inlet temperature vs. pressure ratio at ROT 900 °C*

Figure 6.75 shows that only Cycles G, H, I and J have solutions at both 400 MW and 600 MW. The same percentage leak flows were assumed for all the single-shaft cycles. The Brayton cycle compressor outlet temperature is in the region of 100 °C while the Combined Cycle outlet temperatures are in the region of 400 °C. Although the same percentage leak flows were assumed for the Brayton and Combined Cycle, the Combined Cycle will probably require larger leak flows in order to cool the turbine. The larger leak flows will result in a smaller mass flow through the reactor and therefore it is assumed that the Combined Cycle mass flows only need to be smaller than pressure ratio 1.8 and not 1.5.

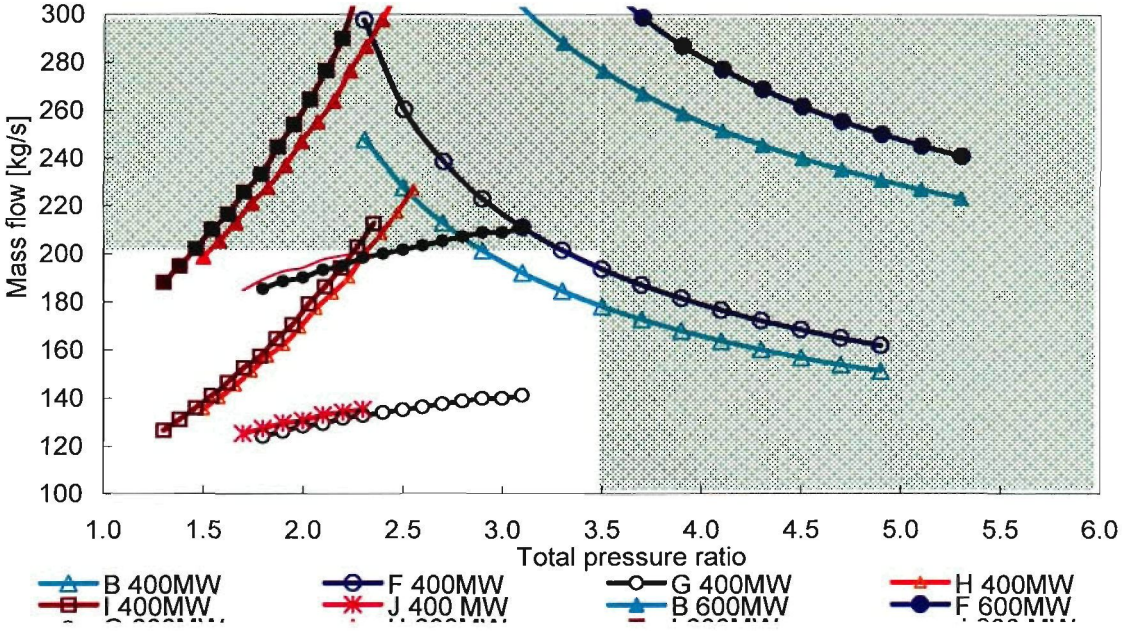


Figure 6.75 *Mass flow vs. pressure ratio at ROT 900 °C*

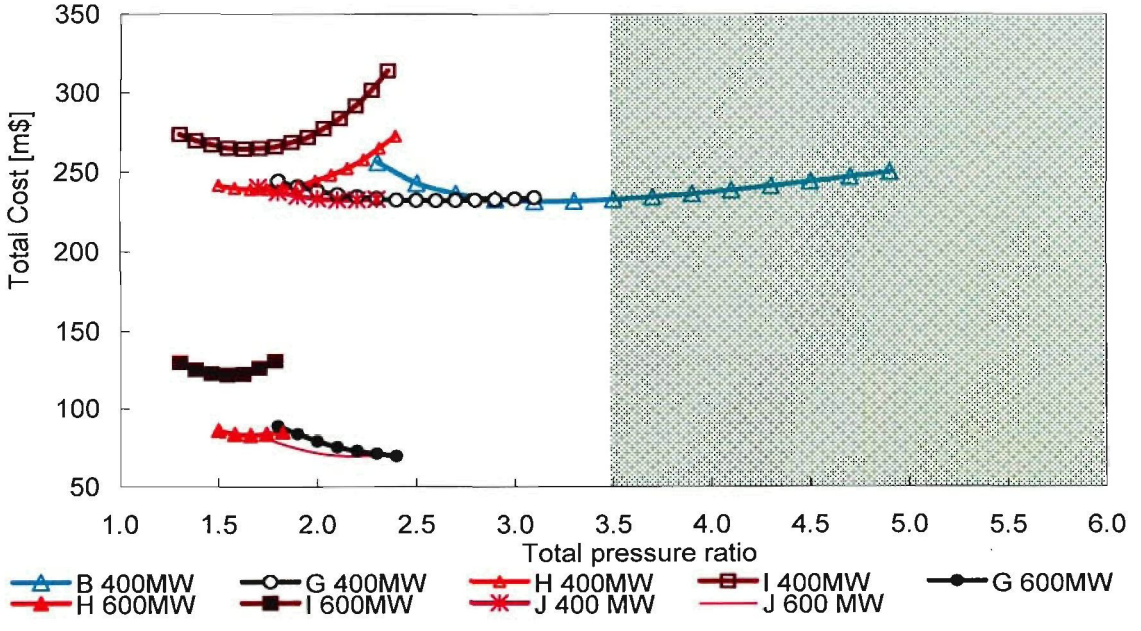


Figure 6.76 *Total plant order of magnitude capital cost vs. pressure ratio at ROT 900 °C cycles*

6.5.3 Reactor outlet temperature: 1100 °C

Figure 6.77, *Figure 6.78*, *Figure 6.79* and *Figure 6.80* present the thermal cycle efficiency, reactor inlet temperature, mass flow and total order-of-magnitude plant cost as function of total pressure ratio. The green shaded areas indicate the region where no solutions were found.

Figure 6.78 indicates that Cycles G, H, I and J are able to operate at their design points at both 400 MW and 600 MW. Neither Cycle B nor Cycle F has any solutions for 400 or 600 MW at 1100 °C.

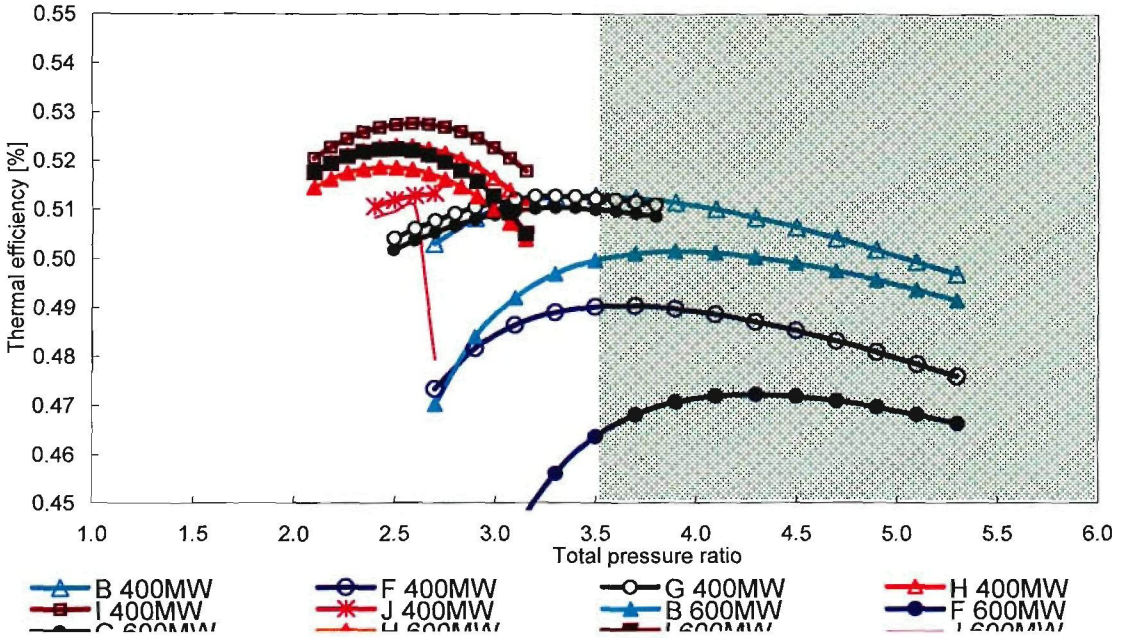


Figure 6.77 *Thermal efficiency vs. pressure ratio at ROT 1100 °C*

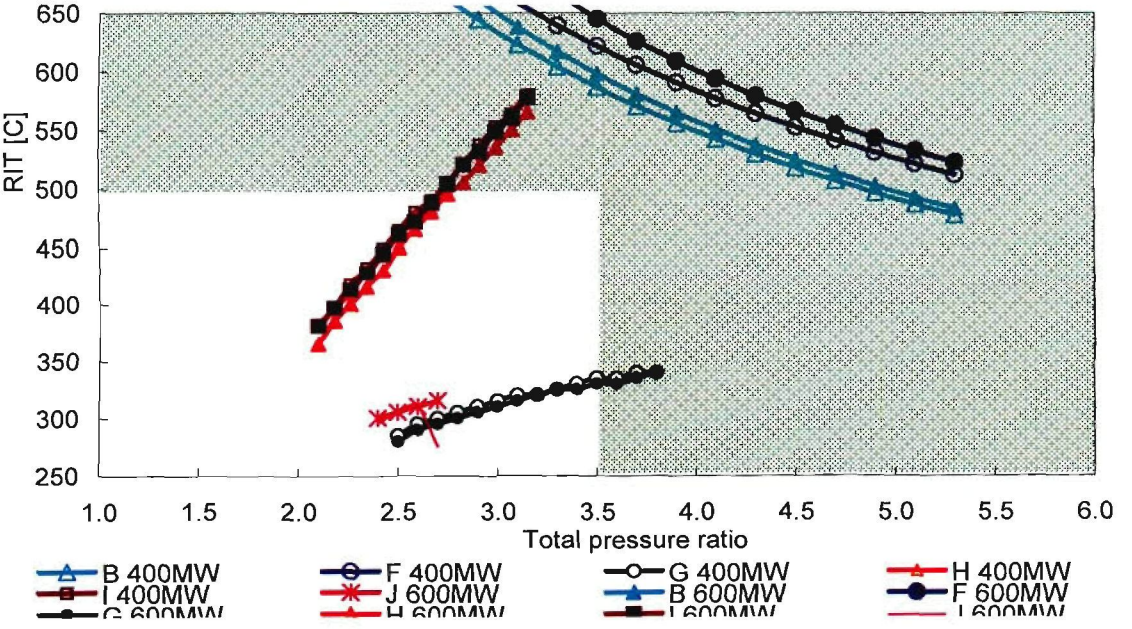


Figure 6.78 *Reactor inlet temperature vs. pressure ratio at ROT 1100 °C*

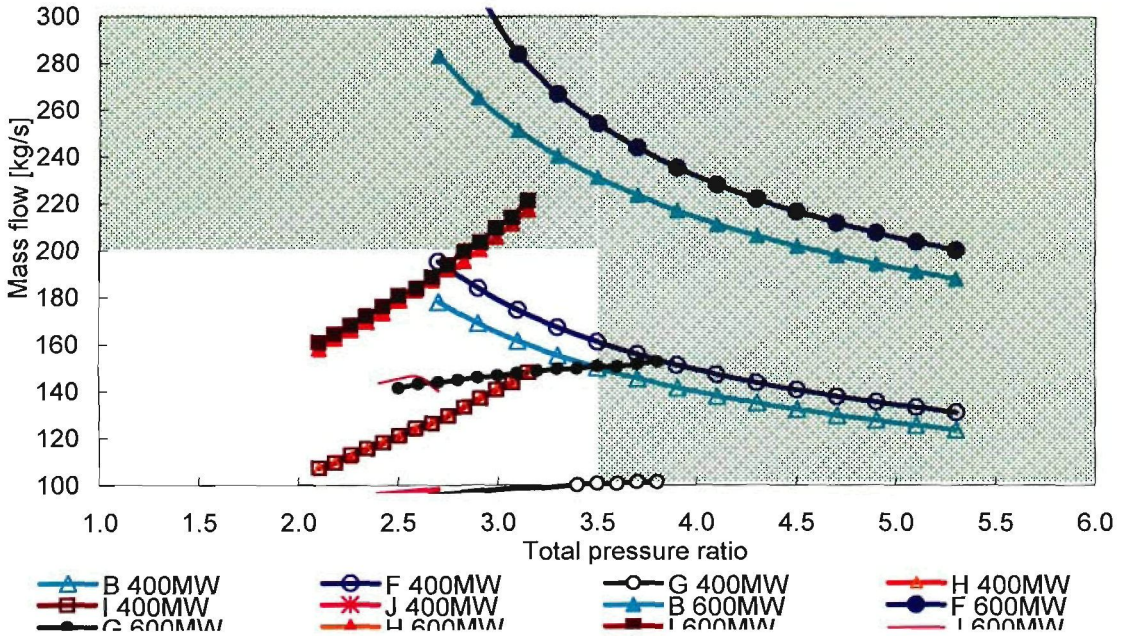


Figure 6.79 *Mass flow vs. pressure ratio at ROT 1100 °C*

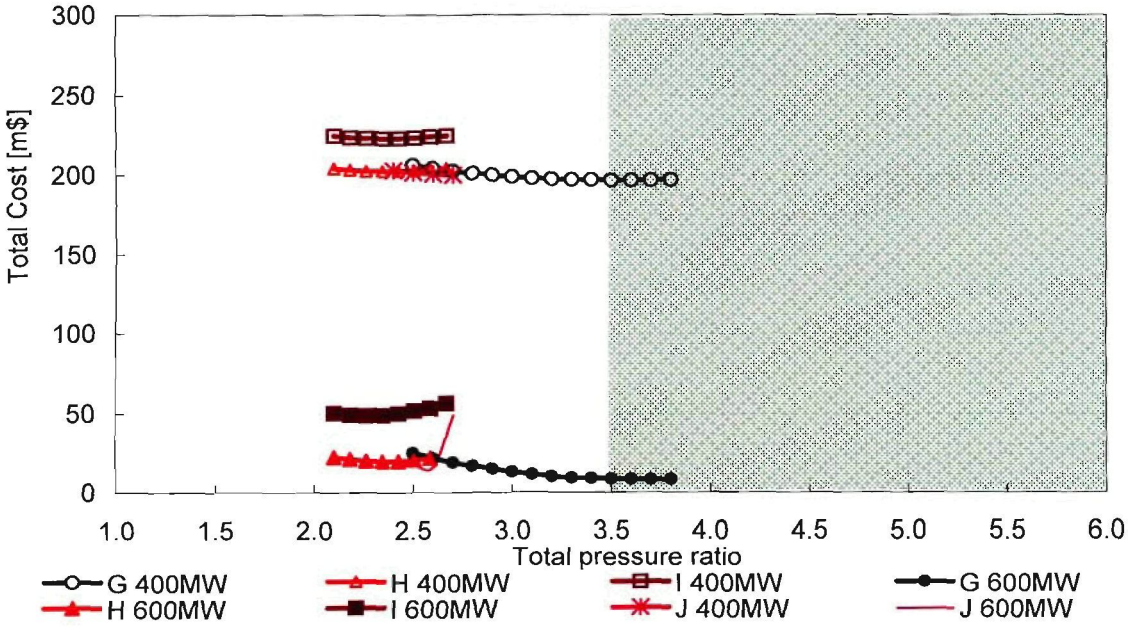


Figure 6.80 *Total plant order of magnitude capital cost vs. pressure ratio at ROT 1100 °C cycles*

6.6 GENERAL RESULTS

6.6.1 Cycles G, H and J without the Intermediate loop

Cycles G, H and J have an intermediate loop between the Brayton and the Rankine cycle in order to prevent steam ingress into the reactor. The temperature difference across the IHX results in a significant efficiency loss for these three cycles. It might be possible to dispose of the intermediate loop by designing the IHX in such a way that steam ingress will not be possible. *Figure 6.81* shows the increase in efficiency for these three cycles in the absence of the intermediate loop. The cycle efficiency of Cycle H increased with 1.5 % and Cycle G and Cycle J both increased with 0.5 %.

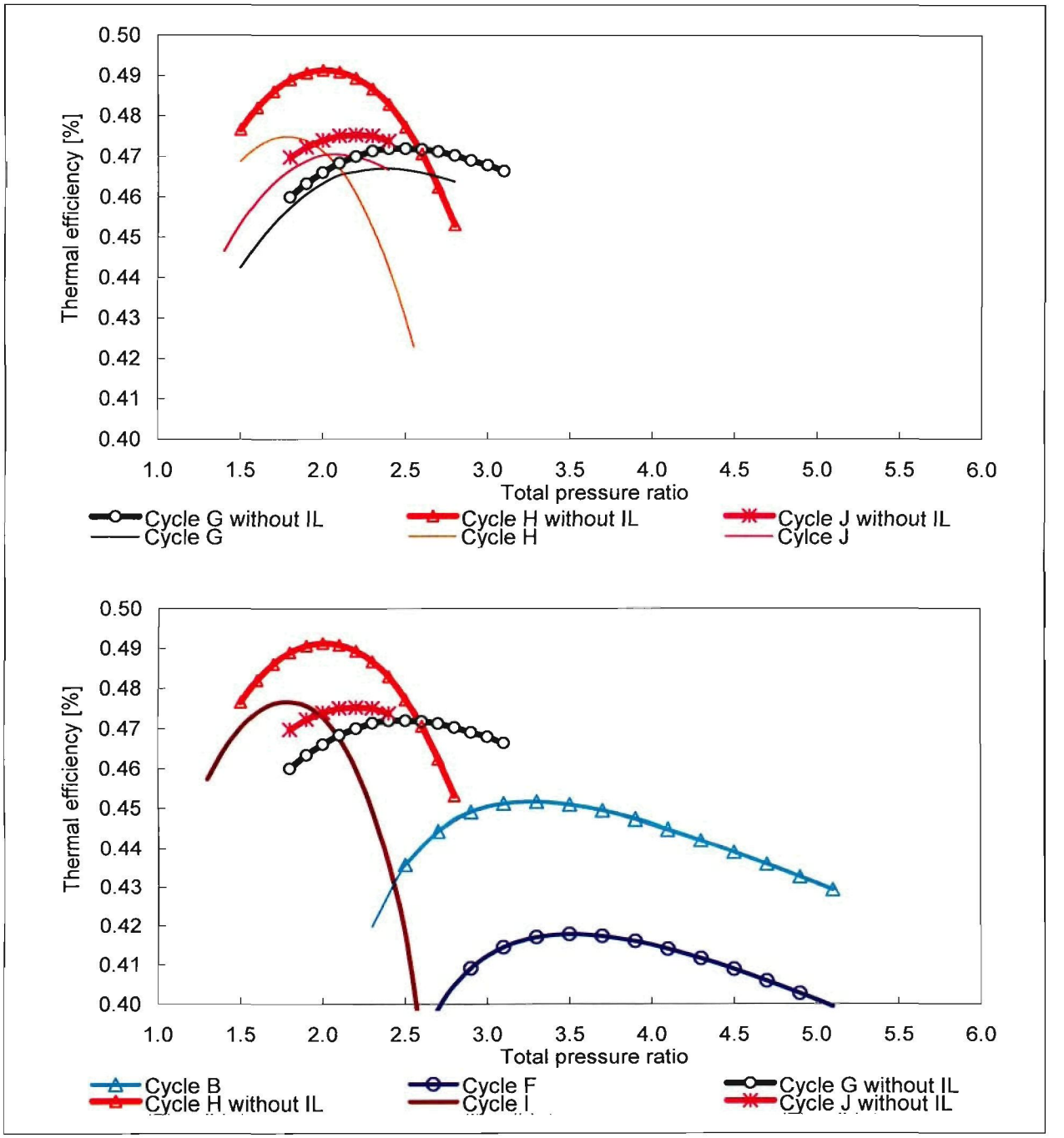


Figure 6.81 *Thermal efficiency vs. pressure ratio for Cycles G, H and J without the intermediate loop*

6.6.2 Blower size

Figure 6.82 presents the blower size for the combined and indirect cycles. Cycle F's blower size is significantly higher than the Combined Cycles due to higher mass flows – see *Figure 6.61*. The blowers of Cycles G, H and J are smaller than Cycle I due to their lower inlet temperatures.

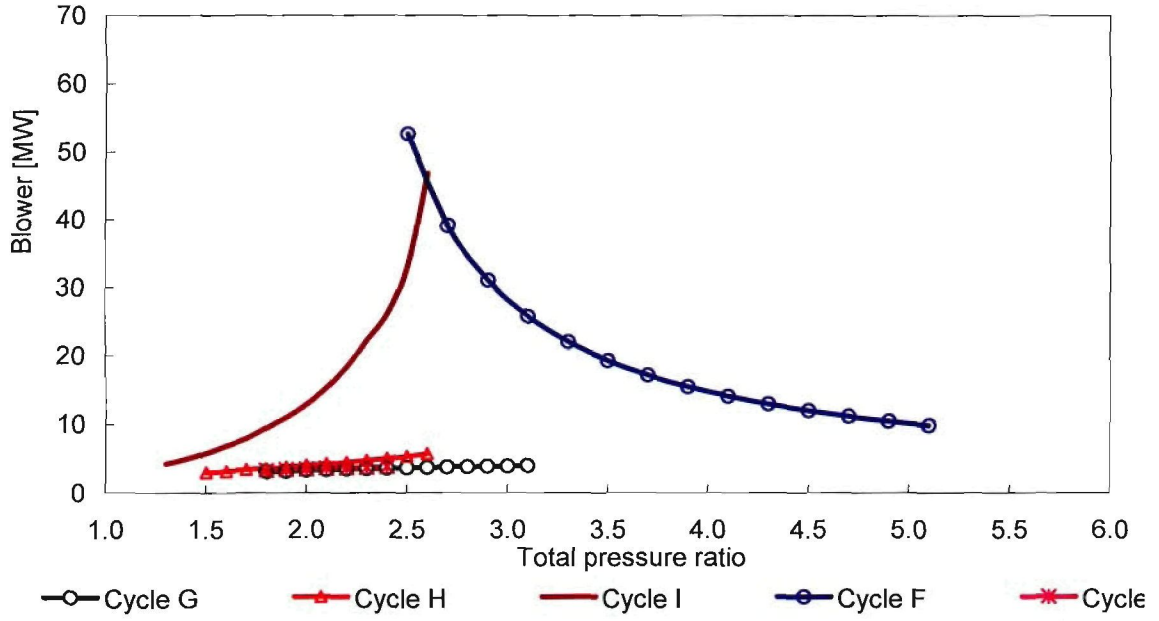


Figure 6.82 *Blower Sizes*

6.6.3 Steam generator inlet temperature

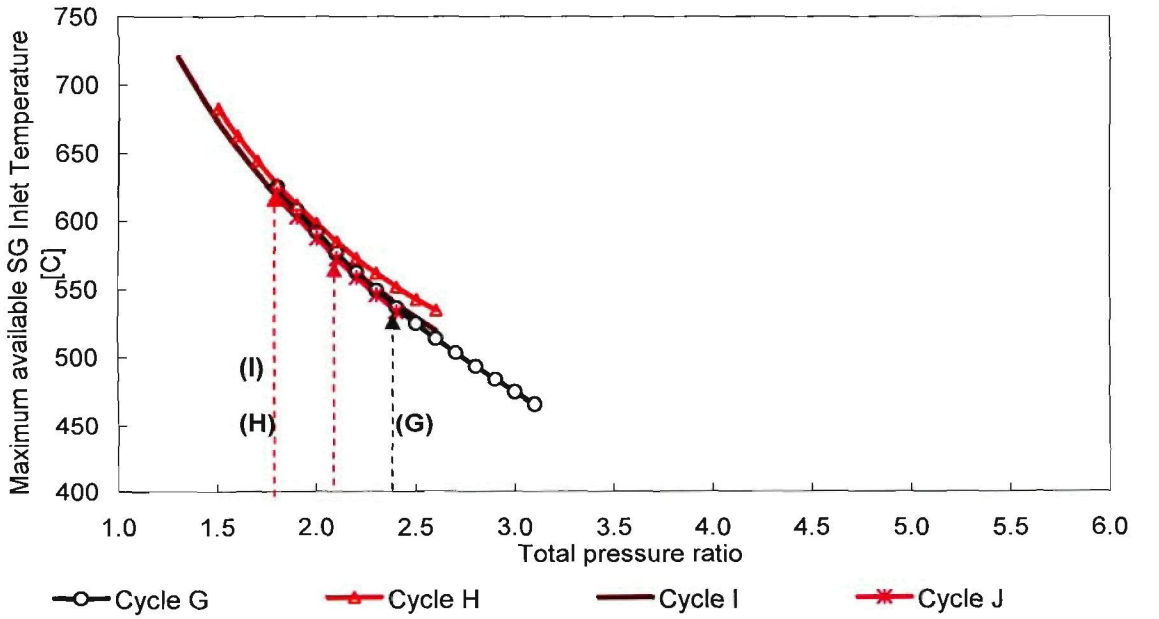


Figure 6.83 *Steam generator inlet temperatures*

Figure 6.83 shows the maximum available steam generator inlet temperature for the Combined Cycles. The steam generator inlet temperature is fixed as 540 °C. Cycles H and Cycle I will therefore not utilize 60 °C, whereas Cycle G and Cycle J will be able to fully use all the available heat.

6.6.4 Turbine blade stress safety factors

Figure 6.84 shows the turbine blade stress safety factor as function of reactor outlet temperature. As expected, the safety factor decreases with increasing temperature.

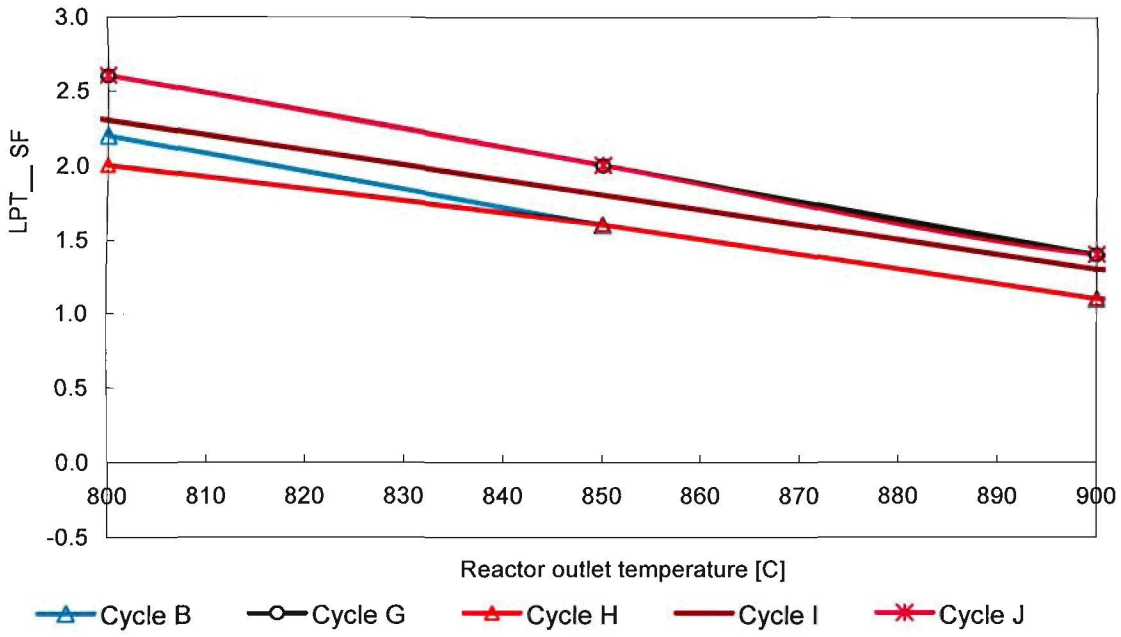


Figure 6.84 *Turbine blade stresses*

The blade stresses are a function of both the turbine inlet temperature (which determines the maximum allowable blade stress) and the rotational speed. At higher temperatures the maximum allowable blade stress decreases and therefore the safety factor decreases as well. The safety factor is defined by:

$$\sigma_{real} = \frac{\sigma_{max}}{SF} = \frac{2}{3}\left[\frac{\rho_b}{2}U_t^2\left(1-\left(\frac{r_r}{r_t}\right)^2\right)\right] \text{ - see Chapter 5} \qquad (5.80)$$

For Cycle B, the safety factor increases 50 % from 900 °C to 850 °C. The lower safety factor has a direct impact on the lifetime of the blades. Although a lower reactor outlet temperature has a lower cycle efficiency, there is a definite cost advantage for the turbo machines from a lifetime and risk perspective at lower reactor outlet temperatures.

The safety factors for the Combined Cycles are between 20% and 50 % higher than the Brayton cycles. This is because the lower mass flows of the Combined Cycles result in smaller machines where the smaller tip radius implies smaller stresses. Data for the turbine blade maximum allowable stress are only available up to 900 °C. *The maximum allowable stress was kept constant beyond 900 °C – see Chapter 5 Figure 5.9.*

6.6.5 Comparing PBMR vs. Framatome

This section compares the thermal efficiency of Framatome's proposed cycle (Cycle I) with PBMR Cycle I. Both are indirect Combined Cycles. The only differences between the two are:

- *Reactor pressure loss coefficient:*

$$\Delta P_{PBMR} = K \tfrac{1}{2} \rho \frac{m^2}{\rho^2 A^2} = K_{PBMR} \frac{m^2}{\rho} \qquad K_{PBMR} = 40\ m^{-4} \qquad (5.81)$$

$$\Delta P_{Framatome} = K \tfrac{1}{2} \rho \frac{m^2}{\rho^2 A^2} = K_{Framatome} \frac{m^2}{\rho} \qquad K_{Framatome} = 4\ m^{-4} \qquad (5.82)$$

- *Maximum cycle pressure:* PBMR = 90 bar
  Framatome = 50 bar
- *Secondary Fluid:* PBMR = Helium
  Framatome = Mixture (20% Helium and 80% Nitrogen)

Figure 6.85 quantifies the effect of the reactor pressure loss coefficient, maximum cycle pressure and the chosen secondary fluid on the thermal efficiency.

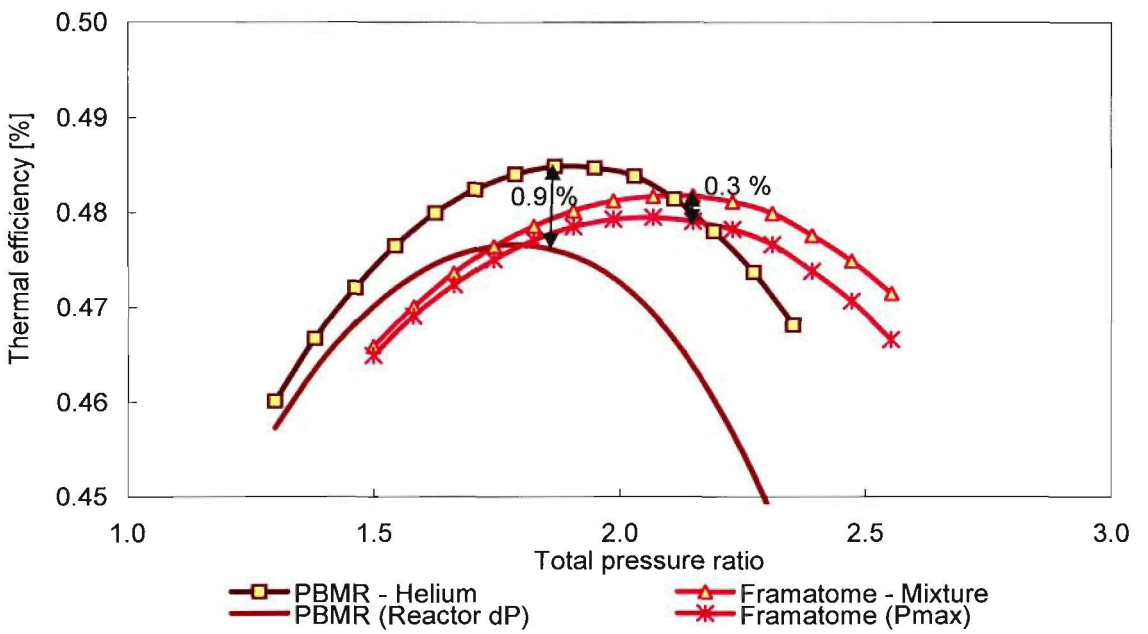


Figure 6.85 *Thermal efficiencies of PBMR (k=40, helium, 90bar) vs. Framatome (k=4, mixture, 50bar)*

PBMR - Helium	: Helium	K = 4 m^{-4}	P_{max} = 90 bar	48.5 %
PBMR (dP)	: Helium	K = 40 m^{-4}	P_{max} = 90 bar	47.6 %
Framatome - Mixture	: Mixture	K = 4 m^{-4}	P_{max} = 90 bar	48.2 %
Framatome (Pmax)	: Mixture	K = 4 m^{-4}	P_{max} = 50 bar	47.9 %

The highest efficiency for the PBMR cycle is with a pressure loss coefficient of 4 m^{-4} at 90 Bar. Next the actual pressure loss of 40 m^{-4} is introduced. *Figure 6.85* shows that PBMR cycle loses 0.9% to the Framatome efficiency due to the higher reactor pressure losses (40 vs. 4 m^{-4}).

The Framatome cycle loses 0.3 % to the PBMR cycle due to the mixture properties. The mixture also increases the optimum pressure ratio for the Framatome cycle. Framatome loses an additional 0.3% to the PBMR efficiency due to the lower maximum pressure.

Overall, the Framatome cycle is 0.3% more efficient than the PBMR cycle. From purely a thermodynamic efficiency viewpoint the PBMR and Framatome cycle are very similar.

6.6.6 Comparing Hydrogen plant - series vs. parallel

In this section the effect of the secondary intermediate heat exchanger (SIHX) placement on the thermal efficiency is investigated. *Figure 6.86* shows the graphical layout for the series and parallel configuration.

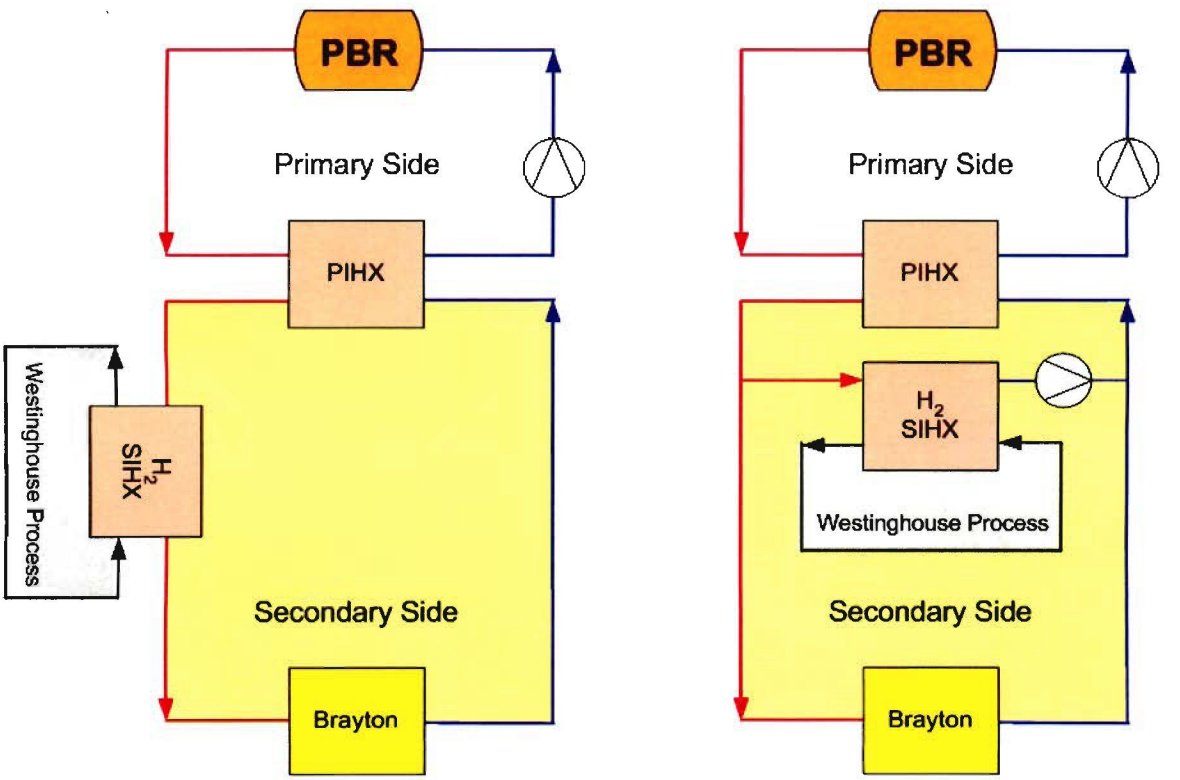


Figure 6.86 *Graphical representation of SIHX in series and parallel*

Figure 6.87 presents the thermal efficiency for the series and parallel configuration for all the cycles as function of total pressure ratio. The thick lines present the parallel configuration and the thin lines the series configuration. It was found that the thermal efficiency for the parallel efficiency is basically exactly the same as without the SIHX (see *Figure 6.59*). This is because the reactor outlet temperature stayed fixed at 900 °C and only the mass flow through the PCU changed. The thermal efficiency for the series configuration is substantially lower than the parallel configuration. This is because the turbine inlet temperature dropped by almost 60 °C, resulting in a lower thermal efficiency. Note that the pressure losses through the secondary loop piping and SIHX were not included and the

effect of the parallel configuration blower was not included.

The mass flow through the series SIHX is in the order of 200 kg/s, whereas the mass flow through the parallel SIHX is in the region of 25 kg/s (example Cycle B). This implies that the parallel SIHX would be considerably smaller than the series SIHX. Conclusions are reserved for section 7.1.

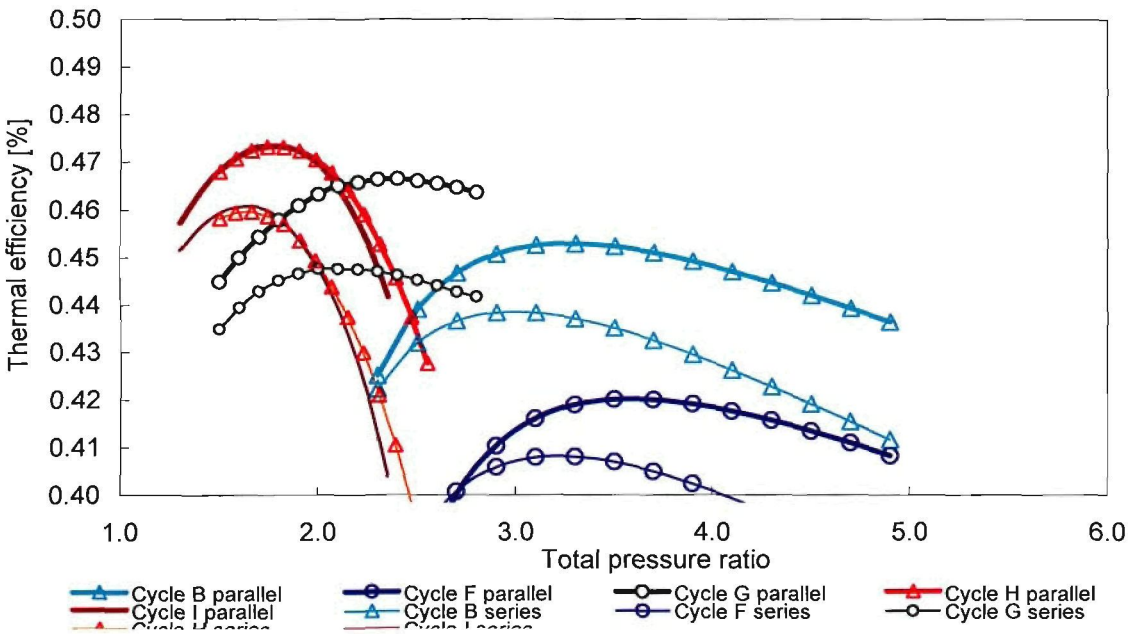


Figure 6.87 *Thermal efficiencies for Hydrogen plant: series vs. parallel*

6.6.7 Comparing Helium vs. Nitrogen

This section comments on the capital costs of the turbo units and heat exchangers for secondary fluids Helium, Nitrogen and a mixture of the two.

Turbo Unit

Figure 6.88 shows that pure Nitrogen produces the cheapest (implying smallest) turbo machines and Helium the most expensive. This can be explained by investigating the turbo machine equations:

$$t_{outlet} = t_{inlet} + \frac{t_{inlet}}{\eta_{blower}}\left[\left(\frac{p_{inlet}}{p_{outlet}}\right)^{(\gamma-1)/\gamma} - 1\right] \qquad (5.83)$$

$$Q_{Turbo\ Machine} = \dot{m} C_p (t_{outlet} - t_{inlet}) \qquad (5.84)$$

A larger ratio of specific heats (γ) results in a larger outlet temperature (t_{outlet}), which in turn results in a larger ($Q_{Turbo\ Machine}$) and more expensive turbo unit. A smaller value of γ implies that a fluid is more compressible.

γ Helium = 1.667 see Chapter 3

γ Mixture = 1.535 see Chapter 3

γ Nitrogen = 1.400 see Chapter 3

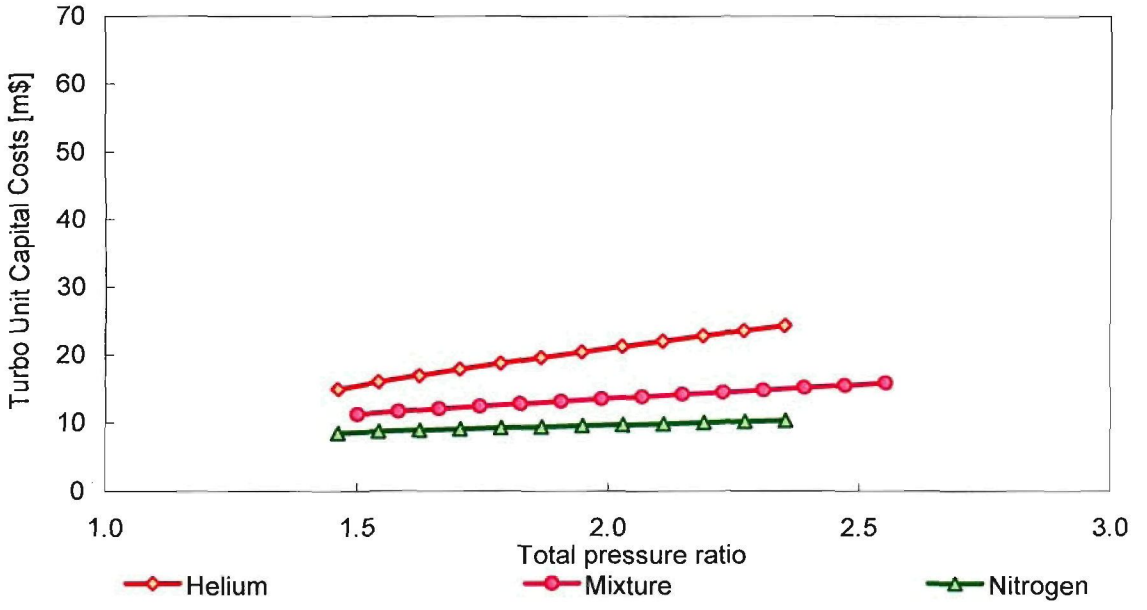


Figure 6.88 *Turbo unit capital cost vs. pressure ratio for Cycle H with Helium, Mixture and Nitrogen*

IHX (see Chapter 5)

Figure 6.89 shows that the Helium IHX is the cheapest and Nitrogen the most expensive. The capital cost of the heat exchangers is directly proportional to the heat transfer area. The heat transfer area is given by:

$$A_{IHX} = \frac{\left(\frac{\eta_{IHX}}{1 - \eta_{IHX}}\right)\dot{m}C_p}{U_{IHX}} \qquad (5.85)$$

The heat transfer coefficient (U_{IHX}) is calculated with the following relation:

$$U_{IHX} = \left(\frac{1}{h_1} + \frac{1}{h_2}\right)^{-1} \qquad (5.86)$$

The convection heat transfer coefficients (h) are calculated with the following relations:

$$h_1 = \frac{Nu\ k_1}{d_{IHX}},\ where\ Nu = 3.66 \text{ - see Chapter 3, } d_{IHX} \qquad (5.87)$$

$$h_2 = \frac{Nu\ k_2}{d_{IHX}},\ where\ Nu = 3.66 \text{ - see Chapter 3, } d_{IHX} \qquad (5.88)$$

where

k_1 and k_2 are the conductive heat transfer coefficients and are calculated as function of temperature (see Chapter 3). Helium has a larger conductive heat transfer coefficient (k) than does Nitrogen. The larger *k* results in a larger *h*, larger *U* and smaller *A* which results in a smaller and cheaper heat exchanger.

The combined cost of the PCU (turbo units, heat exchangers and blowers) is smaller for Helium than for Nitrogen. Interesting to note is that the PCU capital cost of the mixture is the smallest, combining both a low turbo unit and heat exchanger cost – see *Figure 6.90*.

Figure 6.91 shows that the maximum thermal cycle efficiency of the Helium, Nitrogen and Mixture cycles is within 1 %. Although the fluid does not have a large impact on the thermal efficiency, it does have a large impact on the component capital costs.

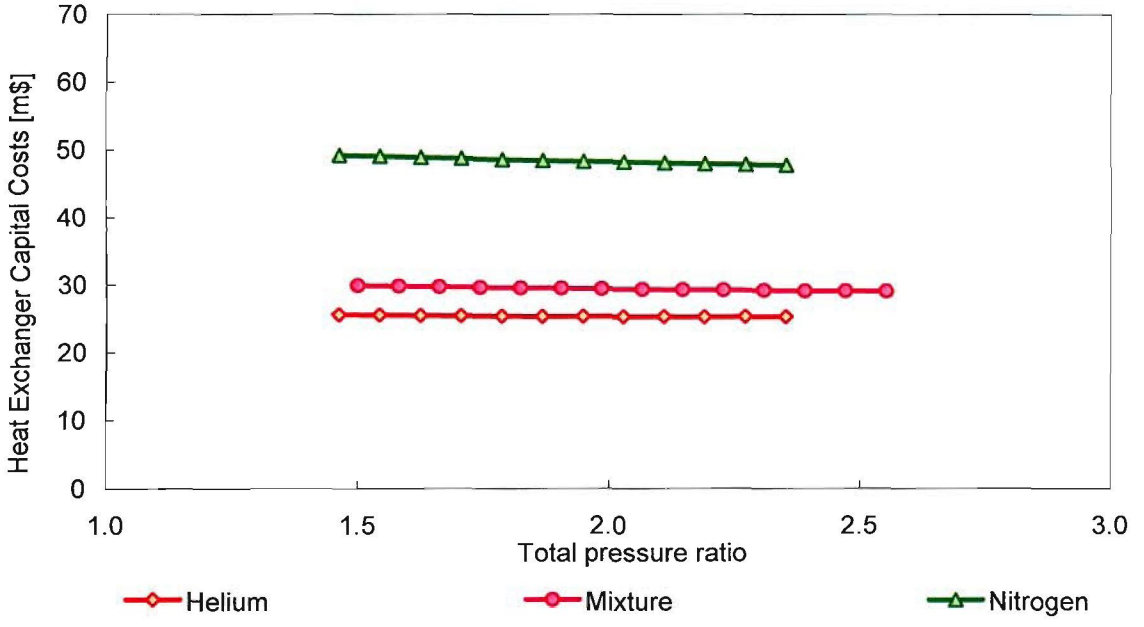


Figure 6.89 *Heat exchangers capital cost vs. pressure ratio for Cycle H with Helium, Mixture and Nitrogen*

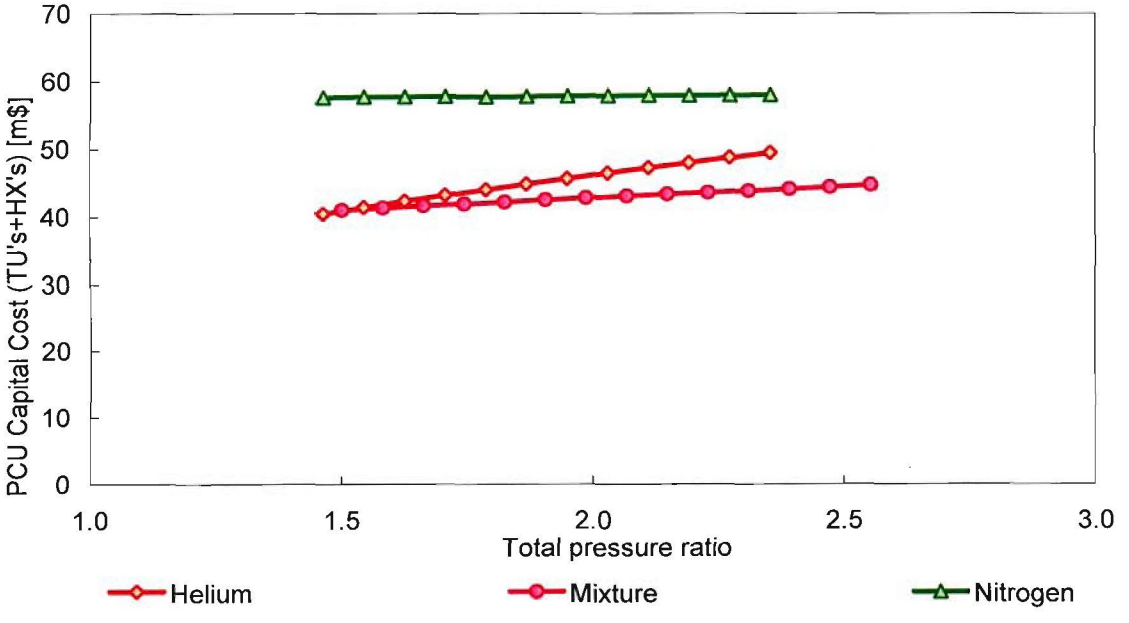


Figure 6.90 *PCU order-of-magnitude capital cost vs. pressure ratio for Cycle H with Helium, Mixture and Nitrogen*

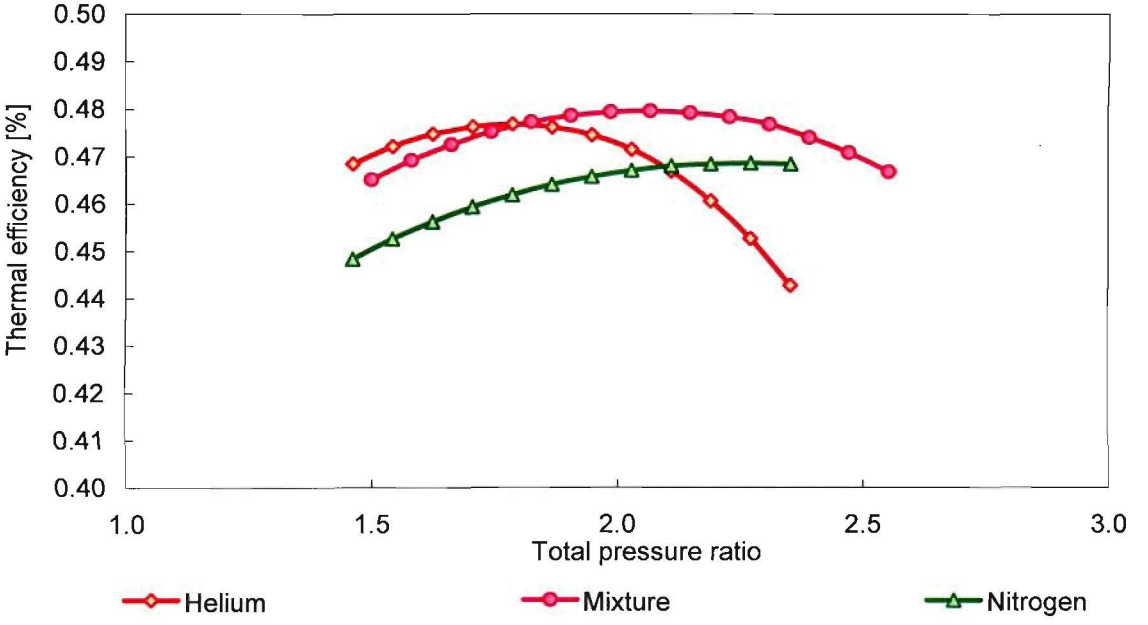


Figure 6.91 *Thermal efficiency vs. pressure ratio for Cycle H with Helium, Mixture and Nitrogen*

6.6.8 Comparing Direct vs. Indirect

This section quantifies the effect of the losses on the thermal efficiency from a direct (Cycle H) to an indirect (Cycle I) configuration and briefly comments on the advantages of the indirect cycle.

Direct : 49.7 % Direct cycle

Losses : 49.2 % *Indirect cycle: Includes pressure losses through piping and IHX and the low blower efficiency.*

Delta T : 47.7 % Indirect cycle: Includes the above losses plus the effect of the temperature difference across the IHX.

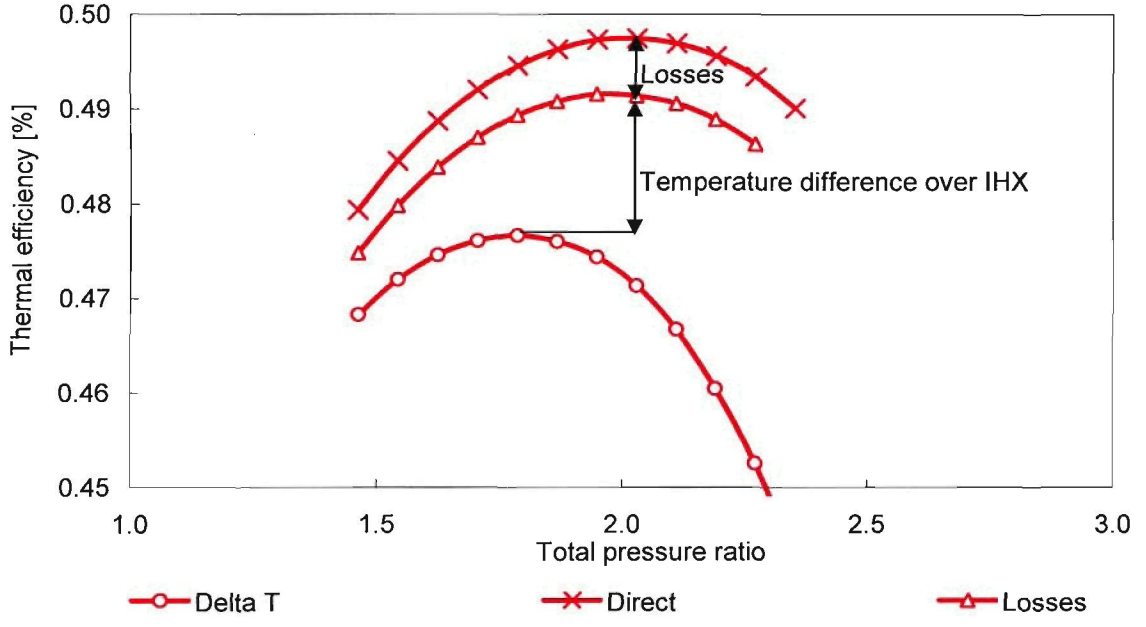


Figure 6.92 *Direct vs. Indirect thermal efficiency*

The axial compressor efficiency is typically 89 % whereas the radial blower efficiency is typically in the region of 81 %. In the direct cycle the compressor overcomes the pressure losses through the reactor and for the indirect cycle the blower overcomes the pressure losses through the reactor. The blower loss in efficiency implies that a larger blower than compressor is required to overcome the reactor losses. The pressure loss due to the piping, IHX and the low blower efficiency accounts for 0.5% of the loss in thermal efficiency. The temperature difference over the IHX accounts for 1.5 % of the loss in thermal efficiency.

Although 1.5 % efficiency is lost due to the temperature difference in the IHX, the indirect cycle has a couple of practical advantages. The IHX shields the PCU from radio active contamination. This reduces risk and saves decommissioning costs. From a controllability viewpoint, the blower in the primary loop can be used to effectively control the HPT inlet temperature during a loss of load or PCU trip. The blower controls the mass flow in the primary loop which directly influences the IHX power. The IHX power controls the HPT inlet temperature.

6.6.9 Cycle thermal efficiency sensitivities

This section shows the sensitivity of the thermal cycle efficiency to the reactor outlet temperature, cooling water temperature, maximum Brayton cycle pressure and the turbine isentropic efficiency.

- *Figure 6.93* shows that the Brayton thermal cycle efficiency increases about 1.8 % (and the Combined Cycle about 1.5 %) for every 50 °C increase in reactor outlet temperature.
- *Figure 6.94* shows that the Brayton thermal cycle efficiency decreases about 0.13 % (and the Combined Cycle about 0.04 %) for every 1 °C increase in cooling water temperature.

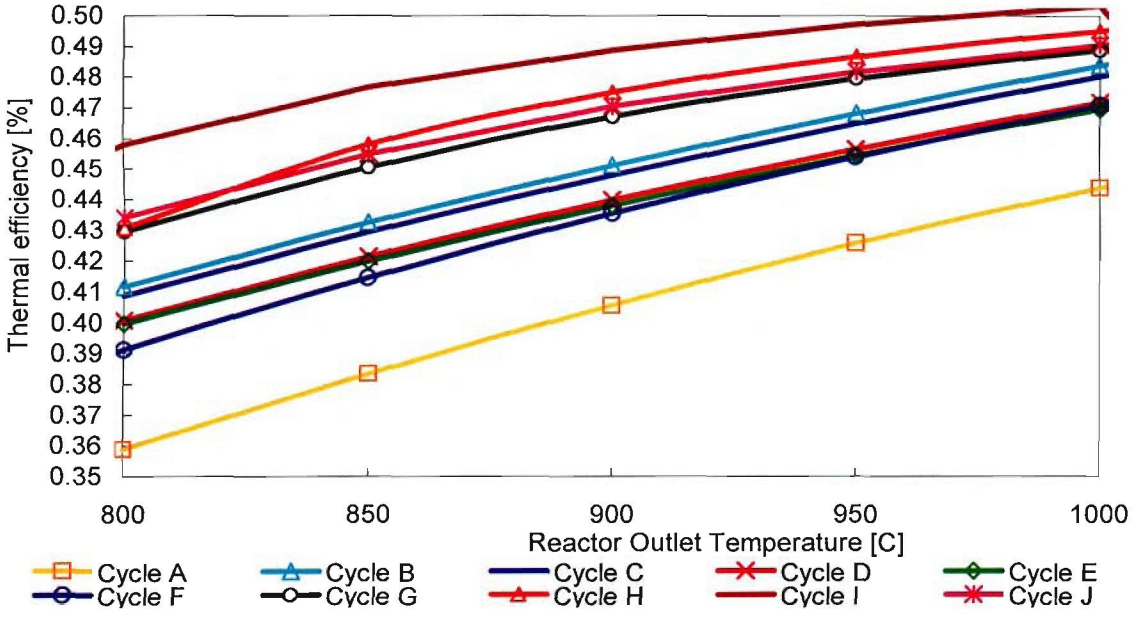


Figure 6.93 *Thermal efficiency sensitivity to reactor outlet temperature*

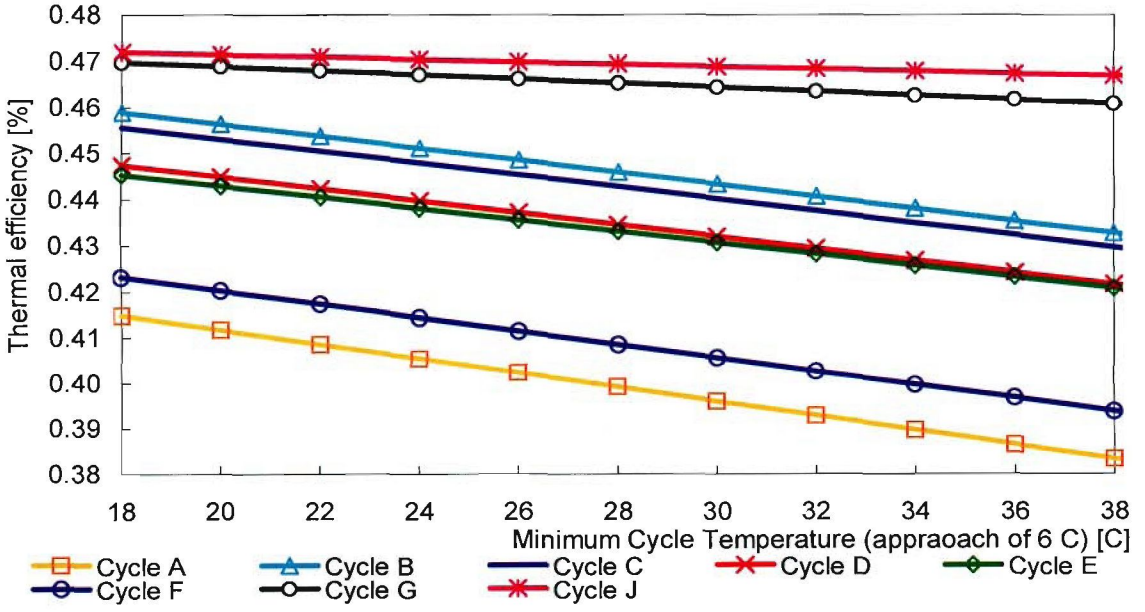


Figure 6.94 *Thermal efficiency sensitivity to cooling water temperature*

- *Figure 6.95* shows the increase in thermal cycle efficiency for increasing maximum Brayton

cycle pressure.

- *Figure 6.96* shows that the Brayton thermal cycle efficiency increases about 0.65 % (and the Combined Cycle about 0.25%) for every 1% increase in turbine isentropic efficiency.

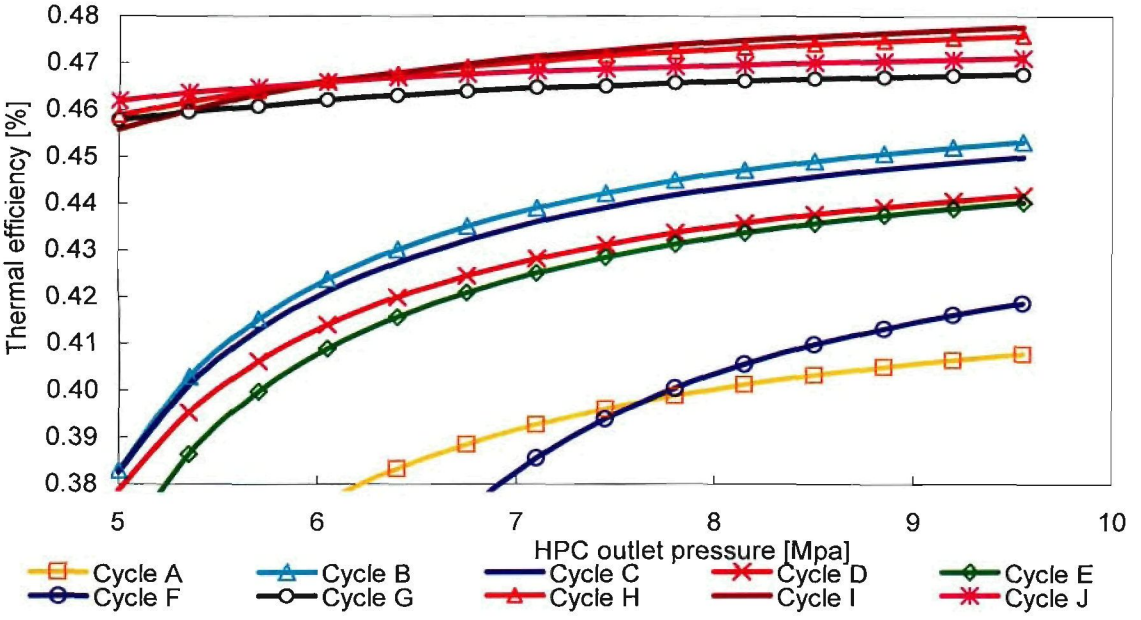


Figure 6.95 *Thermal efficiency sensitivity to maximum Brayton cycle pressure*

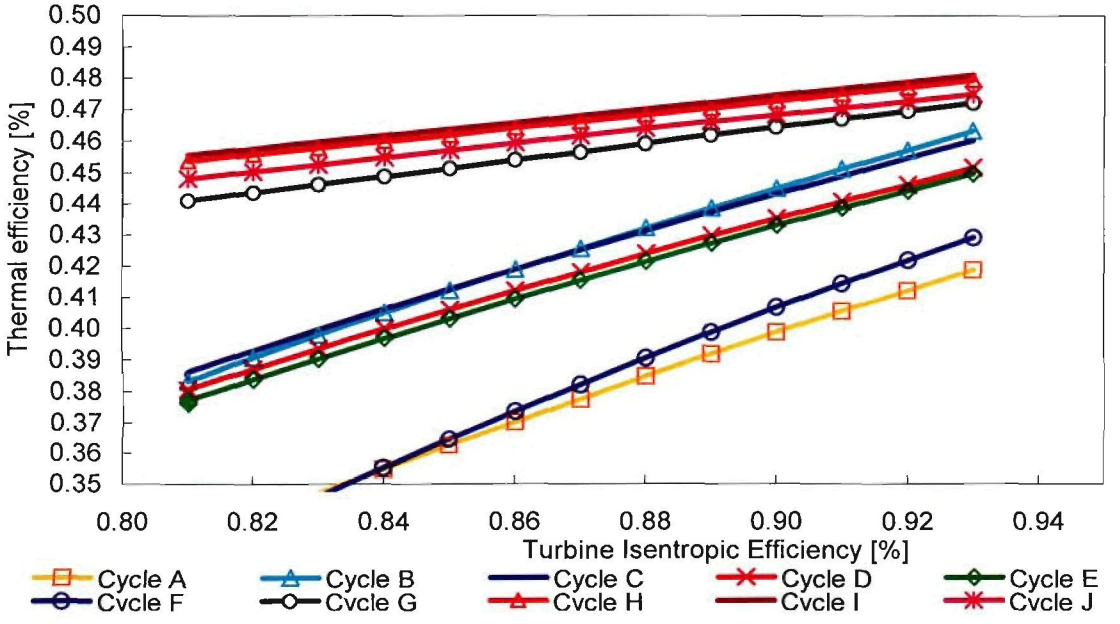


Figure 6.96 *Thermal efficiency sensitivity to turbine isentropic efficiency*

6.7 VALIDATION AND VERIFICATION OF RESULTS

6.7.1 Costing Results

The validation and verification of the costing results fall outside the scope of this study. Cost data are not readily available. Manufacturers regard cost information as important intellectual property. Cost data for nuclear plants are also difficult to come by. Due to the strong market competition, developers regard all costs as confidential.

6.7.2 Thermodynamic Results

Verification

The thermodynamic cycle solution of Cycles B, G, H, I and J were verified with EES models. It was found both C++ and EES give the exact same results for the cycle efficiency, pressures, temperatures, entropy, enthalpy and mass flow.

Validation

Only Cycles A, B, F, H and I were validated. Current international programs on the Brayton cycle focus on Cycle A and Cycle B. Cycles C, D and E are regarded as less important cycles for our purposes and were not validated. Cycle G and Cycle J are new inventions and are in the process of being patented by PBMR Pty. Ltd. Consequently they cannot be validated from the literature. Only the thermal cycle efficiencies of the CYCLE-C tool were validated (for Cycles A, B, F, H and I).

- The published efficiency of the GTHTR300 (Kunitomi et al, 2004) was used to validate Cycle A.
- The published efficiency of the PBMR, GT-MHR (Kostin et al, 2004) and the article of Frohling et al (2002) were used to validate Cycle B.
- The published efficiency of the article of Frohling et al (2002) was used to validate Cycle F.
- The published efficiency of the article of Frohling et al (2002) and work of Kugeler (2003) were used to validate Cycle H.
- The published efficiency of the Framatome ANP cycle (Copsey et al, 2004) was used to validate Cycle I.

The cycle efficiency is a function of all the variables listed in *Table 6.9*. The values of each of these variables are required in order to be capable to fully validate a cycle's efficiency. Unfortunately, the values of all these variables are not given when a cycle's efficiency is quoted in literature. In literature, the values that are given when a cycle efficiency is quoted is mostly only the reactor thermal power, reactor outlet temperature, maximum cycle pressure, minimum cycle coolant temperature and total pressure ratio over all compressors are given. Sometimes, the turbo machine isentropic efficiencies, the recuperator effectiveness and leak flows are also given.

In validating the cycle efficiencies of Cycle A, B, F, H and I, the input values of the respective literature were used, but whenever a value wasn't qualified the default input values of CYCLE-C were used. In some cases, where a value wasn't qualified a different value (other than CYCLE-C's default input) was used. *Table 6.10* lists all the input values to Cycle A, B, F, H and I as found in literature. The values printed in **bold** and shaded green in *Table 6.10* are those values that were not qualified in literature.

Some of these variables have different values than the default CYCLE-C input – depending on the cycle.

	Brayton - Validated		Rankine - Validated
Reactor	reactor thermal power	t_{max}	maximum allowable oulet temperature for steam generator
t_{max}	maximum cycle coolant temperature	p_{max}	pressure in steam generator
p_{max}	maximum cycle pressure		
t_{min}	minimum cycle coolant temperature		
η_t	turbine isentropic efficiency		
η_c	compressor isentropic efficiency		
$\eta_{Recuperator}$	recuperator effectiveness		
Leak flows	leak flows		
PR	total pressure ratio over all compressors		
Fluid			
	Brayton – fixed		**Rankine - fixed**
k_{comp}	loss coefficient for diffuser - compressor	t_{min}	condenser temperature
k_{turb}	loss coefficient for diffuser - turbine	$\%dP_{RH}$	losses in reheater
$\%dP_{HXs}$	pressure loss through heat exchangers	$\%dP_{SG}$	losses in steam generator
$\%dP_{PIPING}$	pressure loss through piping	t_{Pinch}	pinch temperature for steam generator
η_{blower}	blower isentropic efficiency	**CDx**	minimum allowable condensor two-phase fraction
$\eta_{mechanical}$	mechanical shaft efficiency	$\eta_{turbine}$	steam turbine efficiency
$C_{a,c}$, $C_{a,t}$	diffuser outlet velocity	η_{pump}	pump efficiency
k_{PBMR}	loss coefficient for reactor $k_{PBMR} = \frac{1}{2}\frac{1}{A^2}K = \frac{\rho_{avg}\Delta P}{\dot{m}^2}$		

Table 6.9 *Cycle input parameters*

Validating Cycle A

Figure 6.97 (left) shows that the cycle efficiency of CYCLE-C and the published efficiency of the GT-HTR300 correspond favourably.

Validating Cycle B

Figure 6.97 (right) shows that the cycle efficiency of CYCLE-C and the published efficiency of the GT-MHR correspond favourably. The cycle efficiency of the PBMR corresponds favourably with the default CYCLE-C inputs. The cycle efficiency of CYCLE-C for the Frohling et al (2002) inputs is lower than the published value. This difference may be ascribed to wrong input values for the leak flows, recuperator effectiveness and pressure loss through the reactor. Frohling did not publish the values for the leak flows and recuperator effectiveness. The turbine efficiency of 85 % is suspiciously low.

Validating Cycle F

Figure 6.98 shows that the cycle efficiency of CYCLE-C and the published efficiency of Frohling correspond favourably.

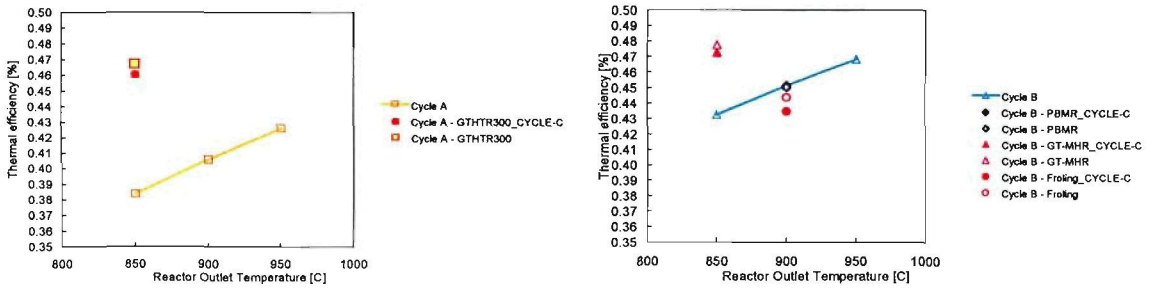


Figure 6.97 *Validation of the thermal efficiency of Cycle A and Cycle B*

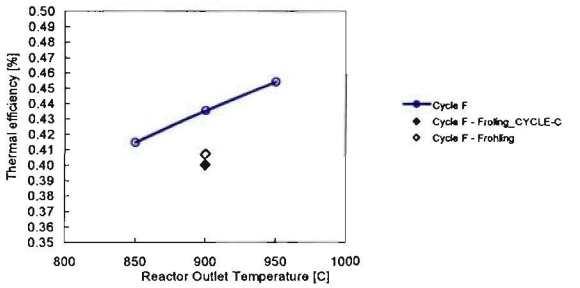


Figure 6.98 *Validation of the thermal efficiency of Cycle F*

Validating Cycle H

Figure 6.99 (left) shows that the cycle efficiency calculated with CYCLE-C with the Frohling et al (2002) inputs is lower than the published value of Frohling. Again, this difference may be ascribed to wrong input values for the leak flows, recuperator effectiveness and pressure loss through the reactor. Frohling did not publish these values. Again, the turbine efficiency of 85 % is suspiciously low. The cycle efficiency of CYCLE-C with the Kugeler (2003) inputs corresponds acceptably well with the published value. Both the published values correspond favourably with the CYCLE-C efficiency for CYCLE-C's default inputs, although this is with different inputs than the published inputs.

Validating Cycle I

Figure 6.99 (right) shows that the cycle efficiency calculated with CYCLE-C with the Framatome (Copsey et al, 2004) inputs are lower than the published values. This difference can be ascribed to different input values. Framatome did not publish the steam conditions of the cycle. The Framatome cycle provides process heat to a Hydrogen process. The Hydrogen efficiency was not published.

Overall, CYCLE-C is believed to correspond well with published efficiencies given the uncertainty surrounding input values.

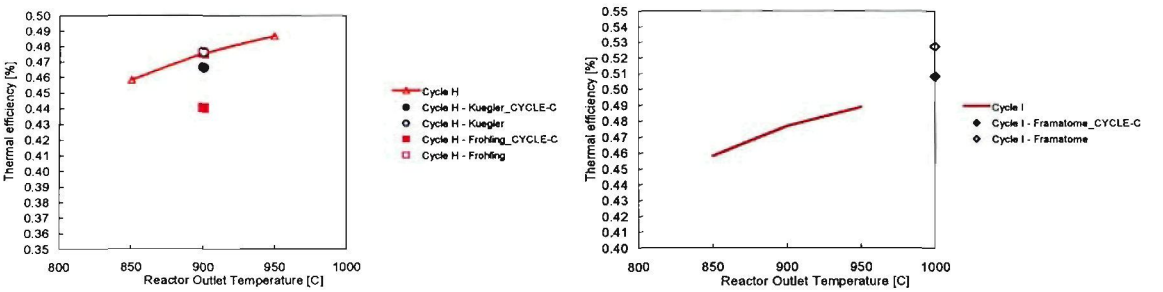


Figure 6.99 *Validation of the thermal efficiency of Cycle H and Cycle I*

			Literature													CYCLE-C
Cycle	**Ref.**	**Ref.**	**Power**	**ROT**	**P_{max}**	**T_{min}**	**Turbine**	**Compressor**	**Recuperator**	**Leak flows**	**$k_{reactor}$**	**PR**	**Steam**	**Steam**	**$\eta_{thermal}$**	**$\eta_{thermal}$**
		-	**MW_{th}**	**°C**	**Bar**	**°C**	**%**	**%**	**%**			-	**T**	**P**	**%**	
A	GTHTR300	[17]	600	850	70 Bar	28	0.928	0.905	0.950	**1.2**	**4**	-	-	-	0.467	0.460
B	PBMR	-	400	900	90 Bar	24	0.910	0.890	0.960	5.6	**40**	3.1	-	-	0.450	0.451
B	GT-MHR	[15]	600	850	71 Bar	24	0.930	0.88 / 0.87	0.950	2.1	**4**	-	-	-	0.477	0.472
B	Frohling	[6]	200	900	**90 Bar**	30	0.855	0.855	**0.960**	**2.0**	40	2.7	-	-	0.443	0.434
C	-	-	-	-	-	-	-	-	-	-	-	-	-	-	-	0.448
D	-	-	-	-	-	-	-	-	-	-	-	-	-	-	-	0.440
E	-	-	-	-	-	-	-	-	-	-	-	-	-	-	-	0.438
F	Frohling	[6]	200	900	**90 Bar**	30	0.855	0.855	**0.960**	**2.0**	**40**	-	-	-	0.407	0.400
G	-	-	-	-	-	-	-	-	-	-	-	-	-	-	-	0.467
H	Frohling	[6]	200	900	**90 Bar**	-	0.855	0.855	-	**5.6**	**40**	-	547	110 Bar	0.475	0.440
H	Kugeler	[16]	200	900	**90 Bar**	-	0.910	0.890	-	**5.6**	**40**	-	547	110 Bar	0.476	0.466
I	Framatome	[4]	600	1000	50 Bar	-	**0.910**	**0.890**	-	**5.6**	**4**	-	STD	**180 Bar**	0.527	0.508
J	-	-	-	-	-	-	-	-	-	-	-	-	-	-	-	0.470

Table 6.10 *Cycle input parameters*

6.8 COMBINED CYCLE PRACTICALITIES

Figure 6.59 indicated that Combined Cycles H and Cycle I have the highest cycle efficiency and *Figure 6.66* indicated that both Cycle H and Cycle I compare favourably with Cycle B from a relative cost perspective. This section discusses some possible practical issues associated with the Combined Cycle H and Cycle I. Section 6.8.1 will discuss the identified practicalities for the Brayton section and section 6.8.2 will discuss the practicalities associated with the steam plant. Section 6.8.3 investigates the practicalities associated with coupling the PBMR reactor via an IHX to a conventional off-the-shelf Combined Cycle. See *Figure 6.104* and *Figure 6.105* for the identification diagram of Cycle H and Cycle I respectively.

6.8.1 Brayton

The following practicalities are highlighted:

- The LPC inlet temperature is 246 °C for Cycle H and 211 °C for Cycle I. In the event of loss of cooling from the steam plant, the LPC inlet temperature will increase to the region of 670 °C, which is unacceptable.

  Possible solution:

  Insert a small heat exchanger between the IHX (Cycle H) or Steam generator (Cycle I) and the LPC. Bypass the heat exchanger during normal operation. The additional cost of such a heat exchanger was not taken into account.

  An alternative is to bypass the steam turbines from the steam generator outlet to the condenser inlet.

- The pressure boundary temperature is limited to 371°C. For Brayton Cycle B, the HPC outlet temperature is around 100 °C. The LPC outlet temperature for Cycle H is 400 °C which exceeds the allowable pressure boundary temperature.

  Possible solution:

  Both the turbine and compressor casing materials will need to be upgraded to ASME 316. ASME 316 is expensive and this additional cost was not included for Cycle H and Cycle I.

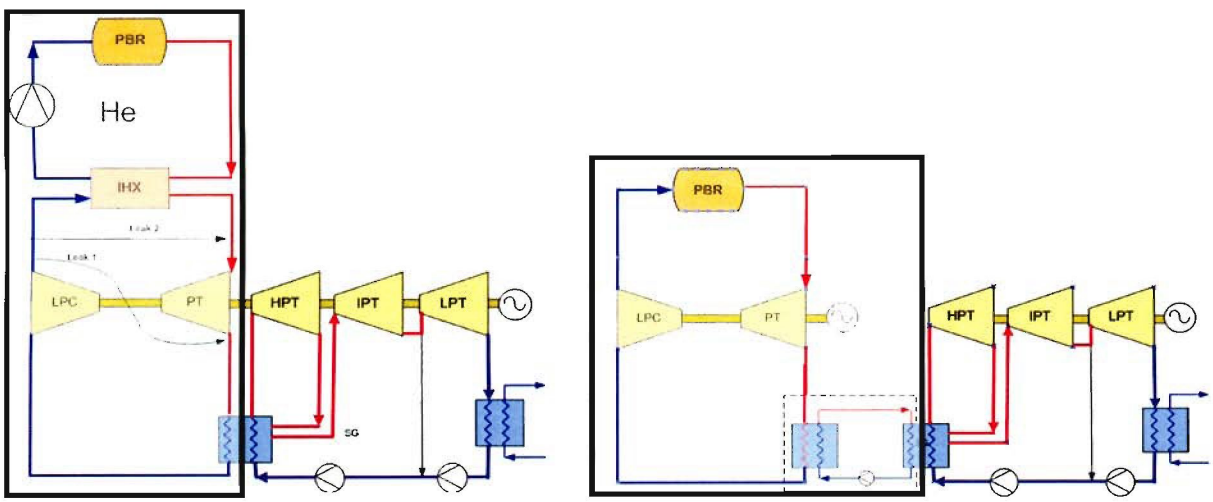


Figure 6.100 *Schematic drawing for Cycle H and Cycle I – Brayton (CC)*

- For current technology, the recuperator inlet temperature is limited to 600 °C. The recuperator

inlet temperature for Cycle H is 670 °C and the temperature for Cycle I is 628 °C.

Possible solution:

The SIHX for the hydrogen plant needs to withstand temperatures of 900 °C. It is assumed that the same material may be used for the recuperator and that this new technology would have matured by the time of construction.

- For Cycle B, the HPC outlet temperature of 100 °C is used to cool the dry-gas seal (DGS) which is situated at the power turbine at 900 °C. For both Cycle H and Cycle I the LPC outlet temperature exceeds 400 °C which would not be sufficient to cool the DGS.

Possible solution:

Larger leak flows might produce sufficient cooling, but at the cost of a lower cycle efficiency. Constant active cooling will probably need to be introduced to cool the DGS.

The following comments can be made:

- The pressure ratio of 1.8 is not a problem.
- The low reactor inlet temperature of 400 °C is very favourable.
- The blower size of 3.5 MW is not a problem.
- For the current PBMR design Cycle B, turbine blade cooling is a problem due to the large temperature difference (900-100 °C) over the turbine blades which results in unacceptably high blade stresses. Although further investigation is needed, it seems that the higher LPC outlet temperature for Cycle H and Cycle I makes turbine blade cooling possible (900-400 °C). Turbine blade cooling has the advantage of possibly higher reactor outlet temperatures.

None of the practical issues mentioned are perceived to be insoluble and it is believed that these issues can be mitigated.

6.8.2 Steam plant

Conservative inputs were used for the Rankine cycle – see Chapter 3. By investigating *Figure 6.104* and *Figure 6.105* it is the opinion of PBMR experts than none of the pressures and temperatures mentioned indicate impractical designs.

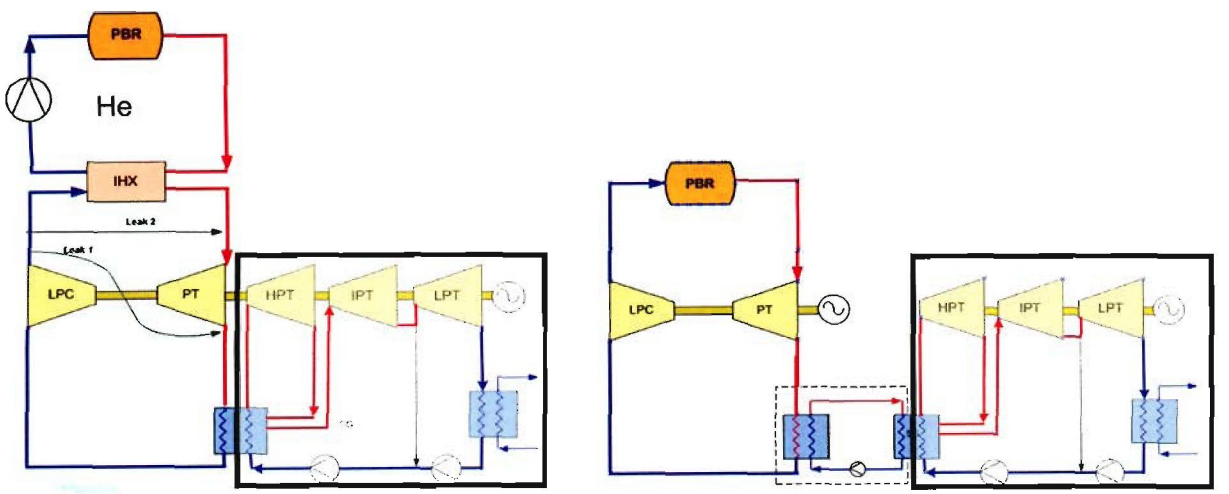


Figure 6.101 *Schematic drawing for Cycle H and Cycle I – Steam plant (CC)*

Caution is given to the low steam generator inlet temperature. Conventional nuclear steam plants have steam generator inlet temperatures in the order of 250 °C. At his stage this is not perceived as a problem, but needs to be further investigated. **The steam plant will need to be custom designed for the Combined Cycle application.** Although this involves effort, it is not impossible since the steam plant relies on proven technology.

6.8.3 Standard off-the-shelf Combined Cycle

It would be ideal to only design the PBMR reactor and then couple it to a conventional off-the shelf Combined Cycle via an IHX. The following practicalities were identified:

- Traditional off-the-shelf Combined Cycles have maximum cycle temperatures in excess of 1100 °C. The IHX limits the reactor outlet temperature to 900 °C. This implies that the off-the-shelf design will be operated at 900 °C. Operating at 900 °C effectively means that the turbo machines will be operated at an off-design point. This implies firstly that the turbo machine efficiencies will decrease and secondly that one pays the capital cost of a large turbo machine but not utilising its full capacity. The entire steam plant will also be operated at off-design conditions. *Figure 6.102* illustrates the above mentioned arguments.

  Possible solution:

  It is therefore recommended that when coupling to an off-the-shelf design that the reactor outlet temperature be in excess of 900 °C and as close as possible to 1100 °C.

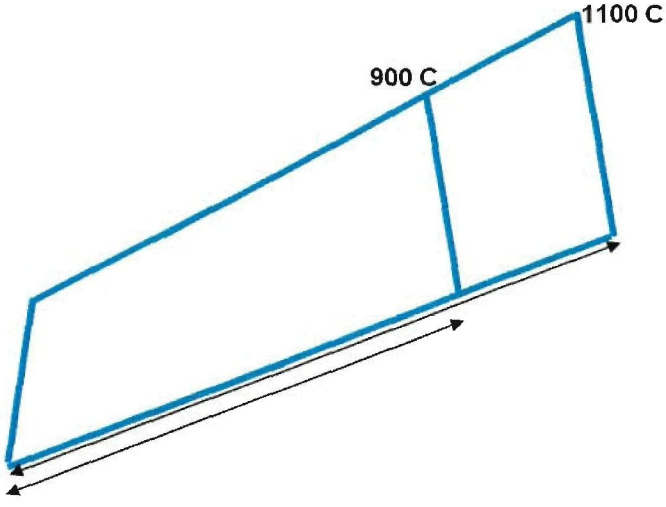


Figure 6.102 *T-s diagram for off-the-shelf Combined Cycle operated at off-design conditions*

- Traditional off-the-shelf Combined Cycles are open to atmosphere. This poses a problem for possible radio activity release. The IHX is designed according to ASME 3 standards. Should a medium pipe break (IHX break) occur (10-230 mm) the IHX fails and full radio activity release occurs as would be the case if a pre-cooler or inter-cooler breaks. The problem is when a small pipe break occurs (<10 mm). For a closed system, the radio activity release of small pipe breaks are removed via the HVAC (heating ventilation an air conditioning) system. Small pipe breaks are a problem for conventional off-the shelf Combined Cycles since activity release would occur.

  Possible solution:

  A pre-cooler could possibly be inserted between the steam generator and the LPC in order to force a closed-loop system.

- Traditional off-the-shelf Combined Cycles operate at pressure ratios between 15:1 and 40:1. General Electric is said to be designing a plant with a 50:1 pressure ratio. This implies that at best the compressor outlet pressure is in the region of 50 Bar. The primary loop for the PBR needs to be above 90 bar pressure to minimize the velocities in the reactor. This is a problem

since the IHX needs to withstand a pressure difference of 40 Bar, which is not acceptable.

Possible solution:

The PBR primary loop will need to operate at around 60 bar, ensuring a pressure difference of around 10 Bar across the IHX. At 400 MW this is not possible due to high reactor velocities. This problem might be overcome by reducing the reactor power to 300 MW which would bring the pressure down from 90 Bar to 68 Bar. This implies that the reactor becomes shorter resulting in lower costs. For the shorter 300 MW design, the fuel pebbles only need to travel once through the reactor, mitigating the use of the fuel handling system which also has a cost benefit. These statements need to be investigated.

These practicalities mentioned seem to imply that it is not feasible to couple the 400 MW 90 bar PBR to a conventional off-the-shelf designed Combined Cycle, although a 300 MW 50 bar PBR seems practical and economical. This implies that a different reactor design is needed. Standard off-the-shelf Combined Cycles cost in the region of 400 $/kW [2003 GTW Handbook].

The current PBMR design Cycle B costs 250 m$:

a) Reactor 77 m$

b) Building and balance of plant 113 m$

c) PCU 60 m$

Should the PBR couple to an off-the-shelf design the expected cost could be as low as 222 m$:

a) Combined Cycle 120 m$ (300 MW at 400 $/kW)

b) Reactor 77 m$ (possibly cheaper due to shorter design)

c) IHX 25 m$

The additional cost advantages for the Combined Cycle due to higher cycle efficiency, lower reactor costs and the possible absence of the fuel handling system is not included. The cost disadvantage due to lower power level has not been included.

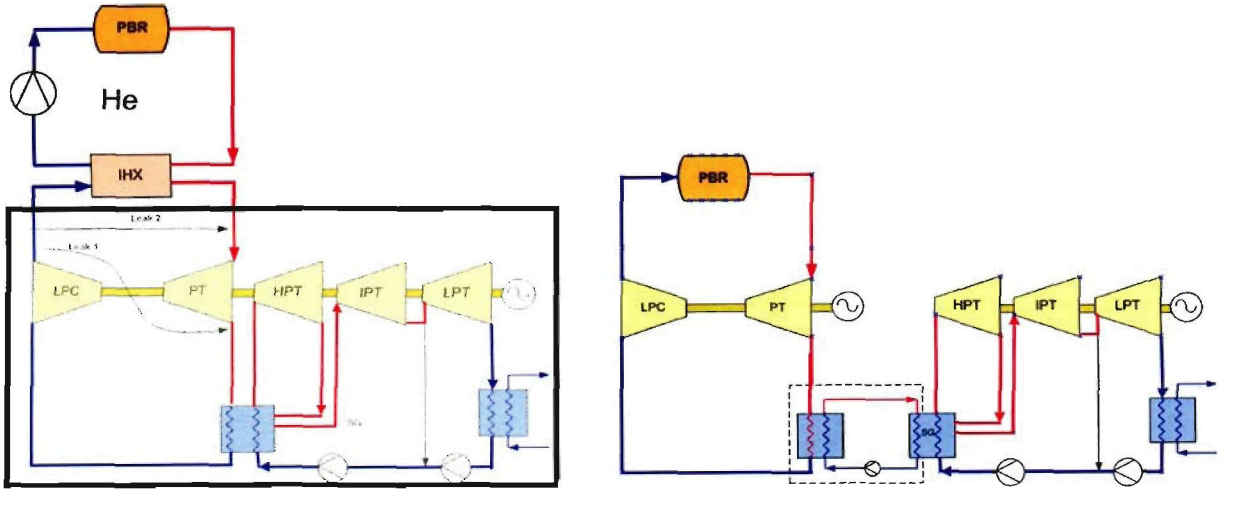


Figure 6.103 *Schematic drawing for Cycle H and Cycle I – Standard off-the shelf CC*

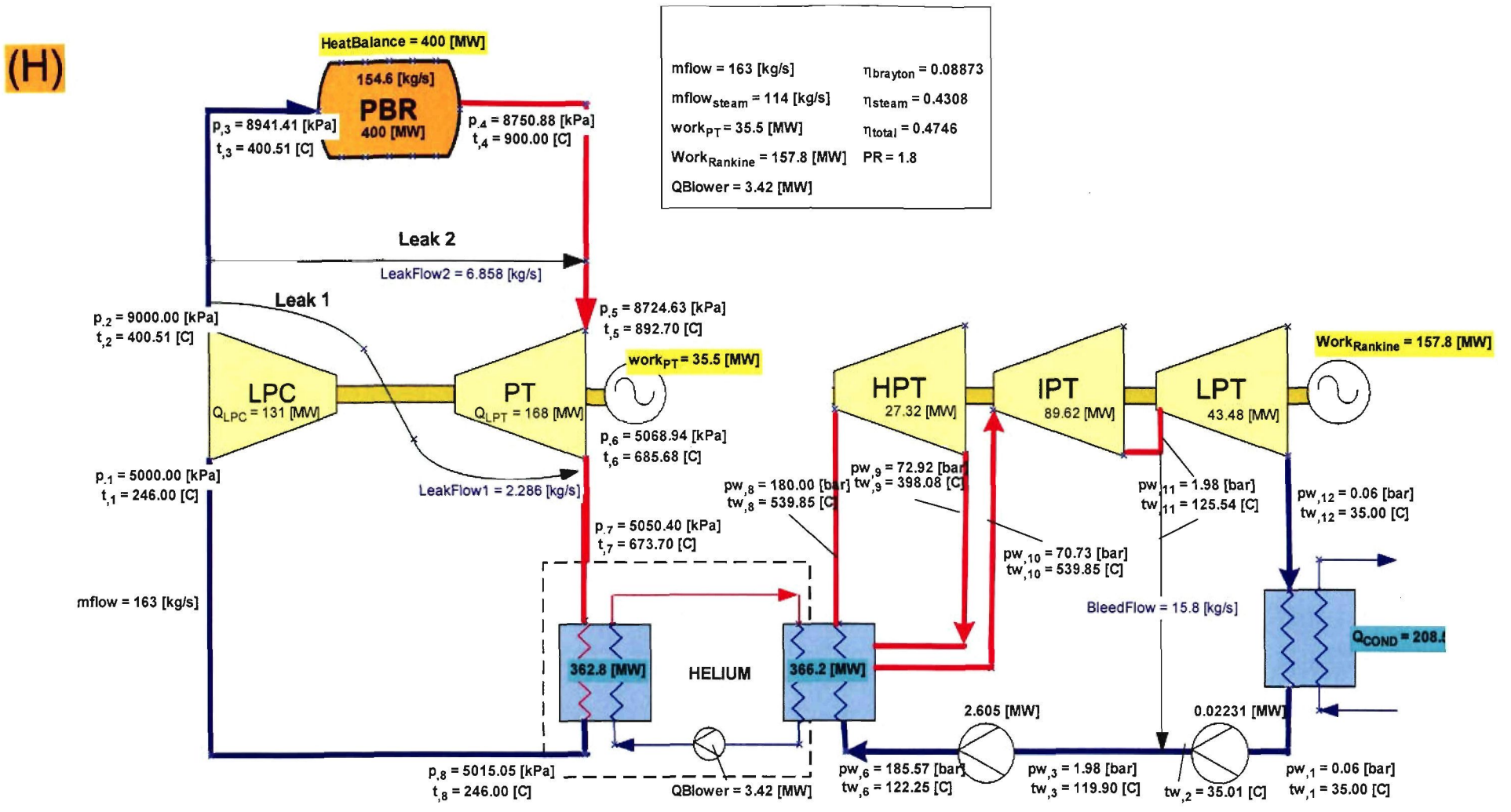


Figure 6.104 *Identification Diagram – Cycle H*

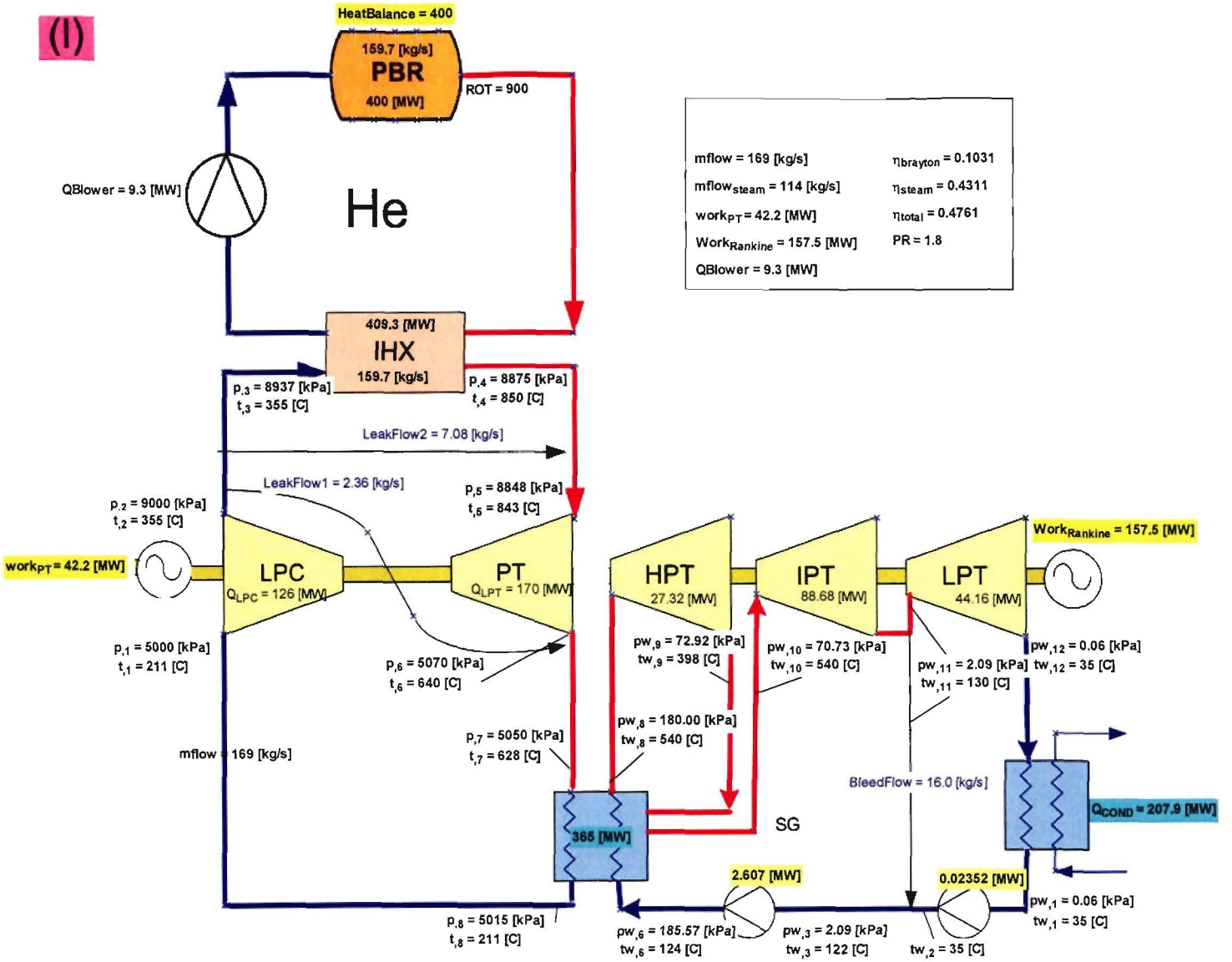


Figure 6.105 *Identification Diagram – Cycle I*

6.9 SUMMARY OF RESULTS

Brayton Cycles

(A) Single-shaft – The reactor inlet temperature limitation of 500 °C (*Figure 6.48*) limits the pressure ratio of this cycle to 3.1, which corresponds with a low thermal efficiency. Cycle A has the lowest cycle efficiency of all the cycles under investigation. The size of this cycle's single compressor is larger than the two compressors of Cycle B combined. Remember that the cost is only based on the physical size. *Figure 6.53* indicates that Cycle A is relatively speaking the most expensive.

(B) Single-shaft with inter-cooling - This cycle has the highest thermal efficiency of the Brayton cycles and also the lowest order-of-magnitude cost of all the cycles. Apart from Cycle A, this cycle also has the least number of components. Interesting to note is that the turbo machines for this cycle are smaller than those for Cycle A because of lower volumetric flows in the HPC, which results in a smaller machine. The single-shaft also offers the advantage of higher turbine efficiencies, because a larger pressure ratio over the single turbine results in more stages. Cycle B is relatively speaking the cheapest of all the cycles (for a power turbine speed of 100 rev/s) – see *Figure 6.66* and *Figure 6.67*. This is however a function of the NCC. Should the nuclear plant be sold for more than 2000 $/kW, the Combined Cycles would be relatively speaking the cheapest. However, Cycle B has the disadvantage of not being able to operate at higher power levels because the reactor inlet temperature and mass flow limitations will be exceeded – see *Figure 6.72*, *Figure 6.76* and *Figure 6.80*. Although *Figure 6.55* indicated that higher reactor outlet temperatures are possible from a turbo machine cost viewpoint, the practical constraints do not make this possible. *Figure 6.84* indicated that the reactor outlet temperature should be kept below 900 °C from a turbine blade stress viewpoint. *Figure 6.56* shows that a gearbox will be compulsory for the single-shaft design in order to be competitive with the three-shaft design (Cycle D). At 50 rev/s the turbo machine capital costs of Cycle B are the most expensive of all the cycles.

(C) Two-shaft with inter-cooling – This cycle has a slightly lower efficiency than Cycle B and is only slightly more expensive than Cycle B. This cycle has the disadvantage of expensive turbo machines at high reactor outlet temperatures. An alternative for Cycle C would be to operate the HPT as the power turbine and to remove the HPC – see *Figure 7.106*.

(D) Three-shaft with inter-cooling - The three-shaft design with single inter-cooling has low turbo machine costs because both the high-pressure and low-pressure turbo machines can be optimized. *Figure 6.55* shows that the turbo machine costs increase significantly at higher reactor outlet temperatures. Unless stronger turbine blade materials are developed, it does not seem feasible from a technology growth viewpoint to use a three-shaft design. At reactor outlet temperatures below 870 °C, the three-shaft design holds the advantage that a gearbox is not needed. This cycle has more components than Cycle B without a cost or an efficiency advantage.

(E) Three-shaft with two-step inter-cooling - When comparing the two three-shaft designs, the two-step inter-cooling has the advantage of a higher thermal efficiency, but the turbo machine costs are significantly higher due to the compressor connected to the power turbine. This compressor's cost is high because its speed is fixed.

(F) Indirect single-shaft with inter-cooling – The indirect cycle is about 3 % less efficient than Cycle B, has a higher reactor inlet temperature due to the temperature increase over the blower and therefore also higher mass flows. The indirect cycle is relatively speaking also considerably more expensive than Cycle B due to the expensive IHX and the loss of capitalised income due to the low cycle efficiency. Furthermore, there doesn't seem to be any practical solutions for Cycle F at reactor outlet temperatures 850 °C and 900 °C for 400 and 600 MW. The only solution occurs at 400 MW for a reactor outlet temperature of 1100 °C - see *Figure 6.72*, *Figure 6.76* and *Figure 6.80*.

Combined Cycles

(G) Single-shaft recuperative Brayton with inter-cooling – This cycle has the fourth highest cycle efficiency (46.6%) and the second cheapest relative cost. This cycle's mass flow and reactor inlet temperature are the lowest of all the cycles. The low reactor inlet temperature (320 °C) is very favourable for the reactor and the low mass flows imply a small PCU. Although this cycle has the highest number of components and may seem to be complex, the additional components are small and simple. This cycle also has the advantage that practical solutions are obtained for 400 and 600 MW at 900 °C and 1100 °C. Another advantage is that no practical problems have been identified with this cycle. It was illustrated in *Figure 6.84* that Cycle G has the largest turbine blade stress safety factor of all the cycles. The large safety factor of Cycle G can be ascribed to the low mass flows in the PCU that results in smaller turbo machines. Cycle G has the advantage that the compressor design is conventional, where as the compressor designs of Cycle H and Cycle I are not conventional due to the high inlet temperatures. The thermal mass of the recuperator has the advantage that Cycle G is less sensitive to transients. Cycle G does not have the same problem with cooling as do Cycle H and Cycle I.

(H) Single-shaft Brayton without inter-cooling – This cycle (together with Cycle I) has the highest thermal efficiency. This is because all the cycle's heat is rejected in the condenser at a low temperature. Cycle H has a low reactor inlet temperature (400 °C) and low mass flows (160 kg/s). The low mass flows result in small turbo machines. *Figure 6.65* showed that only 20 % of the total work output is produced by the Brayton cycle and 80 % by the steam plant. The total cost of Cycle H compares favourably with Cycle B and Cycle G. Cycle H has the advantage of practical solutions at 900 °C and 1100 °C for both 400 and 600 MW. The practical issues associated with this cycle were discussed in section 6.7.

(I) Indirect Single-shaft Brayton without inter-cooling - This cycle (together with Cycle H) has the highest thermal efficiency. Cycle I also has a low reactor inlet temperature (400 °C) and low mass flows (160 kg/s). *Figure 6.65* showed that only 20 % of the total work output is produced by the Brayton cycle and 80 % by the steam plant. The total cost of Cycle I is approximately 25 m$ more expensive than Cycle H due to the expensive IHX. The 25 m$ consists of 60 % development costs and 40 % capital cost. The additional advantages of an indirect cycle need to be compared to the additional capital costs. The IHX shields the PCU from contamination. This is a big advantage due to lower risks and also lower decommissioning costs. Cycle I also has the advantage of practical solutions at 900 °C and 1100 °C for both 400 and 600 MW. From a technology growth path viewpoint Cycle I is a good choice. The development of the IHX will enable PBMR to explore markets other than the electricity generation business. The IHX will enable the PBR to be coupled to other high-process temperatures. The development of the IHX may enable PBMR to couple with a standard off-the shelf

Copyright 2005 by PBMR

Combined Cycle in future. The practical issues associated with this cycle were discussed in section 6.7.

(J) Single-shaft recuperative Brayton without inter-cooling – This cycle has the third highest cycle efficiency (47.5%) and the second cheapest relative cost. This cycle's mass flow and reactor inlet temperature are the lowest of all the cycles. The low reactor inlet temperature (320 °C) is very favourable for the reactor and the low mass flows imply a small PCU. This cycle also has the advantage that practical solutions are obtained for 400 and 600 MW at 900 °C and 1100 °C. Another advantage is that no practical problems have been identified with this cycle. Cycle J has the advantage that the compressor design is conventional, where as the compressor designs of Cycle H and Cycle I are not conventional. The thermal mass of the recuperator has the advantage that Cycle J is less sensitive to transients. Cycle J does not have the same problem with cooling as do Cycle H and Cycle I.

The turbine blade safety factors for the Combined Cycles are between 20% and 50 % higher than the Brayton cycles. This is favourable from both a blade lifetime and risk perspective.

Practicalities

None of the practical issues mentioned for Cycle H and Cycle I are perceived as insoluble and it is believed that the issues can be mitigated. The steam plant will need to be custom designed for the Combined Cycle application. Although this involves effort, it is not impossible.

As mentioned, the pressure difference over the IHX is a big problem when coupling to an off-the-shelf Combined Cycle, which will force the PBR to probably operate at 300 MW or lower in order to reduce to maximum pressure in the primary loop or re-design the PBR.

Framatome vs. PBMR

Overall, the Framatome cycle is 0.3% more efficient than the PBMR cycle. From purely a thermodynamic efficiency viewpoint neither the PBMR nor the Framatome cycle has a significant advantage.

Series vs. Parallel configuration for the SIHX

The thermal efficiency for the series configuration is substantially lower than the parallel configuration. This is because the turbine inlet temperature has dropped with almost 60 °C, resulting in a lower thermal efficiency. The parallel configuration SIHX sees only 12% of the total cycle mass flow, resulting in a considerably smaller design than for the series configuration, while the turbine inlet temperature stays constant.

Helium vs. Nitrogen

Nitrogen produces smaller turbo machines than Helium because Nitrogen is more compressible. The helium heat exchanger is considerably smaller than the nitrogen heat exchanger due to a higher conductive heat transfer coefficient. The combined cost of the PCU (turbo units, heat exchangers and blowers) is smaller for Helium than for Nitrogen. Interesting to note is that the PCU capital cost of the

mixture is the smallest, combining both a low turbo unit and heat exchanger cost – see *Figure 6.90*.

Direct vs. Indirect

The pressure loss due to the piping, IHX and the low blower efficiency accounts for 0.5% of the loss in thermal efficiency. The temperature difference across the IHX accounts for 1.5 % of the loss in thermal efficiency. The indirect cycle has the advantage of shielding the PCU from contamination which reduces both decommissioning costs and risks. The blower in the primary loop adds an additional parameter with which to control the plant, which might be favourable from a controllability viewpoint.

ITRG requirements

Cycles B, G, H and I have thermal cycle efficiencies higher than 45 % at 900 °C, as recommended by the ITRG.

Chapter 7

Recommendation and Conclusion

In this chapter recommendations are made, conclusions are drawn and future work is mentioned.

7. RECOMMENDATION AND CONCLUSION

This chapter documents the recommendation of this study based on the results presented in Chapter 6. The final conclusion is drawn in section 7.2 and possible future work is mentioned in section 7.3.

7.1 RECOMMENDATION

The following cycles are not recommended

- *Cycle A* - This cycle is relatively speaking the most expensive and also the least efficient.
- *Cycle C* - This cycle has a slightly lower efficiency than Cycle B and is only slightly more expensive than Cycle B. A better alternative for Cycle C would be to operate the HPT as the power turbine and to remove the HPC – see *Figure 7.106*.
- *Cycle D* - This design also has more components than the single- and two-shaft design and also has lower cycle efficiencies than the single- and two-shaft due to more pipe losses, turbo machine diffuser losses and lower turbine isentropic efficiencies. The increased turbo machine costs at higher reactor outlet temperatures do not make this cycle feasible from a technology growth potential viewpoint.
- *Cycle E* – This cycle is expensive and complex - not recommended.
- *Cycle F* – This cycle is expensive and inefficient - not recommended. This cycle also has the disadvantage of no practical solutions at 850 °C and 900 °C for neither 400 nor 600 MW.

The following cycles are recommended to be further investigated:

- *Cycle B* - This cycle has the highest thermal efficiency of the Brayton cycles and also the lowest order-of-magnitude cost of all the cycles.
    - Should Cycle B be chosen, it is compulsory that a gearbox be implemented and that the power turbine speed should exceed 80 rev/s.
    - Cycle B becomes more expensive than the Combined Cycles at NCC costs of higher than 2000 $/kW. Cycle B is only recommended if the selling price of the plant is below 2000 $/kW.
    - Due to reactor inlet temperature and mass flow limitations, Cycle B cannot operate at 600 MW or at 1100 °C. Cycle B is only recommended if it is clear that neither 600 MW nor higher reactor outlet temperatures will be pursued in future (unless of course the reactor inlet temperature may be increased and the reactor can operate at higher velocities).
- *Alternative to Cycle B and C* - The LPT blade stresses for Cycle B, though acceptable, is uncomfortably high at 900 °C. The blade stresses is a function of both the inlet temperature and the rotational speed. Lowering the inlet temperature or lowering the rotational speed will reduce the blade stresses. It is not really feasible to lower the reactor inlet temperature – see *Figure 6.69* and *Figure 6.72* compared to 900 °C. The blade stresses can be lowered by an additional power turbine between the LPT and the reactor which operates without a gearbox at 50 rev/s - see *Figure 7.106*. This has two advantages:
    - The gearbox is mitigated because the LPT, LPC and HPC are free to operate at

higher rotational speeds which still implies (as with the gear box) smaller and cheaper designs.

- The advantage of a multi shaft system is that the higher rotational speeds produce smaller and cheaper designs. At high temperatures though, the blade stresses increase and the turbine is forced to operate at lower speeds. Operating the power turbine for the alternative configuration at 50 rev/s significantly reduces the blade stresses because of the lower rotational speed. The LPT operates at lower temperatures. The advantage is that the LPT can operate at higher speeds at the lower temperatures where the advantage of smaller machines can be fully realised.

The alternative cycle has the following disadvantages:

- The power turbine will be very large and expensive.
- The power turbine will encounter fourth quadrant problems.
- The large power turbine will require large leak flows.
- A start-up blower will be required.

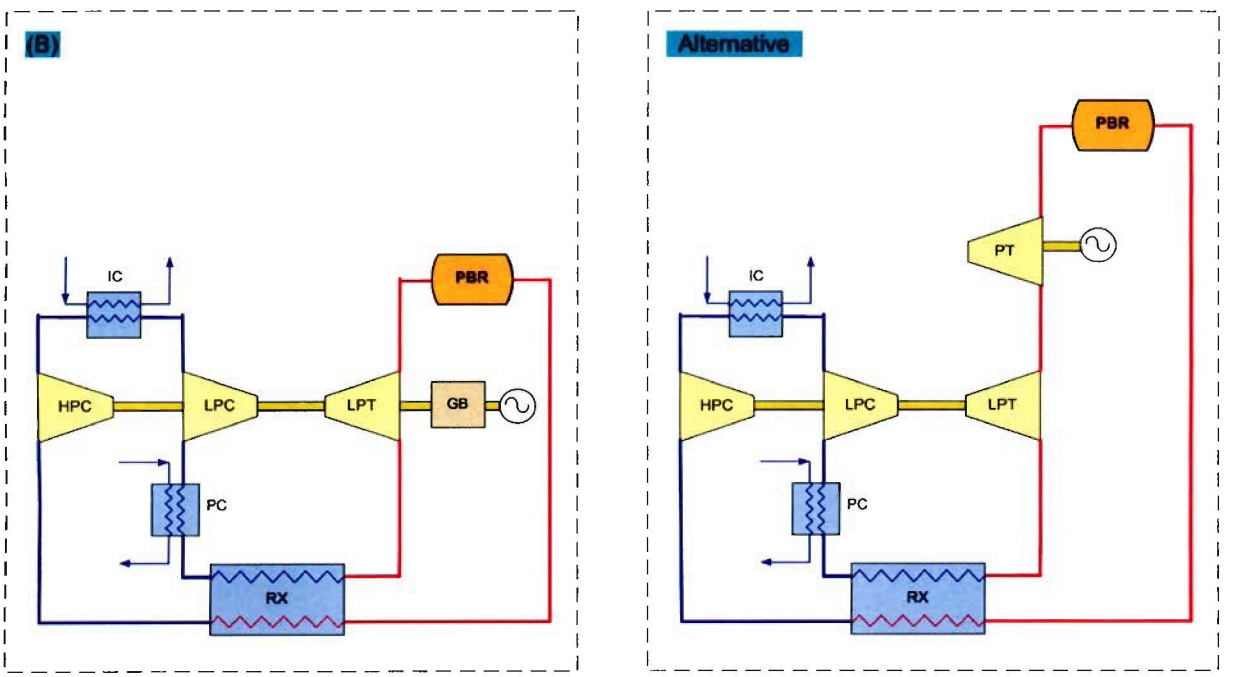


Figure 7.106 *Alternative: Combining Cycle B and Cycle C*

- *Cycle G* – Although this cycle has the highest number of components and may seem to be complex this cycle has the advantage that practical solutions are obtained for 400 and 600 MW at 900 °C and 1100 °C and that no practical problems have been identified with this cycle. This cycle is strongly recommended. **Cycle G has the advantage that the mass flow at 600 MW (pressure ratio 2.1) is the same as the mass flow for the current PBMR design Cycle B at 400 MW (pressure ratio 3.1) – see *Figure 6.75*. This implies that the same turbo machines might easily be used to upgrade the current design (B) to 600 MW.**
- *Cycle H* – This cycle seems to be practical and has a very high cycle efficiency and low

relative cost. This cycle holds the advantage of a technology growth path which leads to both higher reactor outlet temperature and higher power levels. From a technology growth path viewpoint Cycle H is a good choice.

- *Cycle I* - This cycle has all the same advantages as Cycle H. The added disadvantage is the costly IHX and the effort and time needed to qualify materials to use for the IHX. The developed and qualified IHX will not only realise Cycle I, but also opens the market for other opportunities. The IHX can be coupled to a conventional Combined Cycle and also with many high temperature process heat applications.
- *Cycle J* – This cycle has the advantage that practical solutions are obtained for 400 and 600 MW at 900 °C and 1100 °C and that no practical problems have been identified with this cycle. This cycle is strongly recommended. **Cycle J has the advantage that the mass flow at 600 MW (pressure ratio 1.6) is the same as the mass flow for the current PBMR design Cycle B at 400 MW (pressure ratio 3.1) – see *Figure 6.75*. This implies that the same turbo machines might easily be used to upgrade the current design (B) to 600 MW.** The pressure ratio of Cycle J at 600 MW needs to be around 1.6 in order to have the same mass flow as the Brayton Cycle B at a pressure ratio of 3.1. This efficiency of Cycle J at a pressure ratio of 1.6 is not optimum. **Cycle J only has solutions at a small number of pressure ratios.**

SIHX configuration for hydrogen plant

A parallel configuration has higher cycle efficiencies and the SIHX is smaller therefore a parallel configuration is recommended.

Final Recommendation

The optimum solution is a function of whether an IHX is compulsory, if it is important to operate at higher reactor outlet temperatures and power levels in future (potential technology growth), if new turbo machines will be designed and lastly what the nuclear capacity cost is. See *Figure 7.107* for discussion to follow.

The direct Brayton Cycle B is only recommended if it is decided that no IHX will be developed, that potential technology growth is not required or envisaged within the next 20 years and if the NCC is smaller than 2000 $/kW. If the NCC is larger than 2000 $/kW Cycle H, G or J are recommended. If it is required to use the same turbo machines as the current PBMR design for the NGNP, Cycle G or Cycle J are recommended. If it is decided to develop the IHX, Cycle I is recommended. For a custom designed plant either Helium or a mixture of Helium and Nitrogen can be used for the secondary loop. If it is decided to develop the IHX and buy an off-the-shelf design a gas mixture is recommended. When coupling to an off-the-shelf Combined Cycle design, a different reactor design is needed in order to operate at lower pressure levels due to the low pressure in the Combined Cycle.

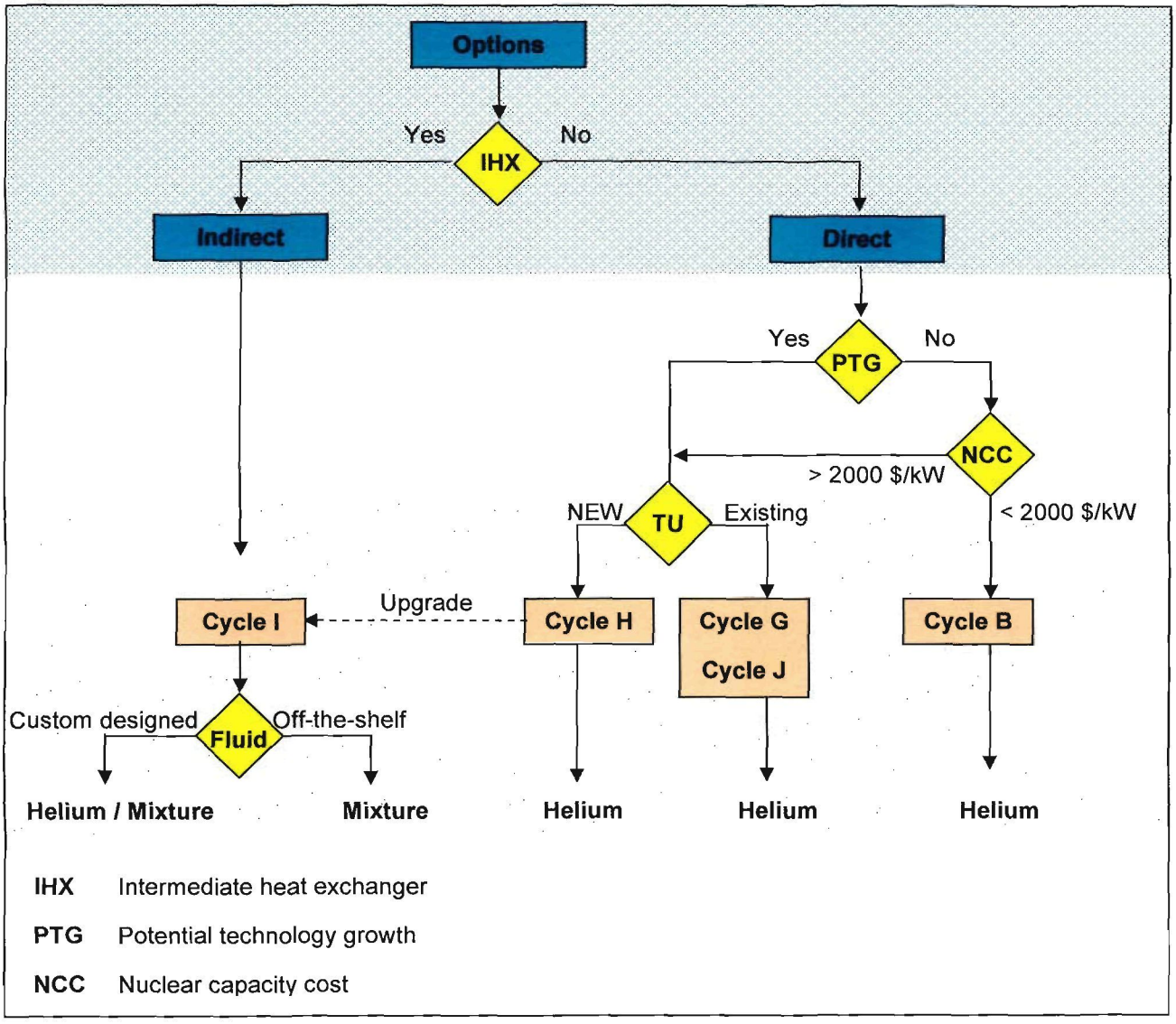


Figure 7.107 *Recommendation tree*

All said, Cycle G or Cycle J is recommended for the INEEL project. Strategically Cycle G and Cycle J are believed to be the best cycle for the following reasons:

- Both cycles provide the possibility of upgrading to higher reactor outlet temperatures and higher power levels.
- Both cycles are efficient.
- Both cycles are believed to be practical.
- PBMR already has specialised knowledge in helium turbo machinery design.
- The current PBMR plant layout and turbo machine design can be used as it is, while operating at 600 MW without any perceived practical problems.

7.2 CONCLUSION

The objective of this study was to compare the most promising one-, two- and three-shaft Brayton- and Combined-cycle configurations in order to evaluate the technical performance, practical considerations and economical competitiveness when employed in conjunction with a given Pebble Bed Reactor.

The technical performance (thermo-dynamic solution), practical considerations (design envelopes) and economical competitiveness (costs) of each of the ten selected cycles were evaluated. Of the ten cycles under evaluation, it was found that Cycle G and Cycle J are most appropriate as PCUs for the NGNP (600MWth).

The outcomes of this study are as following:

- This study succeeded in identifying a suitable PCU for the NGNP (Cycle G and Cycle J).
- This study assisted PBMR in long-term strategic planning as to which PCU is best for VHTR application. PBMR (Pty) Ltd. is currently in the process of procuring funds to build a demonstration plant for either Cycle G or Cycle J. The demonstration plant (micro model) will typically operate using a heater of 700 KW and a maximum cycle pressure of 2 Bar.
- This study succeeded to integrate knowledge from within PBMR.
- PBMR (Pty) Ltd is in the process of patenting both Cycle G and Cycle J.
- This study succeeded in providing PBMR with a tool which will give quick, meaningful results of PCU temperatures, pressures, mass flows, cycle efficiencies, comparative costs and PCU component designs. CYCLE-C was used to determine a working point for the proposed micro model.

7.3 FUTURE WORK

The following outstanding issues still need to be addressed:

- *Chapter 2: Literature survey*
  - Document the history of high temperature gas reactors (HTGR).
  - Document thermodynamic assessment of plant efficiencies for HTR power conversion as found in literature
- *Chapter 3: System thermo-hydraulic design*
  - The compressor and turbine designs were only optimized for capital cost. Since the axial velocity determines the diffuser outlet loss, the cycle needs to be optimized together with the turbo machine model to find an optimum value for C_a as well.
  - In designing the compressors and turbines, only the centrifugal stresses were evaluated. The turbine model needs to be extended to also evaluate the effect of gas bending stresses. The gas bending stresses are influenced by the number of blades, which in turn will have an impact on the cost of the turbine. The cycle needs to be optimised with regard to the gas bending stresses. This has not been done.
  - The amount of leak flow needed for a particular cycle is determined by the size of the turbo machines. The leak flows have a large impact on the thermal efficiency of the plant. The turbo machines need to be optimized to also take the effect of leak flows into account. At this stage the leak flows were simply calculated as fixed percentage of the total cycle flow.
  - The pressure loss over the piping is calculated as a percentage of the pipe inlet pressure. This percentage was kept the same for all the pipes. The percentage needs to be varied, depending on the pipe location.
- *Chapter 4: Costing models*
  - The costing models need to be refined to also incorporate development costs and engineering effort.
- *Chapter 5: Component models*
  - Turbo machine
    - The component model can be refined to also take into account the number of blades.
    - The stage prediction for the compressor must be implemented, using the loss model of *Koch and Smith* for the compressor and the loss model of *Ainley and Matthiesen* for the turbine. At this stage a fixed stage efficiency was assumed.
    - The fixed stage efficiency needs to be confirmed and refined.
  - Heat exchangers
    - The recuperator and heat exchanger models need to be refined to calculate the pressure loss through the heat exchanger as function of the heat exchanger design. In order to evaluate the pressure loss, a detailed design for the recuperator and heat exchangers are needed.
    - At this stage, the overall heat transfer coefficient U for the heat exchangers

was fixed. The heat exchanger models need to be extended to calculate the overall convection coefficient.

- Reactor
  - A reactor model needs to be integrated with the cycle analyses.
- Piping and pressure boundary
  - The piping sizes and cost need to be calculated.

- *Chapter 6: Results*
- A generic economic model which incorporates those variables that will have an impact on the overall cost of a nuclear plant needs to be developed:
  - capital costs , depreciation of capital, interest on capital
  - fuel costs, operation costs, maintenance, waste disposal
  - *complexity, construction time, licensing cost, decommissioning*
- A number of qualitative attributes such as maintenance, decommissioning, safety, licensing, market flexibility, risk and suppliers will need to be evaluated for each cycle configuration.
- The controllability of each configuration needs to be assessed.
- Standard off-the-shelf steam and combined plants need to be investigated to confirm whether the designs proposed are practical.
- Scoping analyses need to be done for multi module configurations as well.
- *The sensitivity analyses of section 6.6.9 need to be documented.*

8. REFERENCES

[1] **008472-052 REV1**. PBMR Material Properties Database. (Internal PBMR document).

[2] **ANON**. 8 April 2002. *Newsweek*.

[3] **BILLOT, P & BARBIER, D.** 2004. VHTR The French Atomic Energy Commission (CEA) R&D program. (Paper presented at the 2nd International Topical meeting of HTGR technology hosted in Beijing China during September 2004).

[4] **COPSEY, B & LECOMTE, M & BRINKMAN, G & CAPITAINE, A & DEBERNE, N. 2004.** The Framatome ANP Indirect Cycle VHTR. (Paper precented at the proceedings of ICAPP during June 2004).

[5] **DA CRUZ, D.F & DE HAAS, J.B.M & VAN HEEK A.I. 2002.** ACACIA-Indirect: A small scale Nuclear power plant. (Paper presented at the 1st International Topical meeting of HTGR technology hosted in Beijing China during September 2002).

[6] **FROHLING, W & UNGER, H.M & DONG, Y.** 2002. Thermodynamic assessment of plant efficiencies for HTR power conversion systems. (Paper presented at the 1st International Topical meeting of HTGR technology hosted in Beijing China during September 2002).

[7] **FUJIMOTO, N.** 2004. Present status of HTTR project – Achievement of 950 °C of reactor outlet coolant temperature. (Paper presented at the 2nd International Topical meeting of HTGR technology hosted in Beijing China during September 2004).

[8] **HITTNER, D.** 2004. The European programme of development of HTR/VHTR technology". (Paper presented at the 2nd International Topical meeting of HTGR technology hosted in Beijing China during September 2004).

[9] **IAEA (International Atomic Energy Agency).** 2001**a**. IAEA-TECDOC-1198 - Current status and future development of modular high temperature gas cooled reactor technology, February 2001.

[10] **IAEA (International Atomic Energy Agency).** 2001**b**. IAEA-TECDOC-1238 - Gas turbine power conversion systems for modular HTGRs. (Summary of reports from a technical committee meeting held in Palo Alto USA during August 2001). *Specific report by:*

BREY, HL. 2000. Developmental history of the gas turbine modular HTR, November 2000.

[11] **IAEA (International Atomic Energy Agency).** 2001**c**. IAEA-TECDOC-1198 - Current Status and future development of modular hight temperature gas cooled reactor technology, February 2001. Chapter 2.

[12] **INEEL ITRG.** 2004. Design features and technology uncertainties for the Next Generation Nuclear Plant. (Document published by INEEL on 30 June 2004). INEEL/EXT-04-01816.

[13] **JIE, W & ZHIYONG, H & SHUTANG, Z & SUYUAN, Y.** 2004. Design features of the gas turbine power conversion system for HTR-10 GT. (Paper presented at the 2nd International Topical meeting of HTGR technology hosted in Beijing China during September 2004).

[14] **KADAK, A & BALLINGER, R.** 2004. MIT Modular Pebble Bed Reactor (MBMR). (Paper presented at the 2nd International Topical meeting of HTGR technology hosted in Beijing China during September 2004).

[15] **KOSTIN V.I & KODOCHIGOV, N.G & VASYAEV, A.V & GOLOVKO, V.F.** 2004. Power Conversion Unit with Direct Gas-Turbine Cycle for Electric Power Generation as a part of GT-MHR. (Paper presented at the 2nd International Topical meeting of HTGR technology hosted in Beijing China during September 2004).

[16] **KUGELER, K & ALKAN, Z & POPPE, N.** 2003. Course notes on *High Temperature Reactor Technology* presented at Potchefstroom University during April 2003. Chapter 1.

[17] **KUNITOMI, K & KATANISHI, S & TAKADA, S & TAKIZUKA, T & YAN, X.** 2004. Japan's future HTR – the GTHTR300. *Nuclear Engineering and Design,* 233: 309-327. Aug.

[18] **MACDONALD, P *et al.*** 2004b. The NGNP – Insights gained from the INEEL Point Design Studies. (Paper presented at the proceedings of ICAPP during June 2004).

[19] **MACDONALD, P.** 2004a. The Next Generation Nuclear Plant (NGNP) Program. (A presentation by the NGNP Program Manager for INEEL on 16 November 2004).

[20] **MATZNER, D & MATZIE, R & NICHOLLS, D.** 2003. PBMR The first Generation IV reactor to be constructed. (Presentation held at the *WNA Annual Symposium* 2003).

[21] **MATZNER, D.** 2004. PBMR project status and the way ahead. (Paper presented at the 2nd International Topical meeting of HTGR technology hosted in Beijing China during September 2004).

[22] **OECD/IEA.** 2003. Annual Report. Energy balances of OECD countries 2001.

[23] PBMR Flownex project file. MPS model S003 Demonstration Plant.

[24] PBMR Flownex project file. MPS model V704 Demonstration Plant.

[25] **PBMR-MHI-032.** 2003. Mitsubushi HPT interim design report for the basic design of the turbo units and power turbine generator. REV 0 (29 August 2003). (Internal PBMR document).

[26] **PBMR-MHI-033.** 2003. Mitsubushi HPC interim design report for the basic design of the turbo units and power turbine generator. REV 0 (29 August 2003). (Internal PBMR document).

[27] **PBMR-MHI-035.** 2003. Mitsubushi LPT interim design report for the basic design of the turbo units and power turbine generator. REV 0 (29 August 2003). (Internal PBMR document).

[28] **PBMR-MHI-036**. 2003. Mitsubushi LPC interim design report for the basic design of the turbo units and power turbine generator. REV 0 (29 August 2003). (Internal PBMR document).

[29] **SARAVANAMUTTOO, H.I.H & ROGERS, G. COHEN, H.** 2001. Gas Turbine Theory. 5th Ed. Prentice Hall.

[30] **SAWA, K & UETA, S.** 2004. Research and development on HTGR fuel in the HTTR project. *Nuclear Engineering and Design,* 233: 163-172. Aug.

[31] **SL-008277**. 2004. PBMR Turbine island design feasibility study. (Prepared for PBMR by Sargent and Lundy). (Internal PBMR document).

[32] **TWG-GCR members**. 2005. Minutes of 19th meeting on the Technical Working Group on Gas-Cooled Reactors (held at the University of Manchester UK during January 2005).

[33] **US DOE (United States Department of Energy)**. 2004. System Research Plan for the VHTR. (Draft document issued by the US DOE and GIF in August 2004).

[34] **VAN HEEK, A & WIERSMA, B & BLOM, F & GROOT, S & BOER, B & PAHLADSINGH, R.** 2004. A private investor's initiative in HTR technology in the Netherlands. (Paper presented at the 2nd International Topical meeting of HTGR technology hosted in Beijing China during September 2004).

[35] **WANG, C & BALLINGER, R.G & STAHLE, P.W.** 2002. Design of a Power Conversion System for an Indirect Cycle, Helium Cooled PBR System. (Paper presented at the 1st International Topical meeting of HTGR technology hosted in Beijing China during September 2002).

[36] **WNA**. 2002**a**. World energy needs and nuclear power. *World Nuclear Association Info Brief: July 2002.*

[37] **WNA**. 2002**b**. World energy needs and nuclear power. *World Nuclear Association Info Brief, July 2002.*

[38] **WNA**. 2003**a**. Advanced Reactors. *World Nuclear Association Info Brief, December 2003.*

[39] **WNA**. 2003**b**. Generation IV nuclear reactors. *World Nuclear Association Info Brief, August 2003.*

[40] **WNA**. 2004**a**. Nuclear power in the world today. *World Nuclear Association Info Brief: March 2004.*

[41] **WNA**. 2004**b**. The economics of nuclear power. *World Nuclear Association Info Brief: March 2004.*

[42] **WNA**. 2005**a**. Small nuclear power reactors. *World Nuclear Association Info Brief, January 2005.*

[43] **WNA**. 2005**b**. US Nuclear Power industry. *World Nuclear Association Info Brief, January 2005.*

[44] **YAN**, X & TAKIZUKA, T & TAKADA, S & KUNITOMI, K & MINATSUKI, I & MIZOKAMI, Y. 2003. Cost and performance design approach for GTHTR300 power conversion system. *Nuclear Engineering and Design,* 226: 351-373. Jul.

[45] **ZHIYONG, H & JIE, W & LI, J**. 2004. Study on the thermodynamic cycle of the HTR-GT. (Paper presented at the 2nd International Topical meeting of HTGR technology hosted in Beijing China during September 2004).

9. APPENDICES

9.1 APPENDIX I – INPUT PARAMETERS

Variables	*C++ var.*	Value	Units	Description
η_c	*a.etac_HP*	= 89	[%]	compressor isentropic efficiency - HPC
	a.etac_LP	= 89	[%]	compressor isentropic efficiency - LPC
	a.etac_PT	= 89	[%]	compressor isentropic efficiency - LPC2
η_t	*a.etat_HP*	= 91	[%]	turbine isentropic efficiency - HPT
	a.etat_LP	= 91	[%]	turbine isentropic efficiency - LPT
	a.etat_PT	= 91	[%]	turbine isentropic efficiency - PT
$C_{a,c}$, $C_{a,t}$	*a.V_PT*	= 100	[m/s]	diffuser outlet velocity - PT
	a.V_Lpt	= 135	[m/s]	diffuser outlet velocity - LPC2
	a.V_HPC	= 135	[m/s]	diffuser outlet velocity - HPC
	a.V_HPT	= 135	[m/s]	diffuser outlet velocity - HPT
	a.V_LPC	= 135	[m/s]	diffuser outlet velocity - LPC
	a.V_LPT	= 135	[m/s]	diffuser outlet velocity - LPT

Table 9.11 *Guessed input variables*

Variables	*C++ var.*	Value	Units	Description
t_{min}	*a.tcold*	= 24	[°C]	minimum cycle coolant temperature
t_{max}	*a.thot*	= 900	[°C]	maximum cycle coolant temperature
p_{max}	*a.ph*	= 90	[bar]	maximum cycle pressure
pressure ratio	*a.PR*	= vary	[-]	total pressure ratio over all compressors
PBR	*a.PBMR*	= 400	[MWth]	Pebble Bed Reactor thermal power
BLOCK	*a.BLOCK*	= 400	[MWth]	Block Reactor thermal power
K_{PBMR}	*a.k_PBMR*	= 40	[-]	loss coefficient for PBR - fixed $k_{PBMR} = \frac{1}{2}\frac{1}{A^2}K = \frac{\rho_{avg}\Delta P}{\dot{m}^2}$
K_{BLOCK}	*a.k_BLOCK*	= 4	[-]	loss coefficient for BlockReactor - fixed
K_{comp}	*a.k_comp*	= 1.0	[-]	loss coefficient for diffuser - compressor
K_{turb}	*a.k_turb*	= 0.8	[-]	loss coefficient for diffuser - turbine
$\%dP_{HXs}$	*a.lossfact2*	= 0.993	[-]	0.7% pressure loss on each side for each heat exchanger in cycle
$\%dP_{PIPING}$	*a.lossfact1*	= 0.997	[-]	0.3% pressure loss assumed for each pipe in the cycle
η_{blower}	*η_b*	= 81	[%]	blower isentropic efficiency

Table 9.12 *Brayton input variables*

Variables	*C++ var.*	Value	Units	Description
t_{min}	*tcond*	= 35	[°C]	condensor temperature
t_{max}	*tmax*	= < 540	[°C]	maximum allowable oulet temperature for steam generator

Variables	C++ var.	Value	Units	Description
p_{max}	*p[8]*	= 180	[bar]	pressure in steam generator
$\%dP_{RH}$	-	= 3	[%]	losses in reheater
$\%dP_{SG}$	-	= 3	[%]	losses in steam generator
t_{Pinch}	-	= 10	[°C]	pinch temperature for steam generator
CDx	*x[12]*	= > 0.88	[-]	minimum allowable condensor two-phase fraction
$\eta_{turbine}$	*etat*	= 89	[%]	turbine efficiency
η_{pump}	-	= 85	[%]	pump efficiency

Table 9.13 *Rankine input variables*

Variables	C++ var.	Value	Units	Description
$gamma_{He}$	*a.gamma*	= 1.667	[-]	helium: ratio of specific heats
R_{He}	*a.R*	= 2078.0		helium: gas constant
Cp_{He}	*a.cp*	= 5195.0		helium: specific heat at constant pressure
k_{He}	*d.k_ihx_He1*	= 0.086063000+ 0.000252000*t		helium: conductivity as function of temperature
$gamma_{N2}$	*a.gamma*	= 1.400	[-]	nitrogen: ratio of specific heats
R_{N2}	*a.R*	= 296.8		nitrogen: gas constant
Cp_{N2}	*a.cp*	= 1038.8		nitrogen: specific heat at constant pressure
k_{N2}	*d.k_ihx_N22*	= 0.011312511+ 0.000053835*t		nitrogen: conductivity as function of temperature
$gamma_{MIX}$	*a.gamma*	= 1.535	[-]	mixure20%He80%N2: ratio of specific heats
R_{MIX}	*a.R*	= 652.8		mixure20%He80%N2: gas constant
Cp_{MIX}	*a.cp*	= 1873.7		mixure20%He80%N2: specific heat at constant pressure
k_{MIX}	*d.k_ihx_N22*	= 0.045830000+ 0.000142200*t		mixure20%He80%N2: conductivity as function of temperature

Table 9.14 *Fluid input variables*

Variables	C++ var.	Value	Units	Description
$H2_{MW\text{-}serie}$	*a.H2_MW_serie*	= 0 OR 50	[MW]	Power available for Hydrogen plant - series configuration
$H2_{eff\text{-}serie}$	*a.H2_eff_serie*	= 46.2	[%]	Hydrogen process efficiency
$H2_{MW\text{-}parallel}$	*a.H2_MW_parallel*	= 0 OR 50	[MW]	Power available for Hydrogen plant - parallel configuration
$H2_{eff\text{-}parallel}$	*a.H2_eff_parallel*	= 46.2	[%]	Hydrogen process efficiency

Table 9.15 *Hydrogen Plant input variables*

Variables	C++ var.	Value	Units	Description
$\eta_{mechanical}$	*a.etamech*	= 99	[%]	mechanical shaft efficiency
Φ	*fi*	= 0.40	[-]	compressor flow coefficient
Ψ	*tsi*	= 0.36	[-]	compressor work coefficient
blade material	-	= 10705BX	[-]	compressor blade material
σ_{max}	*sigmamax*	= 744	[MPa]	compressor blade material maximum allowable yield strength

Variables	C++ var.	Value	Units	Description
ρ_{BLADE}	*rhoblade*	= 7770	[kg/m3]	compressor blade material density
η_s	*etastage[i]*	= 89	[%]	stage efficiency - internal stage - compressor
Φ	*fi*	= 0.50	[-]	turbine flow coefficient
Ψ	*tsi*	= 1.10	[-]	turbine work coefficient
blade material	-	= MGA1400DS	[-]	turbine blade material
σ_{max}	*sigmamax*	= graph	[MPa]	turbine blade material maximum allowable yield strength
ρ_{BLADE}	*rhoblade*	= 7830	[kg/m3]	turbine blade material density
η_s	*etastage[i]*	= 91	[%]	stage efficiency - internal stage - turbine
N_{PT}	*N*	= 100	[rev/s]	the power turbine speed was fixed at 6000 rpm

Table 9.16 *Turbo machine input variables*

Variables	C++ var.	Value	Units	Description
$U_{Recuperator}$	*U_rec*	= 1094	[-]	heat transfer coefficient for the recuperator
$\eta_{Recuperator}$	*η_rec*	= 96	[%]	recuperator effectiveness
d_{IHX}	*a.diameter_ihx*	= 0.000576	[m]	hydraulic diameter - IHX
dT_{IHX}	*c.IHX_deltaT*	= 50	[°C]	temperature difference over the IHX for indirect cycles
$dT_{IHXsteam}$	*a.IHX_steam_deltaT*	= 37	[°C]	temperature difference over the HX for direct cycles
U_{IC}	*U*	= 320	[-]	heat transfer coefficient for the coolers
η_{IC}	*η_ic*	= 83	[%]	inter-cooler effectiveness
U_{PC}	*U*	= 320	[-]	heat transfer coefficient for the coolers
η_{PC}	*η_pc*	= 83	[%]	pre-cooler effectiveness
Cr	*Cr*	= 0.4	[-]	heat capacity ratio

Table 8.17 *Heat exchanger input variables*

Variables	C++ var.	Value	Units	Description
NCC	*$.nuclear_marginal*	= 2.0	[m$/MW]	Nuclear capacity cost
$Steam_{marginal}$	*a.steam_marginal*	= 0.26	[$/kW]	y=ax+b… (a) marginal cost
$Steam_{offset}$	*a.steam_offset*	= 24.0	[m$]	y=ax+b… (b) cost offset
KC1	*$.Comp_cost*	= 0.4311	-	proportionality constant: compressor (material)
KT1	*$.Turbine_cost*	= 2.0400	-	proportionality constant: turbine (material)
$K_{Recuperator}$	*$.rec_cost*	= 0.00025810	-	proportionality constant: recuperator (material)
K_{IC}	*$.IC_cost*	= 0.00007360	-	proportionality constant: Inter-cooler (material)
K_{PC}	*$.PC_cost*	= 0.00007360	-	proportionality constant: Pre-cooler (material)
K_{IHX}	*$.ihx_cost_factor*	= 0.00125502	-	proportionality constant: IHX (material)
$Kbase_{IHX}$	*$.ihx_cost_base*	= 15	[m$]	Cost offset: IHX (development cost)
$C_{Generator\_Gearbox}$	*$_GB_generator*	= 5.0+1.0	[m$]	Capital cost: Generator and Gearbox

Variables	C++ var.	Value	Units	Description
C_{SBS_RB}	*$.SBS_RB*	= 3.0+3.8	[m$]	Capital cost: SBS blower and Resistor bank
C_Reactor_Buiding	*$_reactor_BOP*	= 77+ 113	[m$]	Capital cost: reactor and building (incl. balance of plant) - Brayton
C_Reactor_Buiding_CC	*$_reactor_BOP*	= 77+ 82	[m$]	Capital cost: reactor and building (incl. balance of plant) - CC

Table 9.18 *Costing input variables*

Variables	C++ var.	Value	Units	Description
Single Shaft	*a.leak*	= 5.6	[%]	percentage of total mass flow
leak 1	*a.leak1*	= 25	[%]	percentage of total leak flow before turbine
leak 2	*a.leak2*	= 75	[%]	percentage of total leak flow after turbine
leak 3	*a.leak3*	= 0	[%]	percentage of leak
Single Shaft: No IC	*a.leak*	= 5.2	[%]	percentage of total mass flow
leak 1	*a.leak1*	= 100	[%]	percentage of leak
leak 2	*a.leak2*	= 0	[%]	percentage of leak
leak 3	*a.leak3*	= 0	[%]	percentage of leak
Two Shaft	*a.leak*	= 6.1	[%]	percentage of total mass flow
leak 1	*a.leak1*	= 50	[%]	percentage of leak
leak 2	*a.leak2*	= 50	[%]	percentage of leak
leak 3	*a.leak3*	= 0	[%]	percentage of leak
3-shaft designs	*a.leak*	= 7.3	[%]	percentage of total mass flow
leak 1	*a.leak1*	= 30	[%]	percentage of leak
leak 2	*a.leak2*	= 30	[%]	percentage of leak
leak 3	*a.leak3*	= 40	[%]	percentage of leak
Two Shaft nitrogen	*a.leak*	= 5.2	[%]	percentage of total mass flow
leak 1	*a.leak1*	= 25	[%]	percentage of leak
leak 2	*a.leak2*	= 75	[%]	percentage of leak
leak 3	*a.leak3*	= 0	[%]	percentage of leak

Table 9.19 *Leak flow input variables*

9.2 APPENDIX II – STAGE PREDICTION

Stage prediction is the process by which the stage efficiency of a machine is calculated. Pre-defined loss models, derived from cascade data, are used together with the basic geometry and flow conditions of the machine in order to "predict" the stage efficiency of the machine. Once the stage efficiency of each stage is known, the isentropic efficiency of the machine is calculated.

A variety of loss models for the compressor and turbine exist today, each ranging in its level of accuracy and complexity. For the compressor, the method of *Howell* was chosen. The *Howell* model, as explained in (Saravanamuttoo, 2001), is a very simple model. A more accurate, but much more involved model is that of *Koch and Smith.* See Appendix 9.4 for the documentation of the *Howell* model. For the turbine, the loss model of *Ainley and Matthieson* was chosen, which is documented in Appendix 9.5.

Typically, the loss models for both the compressor and turbine would require the following variables as input:

- All the blade angles: β_1 and β_2 and α_1 and α_2
- Blade height, h
- Pitch, s
- Solidity: s/c where c = chord
- Aspect Ratio: h/c where c = chord
- Reynolds number
- Stage inlet and outlet temperature
- Percentage tip clearance

This section briefly describes how these input parameters are obtained.

Blade angles, β

For a fixed reaction, Φ and ψ, the rotor inlet and outlet relative blade angles for the ***compressor*** are calculated using equations (1.1) and (1.2). These equations are the same as equations (5.37) and (5.38), but now the work done factor, λ is incorporated.

$$\psi = \lambda\phi(\tan\beta_1 - \tan\beta_2) \qquad (1.1)$$

From Eq. (5.23) we have that

$$\Lambda = \frac{\phi}{2}\left(\tan\beta_1 + \tan\beta_2\right) \qquad (1.2)$$

The work-done factor, λ accounts for the reduction in work capacity for the compressor. The work-done factor will always be a number less than unity. Because of the variation of axial velocity profile through the compressor, the mean work-done factor will vary as well. The values for the work-done factor, as function of number of stages, was obtained using Mitsubishi's blockage factors, as obtained in (PBMR-MHI-032, 2003, [25]) - see Figure 9.108.

The compressor absolute blade angles are calculated as function of U_m, C_a (see next section) and β. See *Figure 5.38* and reference (Saravanamuttoo, 2001) for the derivation of these equations.

$$\alpha_1 = a\tan\left(\frac{U_m}{C_a} - \tan\beta_1\right) \tag{1.3}$$

$$\alpha_2 = a\tan\left(\frac{U_m}{C_a} - \tan\beta_2\right) \tag{1.4}$$

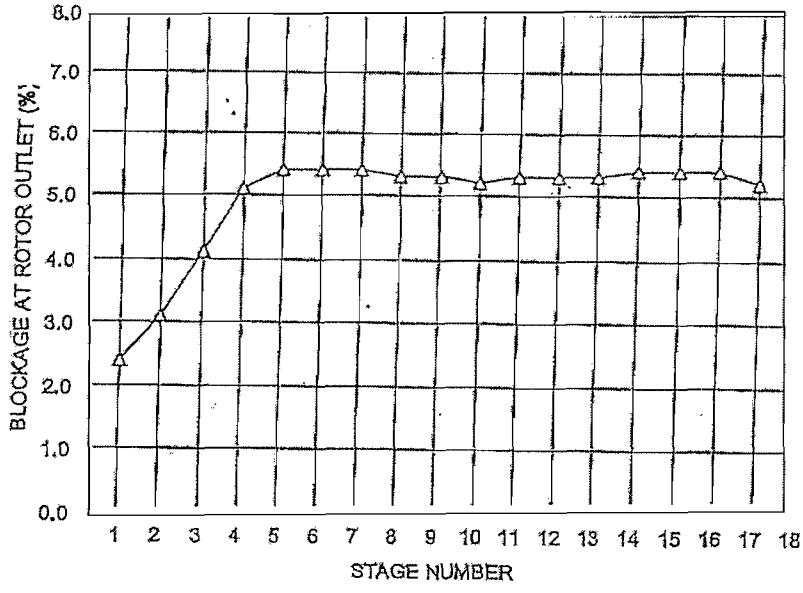


Figure 9.108 *Variation of mean blockage factor with number of stages (PBMR-MHI-032, 2003:1-68, [25])*

For a fixed reaction, Φ and ψ, the rotor inlet and outlet relative blade angles for the ***turbine*** are calculated using equations (1.5) and (1.6).

$$\psi = 2\phi(\tan\beta_2 + \tan\beta_3) \tag{1.5}$$

$$\Lambda = \frac{\phi}{2}(\tan\beta_3 - \tan\beta_2) \tag{1.6}$$

The turbine absolute blade angles are calculated as function of Φ and β. See Figure 5.39 and reference (Saravanamuttoo, 2001) for the derivation of these equations.

$$\alpha_2 = a\tan\left(\tan\beta_2 + \frac{1}{\phi}\right) \tag{1.7}$$

$$\alpha_3 = a\tan\left(\tan\beta_3 - \frac{1}{\phi}\right) \tag{1.8}$$

The blade angles dominate the profile losses over the blades.

Blade height, h

The absolute velocity at the inlet, C_1 (see *Figure 5.38* and *Figure 5.39*), can be calculated from the velocity triangles since the blade angles have been solved, and the axial velocity is known. For both

the compressor and turbine it follows that

$$C_1 = \frac{C_a}{\cos \alpha_1} \tag{1.9}$$

The static inlet temperature and pressure and the inlet density can be calculated since the inlet stagnation properties are known.

$$t1_{static} = t_1 - 2C_p C_1^2$$

$$p1_{static} = p_1 \left(\frac{t1_{static}}{t_1} \right)^{\gamma/(\gamma-1)}$$

$$\rho_1 = \frac{p1_{static}}{t1_{static} R} \tag{1.10}$$

The mass flow is known from the cycle analysis and is used to calculate the inlet area.

$$A_1 = \frac{mflow}{\rho_1 C_a} \tag{1.11}$$

In the following section it is shown how the tip radius and hub-tip-ratio was solved. Therefore the mean radius is known. Lastly, the height at the blade inlet based on the mean radius is calculated:

$$h = \frac{A_1}{2\pi r_{mean}}$$

Pitch

The number of blades is specified, from which the pitch is calculated:

$$s = \frac{2\pi r_{mean}}{n}, \quad where \quad n = number\ of\ blades\ .\ [n\ was\ assumed\ to\ be\ 77]$$

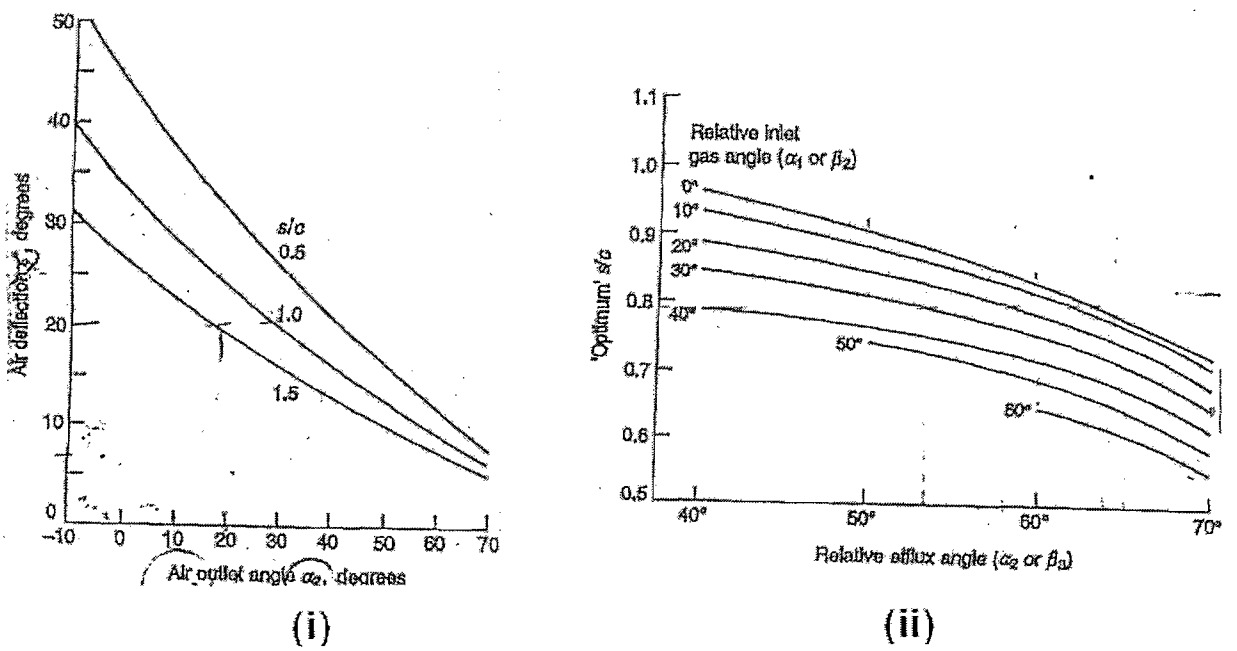


Figure 9.109 *Design deflection curves (i) compressor (Saravanamuttoo, 2001:233) (ii) turbine (Saravanamuttoo, 2001:332)*

Solidity

The solidity at 0° incidence can be calculated from empirical data as a function of the blade inlet angles – see Figure 9.109 for the compressor and turbine solidity. For fixed blade angles, these two graphs give the optimum s/c that will result in the minimum profile losses for the compressor and turbine respectively.

Aspect Ratio

Having solved the height, pitch and solidity, the aspect ratio (AR) and chord (c) can be calculated:

c = s/Solidity

AR = h/c

Reynolds number

Next, the chord-Reynolds number is solved: $\mathrm{Re} = \frac{\rho V c}{\mu}$

where Re = Reynolds number

ρ = inlet fluid density

c = chord

μ = fluid viscosity

Stage inlet and outlet temperature

The inlet and outlet temperature is already known from the cycle analysis.

Tip clearance

The tip clearance is assumed to be 1% of the blade height, but always larger than 1 mm.

Having solved all the required input parameters, the loss model's method is applied to calculate each stage's efficiency – see the Appendix 9.4 and 9.5.

9.3 APPENDIX III – TURBO MACHINE EQUATIONS IN EXPLICIT FORM

In section 5.1.2 it was explained how equations (1.12) to (1.15) are used to solve for

- z: number of stages [-]
- Ca: axial velocity [m/s]
- r_t: tip radius [m]
- $\frac{r_r}{r_t}$: hub-tip-ratio [-]

while identifying the optimum combination for rotational speed N and safety factor SF that will result in the smallest machine.

The *work coefficient* is defined as: $$\psi = \frac{cp.(dT/z)}{U_m{}^2} \quad (1.12)$$

The *flow coefficient* is defined as: $$\phi = \frac{C_a}{U_m} \quad (1.13)$$

The *centrifugal tensile* stress is defined by: $$\sigma_{real} = \frac{\sigma_{\max}}{SF} = 2/3\left[\frac{\rho_b}{2}U_t{}^2\left(1-\left(\frac{r_r}{r_t}\right)^2\right)\right] \quad (1.14)$$

The *continuity equation* states that: $$m = rho \cdot C_a \cdot \pi r_t^2\left(1-\left(\frac{r_r}{r_t}\right)^2\right) \quad (1.15)$$

When programming these equations in *Visual C++*, they need to be written in the explicit form and are then solved with the Newton-Raphson method. The derivation of these 4 equations in explicit form follows:

Equations (1.12) to (1.15) are re-written in the following form, where the mean speed is defined by:

$$U_m = 2\pi N r_m = 2\pi N\left(\frac{r_t + r_r}{2}\right) = \pi N r_t\left(1+\frac{r_r}{r_t}\right) = \frac{U_t}{2}\left(1+\frac{r_r}{r_t}\right) thus \quad (1.16)$$

$$N = \frac{U_m}{\pi r_t\left(1+\frac{r_r}{r_t}\right)} \quad (1.17)$$

$$r_t = \frac{U_m}{N\pi\left(1+\frac{r_r}{r_t}\right)} \quad (1.18)$$

$$U_t = \frac{2U_m}{\left(1+\frac{r_r}{r_t}\right)} \quad (1.19)$$

Substituting (1.19) into (1.14)

$$U_m = \sqrt{\frac{3}{4}\frac{\sigma_{max}}{\rho_b SF}\frac{(1+(r_r/r_t))}{(1-(r_r/r_t))}} \qquad (1.20)$$

Substituting (1.13) into (1.15)

$$r_t = \sqrt{\frac{m}{rho.\phi.U_m \pi\left(1-(r_r/r_t)^2\right)}} \qquad (1.21)$$

Equations, (1.20), (1.21), (1.13) and (1.17) are used to solve for the hub-tip ratio, using a Newton-Raphson method. The number of stages is calculated from Eq. (5.30)

$$z = \frac{C_p dT}{\psi U_m^{\ 2}} \quad where\ \ dT\ =\ total\ temperature\ rise\ over\ compressor$$

9.4 APPENDIX IV – THE HOWELL COMPRESSOR LOSS MODEL

The theory necessary to use the loss model of *Howell* in order to evaluate a compressor's stage efficiency is documented in this section.

The static pressure rise across the blades in a cascade test is given by:

$$\Delta p = p_2 - p_1$$
$$\Delta p = \left(p_{02} - \tfrac{1}{2}\rho V_2^2\right) - \left(p_{01} - \tfrac{1}{2}\rho V_1^2\right)$$

The incompressible flow formula is used because the change of density is negligible. Hence, it follows that

$$\Delta p = \tfrac{1}{2}\rho\left(V_1^2 - V_2^2\right) - (p_{01} - p_{02})$$

$$\Delta p = \tfrac{1}{2}\rho\left(V_1^2 - V_2^2\right) - \bar{w}$$

$$\Delta p = \tfrac{1}{2}\rho C_a^{\,2}\left(\tan^2\alpha_1 - \tan^2\alpha_2\right) - \bar{w} \qquad (1.22)$$

where $\bar{w}$ is the blade loss coefficient. For the rotor blades $\alpha_1 = \beta_1$ & $\alpha_2 = \beta_2$

The overall blade loss must account for the following sources of stagnation pressure loss:

1. *Profile loss, C_{DP}* – associated with boundary layer growth over the blade profile. C_{DP} is defined by:

   Stator:

   $$C_{DP} = \left(\frac{s}{c}\right)\left(\frac{\bar{w}}{0.5\rho V_1^2}\right)_{cascade}\left(\frac{\cos^3\alpha_m}{\cos^2\alpha_1}\right) \qquad (1.23)$$

   Rotor:

   $$C_{DP} = \left(\frac{s}{c}\right)\left(\frac{\bar{w}}{0.5\rho V_1^2}\right)_{cascade}\left(\frac{\cos^3\beta_m}{\cos^2\beta_1}\right) \qquad (1.24)$$

   From cascade data, for a certain s/c, the relationship in *Figure 9.110* can be plotted for C_{DP}. Therefore, one must have $\left(\frac{\bar{w}}{0.5\rho V_1^2}\right)_{cascade}$ if s/c is other than value for *Figure 9.110*.

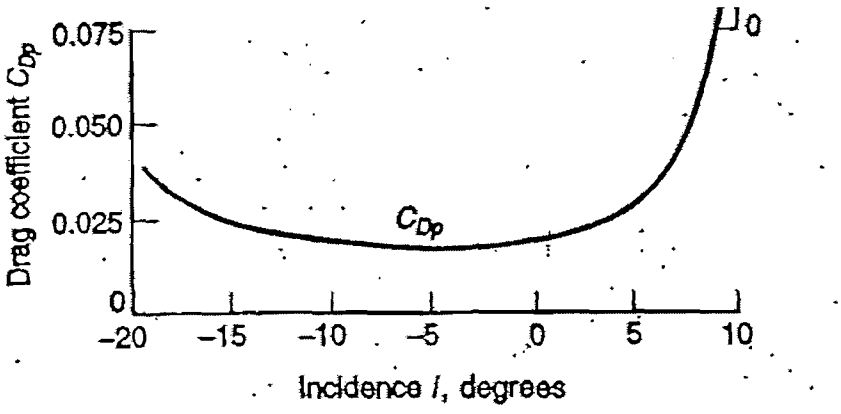


Figure 9.110 Drag coefficient for cascade of fixed geometrical form

From Figure 9.110 , at zero incidence $C_{DP} = 0.018$.

2. *Annulus drag,* C_{DA} – C_{DA} represents a loss due to drag effects on the annulus walls. Eq. (1.25) is derived in reference (Saravanamuttoo, 2001:196)

$$C_{DA} = 0.020\frac{s}{h} \tag{1.25}$$

where *s* and *h* are the pitch and height of the blades respectively.

3. *Secondary losses,* C_{DS} – Secondary losses due to trailing edge vortices and tip clearance are accounted for by C_{DS}. For typical axial compressor designs, the following empirical formula for the additional drag coefficient arising from secondary losses has been derived.

$$C_L = 2\frac{s}{c}(\tan\beta_1 - \tan\beta_2)\cos\beta_m$$

$$C_{DS} = 0.018 \cdot C_L^{\,2} \tag{1.26}$$

On inclusion of these three factors, an overall drag coefficient can be determined which is given by

$$C_D = C_{DP} + C_{DA} + C_{DS} \tag{1.27}$$

Eq. (1.24) can now be rewritten as

$$C_D = \left(\frac{s}{c}\right)\left(\frac{\overline{w}}{0.5\rho V_1^2}\right)\frac{\cos^3\beta_m}{\cos^2\beta_1} \tag{1.28}$$

where $\frac{\overline{w}}{0.5\rho V_1^2}$ represents the total loss in stagnation pressure for the rotor.

Since C_D can be calculated from the empirical data, and the blade angles and solidity is known, $\frac{\overline{w}}{0.5\rho V_1^2}$ for the blade row can be solved. The theoretical static pressure rise through the blade row is found by putting the loss *w* equal to zero in Eq. (1.22), which gives

$$\Delta p_{th} = \tfrac{1}{2}\rho \cdot C_a^{\,2}\left(\tan^2\alpha_1 - \tan^2\alpha_2\right)$$

$$\Delta p_{th} = \tfrac{1}{2}\rho \cdot C_a^{\,2}\left(\sec^2\alpha_1 - \sec^2\alpha_2\right)$$

Therefore

$$\frac{\Delta p_{th}}{\tfrac{1}{2}\rho \cdot C_a^{\,2}\sec^2\alpha_1} = \left(1 - \frac{\sec^2\alpha_2}{\sec^2\alpha_1}\right)$$

$$\frac{\Delta p_{th}}{\tfrac{1}{2}\rho \cdot V_1^2} = \left(1 - \frac{\cos^2\alpha_1}{\cos^2\alpha_2}\right) \qquad \text{cascade notation} \tag{1.29}$$

$$\frac{\Delta P_{th}}{\tfrac{1}{2}\rho \cdot V_1^2} = \left(1 - \frac{\cos^2\beta_1}{\cos^2\beta_2}\right) \qquad \text{blade row notation} \tag{1.30}$$

The efficiency of the blade row, η_b, is defined as the ratio of the actual pressure rise to the theoretical pressure rise $\eta_b = \frac{\Delta p_{th} - \overline{w}}{\Delta p_{th}}$, reducing to

$$\eta_b = 1 - \frac{\overline{w}/\left(0.5 \cdot \rho V_1^2\right)}{\Delta p_{th}/\left(0.5 \cdot \rho V_1^2\right)} \tag{1.31}$$

For stages of 50% reaction, the efficiency of the blade row is assumed to be the same as the stage efficiency, $\eta_b = \eta_s$ (Saravanamuttoo, 2001). The static pressure ratio of the stage is found to be

$$PR_s = \left[1 + \frac{\eta_s \Delta T_s}{T_1}\right]^{\gamma/(\gamma-1)} \tag{1.32}$$

After the efficiency of all the stages were solved, the actual pressure ratio over each of the stages is calculated. This calculated pressure ratio per stage is used to determine the actual pressure ratio over the compressor, from which the actual compressor efficiency is calculated.

9.5 APPENDIX V – THE AINLEY & MATTHIESON TURBINE LOSS MODEL

The theory necessary to use the loss model of *Ainley and Matthiesen* in order to evaluate a turbine's stage efficiency is documented in this section. See *Figure 5.42* for the discussion to follow.

The loss coefficient for the nozzle blades is defined by either: (see *Figure 5.42* for notation)

$$\lambda_N = \frac{T_2 - T_2'}{C_2^2 / 2c_p} \quad or \quad Y_N = \frac{p_{01} - p_{02}}{p_{02} - p_2} \tag{1.33}$$

The loss coefficient for the rotor blades is defined by either: (see *Figure 5.42* for notation)

$$\lambda_R = \frac{T_3 - T_3''}{V_3^2 / 2c_p} \quad or \quad Y_R = \frac{p_{02rel} - p_{03rel}}{p_{03rel} - p_3} \tag{1.34}$$

See (Saravanamuttoo, 2001) for the theory in deriving the stage efficiency, η_s.

$$\eta_s = \frac{1}{1 + \left[\lambda_R (V_3^2 / 2c_p) + (T_3 / T_2)\lambda_N (C_2^2 / 2c_p)\right] / (T_{01} - T_{03})} \tag{1.35}$$

The stage prediction needs to solve for λ_N and λ_R. The overall blade loss coefficient Y (or λ) must account for the following sources of friction loss

1. *Profile loss, Y_P* – associated with boundary layer growth over the blade profile (including separation loss under adverse conditions of extreme angles of incidence or high inlet Mach number).
2. *Annulus loss and secondary loss, Y_S* – The annulus loss is associated with boundary layer growth on the inner and outer walls of the annulus. The secondary loss arises from secondary flows which are always present when a wall boundary layer is turned through an angle by an adjacent curved surface.
3. *Tip clearance loss, Y_K* – near the rotor blade tip the gas does not follow the intended path, fails to contribute its quota of work output, and interacts with the outer wall boundary layer.

The method to be outlined here is that of *Ainley and Mathieson*, which estimates the performance on flow conditions at the mean diameter of the annulus. We are concerned now to only estimate the efficiency at the design point. Two correlations for profile loss coefficient Y_P obtained from cascade data are shown in *Figure 9.111*. These refer to conventional profile (e.g. T6) having a thickness/chord ratio (t/c) of 0.2 and a trailing edge thickness/pitch ratio (t_e/s) of 0.02. Rotor blade notation is used in *Figure 9.111*.

When the nozzle row is being considered β_2 becomes α_1 and β_3 becomes α_2; there is no need to duplicate equations which equally apply to both rows. The values of Y_P in *Figure 9.111* refer to blades operating at zero incidences.

STEP 1: Estimation of Y_p

Estimate $(Y_P)_N$ and $(Y_P)_R$ from the gas angles of the proposed design by using *Figure 9.111* together

with the interpolation formula:

$$Y_P = \left\{ Y_{P(\beta_2=0)} + \left(\frac{\beta_2}{\beta_3}\right)^2 \left[Y_{P(\beta_2=\beta_3)} - Y_{P(\beta_2=0)} \right] \right\} \left(\frac{t/c}{0.2}\right)^{\beta_2/\beta_3} \qquad (1.36)$$

For the nozzle, replace β_2 with α_1 and β_3 with α_2 in Eq. (1.36). This correction is considered reliable only for $0.15 < t/c < 0.25$.

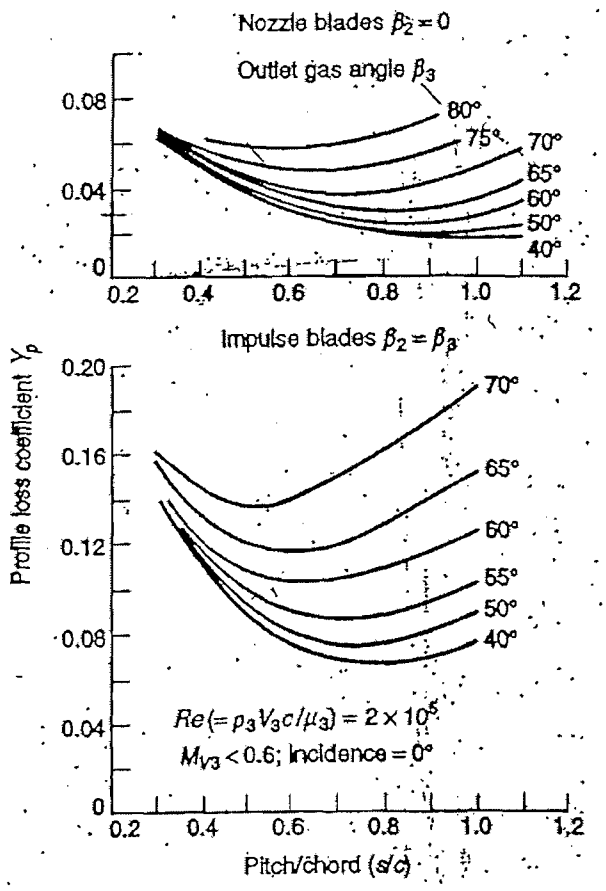


Figure 9.111 *Profile loss coefficient for conventional blading with t/c = 0.2*

Should it be decided to design the blades to operate with some incidence at the design point, a correction to Y_P would be required. As this correction is really only important when estimating performance at part load, we refer to (Saravanamuttoo, 2001).

STEP 2: Estimation of Y_s and Y_k

Secondary and tip-clearance loss data for Y_s and Y_k have been correlated using the concepts of lift and drag coefficient. For the turbine cascade, it follows that

$C_L = 2\frac{s}{c}(\tan\beta_2 + \tan\beta_3)\cos\beta_m$, where

$\beta_m = \tan^{-1}\left[(\tan\beta_3 - \tan\beta_2)/2\right]$

It is convenient to treat Y_s and Y_k simultaneously. The proposed correlation is

$$Y_s + Y_k = \left[\lambda + B\left(\frac{k}{h}\right)\right]\left[\frac{C_L}{s/c}\right]^2 \frac{\cos^2\beta_3}{\cos^3\beta_m} \tag{1.37}$$

Consider the first bracketed term. The tip clearance is proportional to k/h where *k* is the clearance and *h* the blade height. The constant *B* is 0.5 for a radial tip clearance and 0.25 for a shrouded blade with side clearance. The secondary loss component function is given by

$$\lambda = 0.0334\left(\frac{c}{h}\right)\left(\frac{\cos\beta_3}{\cos\beta_2}\right) \tag{1.38}$$

For nozzle blade row, replace β_2 with α_1 and β_3 with α_2. The total loss coefficients become

$$Y_N = (Y_P)_N + [Y_s + Y_k]_N \tag{1.39}$$

$$Y_R = (Y_P)_R + [Y_s + Y_k]_R \tag{1.40}$$

STEP 3: Calculate stage efficiency

The stage efficiency can now be calculated:

$$\lambda_N = \frac{Y_N}{(T_{02}/T'_2)} \tag{1.41}$$

$$\lambda_R = \frac{Y_R}{(T_{03rel}/T''_3)} \tag{1.42}$$

$$\eta_s = \frac{1}{1 + \left[\lambda_R(V_3^2/2c_p) + (T_3/T_2)\lambda_N(C_2^2/2c_p)\right]/(T_{01} - T_{03})} \tag{1.43}$$

STEP 4: Evaluate mach number

In conclusion, it must be emphasized that the cascade data and other loss correlations are strictly applicable only to designs where the Mach numbers are such that no shock losses are incurred in the blade passages. The additional loss incurred by designing with a blade outlet relative Mach number greater than unity can be accounted for by adjusting the profile loss coefficient Y_P of the blade row. The correction is given by

$$Y_P = \left\{Y_{P(\beta_2=0)} + \left(\frac{\beta_2}{\beta_3}\right)^2\left[Y_{P(\beta_2=\beta_3)} - Y_{P(\beta_2=0)}\right]\right\}\left(\frac{t/c}{0.2}\right)^{\beta_2/\beta_3} x\left[1 + 60(M-1)^2\right] \tag{1.44}$$

However, the Mach number in Helium cycles will always be relatively low.

9.6 APPENDIX VI – VERIFICATION BY MEANS OF EES-MODELS

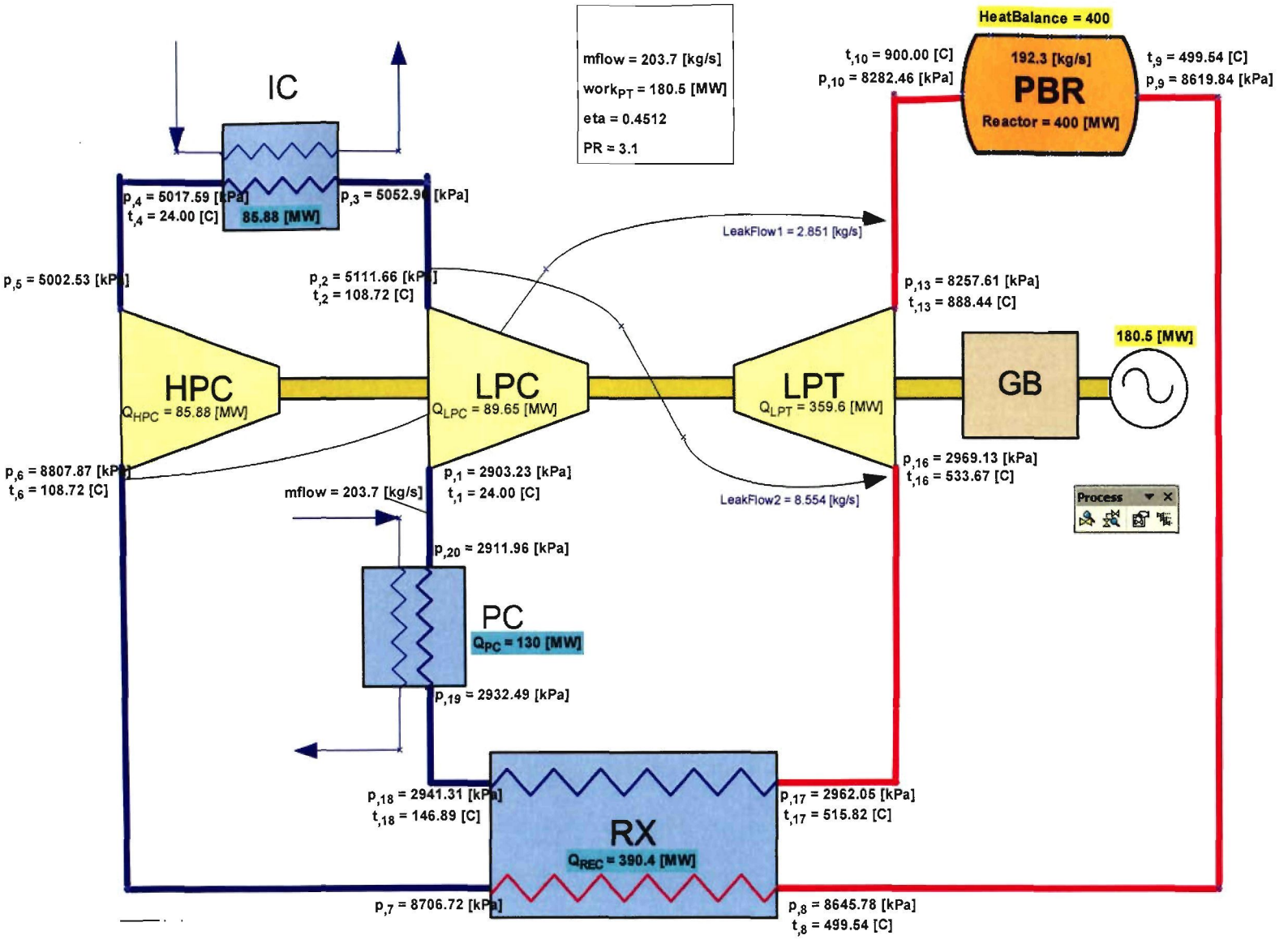


Figure 9.112 *EES identification diagram - (B) Single-shaft with inter-cooling*

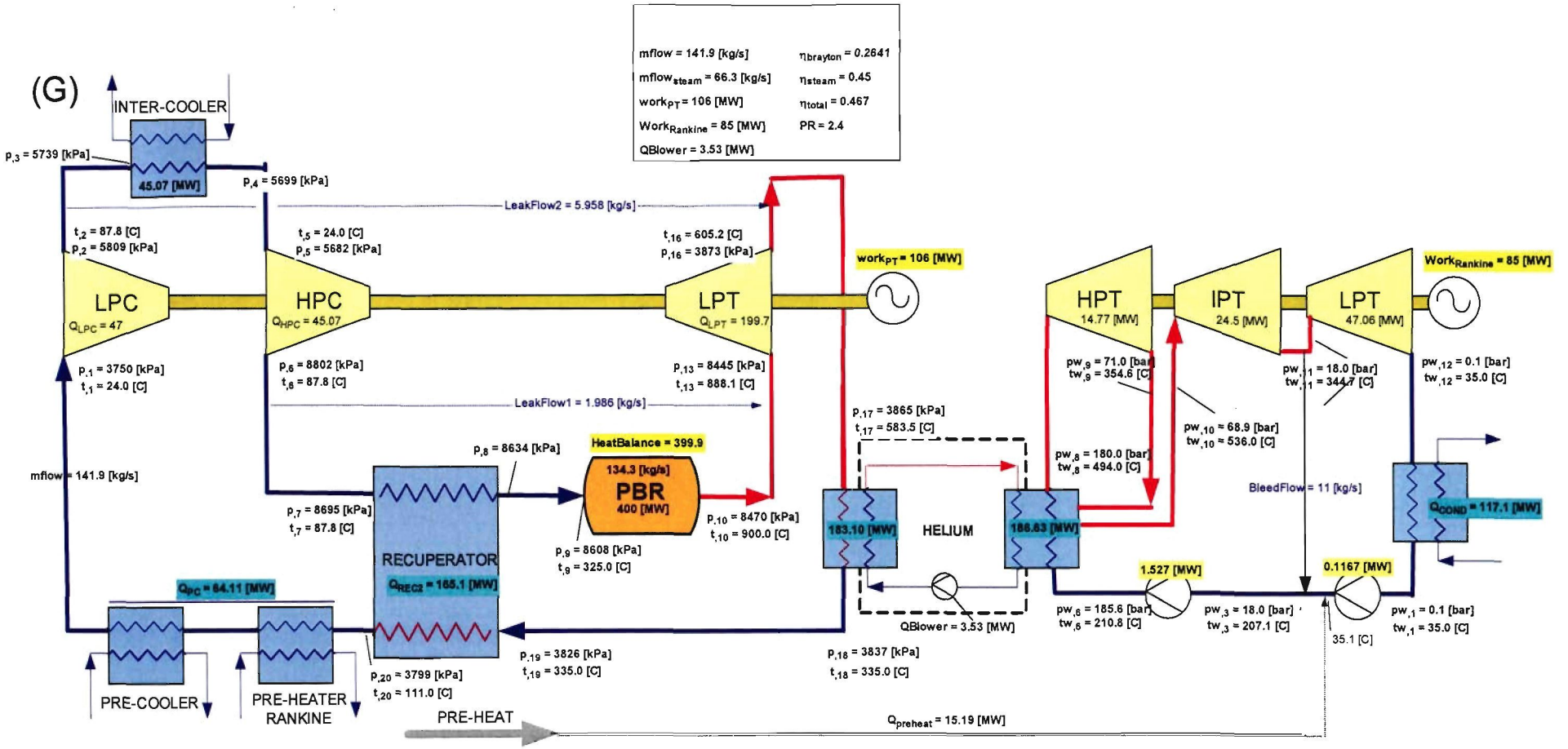


Figure 9.113 *EES identification diagram - (G) Single-shaft recuperative Brayton with inter-cooling*

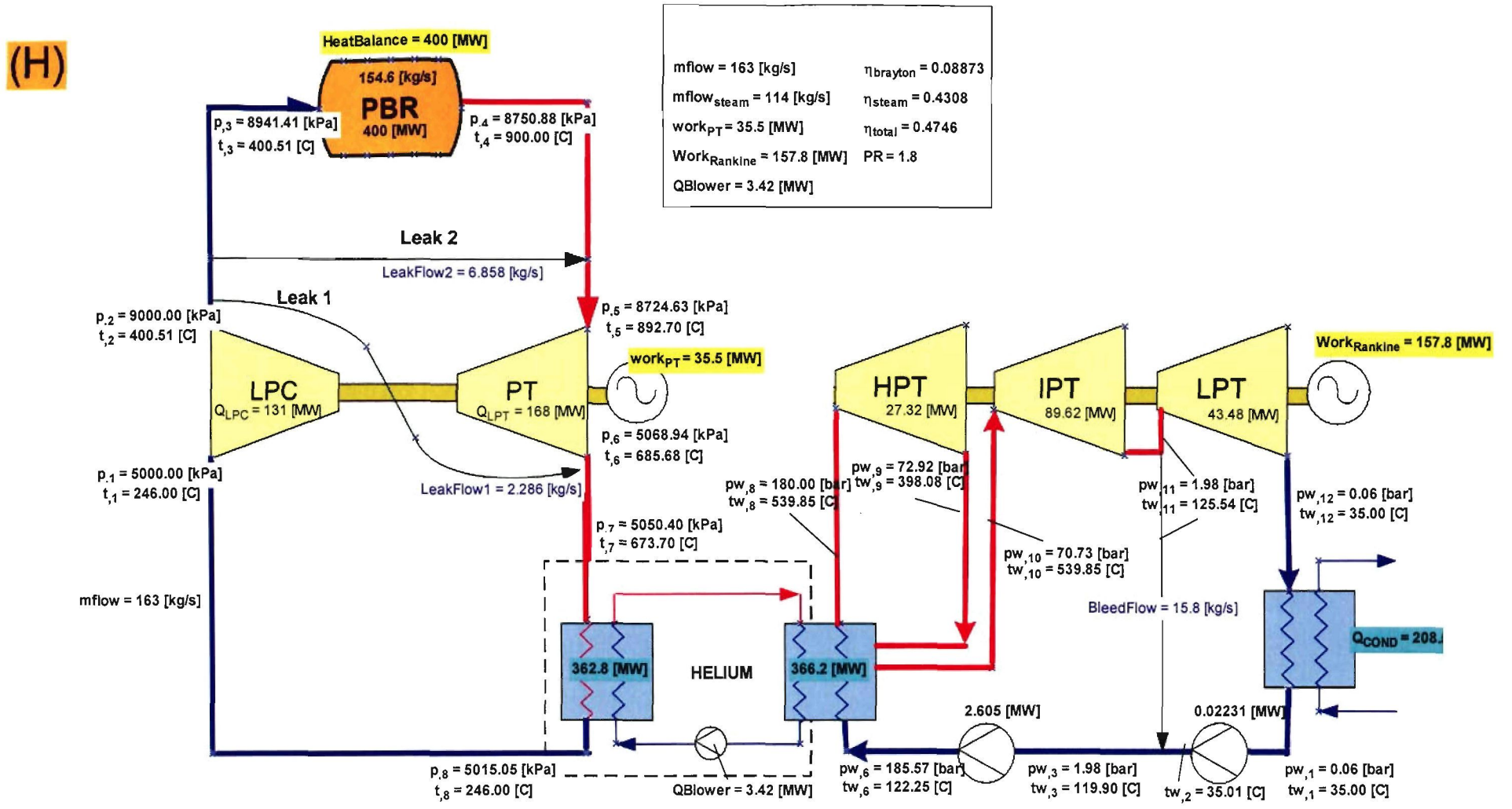


Figure 9.114 *EES identification diagram - (H) Single-shaft Brayton without inter-cooling*

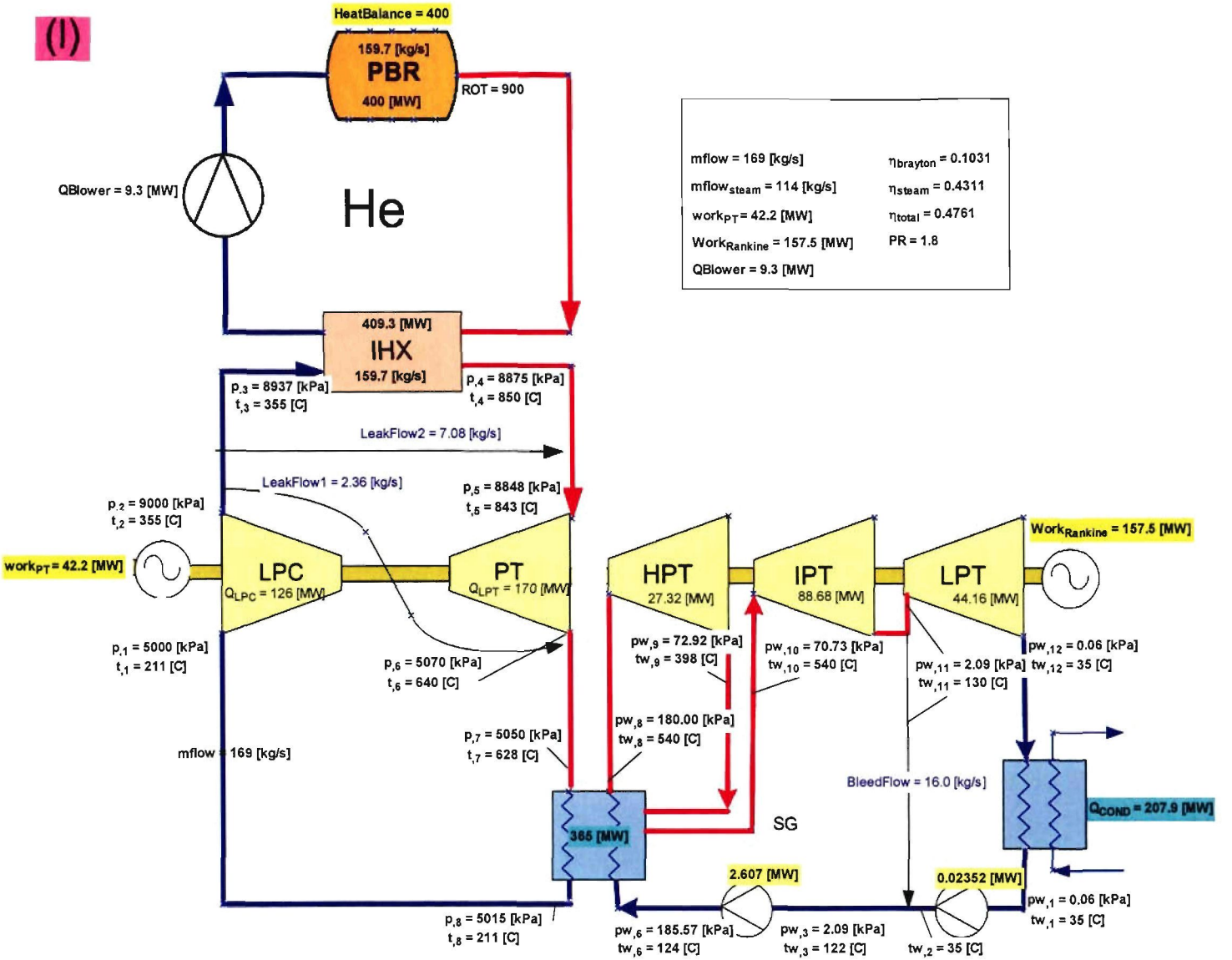


Figure 9.115 *EES identification diagram - (I) Indirect Single-shaft Brayton without inter-cooling – HELIUM*

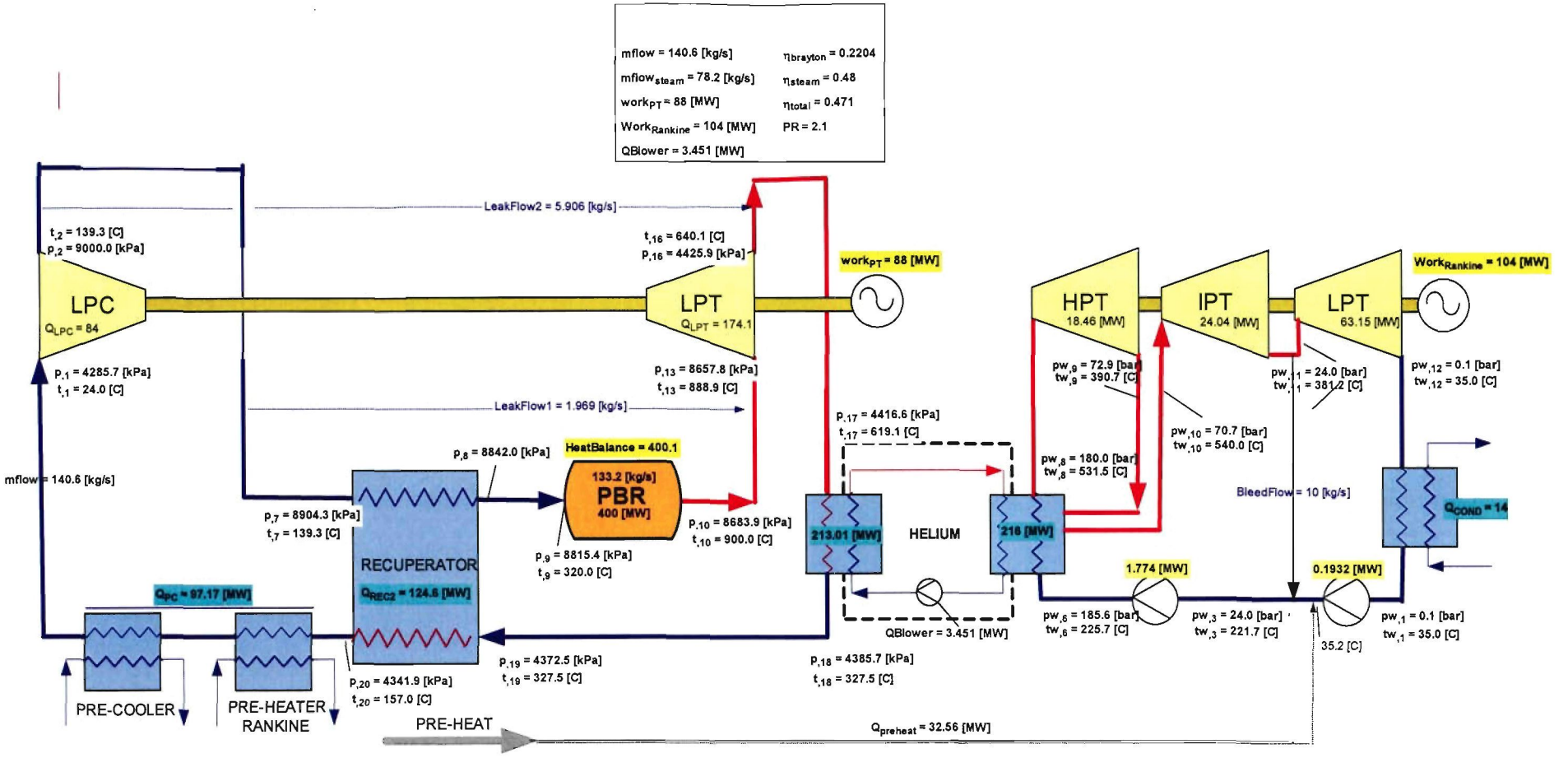


Figure 9.116 *EES identification diagram - (J) Single-shaft recuperative Brayton without inter-cooling*